UNIVERSITÀ DEGLI STUDI DI MESSINA

Dipartimento di scienze Chimiche, Biologiche,
Farmaceutiche e Ambientali

Dottorato di Ricerca in Scienze Chimiche
XXIX Ciclo

Transition metal anion complexation agents: sensors, molecular carriers and acid-base titrants

Ileana Ielo

Supervisor

Prof. Antonino Giannetto

Coordinator

Prof. Sebastiano Campagna

Contents

Introduction

Studies on the noncovalent coordination of anions may be considered to have started in 1968, with early contributions by Park and Simmons, [1] later developed in particular by Schmidtchen [2] and Lehn. [3] After this pioneering start, there was extensive diffusion in 1990s. [4,5] Since then, design and development of new anion receptors has become a more and more attractive aim.

In fact, a full understanding of the reversible intermolecular interaction between a receptor and its complementary anion paves the way toward the availability of high-sensitivity anion sensors, which is particularly interesting for anionic species that are the cause of serious environmental problems. In such cases, stable and reversible receptor–anion complexes could function as carriers of a pollutant anion and thus to remove it from blood, cells, soil, water, and so on. Furthermore, anion transport by receptor–anion carriers through a lipid bilayer membrane by a receptor that can function as a mobile carrier or may form a channel, could find application in biology and medicine. [6]

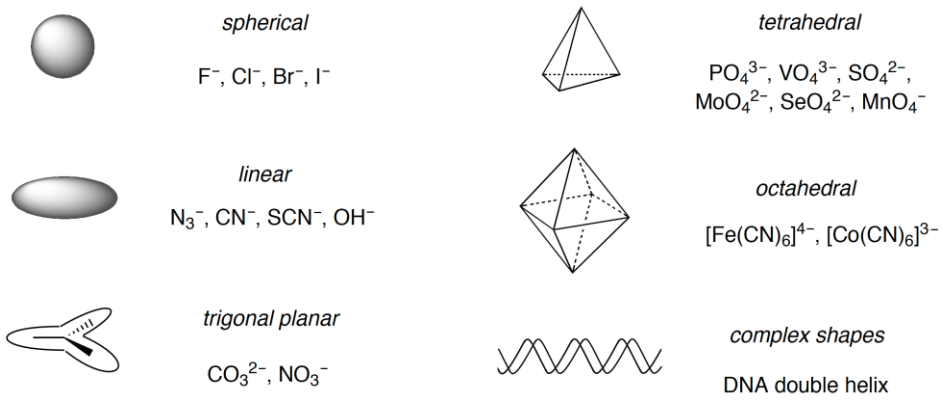

Fig. 1 - The structural variety of anions

A proper design of a suitable anion receptor must take into account a series of factors: i) electrostatic binding interactions, substantially ruled by charge to radius ratio; ii) pH window in which the target anion are not yet protonated; iii) geometric complementarity with the shape of the anions to be received. In fact the wide range of geometries possible for an anionic species (Fig. 1) requires a higher degree of design for the complementary accommodation of the anionic guest.[7]

The design anion receptor must also take into consideration the nature of the solvent in which the designed molecule could work; for example an neutral receptor may only complex anions in aprotic organic solvents, where it can form strong hydrogen bonds with anions. On the contrary a charged receptor has the capacity to bind highly solvated (hydrated) anions in protic solvent media.

Anion receptors that match the above requisites are usually classified as: [8] charged anion receptors, like those based on the presence of ammonium, guanidinium, imidazolium, and triazolium groups; neutral anion receptors, which, in turn, can be further divided into Lewis acid receptors and molecules containing hydrogen-bond-donor (**HBD**) groups. These latter are essentially based on urea, thiourea, amide, indole, pyrrole, and alcohol moieties.

In the following a survey of the above classes of charged and neutral receptors will be done; the survey not pretends to be exhaustive but provides only adequate illustrative examples of the various classes of receptors.

References

[1] C. H. Park and H. E. Simmonds, *J. Am.Chem.Soc*., **1968**, *90*, 2428.

[2] a) F. P. Schmidtchen, *Angew. Chem., Int. Ed. Engl.* , **1981**, *20*, 466; b) F. P. Schmidtchen, *Chem. Soc. Rev.* **2010**, *39*, 3916.

[3] J. M. Lehn, *Angew. Chem., Int. Ed. Engl*., **1988**, *27*, 89 and references therein.

[4] A. Bianchi, K. Bowman-James and E. Garcia-Espana, *Supramolecular Chemistry of Anions*, Wiley-VCH New York **1997**,

[5] F. B. Schmidtchen and M. Berger, *Chem. Rev.* **1997**, *97*, 1609.

[6] a) G. A. Jeffrey and W. Saenger, *Hydrogen Bonding in Biological Structures*; Springer-Verlag: Berlin, **1991**; b) M. P. Hughes and B. D. Smith, *J. Org. Chem.* **1997**, *62*, 4492; c) D. C. Gadsby, *Nature* **2004**, *427*, 795–7; d) S. Y. Noskov, S. Berneche and B. Roux, *Nature* **2004**, 431.

[7] P. A. Gale, N. Busschaert, C. J. E Haynes, L. E. Karagiannidis and I. L. Kirby *Chem. Soc. Rev*., **2014**, *43*, 205.

[8] V. Amendola and L. Fabbrizzi, *Chem. Commun*. **2009**, 513.

1. Ammonium based anion receptors

Ammonium based anion receptors may be classified according to their complexity. Then, we can distinguish:

1) Acyclic ammonium receptors

2) Monocyclic ammonium receptors

3) Bicyclic ammonium receptors

1.1 Acyclic ammonium receptors

This kinds of compound are the simplest receptors in terms of design, in that they include alkyl ammonium salts. In the protonated form they can readily complex anions, and do so in biological systems. The diprotonated extended chain diamine and putrescine (1,4-diamino-n-butane), binds $H_2PO_4^-$ in what can be considered as a model for nucleic acid interactions with amines (Fig. 1.1A) [1, 2].

Even simple protonated ethylenediamine can form complexes, as seen in the crystal structure of the ethylenediammonium salt with citrate (Fig. 1.1B).

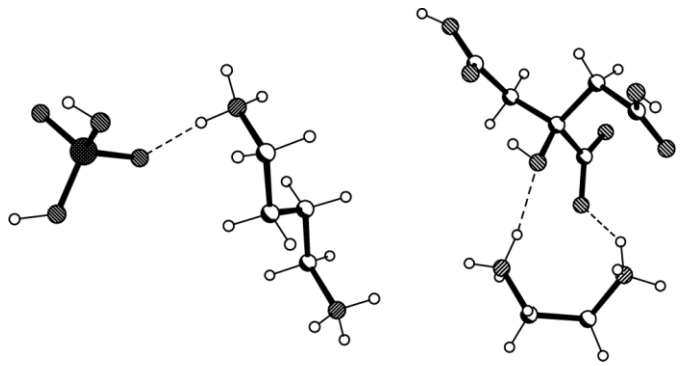

Fig. 1.1 - (**A**) Complex of diprotonated putrescine with $H_2PO_4^-$ [9]. (**B**) Ethylenediammonium complex with citrate [2].

Some Polyamine anion receptors (figure 1.2). anthrylpolyamines, **1** and **2**, exhibit fluorescence capabilities. Interactions with oxo anion groups, carboxylate, phosphate, and sulfate were examined [3]

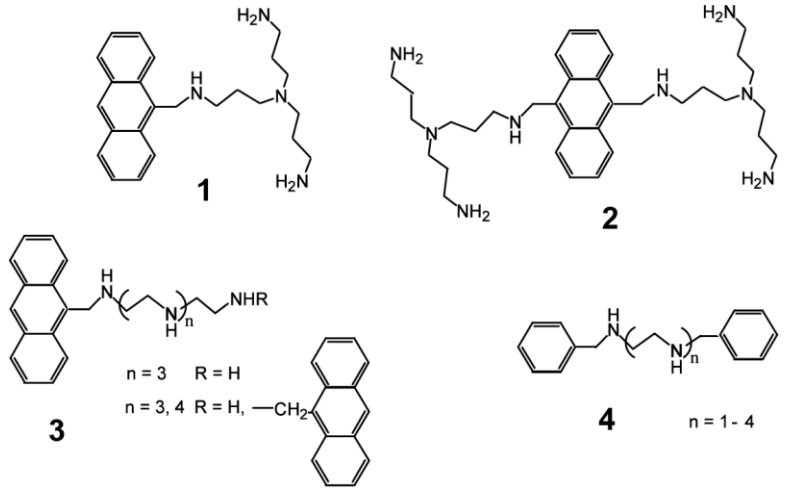

Fig. 1.2

A later study focused on a variety of linear amines, **3**, of varying chain lengths with one or two terminal anthracenes as fluorescence-signaling receptors for ATP, ADP and AMP. The findings indicated that the binding of ATP compared to the other nucleotides was significantly higher (Ks = 8.1-9.9) [4].

The ability of dibenzylated linear amines, **4**, to bind $[Co(CN)_6]^{3-}$ was also examined [5].

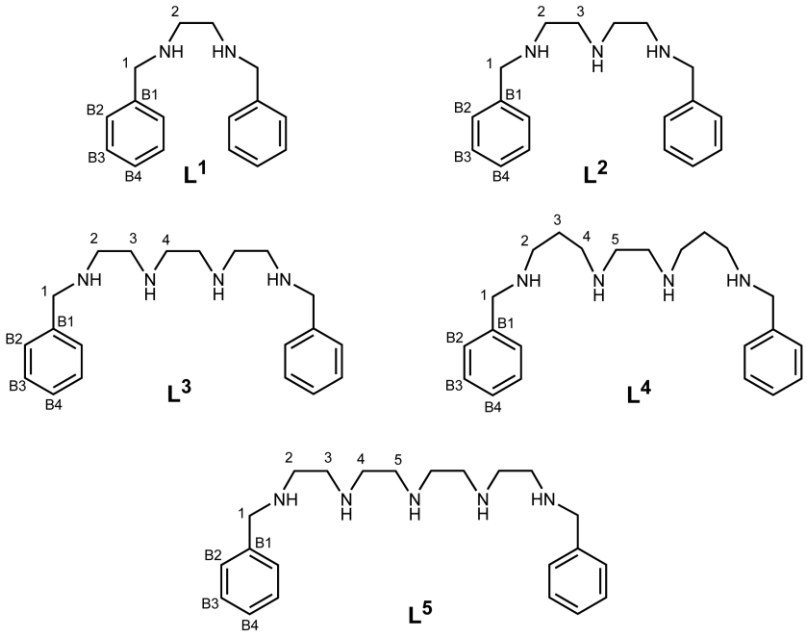

Fig 1.3

The supramolecular adducts of L^1-L^5 (Fig. 1.3) with $[Co(CN)_6]^{3-}$ have been studied with photochemical methods: The emission of the fully protonated forms of the polyamines L^1-L^5 were followed as a function of the added concentration of hexacyanocobaltate(III) in 0.15 mol dm^{-3} NaClO, or NaCI. addition of the anion gives rise to a quenching effect on the emission of the fully protonated form of the L^1-L^5 receptor, and it has been possible the calculation of association constants.

1.2 Monocyclic ammonium receptors.

Monocylic ammonium receptors can be divided according to molecular complexity of hosted anions.

2.2.1 Simple inorganic anions

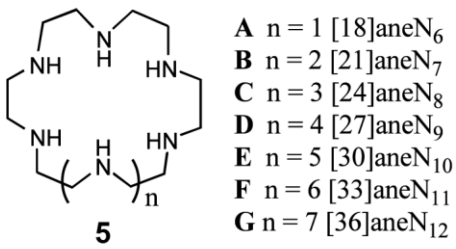

5

A n = 1 [18]aneN$_6$
B n = 2 [21]aneN$_7$
C n = 3 [24]aneN$_8$
D n = 4 [27]aneN$_9$
E n = 5 [30]aneN$_{10}$
F n = 6 [33]aneN$_{11}$
G n = 7 [36]aneN$_{12}$

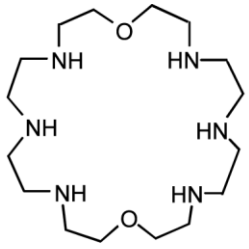

6

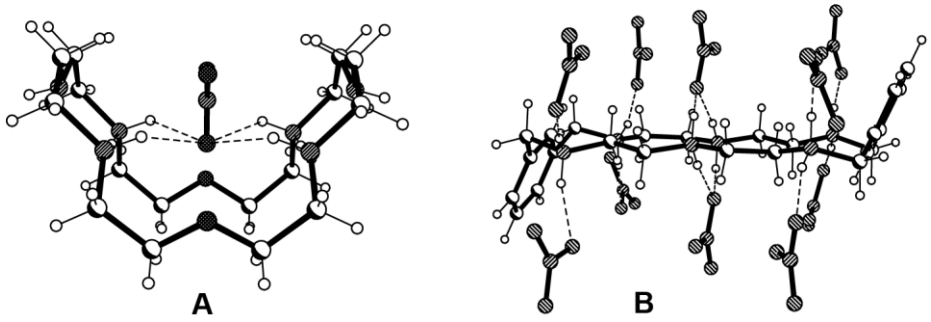

A B

Fig. 1.4 - (**A**) Encapsulation of nitrate in the complex of $H_4\mathbf{6}^{4+\cdot}$ $4NO_3^-$ [7]. (Only the encapsulated nitrate is shown) (**B**) Layered structure of the nitrate complex of $H_6\mathbf{7A}^{\cdot}$ $6NO_3^-$ [11]. (Eight surrounding nitrates are shown.)

The first crystallographic example in this area was reported [6] for the 18 membered system [18]aneN6 (Fig. 1.4). Nomenclature for the monocycles will include the ring size in brackets followed by "ane" for saturated carbon chain, followed by the number(s) of heteroatoms. Hence, [18]aneN6 is an 18-membered ring with six nitrogens, the amine corollary to the well-known 18-crown-6.], **5A**.

Molecular dynamics studies on **6** and several related systems indicated that in solution solvation effects come into play, and the folded structure is very flexible [7-9].

More recently, some researchers have shifted their synthetic strategies [10] to receptors readily obtainable by simple Schiff base condensations followed by borohydride reductions (Fig. 1.5)

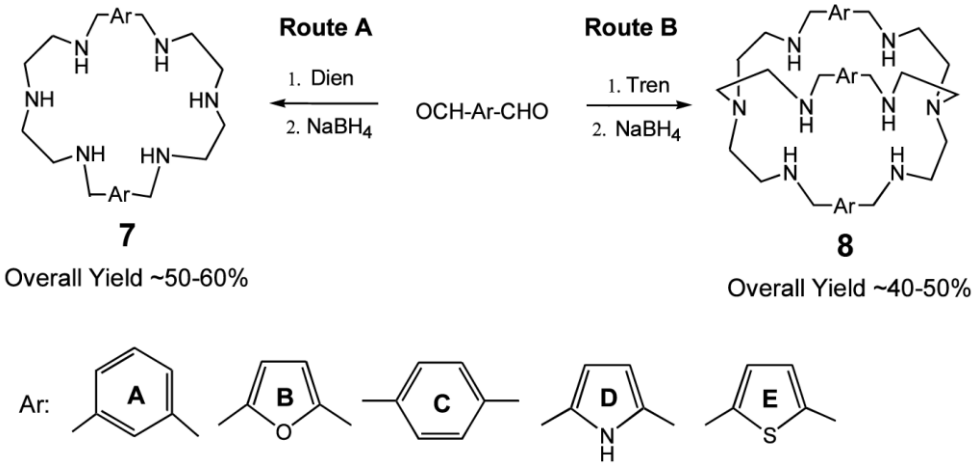

Fig. 1.5 - Synthetic route to polyaza macrocycles and aza cryptands using Schiff base methodology [18].

Many of these aza monocycles (**Route A**) also tend to show layered structures, including complexes of **7A** with nitrate [11], sulfate [11], bromide [12] and fluoride [13]. An example is the nitrate structure of **7A** (Fig. 1.4B), where two 'layers' of nitrates are shown.

1.2.2 Organic anions

Macromonocycles have also been found to bind organic ions, including carboxylates and nucleotides [14-18].

A paper by Lehn and co-workers in 1981 described the interaction of three different polyamine macromonocycles, **9-10** (Fig. 1.6), with a series of organic anions (as well as with sulfate, nucleotides and transition metal anionic complexes) [14].

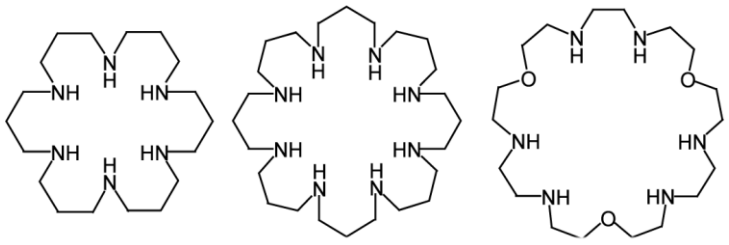

Fig. 1.6

Dicarboxylates could be bound by using ditopic receptors. One method is to attach two monotopic macrocyclic receptors together as was done to obtain **12** (fig. 1.7) [17].

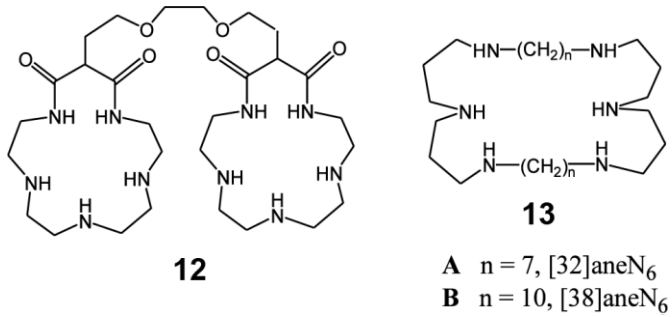

Fig. 1.7

Rather than linking together two separate macrocycles, another strategy for introducing ditopic binding is to place two binding sites at opposite ends of a macrocycle separated by a bridging chain or 'spacer', **13** (fig. 1.7) [18].

1.2.3 Anionic metal complexes

Large ring polyammonium monocycles with six or more nitrogens form complexes with anionic transition metal complexes in second sphere coordination[14,19,20]. Some examples are given in the figure 1.8.

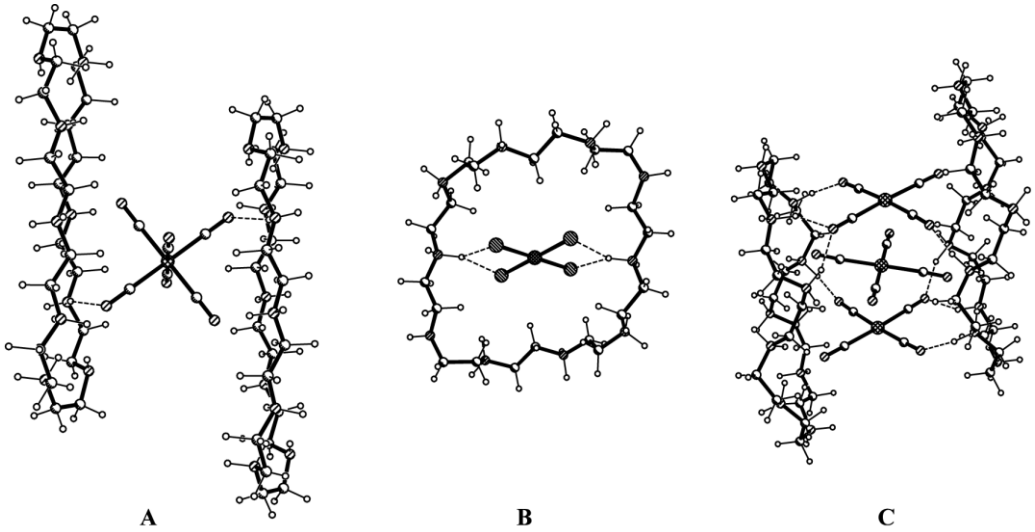

Fig. 1.8 - Structures of metallate anions with the hexaprotonated [21]aneN_{10}. (**A**) $Co(CN)_6^{3-}$ [19,20,22]; (**B**) $PdCl_4^{2-}$ [21]; **(C**) $Pt(CN)_4^{2-}$ [20].

1.3. Bicyclic ammonium receptors

The bicyclic polyammonium receptors are also known as azacryptands because of their structural similarity with the early ether-derived cryptands of Lehn and coworkers [23]. In their polyprotonated states, these bicyclic amine-based receptors bind more strongly to anions, even monoanions, compared to monocycles, often by two or more orders of magnitude.

1.3.1. Halides and pseudohalides

The katapinands, **14** (Fig. 1.9), are diaza bicyclic receptors named from a Greek word meaning "to swallow-up! [24]. In the series of varying chain lengths. The field expanded with the introduction of the linear bis-tren azacryptand **15** [25,26], which was found to be exceptionally complementary

for encapsulating the linear azide ion (Fig. 1.8A), with an aqueous stability constant of log Ks = 4.3. Crystallographic studies also indicated halide inclusion within the cavity. Chloride and bromide (Fig. 1.9B) are centrally located. In the fluoride structure a single fluoride sits off-center, closer to one of the tren units (Fig. 1.9C) [26], although it had been speculated that bifluoride could be encapsulated as well.

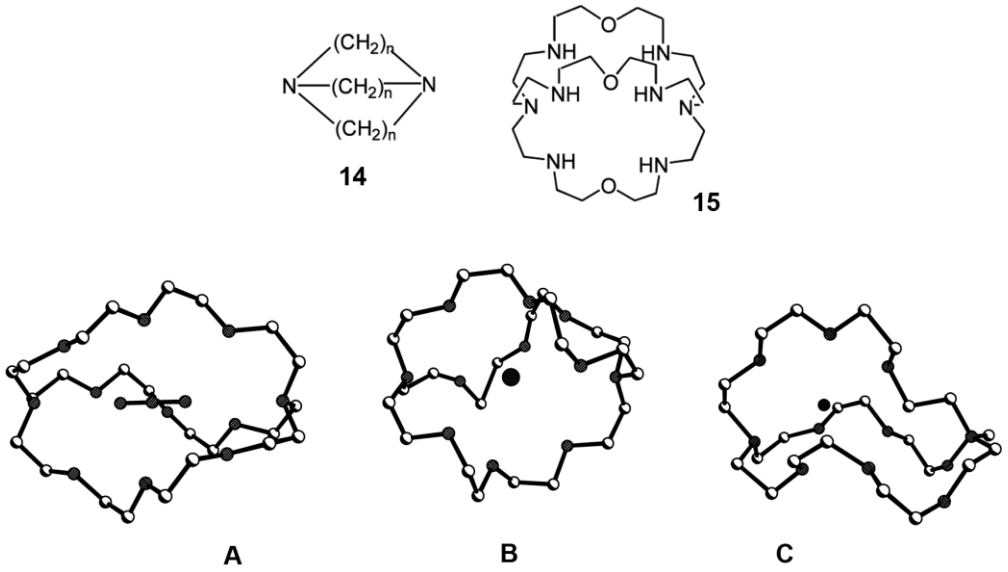

Fig. 1.9 - Crystal structures of $\mathbf{H_6 18^{6+}}$ with (**A**) azide (**B**) bromide, and (**C**) fluoride [26].

1.3.2. Oxo anions

In 1998 an encapsulated nitrate was observed crystallographically in an azacryptand, in this instance for **8A** (Fig. 1.5) [11,27].

The C_3 symmetry of the receptor is perfectly suited to the D_{3h} geometry of nitrate, such that the cavity contains two nitrates, perfectly aligned in an eclipsed conformation (Fig. 1.10B). More recently several nitrate complexes with the hexaprotonated **8C** have been isolated, some of which show a single nitrate in the cavity (Fig. 1.10C) [28].

The complex shown is the pentatosylate mononitrate salt of **8C**. The very first crystallographic verification of internal binding of an oxo anion, however, was reported for a perchlorate encapsulated in the furan cryptand **8B** [29].

Likewise, host **8A** has been found to be a versatile receptor for tetrahedral species, encapsulating thiosulfate and chromate [30], as well as perchlorate [40] (Fig. 1.10).

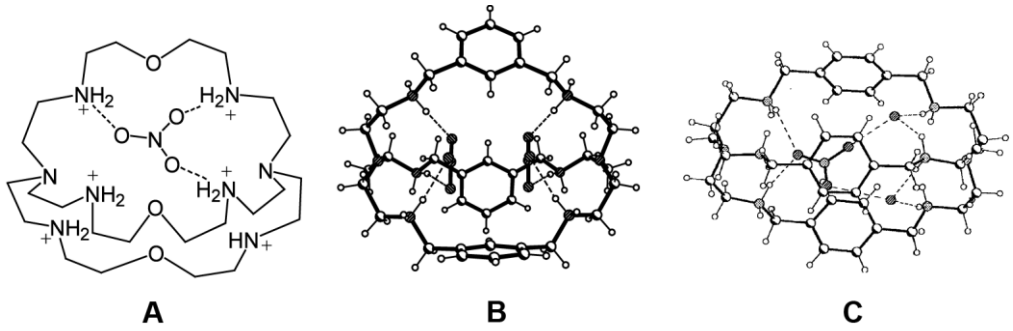

Fig. 1.10

Of the tetrahedral species, hydrogen bonding interactions appear to be maximized in the thiosulfate structure, probably due to the longer S-S bond, which can extend farther along the cavity. The apical sulfur is bound by three protonated amines on one side of the bicycle, while each of the three oxygens are held by the other side in a fashion similar to that observed for the nitrate complex of **8A** (Fig. 1.10B). The other tetrahedral molecules, chromate and perchlorate, do not appear to be as perfectly accommodated (Fig. 1.11B and C).

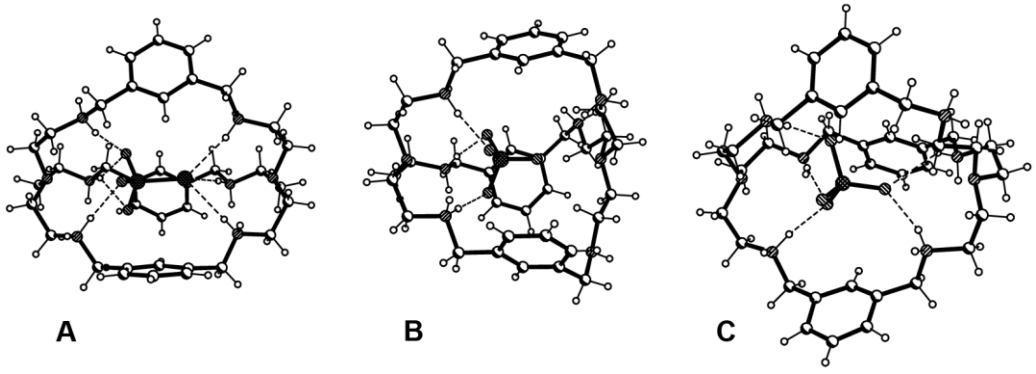

Fig. 1.11

In these structures at least one oxygen is not hydrogen bonded with the receptor, but instead often with nearby water molecules.

A similar situation of non-ideal topology was observed for the perchlorate complex with **8B** [29].

Most of these structures contain significant disorder in the azacryptand and/or the counterions and solvent, and thus present challenges to the chemist and crystallographer. It is unfortunate that there are no comprehensive studies of systematic binding of a variety of anions with a series of these interesting and readily available azacryptands. However, in the binding studies that have been reported, there are no major selectivity successes observed for the binding of oxo anions, with the exception perhaps that dinegative species are bound more strongly than mononegative anions [11,27,30,31]

1.3.3. Organic anions

Despite the increased steric congestion in the bicycles, they can, however, engulf dicarboxylates as seen in the crystal structure of terephthalate with **16** (Fig. 1.12) [32]. In a related series of receptors, including the wellstudied **15** bis-tren, significant affinities for dicarboxylates, and especially oxalate, were observed. For example, the log Ks of **15** with oxalate and malonate are 4.95 and 3.10, respectively [26].

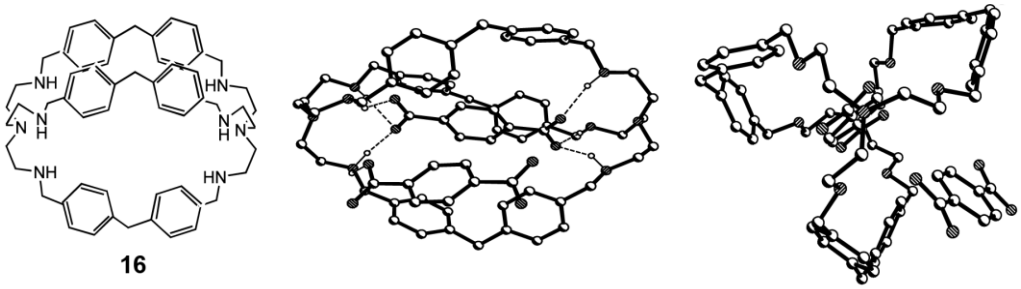

Fig. 1.12

1.4. Polycyclic ammonium receptors.

The macrotricyclic 'soccer ball' ligand, **17**, was first designed as a receptor for alkali metal ions [33], along with a slightly modified host, with the fourth bridge consisting of a simple hydrocarbon chain, **28** (Fig. 1.13).

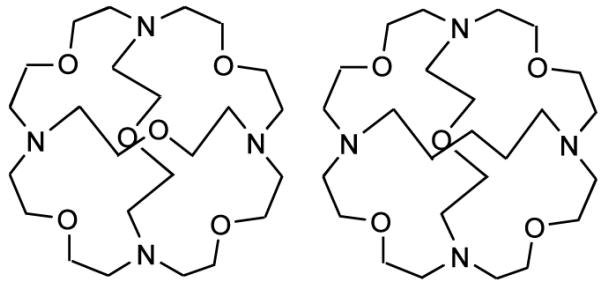

17 **18**

Fig. 1.13

These ligands are also especially well-suited for spherical recognition, incorporating halides internally with high affinities. Size and shape of the macrocycle play a definite role, as the affinity of **17** for Cl^- over Br^- exceeds 10^3, while NO_3^-, CF_3COO^- and ClO_4^-, because of their the wrong shapes, and iodide (too large) do not form complexes.

Shortly after the introduction of the soccer ball ligand, **17**, Schmidtchen synthesized a quaternized analog, **19** (Fig. 1.14), to explore ammonium receptors insensitive to pH [34]. This series has expanded over a wide range of studies illustrating the utility of these systems for anion recognition [35,36].

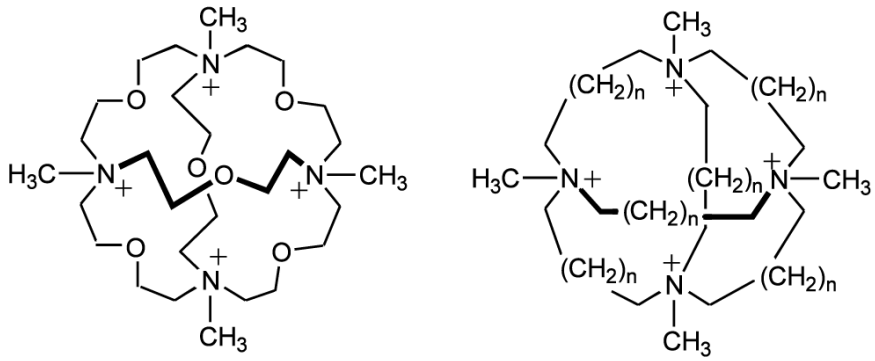

19 **20**

A n = 4
B n = 6

Fig. 1.14

All three quaternized hosts (**19**, **20A**, and **20B**) showed selectivity for Br^- over other halides in aqueous solution. The higher binding for **20A** and **20B** was attributed to the greater flexibility of the hydrocarbon chains (Fig 1.14).

By modifying the quaternary ammonium hosts, dual anion/cation ditopic receptors for zwitterionic guests were synthesized, **21** [37].

When association of the zwitterioinic guests was compared between the ditopic **21** (Fig. 1.15) and a monotopic crown ether control **22**, binding was higher for the monotopic system, but the selectivity factor was higher for the ditopic receptor by a factor of 2.5 [37].

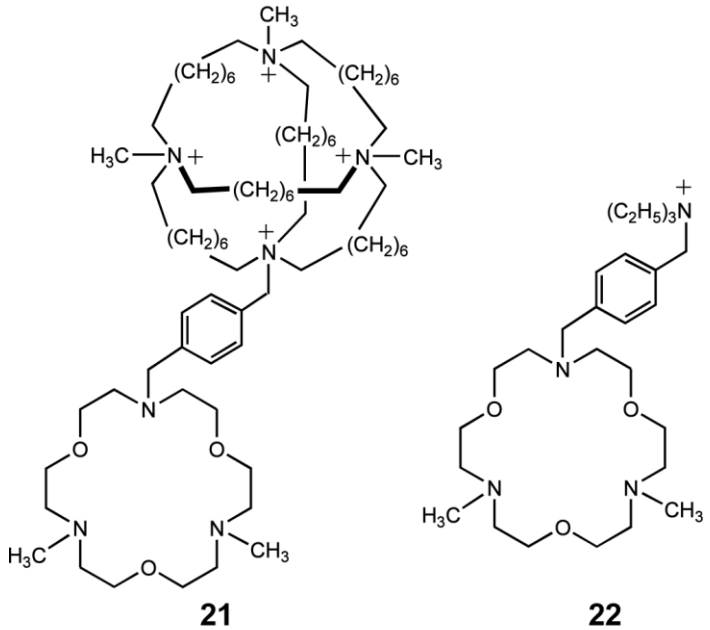

Fig. 1.15

In a slightly different variation of the zwitterionicidea, Schmidtchen synthesized a zwitterionic receptorusing phenylcarboxylates to quaternize the receptors, **23** (Fig. 1.16) [36].

The rationale was to obtain a neutral receptor that would obviate the need for the corollary negative counterion. Rigid phenyl groups were used to maximize the distance between the positive and negative ends, and therefore to interfere as little as possible with the binding.

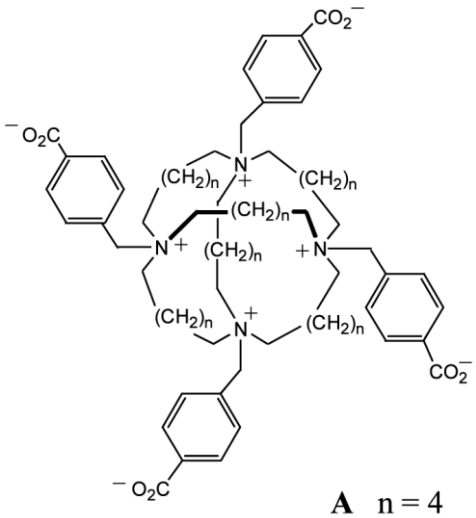

23

Fig. 1.16

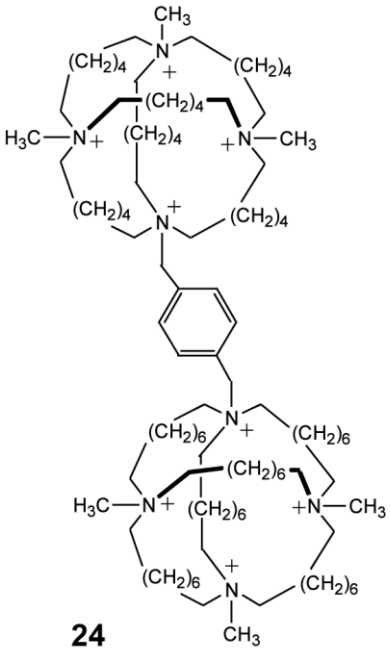

24

Fig. 1.17

By linking two of the quaternary ammonium polycycles together, a ditopic receptor **24** (Fig. 1.17) was synthesized as a host for dianionic guests [38,39].

A corollary to the polyaza cryptands that imposes more rigidity to the receptor consists of two face-to-face, 1,3,5-trisubstituted benzenes with bridges containing amines, **25**-**27** (Fig 1.18) [40,41].

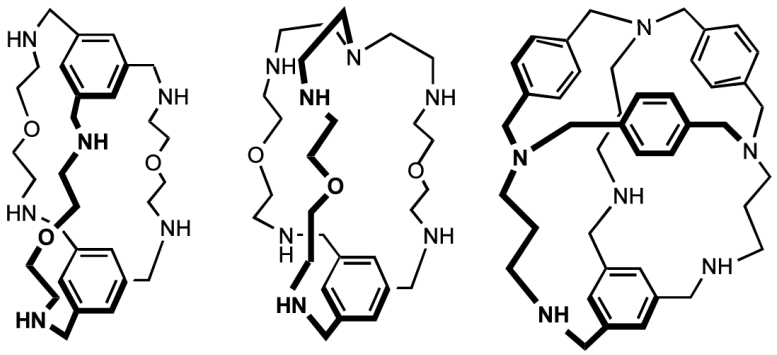

25 26 27

Fig. 1.18

While these could also be categorized as bicyclic, with the phenyl rings as the bridgehead 'atom', for the purposes of this review they shall be considered as polycyclics. Small anions are bound with relatively high affinity in **25**-**27** and NMR studies indicate 1:1 complex formation.

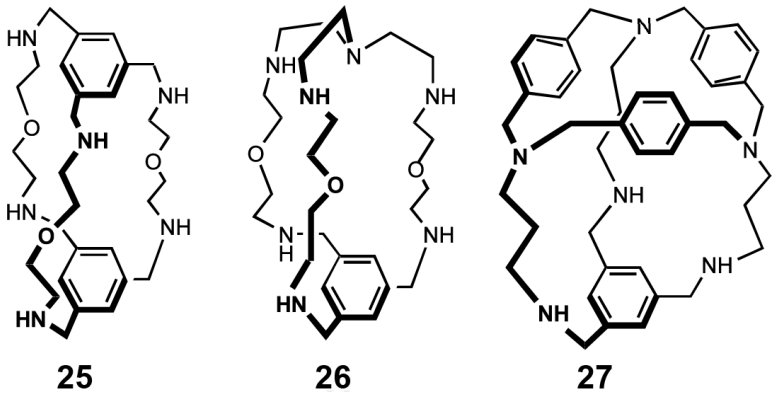

25 **26** **27**

Fig. 1.18

A more complex polycyclic azaparacyclophane, an extension of the concept behind **27**, is **28** (Fig 1.19). Called Kyuphane, this receptor has six faces and is soluble in aqueous media below pH 4 [42]. Kyuphane displays a pH dependent binding capability as well as size and shape selectivity. The polycyclic **28** binds anionic fluorescent molecules such as 1-anilinonaphthalene-8-sulfonate (ANS) at pH 4, in the tetraprotonated state.

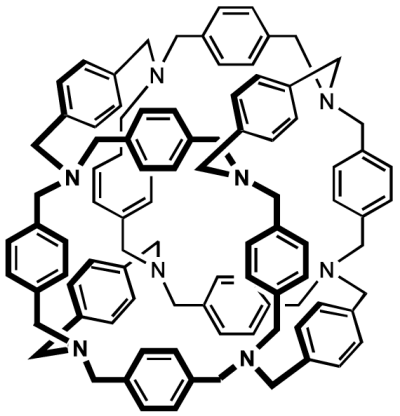

28

Fig. 1.19

References

[1] F. Takusagawa, T.F. Koetzle, *Acta Crystallogr. Sect. B* 35 (**1979**) 867

[2] N.H. Woo, N.C. Seeman, A. Rich, *Biopolymers* 18 (**1979**) 539.]

[3] M.E. Huston, E.U. Akkaya, A.W. Czarnik, *J. Am. Chem. Soc*.40 (**1989**) 8735.

[4] M.T. Albelda, M.A. Bernardo, E. Garcìa-España, M.L. Godino-Salido, S.V. Luis, M.J. Melo, F. Pina, C. Soriano, *J. Chem. Soc. Perkin Trans*. 2 (**1999**) 2545.

[5] M.A. Bernardo, J.A. Guerrero, E. Garcìa-España, S.V. Luis,J.M. Llinares, F. Pina, J.A. Ramı´rez, C. Soriano, *J. Chem. Soc. Perkin Trans*. 2 (**1996**) 2335].

[6] J. Cullinane, R.I. Gelb, T.N. Margulis, L.J. Zompa, *J. Am.Chem. Soc*. 104 (**1982**) 3048.

[7] G. Papoyan, K. Gu, J. Wiórkiewicz-Kuczera, K. Kuczera, K. Bowman-James, *J. Am. Chem. Soc.* 118 (**1996**) 1354.

[8] S. Boudon, A. Decian, J. Fischer, M.W. Hosseini, J.-M. Lehn, G. Wipff, *J. Coord. Chem*. 23 (**1991**) 113.

[9] J. Wiórkiewicz-Kuczera, K. Kuczera, C. Bazzicalupi, A. Bencini, B. Valtancoli, A. Bianchi, K. Bowman-James, *New J. Chem*. 23 (**1999**) 1007.

[10] D. Chen, A.E. Martell, *Tetrahedron* 47 (**1991**) 6895.

[11] T. Clifford, A. Danby, J.M. Llinares, S. Mason, N.W. Alcock, D. Powell, J.A. Aguilar, E. Garcìa-España, K. Bowman-James, *Inorg. Chem*. 40 (**2001**) 4710.

[12] D.A. Nation, J. Reibenspies, A.E. Martell, *Inorg. Chem.* 35 (**1996**) 4597.

[13] J.A. Aguilar, T. Clifford, A. Danby, J.M. Llinares, S. Mason, E. Garcìa-España, K. Bowman-James, *Supramol. Chem*. 13 (**2001**) 405.

[14] B. Dietrich, M.W. Hosseini, J.M. Lehn, R.B. Sessions, *J. Am. Chem. Soc.* 103 (**1981**) 1282.

[15] E. Kimura, A. Sakonaka, T. Yatsunami, M. Kodama, *J. Am. Chem. Soc.* 103 (**1981**) 3041.

[16] A. Bencini, A. Bianchi, M.I. Burguete, P. Dapporto, A. Dome´nech, E. Garcìa-España, S.V. Luis, P. Paoli, J.A. Ramirez, *J. Chem. Soc. Perkin Trans*. 2 (**1994**) 569.

[17] E. Kimura, Y. Kuramoto, T. Koike, H. Fujioka, M. Kodama, *J. Org. Chem.* 55 (**1990**) 42.

[18] M.W. Hosseini, J.M. Lehn, *Helv. Chim. Acta* 69 (**1986**) 587.

[19] A. Bianchi, M. Micheloni, P. Paoletti, *Pure Appl. Chem*. 60 (**1988**) 17.

[20] A. Bencini, A. Bianchi, P. Dapporto, E. Garcìa-España, M. Micheloni, J.A. Ramirez, P. Paoletti, P. Paoli, *Inorg. Chem.* 31 (**1992**) 1902.

[21] A. Bencini, A. Bianchi, P. Dapporto, E. Garcìa-España, M. Micheloni, P. Paoletti, P. Paoli, *J. Chem. Soc. Chem. Commun*. (**1990**) 753.

[22] A. Bianchi, E. Garcìa-España, S. Mangani, M. Micheloni, P. Orioli, P. Paoletti, *J. Chem. Soc. Chem. Commun.* (**1987**) 729.

[23] B. Dietrich, J.-M. Lehn, J.P. Sauvage, *Tetrahedron Lett*. 34 (**1969**) 2889.

[24] C. H. Park and H. E. Simmonds, *J. Am.Chem.Soc*., **1968**, *90*, 2428.

[25] J.-M. Lehn, E. Sonveaux, A.K. Willard, *J. Am. Chem. Soc.* 100 (**1978**) 4914.

[26] B. Dietrich, J. Guilhem, J.-M. Lehn, C. Pascard, E. Sonveaux, *Helv. Chim. Acta* 67 (**1984**) 91.

[27] S. Mason, T. Clifford, L. Seib, K. Kuczera, K. Bowman-James, *J. Am. Chem. Soc.* 120 (**1998**) 8899.

[28] N. Alcock, K. Bowman-James, submitted to Cambridge Data Base.

[29] G. Morgan, V. McKee, J. Nelson, *J. Chem. Soc. Chem. Commun.* (**1995**) 1649.

[30] B.M. Maubert, J. Nelson, V. McKee, R.M. Town, I. Pál, *J. Chem. Soc. Dalton Trans.* (**2001**) 1395.

[31] M.J. Hynes, B. Maubert, V. McKee, R.M. Town, J. Nelson, *J. Chem. Soc. Dalton Trans.* (**2000**) 2853.

[32] J.-M. Lehn, R. Méric, J.-P. Vigneeron, I. Bkouche-Waksman, C. Pascard, *J. Chem. Soc. Chem. Commun.* (**1991**) 62.

[33] E. Graf, J.-M. Lehn, *J. Am. Chem. Soc.* 97 (**1975**) 5022.

[34] J. M. Lehn, *Angew. Chem., Int. Ed. Engl*., **1988**, *27*, 89 and references therein.

[35] B. Owenson, R.D. MacElkro, A. Pohorille, *J. Am. Chem. Soc.* 110 (**1988**) 6992.

[36] K. Worm, F.P. Schmidtchen, *Angew. Chem. Int. Ed. Engl*. 34 (**1995**) 65. and references therein.

[37] F.P. Schmidtchen, *J. Org. Chem.* 51 (**1986**) 5161.

[38] F.P. Schmidtchen, *J. Am. Chem. Soc.* 108 (**1986**) 8249.

[39] F.P. Schmidtchen, *Tetrahedron Lett.* 27 (**1986**) 1987.

[40] D. Heyer, J.-M. Lehn, *Tetrahedron Lett.* 27 (**1986**) 5869.

[41] T. Fujita, J.-M. Lehn, *Tetrahedron Lett.* 29 (**1988**) 1709.

[42] Y. Murakami, J. Kikuchi, T. Ohno, T. Hirayama, Y. Hisaeda, H. Nishimura, J. Snyder, K.J. Steliou, *J. Am. Chem. Soc.* 113 (**1991**) 8229.

2. Abiotic guanidinium containing receptors for anionic species

The guanidinium is a functional group suitable to be introduced molecules in synthetic host molecules designed for the binding of anionic guest. This moiety forms strong non-covalent interactions with anionic groups such as carboxylates, phosphates, sulfates and nitrates through hydrogen bonding and charge pairing interactions. This phenomenon is often present in biological systems, where guanidinium groups, in the form of the side chain of the amino acid arginine, are vital components of enzymatic catalytic domains that participate in the binding of anionic substrates [1,2].

2.1. A bicyclic scaffold containing a guanidinium group

The most prevalent scaffold into which the guanidinium group has been included involves a bicyclic system, as seen in **1** (Fig. 2.1). The geometry of this structure is beneficial for the formation of discrete complexes, as the guanidinium group is constrained such that only one face contains protons available for hydrogen bonding, and thus is accessible for complexation. The synthesis of this bicyclic system was reported by McKay and Kresling in 1957 [3], and then augmented by Schmidtchen for the purpose of developing receptors [4].

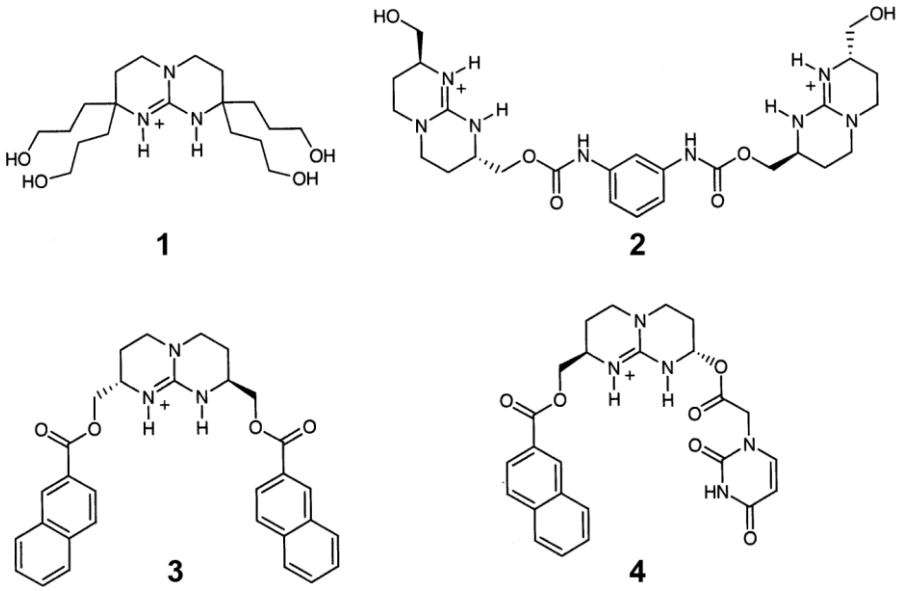

Fig. 2.1

Compound **2** (Fig. 2.1) consists of two bicyclic guanidiniums attached via a urethane linke. ^{1}H-NMR binding studies with dicarboxylates and biologically relevant phosphates pointed to the utility of this compound as a ditopic binder of anionic guests [5].

The host was found to extract dicarboxylate guests from the aqueous phase into chloroform. Receptor **3**, which containis naphthoyl substituents, was reported by de Mendoza and co-workers [6a]. Receptor **4** (Fig. 2.1) include a nucleotide derivative [6b].

A 1:1 complex with p-nitrobenzoate was determined for this structure using ^{1}H-NMR titrations, as well as the extraction of the guest from aqueous to organic media. Interestingly, in this case, slight diastereomeric excesses were observed in the extraction of racemic salts, such as mandelate, naproxenate and tryptophan. This selectivity was ascribed to a three-point binding interaction between the host and guest

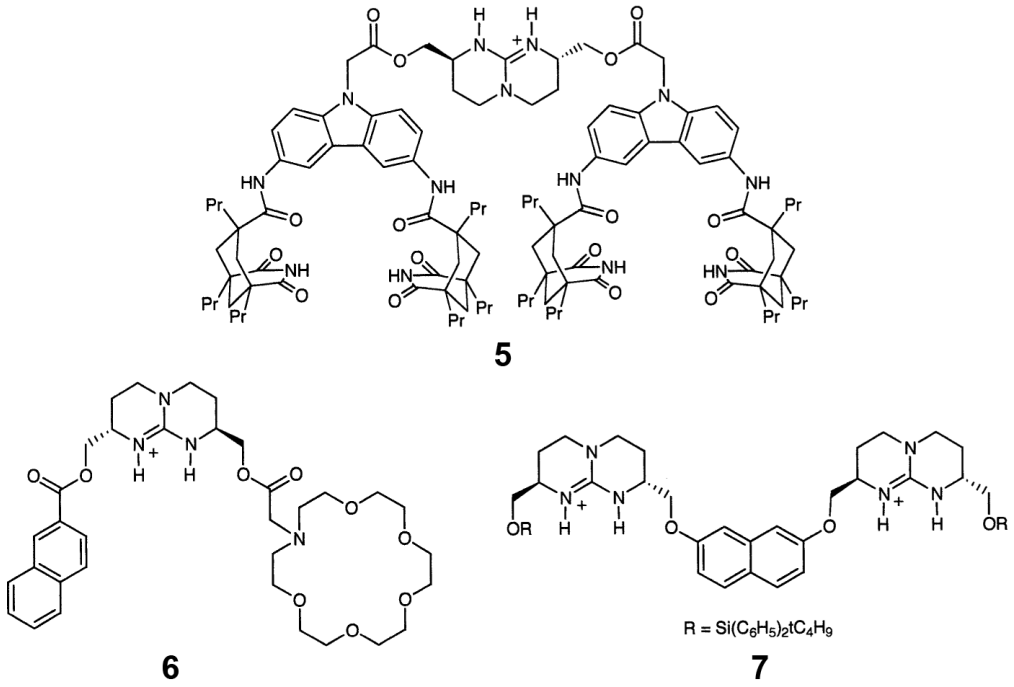

Fig. 2.2

Further development of the bicyclic guanidinium was performed through the attachment of a lipophilic substituent derived from Kemp's triacid which is attached to the core through a 3,6-diaminocarbazole linker (**5**) (Fig. 2.2) [7]. This compound was found to complex dideoxyadenine dinucleotide.

Another functionalization which yielded a receptor based on the bicyclic guanidinium core involved the introduction of one naphthalene ring as well as a crown ether into the system [8]. This structure (**6**) (Fig. 2.2) was designed to bind amino acids guests through interactions between the ammonium group and the host crown, the guest carboxylate with the host guanidinium group and p-stacking interactions between the aromatic groups. Selectivity in the binding of amino acids with aromatic sidechains (phenylalanine and tryptophan) over those with aliphatic chains provided evidence of associations involving the aromatic moieties.

Receptor **7** (Fig. 2.2), which contains two bicyclic guanidiniums linked by a naphthalene spacer, is another example based on this system [9]. This compound was found to bind a variety of nucleotides in methanol and water.

The next advancement on this host scaffold was the introduction of a closo-borane substituent to a structure with two linked guanidinium groups (**8**) (Fig. 2.3) [10]. This alteration was made in an attempt to develop a bicyclic guanidinium host which had an overall neutral charge, but retained hydrophobic character.

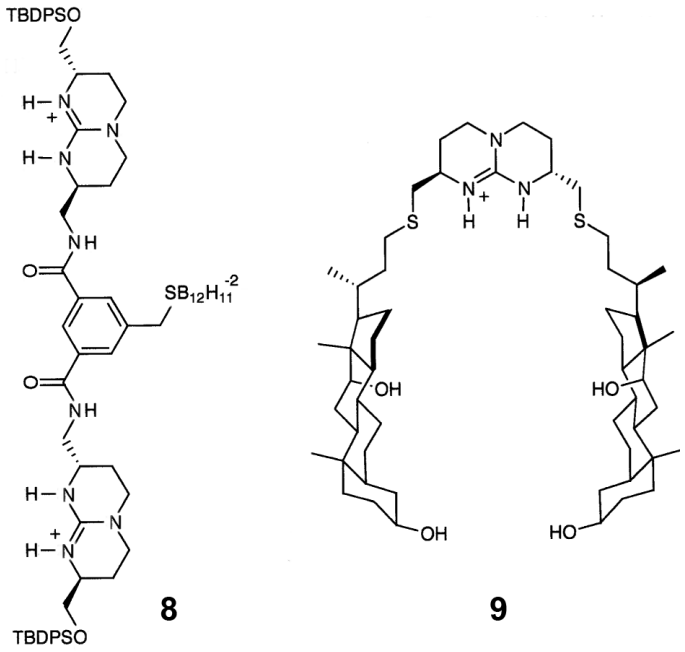

Fig. 2.3

In another example involving this scaffold with appended guanidinium groups, modified deoxycholicacid arms were appended to the core (**9**) (Fig. 2.3) to bind uronicacid guests [11].

Further development of the bicyclic scaffold led to its inclusion within a macrocyclic system [12].

Then, receptor **10** (Fig. 2.4) was designed and synthesized in which multiple functional groups capable of forming hydrogen bonds to anionic guest molecules are constrained within the macrocycle such that they point towards the interior.

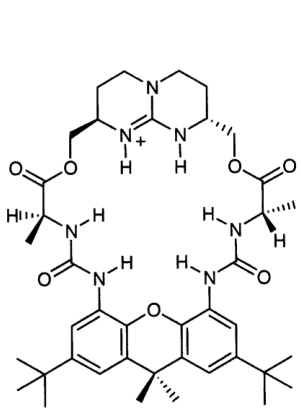

10

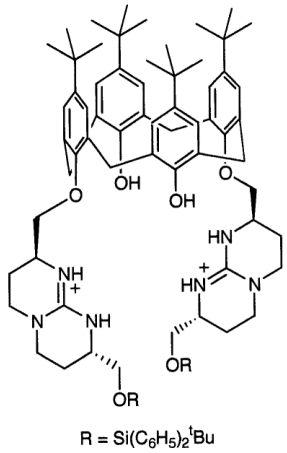

11

Fig. 2.4

Finally, an example of the attachment of bicyclic guanidiniums to calix[4]arene was recently reported [13]. Here, receptor **11** (Fig. 2.4) and the corresponding monoguanidinium were found to enantioselectively extract amino acids into organic solvent. Results obtained indicated selectivity for both the binding and extraction of the L isomers, and up to 90% for phenylalanine.

Another series of compounds with preorganized guanidinium groups involves a variety of cyclic spacers linking two of these functional groups. In these cases, rigid spacers with defined geometries are generally implemented to preorganize the guanidinium moieties and thus provide the orientation for guest binding purposes. This was first exemplified in 1978 when Lehn and co-workers reported the incorporation of guanidinium groups into macrocycles **12**, **13**, and **14** (Fig. 2.5) [14].

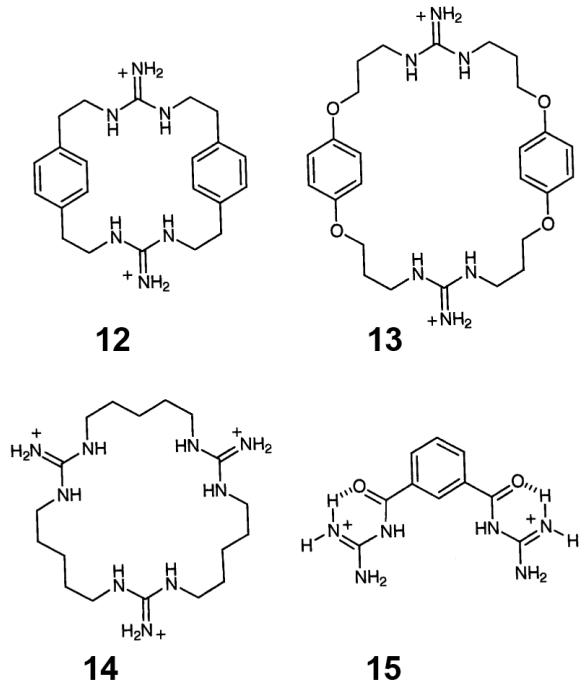

Fig. 2.5

Later, Hamilton and co-workers [15] reported bisguanidiniumcontaining host **15** (Fig. 2.5) which they synthesized for the purpose of binding phosphodiester guests. The isophthaloyl spacer was used to situate the guanidinium groups in a suitable geometry to bind the trigonalbipyramidal guests.

Two tetraguanidines were developed, **16(a)** and **16(b)** (Fig. 2.6), for the purpose of binding DNA [16]. The multilayered structure of these compounds makes them suitable for binding into the minor grooves of double stranded DNA. Furthermore, sequence specificity for the 3'-GAA-5' region was determined for the two structures. In addition, the incorporation of guanidinium group into RNA has recently been reported [17]. In these RNA analogs, the phosphodiester linkages in the backbone have been replaced by guanidinium groups to form polycationic strands. The goal of this work is to obtain receptors with increased affinity towards DNA and RNA by increasing electrostatic interactions upon complexation.

Another example of the appending of guanidinium groups to biological compounds is the development of guanidinoglycosides by Tor and co-workers [18].

Here, guanidinium groups were formed on saccharide scaffolds such as tobramycin, in this case generating **17** (Fig. 2.6). This was performed in an effort to increase affinity for RNA over the parent aminoglycosides through the introduction of guanidinium functionalities.

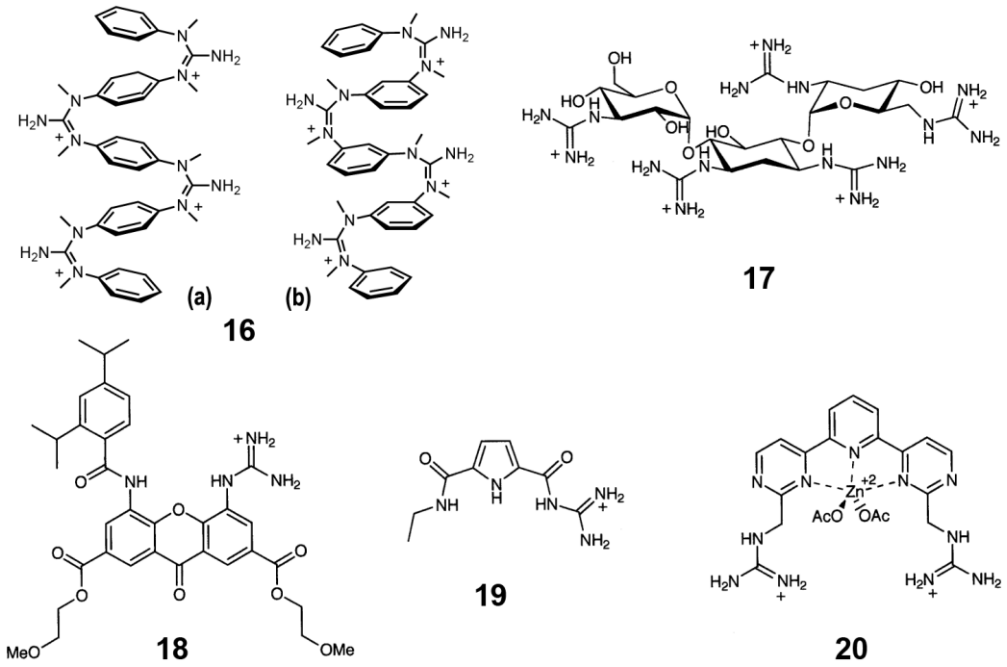

Fig. 2.6

Attachment of a guanidinium groups to xanthone led to the development of receptor **18** (Fig. 2.6) [19]. In this structure, extra interaction sites are built in: the xanthone NH hydrogen bond donor and the diisopropylbenzoate for stacking. Here, data in the analysis of certain carboxylates indicated a proton transfer from the host rather than a binding event. As a result, a series of acids with varying acidities were tested for binding affinity.

In another effort to increase the number of binding sites adjacent to a guanidinium groups, linkage to pyrrole was performed (**19**) (Fig. 2.6) [20]. This design was intended to utilize the pyrrole NH to facilitate the binding of N-acetyl amino acids.

Host compound **20** (Fig. 2.6) was developed which utilizes a 2,2': 6,2" terpyridine-type ligand complexing zinc [21]. This receptor was designed to

bind aspartate and glutamate through three-point interactions in the host-guest complex.

2.2. Guanidinium groups incorporated into the triethylbenzene scaffold.

The triethylbenzene substructure is another molecular design in which guanidinium functionalities have been exploited in the development of host molecules. The utility of this platform has been recently reviewed [22].

In 1997, Anslyn and co-workers [23] reported **21** (Fig. 2.7), based on the threefold substitution of the triethylbenzene scaffold with aminodihydroimidazolium groups. The target guest for this receptor was citrate as the geometrical orientation of the three guanidinium groups complemented the tris-carboxylate containing guest species.

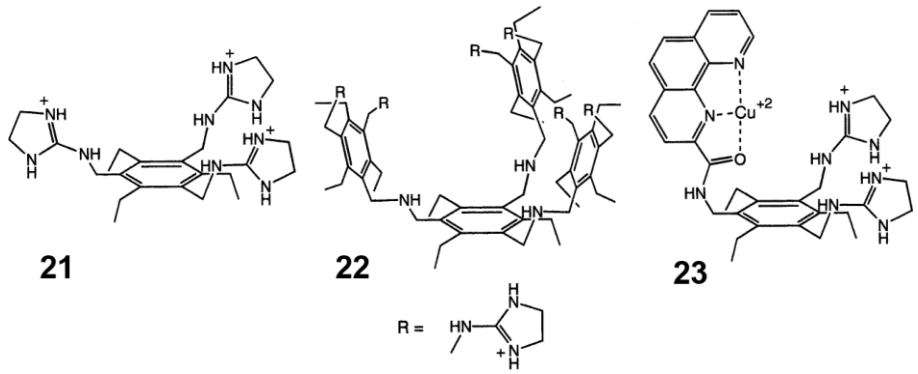

Fig. 2.7

Another receptor based on the triethylbenzene scaffold is compound **22** (Fig. 2.7) [24]. This structure was designed to bind the polyanionic secondary messenger inositol triphosphate (IP3) as it contains six guanidinium groups in such a geometry as they are oriented towards the inside of the cavity.

The next receptor of this type reported (**23**) (Fig. 2.7) included two aminoimidazolium groups and a phenanthroline-copper complex [25]. In this case, the metal complex was introduced both as an extra binding site for the citrate guest and to allow for the signaling of binding. Introduction of the metal to the phenanthroline led to the quenching of the ligand fluorescent signal. The binding of citrate could then be observed due to the reemergence of this signal upon binding of the guest to the metal center.

A different approach to obtaining a receptor of this type involved the formation of a library of compounds based on a rationally designed core [26].

The goal of these studies was to develop a sensor for ATP. The designed core of this structure consisted of a resin-bound triethylbenzene scaffold with two guanidinium groups. A combinatorial library was then obtained by growing peptide arms off the guanidinium groups. Finally, fluorophores were added to the peptide arms and to a lysine linker for detection purposes. The resulting library was screened fluorometrically for ATP binding through inspection using UV light to obtain potential hosts. These were then sequenced and resynthesized. In the final analysis, receptor **24** (Fig. 2.8) with Ser-Tyr-Ser residues on the peptide arms showed selectivity for ATP over AMP and GTP.

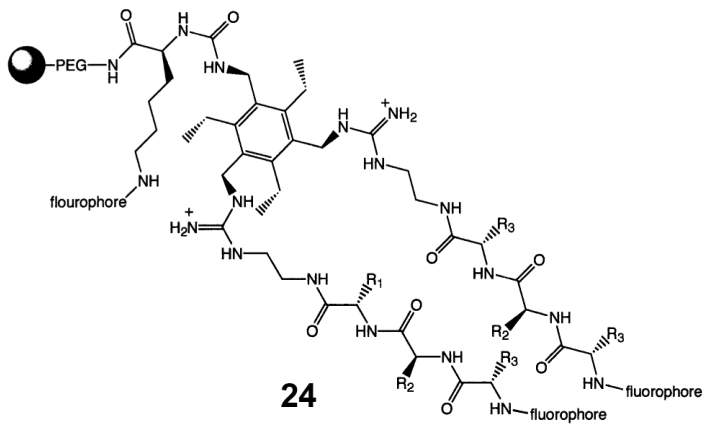

24

Fig. 2.8

2.3. Receptors with covalently attached signalling groups

Another series of guanidinium containing receptors reported have featured the covalent attachment of this binding unit to known signalling devices. In 1996, de Silva et al. [27] reported a receptor of this type, **25** (Fig. 2.30), with azacrown, anthracene and guanidinium groups linked in series.

This host was designed to complex g-aminobutyric acid (GABA) through interactions between the host guanidinium group and guest carboxylate as well as the host azacrown and the guest ammonium.

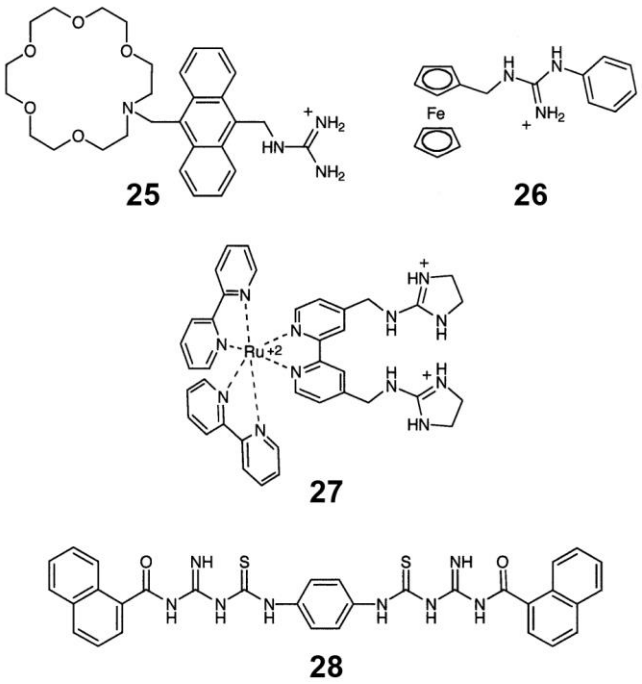

Fig 2.9

The anthracene moiety was included so that binding of the guest by the azacrown amine disrupted photoinduced electron transfer (PET) quenching of the anthracene fluorescence. As was expected, binding of the guest was detected by an increase in fluorescence. A control compound lacking the guanidinium group showed no fluorescence change in the presence of GABA, while glutamic acid, the physiological precursor to GABA also had no detectable effect.

Another example of this concept was published by Beer et al. [28], compound **26** (Fig. 2.9), which consists of a guanidinium group linked to a ferrocene unit.

This host bound inorganic phosphate guest through hydrogen bonding to the guanidinium group. Upon complexation, the redox signal of the ferrocene was affected as oxidation of the group was facilitated by the introduction binding of the guest could be detected through redox analysis.

Next, compound **27** (Fig. 2.9) was established as a luminescent sensor for phosphate and phosphodiester guests [29]. Here, two neutral acylaminoimidazoline groups were linked to bipyridine, which then became one unit of a tris-bipyridine ruthenium(II) complex. Binding was detected by alteration of both the absorbance and fluorescent signals of the host, with a large fluorescence change potentially caused by rigidification of the complex.

Compound **28** (Fig. 2.9), which contains two iminoylthioureas, and the corresponding compound with 1,2,4-thiadiazoles have been reported [30].

Binding of carbonate, bicarbonate and hydrogen phosphate was achieved with these hosts. Fluorescence enhancements and spectral shifts occur.

References

[1] D.W. Christianson, W.N. Lipscomb, *Acc. Chem. Res.* 22 (**1989**) 62.

[2] F.A. Cotton, E.E. Hazen, Jr., M.J. Legg, Proc. Natl. Acad. Sci. 76 (**1979**) 2551.

[3] A.F. McKay, M.E. Kreling, *Can. J. Chem.* 35 (**1957**) 1438.

[4] F.P. Schmidtchen, *Chem. Ber.* 113 (**1980**) 2175.

[5] F.P. Schmidtchen, *Tetrahedron Lett.* 30 (**1989**) 4493.

[6] a) A. Echavarren, A. Galàn, J.-M. Lehn, J. de Mendoza, *J. Am. Chem. Soc.* 111 (**1989**) 4994. b) A. Galàn, E. Pueyo, A. Salmerdzón, J. de Mendoza, *Tetrahedron Lett.* 15 (**1991**) 1827.

[7] A. Galàn, J. de Mendoza, C.M. Bruix, G. Deslongchamps, J. Rebek, Jr., *J. Am. Chem. Soc.* 113 (**1991**) 9421.

[8] A. Galàn, D. Andreu, A.M. Echavarren, P. Padros, J. De Mendoza, *J. Am. Chem. Soc.* 114 (**1992**) 1511

[9] P. Schliessl, F.P. Schmidtchen, *J. Org. Chem.* 59 (**1994**) 509.

[10] M. Berger, F.P. Schmidtchen, *J. Am. Chem. Soc.* 118 (**1996**) 8947.

[11] M. Segura, V. Alcázar, P. Padros, J. de Mendoza, *Tetrahedron* 53 (**1997**) 13119.

[12] V. Alcázar, M. Segura, P. Prados, J. de Mendoza, *Tetrahedron Lett.* 39 (**1998**) 1033

[13] L. Fang, G.-Y. Lu, W.-J. He, Z.-S. Wang, L.-G. Zhu, Chin. *J. Chem. Soc.* 19 (**2001**) 317.

[14] B. Dietrich, T.M. Flyes, J.-M. Lehn, L.G. Pease, D.L. Fyles, *J. Chem. Soc. Chem. Commun.* (**1978**) 934.

[15] R.P. Dixon, S.J. Geib, A.D. Hamilton, *J. Am. Chem. Soc.* 114 (**1992**) 365.

[16] R. Fukutomi, A. Tanatani, H. Kakuta, N. Tomioka, A. Itai, Y. Hashimoto, K. Shudo, H. Kagechika, *Tetrahedron Lett.* 39 (**1998**) 6475.

[17] (a) D.A. Barawkar, B. Linkletter, T.C. Bruice, Bioorg. *Med. Chem. Lett.* 8 (**1998**) 1517; (b) N. Kojima, I.E. Szabo, T.C. Bruice, *Tetrahedron* 58 (**2002**) 867.

[18] N.W. Luedtke, T.J. Baker, M. Goodman, Y. Tor, *J. Am. Chem. Soc.* 122 (**2000**) 12035.

[19] M. Martín, M. Almaraz, J. Hernández, A. Tejeda, M.C. Caballero, J.R. Morán, *Heterocycles* 50 (**1999**) 47.

[20] C. Schmuck, *Chem. Commun.* (**1999**) 843.

[21] H. Aït-Haddou, S.L. Wiskur, V.M. Lynch, E.V. Anslyn, *J. Am. Chem. Soc.* 123 (**2001**) 11296.

[22] G. Hennrich, E.V. Anslyn, *Chem.-Eur. J.* 8 (**2002**) 2119.

[23] A. Metzger, V.M. Lynch, E.V. Anslyn, *Angew. Chem. Int. Ed. Engl.* 36 (**1997**) 862.

[24] K. Niikura, A. Metzger, E.V. Anslyn, *J. Am. Chem. Soc.* 120 (**1998**) 8533.

[25] L.A. Cabell, M.D. Best, J.J. Lavigne, S.E. Schneider, D.M. Perreault, M.-K. Monahan, E.V. Anslyn, *J. Chem. Soc. Perkin Trans*. 2 (**2001**) 315.

[26] S.E. Schneider, S.N. O'Neil, E.V. Anslyn, *J. Am. Chem. Soc.* 122 (**2000**) 542.

[27] A.P. de Silva, H.Q.N. Gunaratne, C. McVeigh, G.E.M. Maguire, P.R.S. Maxwell, E. O'Hanlon, *Chem. Commun.* (**1996**) 2191.

[28] P.D. Beer, M.G.B. Drew, D.K. Smith, *J. Organomet. Chem.* 543 (**1997**) 259.

[29] S. Watanabe, O. Onogawa, Y. Komatsu, K. Yoshida, *J. Am. Chem. Soc.* 120 (**1998**) 229.

[30] G. Hennrich, H. Sonnenschein, U. Resch-Genger, *Tetrahedron Lett.* 42 (**2001**) 2805.

3. Imidazolium receptors for the recognition of anions

Various positively charged imidazolium derivatives have been synthesized and studied as selective anion-receptors. Imidazolium group can make a strong interaction with anions through $(C–H)^{+\cdots}X^-$ type ionic hydrogen bond because the charge–charge electrostatic interaction dominates.[1]

This type of interaction could also be envisaged in the crystal structure of imidazolium based ionic liquids [2a, 2b] and calix-[4]-pyrrole complexing with imidazolium salts.[2c]

In the following, imidazolium based receptors will be grouped according to their topological and structural classification, which includes:

1) benzene tripodal;

2) cyclophane and calix-[n]-imidazolium;

3) cavitand and calixarene;

4) fluorescent imidazolium;

5) ferrocenyl imidazolium.

3.1. Benzene tripodal systems

A benzene based tripodal receptor with three imidazolium groups **1** was reported by Sato et al.[3] . The host **1** displayed a selective binding with Cl^- over Br^- and I^- in acetonitrile, which was confirmed via ^1H NMR titration experiments.[3] Kim and coworkers clarified that this tricationic heterocycle interacts strongly with anions through $(C–H)^{+\cdots}X^-$ type ionic hydrogen bond between the hydrogen on the electron-deficient C(2) carbon atom of the imidazolium ring and the guest anion, and shows a selective binding for F^- over other halide anions. For better anion binding affinity, the benzene based tripodal receptor was theoretically modified and experimentally realized [1] as tripodal nitro-imidazolium receptor **2.**

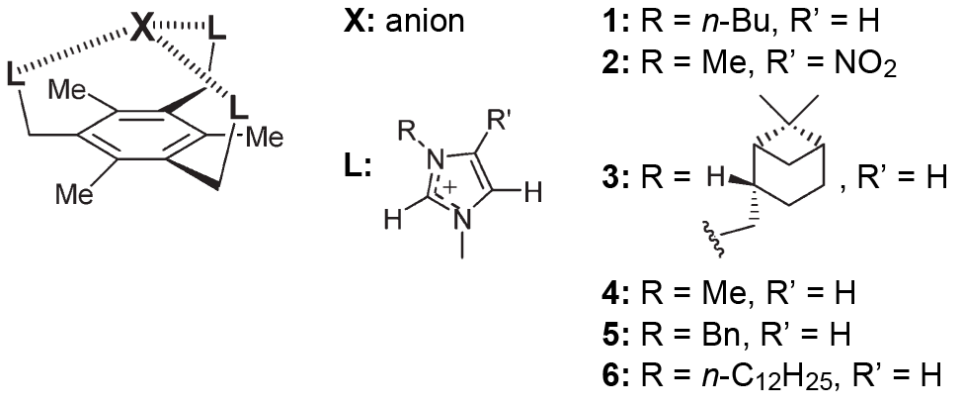

Fig. 3.1 - Benzene tripodal systems

The homochiral tripodal imidazolium system **3** was reported by Howarth et al. [4]. This chiral tripodal system could distinguish between sodium (R)-2-aminopropionate and sodium (S)-2-aminopropionate From the ^{1}H NMR experiments, it has been shown that the imidazolium salt forms a complex with the (R) enantiomer but not with the (S) enantiomer.

3.2. cyclophane and calix-[n]-imidazolium

It has been. recently reported similar benzene tripodal systems (**4**, **5** and **6**) (Fig. 3.1) and bis imidazolium (**7**) [5] (Fig. 3.2)

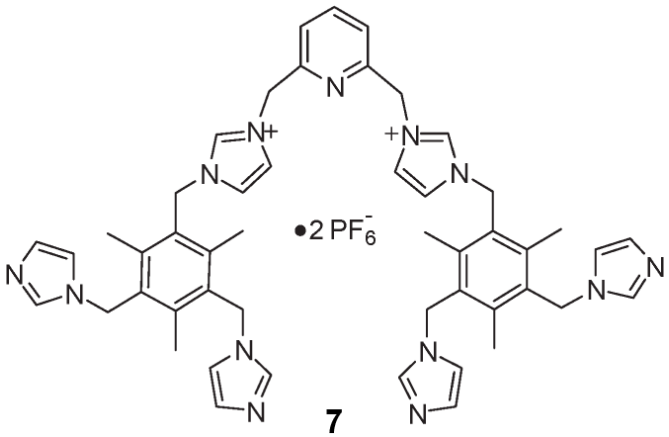

Fig. 3.2 - Bis-imidazolium receptor **7**

Cyclophane and calix-imidazolium systems Alcalde et al. reported cyclophane type receptors as shown in Fig. 3.3 (**8a** and **8b**).[6]

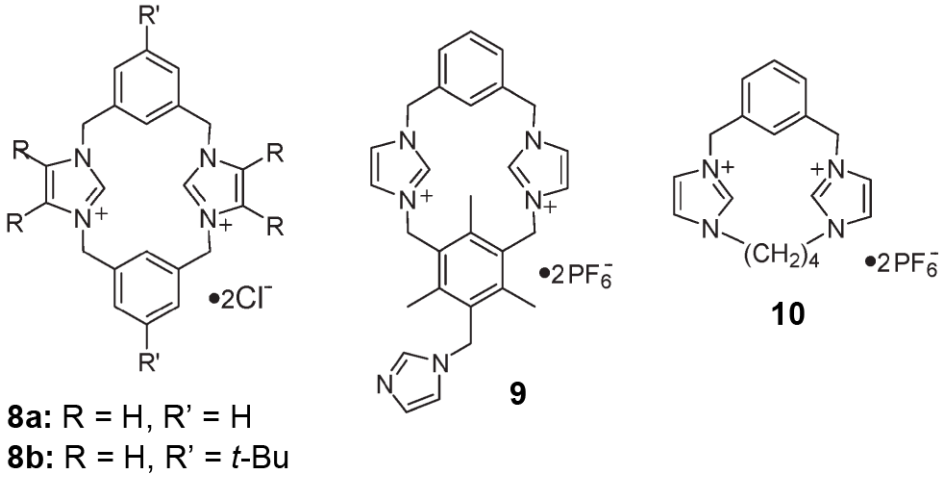

Fig. 3.3 - Structures of cyclophane-type imidazolium receptors **8, 9** and **10**.

Interestingly, in the X-ray crystal structure of **8a**·$2Cl^-$·$2H_2O$, the dication **8a** adopts a chair-like conformation.

On the other hand, the molecular shape of dication **8b** in **8b**·$2Cl^-$ $3.5H_2O$ assumes a cone-like conformation, but both cations **8a** and **8b** have similar molecular cavity dimensions: a square of 5 Å side. The deshielding effects of C(2)–H (in imidazolium rings) were reported to be in the order of $H_2PO_4^-$ > F^-> CH_3COO^- > CN^- > Cl^-.

A tetracationic heterophane (**11**) (Fig. 3.4) has been reported, which forms a 1:1 inclusion complex with halides and oxoanions in DMSO-d_6.[7]

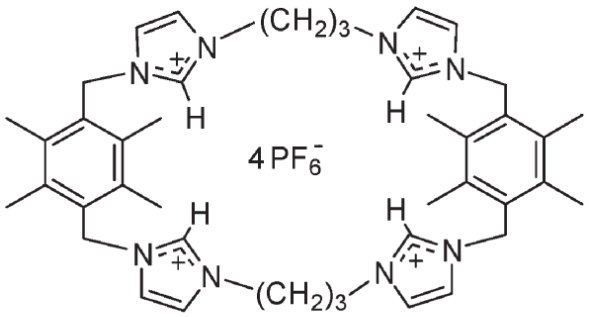

11

Fig. 3.4 - Structures of cyclophane-type imidazolium receptor **11**.

From the ^{1}H NMR titration experiments, the binding affinity of this receptor was reported to be in the order HSO_4^- > Br^- > $H_2PO_4^-$ > Cl^- > I^- > ClO_4^-, which was explained based on the size of anions.

A novel calix[4]imidazolium[2]pyridine **(12)** has been reported (Fig. 3.5).[8]

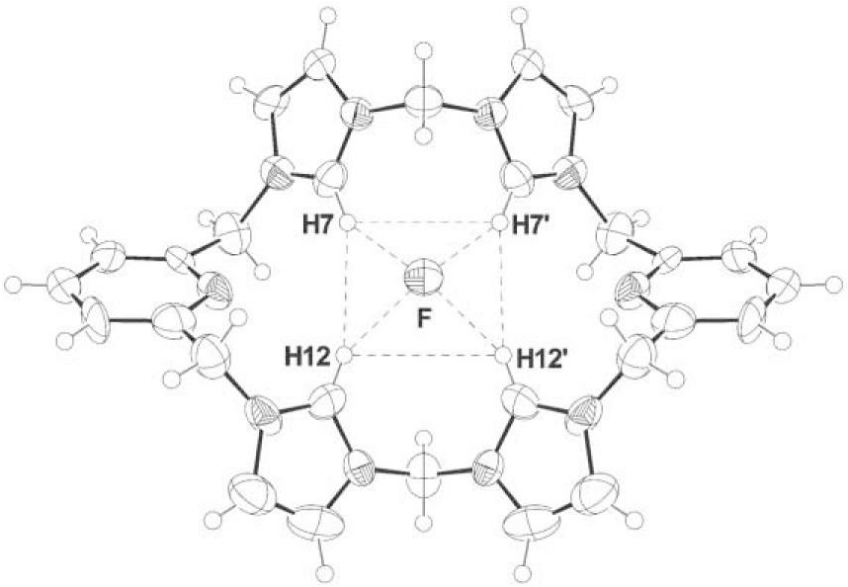

Fig. 3.5 - Crystal structure of calix[4]imidazolium[2]pyridine **12** complexed with anions F^-

Unlike the fluoride anion, the chloride and bromide anions of larger size do not fit in the center of the cavity of **12**, and furthermore these anions favor nonspherical or surface conformations in order to keep the extra electron in a large empty space.[9]

3.3. Cavitand derivative

Recently, reported a new cavitand derivative bearing four imidazolium groups **(12)** as a receptor for anions (Fig. 3.6) has been reported. [10]

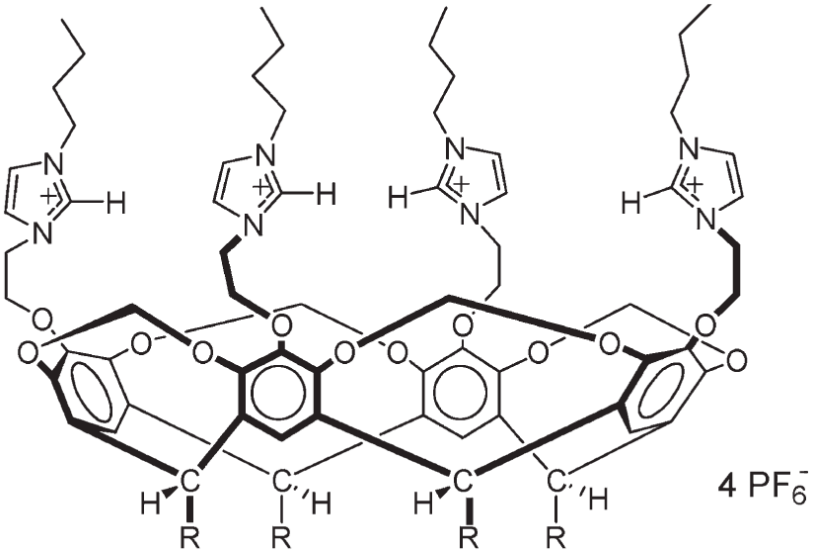

12 , R = CH_2CH_2Ph

Fig 3.6 - Imidazolium receptors based on cavitand (**12**).

The binding properties towards various anions including dicarboxylates were investigated based on the 1H NMR spectroscopic experiments in acetonitrile-d^3. Among the anions examined, cavitand **12** displayed a selective binding with bis(tetrabutylammonium) 1,4-phenylenediacetate.

3.4. Fluorescent imidazolium systems

A few anthracene derivatives bearing imidazolium groups as binding sites have been recently studied.[11]

Two imidazolium moieties were first immobilized on the 1,8-positions of the chemosensor **(13)** (Fig. 3.7), and a unique feature of the binding mode was predicted based on ab initio calculations.[19a] 1,8-Bis-imidazolium anthracene **13** effectively and selectively recognizes the biologically important $H_2PO_4^-$ ion over other anions such as I^-, Br^- and Cl^- in acetonitrile. It has been further demonstrated that the selectivity of these imidazolium receptors against anions can be controlled by the topology of the binding site (e.g. enhancement of rigidity). Compared to host **13**, the greater rigidity in host **14** enhances the binding selectivity for $H_2PO_4^-$ over F^-.[19b]

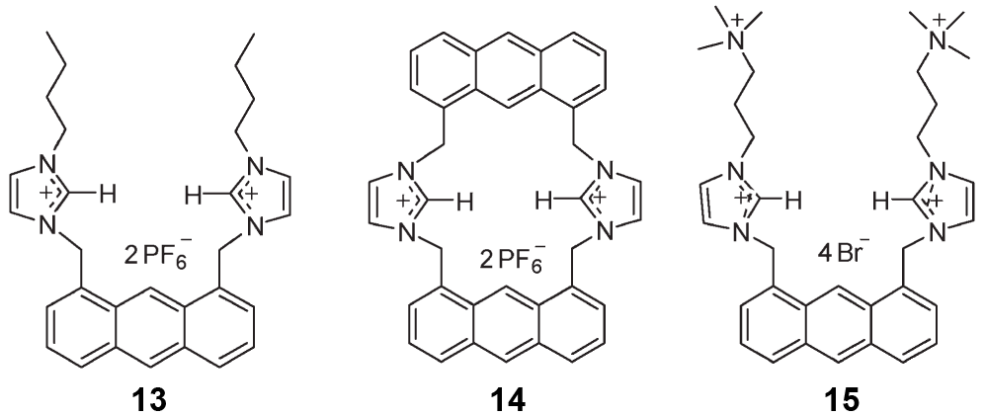

13 **14** **15**

Fig. 3.7 - Anthracene derivatives bearing imidazolium groups

Furthermore it has been reported a novel water-soluble imidazolium anthracene derivative **(15)**, which not only differentiates the structurally similar compounds GTP and ATP but also acts as a potential fluorescent chemosensor for GTP in 100% aqueous solution (pH = 7.4).[19c]

A fluorescent tripodal receptor (**16**) bearing three benzoimidazolium and napthyl groups has been recently synthesized.[12]

This host acts as an ‘‘**off–on**’’ signaling chemical sensor with high selectivity for Cl^- over Br^- and I^- through a guest-induced conformational switching process (Scheme 3.1).

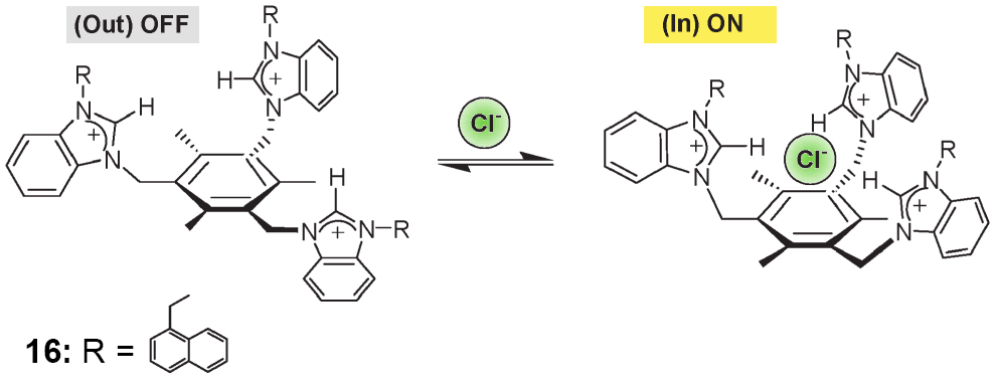

Scheme 3.1 - Conformational switching process of **16** upon the addition of Cl^-

In the presence of Cl^-, the tripodal system adopts a cone conformation, which leads to the excimer fluorescence by bringing the naphthalene groups into close proximity.

It has been also reported a new imidazolium functionalized acyclic ruthenium(II) bipyridyl receptor **(17,18)** (Fig. 3.8).[13]

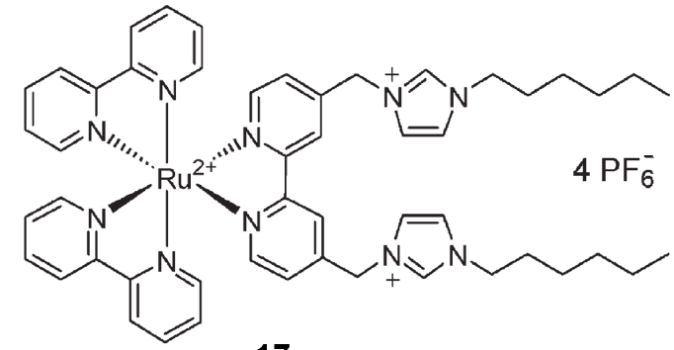

17

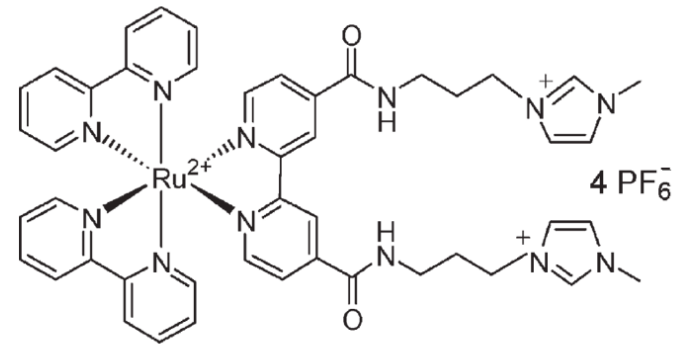

18

Fig. 3.8 - Structures of fluorescent hosts **17** and **18**.

Both receptors displayed a selectivity for Cl^- over the other anions in acetonitrile–water (9: 1, v/v) and **22** sensed ATP in 50:50 acetonitrile–water solvent media.

It has been also reported a naphthalene derivative (**23**) which contains two methylene bridged bis-imidazolium rings (Fig. 3.9).[14a]

The host **19** displayed a selective affinity for I^-, which was confirmed using fluorescence spectroscopy and ^{1}HNMR. They also reported the role of aromatic (C–H)$\cdots$anion interaction on **20** in addition to the imidazolium (C–H)$^+\cdots$anion ionic hydrogen bonding, whose strength was found to be increased with the nitro substitution on the para position.[14b]

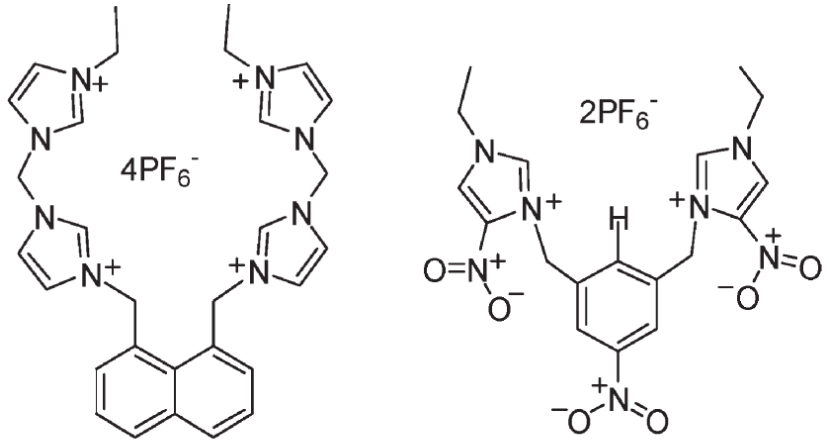

Fig. 3.9 - Structures of hosts **19** and **20**.

A fluorescent cavitand derivative bearing four imidazolium groups as well as four pyrene groups as a fluorescent receptor for **GTP** has been synthesized (Fig. 3.10).[15]

Since host **20** contains pyrene groups, the binding properties towards various anions were investigated based on the fluorescence experiments.

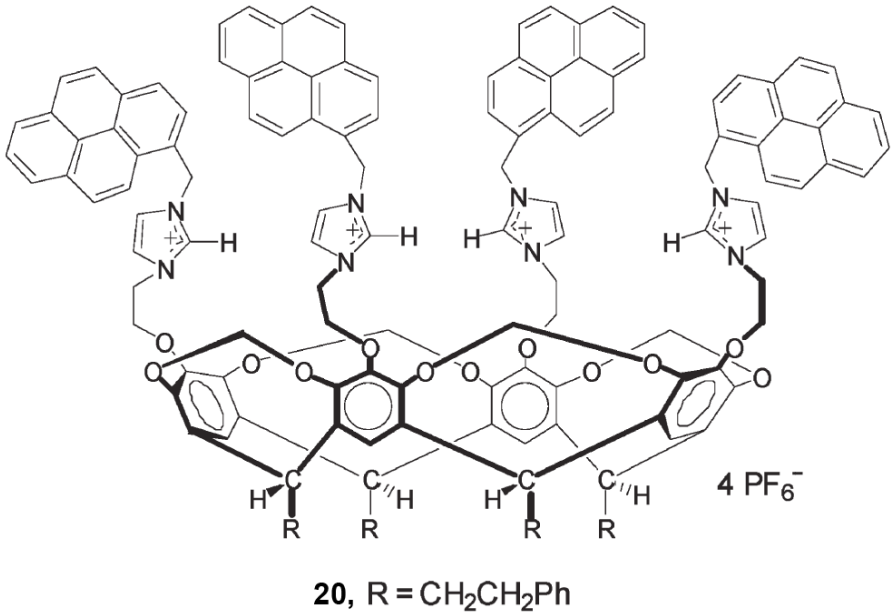

Fig. 3.10 – Imidazolium receptors based on cavitands **25**

3.5. ferrocenyl imidazolium systems

Howarth et al. reported an imidazolium receptor which contains two ferrocene groups **(21)** (Fig. 3.11).[16]

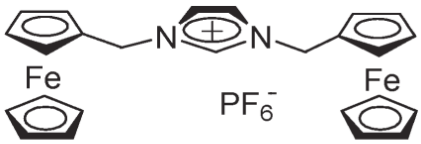

21

Fig. 3.11 - Structures of ferrocenyl imidazolium receptors **21**

This compound adds to a substantial number of artificial organic hosts for anions which incorporate strong hydrogen bonds (H-bonds), usually N-H···X^-,[17] e.g., calixpyrrole, or C-H···X^- H bonding , if the carbon atom is adjacent to a cationic center, e.g., imidazolium.[18] ring and guest anions such as Cl^-, Br^- and I^-.

This novel type of charged hydrogen bonding is very different and intriguing in comparison with many other conventional hydrogen bonds. The role of $(C2\text{-}H)^{+\cdots}$ X^- hydrogen bond during the recognition process is still open to debate [19].

References

[1] H. Ihm, S. Yun, H. G. Kim, J. K. Kim and K. S. Kim, *Org. Lett.*, **2002**, 4, 2897.

[2] (a) J. D. Holbrey, W. M. Reichert, M. Nieuwenhuyzen, S. Johnston, K. R. Seddonb and R. D. Rogers, *Chem. Commun*., **2003**, 1636; (b) J. D. Holbrey, W. M. Reichert and R. D. Rogers, *Dalton Trans*., **2004**, 2267; (c) R. Custelcean, L. H. Delmau, B. A. Moyer, J. L. Sessler, W.-S. Cho, D. Gross, G. W. Bates, S. J. Brooks, M. E. Light and P. A. Gale, *Angew. Chem*., Int. Ed., **2005**, 44, 2537.

[3] K. Sato, S. Arai and T. Yamagishi, *Tetrahedron Lett*., **1999**, 40, 5219.

[4] J. Howarth and N. A. Al-Hashimy, *Tetrahedron Lett*., **2001**, 41, 5777.

[5] Y. Bai, B.-G. Zhang, J. Xu, C.-Y. Duan, D.-B. Dang, D.-J. Liu and Q.-J. Meng, *New J. Chem.*, **2005**, 29,777 .

[6] E. Alcalde, C. Alvarez-Rúa, S. García-Granda, E. García - Rodriguez, N. Mesquida and L. Pérez-García, *Chem. Commun*., **1999**, 295.

[7] K. Sato, T. Onitake, S. Arai and T. Yamagishi, *Heterocycles*, **2003**, 60, 779.

[8] K. Chellappan, N. J. Singh, I.-C. Hwang, J. W. Lee and K. S. Kim, *Angew. Chem*., Int. Ed., **2005**, 44, 2899.

[9] (a) N. J. Singh, A. C. Olleta, A. Kumar, M. Park, H.-B. Yi, I. Bandyopadhyay, H. M. Lee, P. Tarakeshwar and K. S. Kim, *Theor. Chem. Acc*., **2005**, DOI: 10.1007/s00214-005-0057-1; (b) H. M. Lee, D. Kim and K. S. Kim, *J. Chem. Phys*., **2002**, 116, 5509; (c) H.M. Lee and K. S. Kim, *J. Chem. Phys*., **2001**, 114, 4461.

[10] S. K. Kim, B.-G. Kang, H. S. Koh, Y.-J. Yoon, S. J. Jung, B. Jeong, K.-D. Lee and J. Yoon, *Org. Lett*., **2004**, 6, 4655.

[11] (a) S. K. Kim, N. J. Singh, S. J. Kim, H. G. Kim, J. K. Kim, J. W. Lee, K. S. Kim and J. Yoon, *Org. Lett*., **2003**, 5, 2083; (b) J. Yoon, S. K. Kim, N. J. Singh, J. W. Lee, Y. J. Yang, K. Chellappan and K. S. Kim, *J. Org. Chem*., **2004**, 69, 581; (c) J. Y. Kwon, N. J. Singh, H. Kim, S. K. Kim, K. S. Kim and J. Yoon, *J. Am. Chem. Soc*., **2004**, 126, 8892.

[12] Y. Bai, B.-G. Zhang, J. Xu, C.-Y. Duan, D.-B. Dang, D.-J. Liu and Q.-J. Meng, *New J. Chem.*, **2005**, 29, 777.

[13] M. S. Vickers, K. S. Martindale and P. D. Beer, *J. Mater. Chem*., **2005**, 15, 2784.

[14] (a) H. Kim and J. Kang, *Tetrahedron Lett*., **2005**, 46, 5443; (b) S. In, S. J. Cho, K. H. Lee and J. Kang, *Org. Lett*., **2005**, 7, 3993.

[15] S. K. Kim, B.-S. Moon, J. H. Park, Y. I. Seo, H. S. Koh, Y. J. Yoon, K.-D. Lee and J. Yoon, *Tetrahedron Lett*., **2005**, 46, 6617.

[16] (a) J.-L. Thomas, J. Howarth, K. Hanlon and D. McGuirk, *Tetrahedron Lett*., **2000**, 41, 413; (b) J.-L. Thomas, J. Howarth and A. M. Kennedy, *Molecules*, **2002**, 7, 861.

[17] K. A. Nielsen, W.-S. Cho, J. Lyskawa, E. Levillain, V. M. Lynch, J. L. Sessler, J. O. Jeppesen, *J. Am. Chem. Soc*. **2006**, 128, 2444 – 2451;

[18] a) K. Chellappan, N. J. Singh, I.-C. Hwang, J. W. Lee, K. S. Kim, *Angew. Chem*. **2005**, 117, 2959 – 2963; b) K. Chellappan, N. J. Singh, I.-C. Hwang, J. W. Lee, K. S. Kim, *Angew. Chem. Int. Ed*. **2005**, 44, 2899 – 2903; c) N. Alhashimy, D. J. Brougham, J. Howarth, A. Farrell, B. Quilty, K. Nolan, *Tetrahedron Lett*. **2007**, 48, 125– 128.

[19] Zhaochao Xu, Sook Kyung Kim and Juyoung Yoon, *Chem. Soc. Rev*., **2010**, 39, 1457–1466

4. Amide based anion receptors

The anion coordination achieved by amine based anion receptors are here highlighted by halide-H-N amide interections . Halides are the simplest anions in terms of shape and are thus the closest analogue of metal ions. In general, they prefer a four-coordinate, tetrahedral geometry, which is understandable in terms of the four lone pairs in an sp^3-hybridized electronic shell. Indeed, the most common coordination numbers are two, three, and four. However, other coordination numbers up to nine can be cited.

The coordination numbers for most examples of hydrogen-bond coordination of anions begin at two. The bromide complex **1**·Br^- (Fig. 4.1) was characterized by X-ray crystallography, which showed that the bromide is hydrogen bonded in a two-coordinate V-shaped geometry with a *syn,syn* coordination mode and the two amide hydrogen atoms at distances of 2.39 and 2.68 Å from the bromide.[1] The amide groups are out of the phenyl plane, possibly as a result of the large size of the bromide ion.

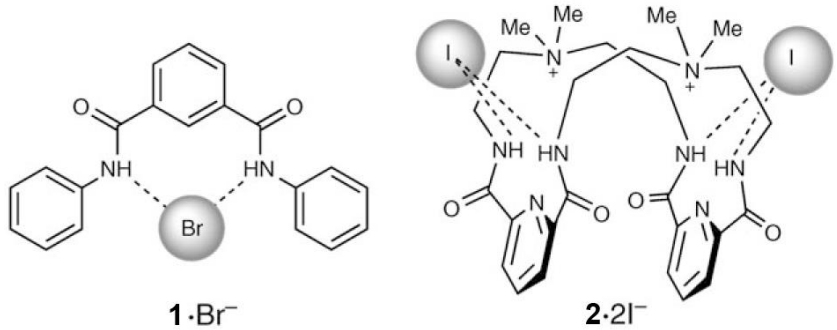

Fig. 4.1

The pyridine nitrogen atom in macrocycle **2** (fig. 4.1) serves to preorganize the two adjacent amide groups for chelation, as illustrated by the two-coordinate V-shaped iodide complex [2].

Smith and co-workers extensively studied dual-host ditopic receptors (for example, receptor **3** in fig. 4.2) for both anions and cations, including halides and alkali-metal ions.[3–6]

The cavity situation in these receptors often leads to a coordination number of two for halides, and the geometry is usually V-shaped. The additional electrostatic binding component provided by an adjacent cation also assists in stabilizing the complex.

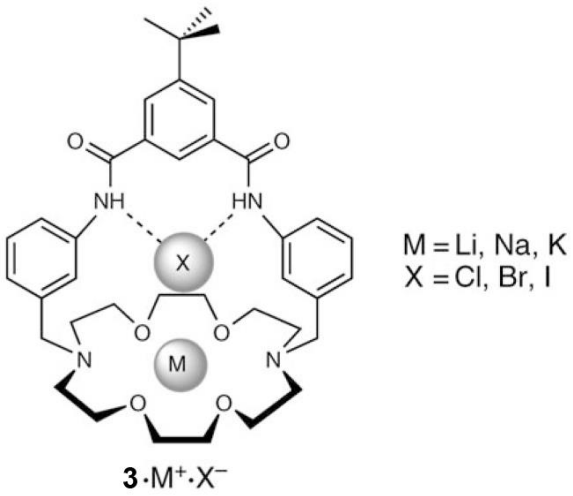

Fig. 4.2

4.1. Coordination Number 3

Coordination number three is often observed with pincer type chelating ligands that contain three available hydrogen bond-donor groups. Diamido-pyrroles are excellent pincer ligands for three-point hydrogen bonding.[7]

For example, in the diamidopyrrole receptor **4** (Fig. 4.3) the chloride ion is bound to the ligand by three hydrogen bonds to the amide and pyrrole hydrogen atoms (**4**·Cl^-).[8]

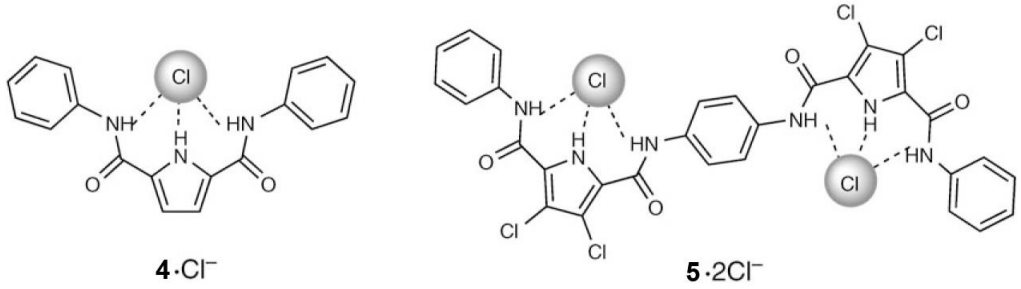

Fig. 4.3

Because of the geometrical placement of the hydrogen bonds imposed by the rigid ligand framework, the geometry of the anion complex probably approximates that of the splayed tines of a fork.

The related ditopic ligand **5** (Fig. 4.3) a dichloro analogue of **4** that was synthesized to enhance the hydrogen-bonding capabilities, readily holds two chloride ions in the two separate binding sites. In the solid state, each Cl^- ion is bound by three NH groups: two amide groups (N···Cl = 3.27 and 3.28 Å) and a pyrrole donor (N···Cl = 3.07 Å).[9]

A related potentially tridentate ligand, the mixed imidazolium/pyrrole **6** (Fig. 4.4), was synthesized as a model for the prodigiosins.[10] Prodigiosins are natural products that contain three pyrrole units and can transport HCl across lipid membranes.[11]

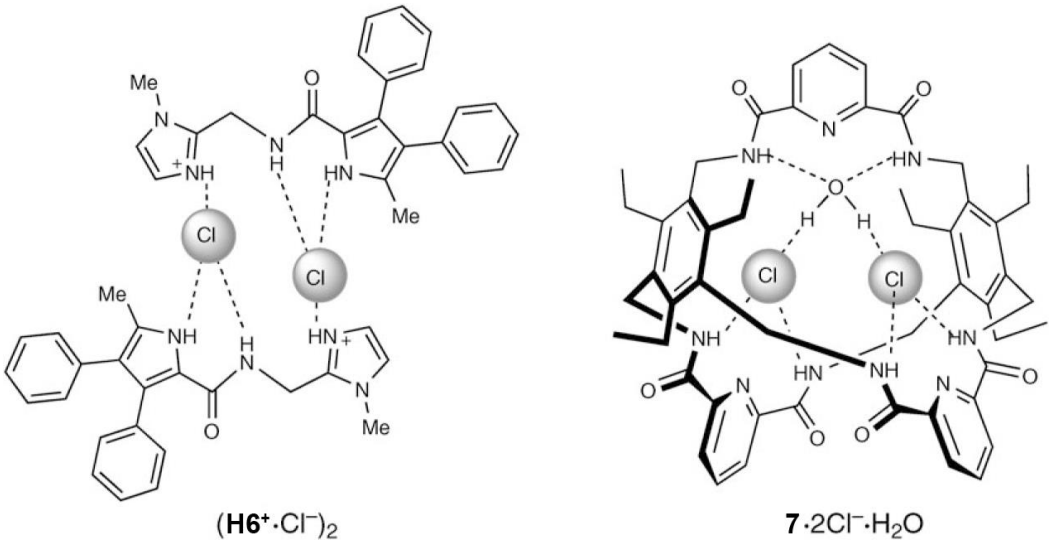

Fig. 4.4

Another three-coordinate halide is found in the chloride complex of the trigonally symmetric amide-based cyclophane **7** (Fig. 4.4). [12] Two chloride ions are held by hydrogen bonding with amide hydrogen atoms of two of the three pyridine spacers. The water molecule is held by the amide groups of the third spacer, and bridges the two chloride ions.

4.2. Coordination Number 4

Probably the most common coordination number for halides is four. The chloride complex of the acyclic pyrrole based ligand **8** (Fig. 4.5) shows a rather unanticipated four-coordinate geometry, with hydrogen bonds from the two

amide hydrogen atoms and two hydrogen atoms on the appended dinitrophenyl rings.

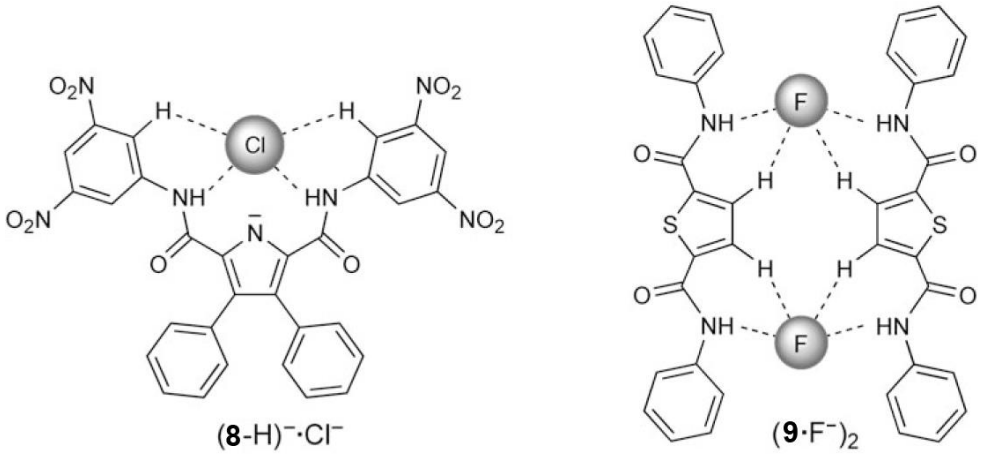

Fig. 4.5

The acyclic thiophene-based amide ligand **9** (fig. 4.5) forms a dimeric complex with flouride $(\mathbf{9}\cdot F^-)_2$,[13]. Two hydrogen bonds in $(\mathbf{9}\cdot F^-)_2$ form from the amide hydrogen atoms and two more from the two CH groups of the thiophene.

Anion complexes of a number of tetraamide macrocyclic hosts were found to have four-coordinate geometries. For example, the 20-membered ring **10** (Fig. 4.6) binds one chloride ion. For most efficient binding, the ligand bends and the chloride ion sits on top of the ligand above the mean plane of the four amide nitrogen atoms,[14] hydrogen-bonded to the four host amide NH groups. The coordination mode is pyramidal and similar to what is sometimes found for transition-metal complexes with macrocyclic ligands that are too small to incorporate the metal ion.

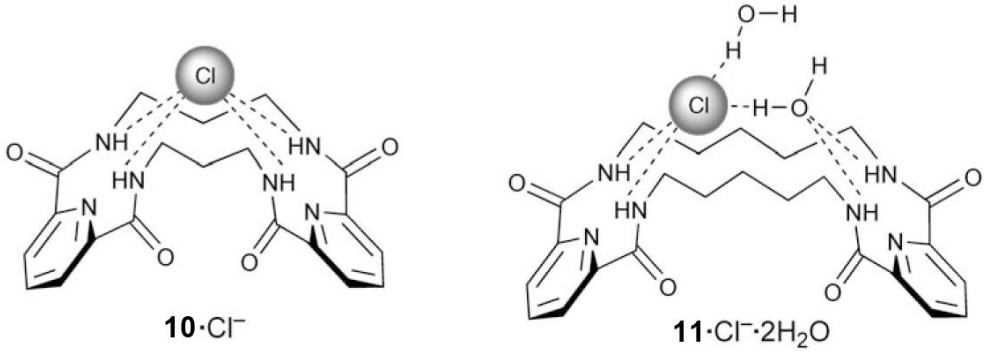

Fig. 4.6

The somewhat larger macrocycle **11** (Fig. 4.6) also binds chloride, together with a water molecule slightly above the macrocyclic cavity.[14]. Two of the coordination sites for the chloride ion are provided by the amide NH groups, a third from the neighboring water molecule, and a fourth from a water molecule from an adjacent macrocycle, which gives what could be described as a distorted tetrahedral geometry.

An expanded version of Jurczak's tetraamide-based macrocycles is the 36-membered-ring lactam **12** (Fig. 4.7) that results from a [4+4]condensation of the methyl ester of pyridine-2,6-dicarboxylate and ethylenediamine.[15]

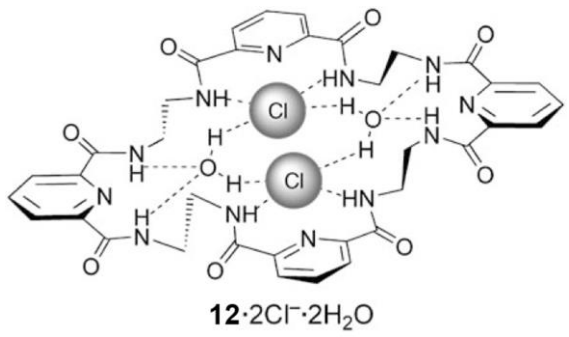

12·2Cl⁻·2H$_2$O

Fig. 4.7

The macrocyclic framework has a steplike geometry, in which two opposing 2,6-pyridinedicarbamoyl groups are essentially coplanar and one of the remaining units is above and one is below that plane. Crystallographic results for the large macrocycle revealed four guests: two chloride ions bridged by two water molecules, all within the macrocyclic cavity (**12**·2 Cl$^-$·2H$_2$O).

The pyridine-based bicyclic receptor **13** (Fig. 4.8) and its methylated quaternary-amine form **14** (Fig. 4.9) were reported by O. Kang et al.[16] In the chloride complex H$_2$**13**$^{2+}$·2 Cl$^-$·H$_2$O, the bridgehead amines are protonated and two of the amide loops fold in one direction while the other loop points in the opposite direction. Two chloride ions are held within the cryptand and are bridged by a water molecule.

The quaternary-amine cryptand **14** also binds chloride (**14**·2Cl$^-$·2H$_2$O).[16] In this case, all three amide loops of the ligand fold in the same direction, thus forming a bowl-like shape. Rather than being encapsulated, one chloride ion sits at the top of the bowl and is centered between the two charged amines. A second chloride ion is located off to one side of the macrocycle and is linked by water molecules to the first chloride ion. The chloride ion directly above the host is bound to two of the amide hydrogen atoms of **14**, with two additional linkages to the waters "floating" on top of the host to result in a pseudotetrahedral geometry.

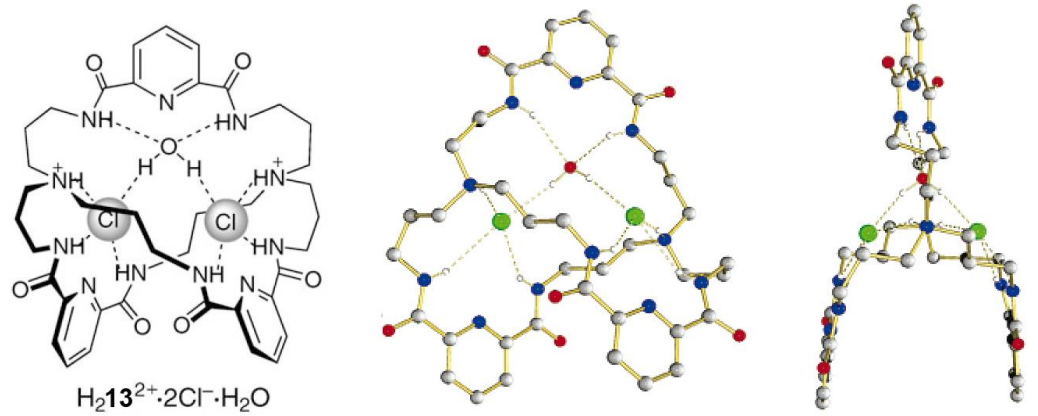

Fig. 4.8 - Chloride complex $H_2\mathbf{13}^{2+}\cdot 2\ Cl^-\cdot H_2O$ in different views

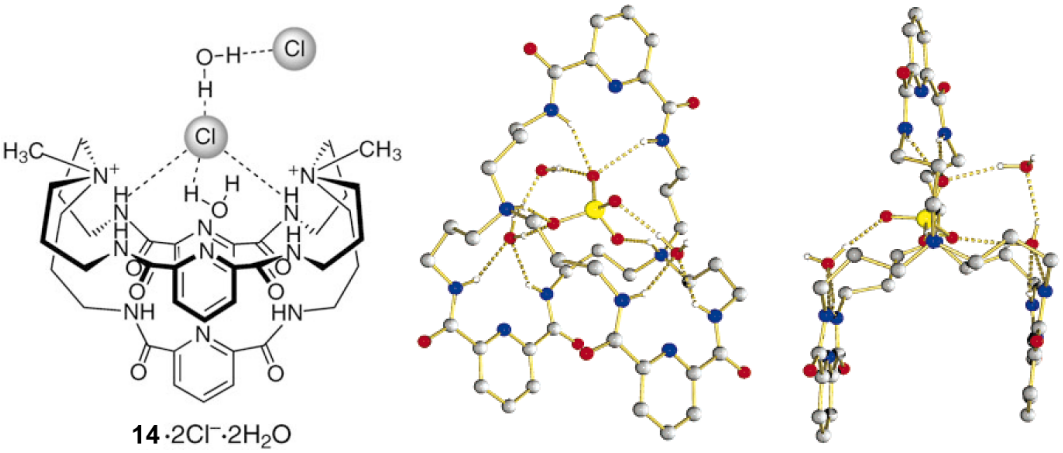

Fig. 4.9 - Chloride complex $\mathbf{14}\cdot 2Cl^-\cdot 2H_2O$ in different views

4.3. Coordination Number 5

The common geometries of five-coordinate transition metal complexes are square pyramidal and trigonal bipyramidal. Five-coordinate halide complexes are frequently found for simple tetraamide hosts, both acyclic and macrocyclic. The acyclic host in $\mathbf{15}\cdot Cl^-\cdot H_2O$ (Fig. 4.10) is deformed slightly from planarity, and the two planar 2,6-pyridinedicarbamoyl groups are canted with respect to each other.[14]

The chloride ion acts as a template and forms four hydrogen bonds to the amide hydrogen atoms. There is an additional hydrogen bond to a water molecule on one side of the macrocycle. The resulting coordination geometry is pseudo square pyramidal.

The 18-membered-ring macrocycle **16** (Fig. 4.10) forms both fluoride and chloride complexes (**16**·X^-·H_2O). Although the 18-membered ring might be considered an ideal size for the relatively small ion, the four amide groups undergo a slight tetrahedral distortion to accommodate the fluoride ion. With the fifth hydrogen bond to a water molecule, the resulting geometry is pseudo square pyramidal.[17]

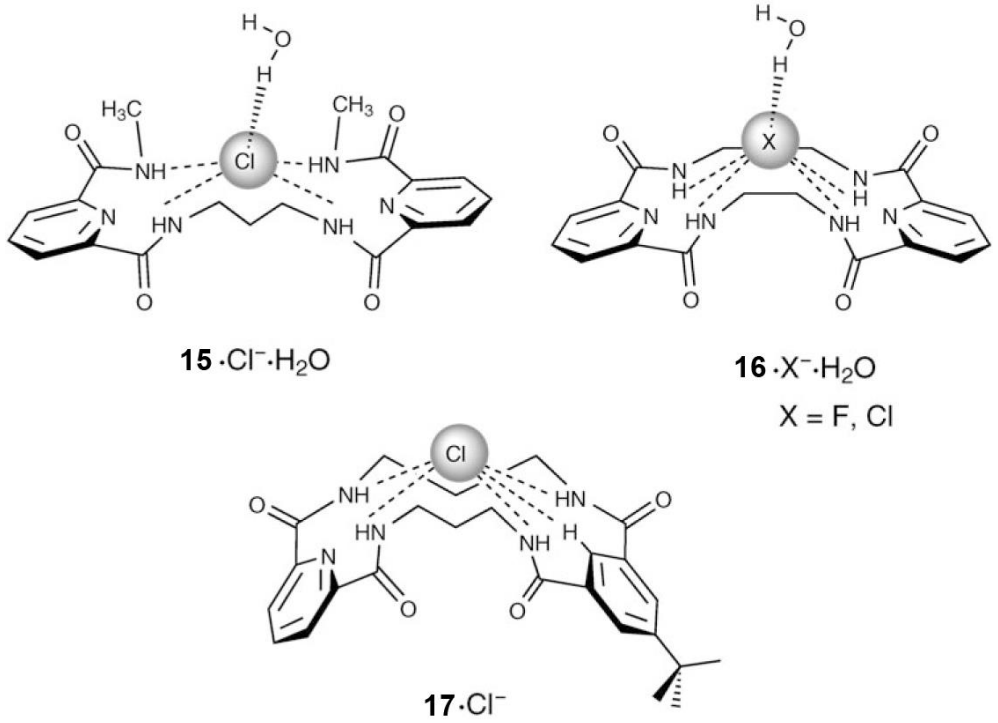

Fig. 4.10

The hybrid tetraamide receptor **17** (Fig. 4.10) contains both 2,6-diamidopyridine and 1,3-diamidobenzene groups and also binds one chloride ion. The solid-state structure of the chloride complex (**17**·Cl^-) shows the chloride ion held through five hydrogen bonds inside the cavity of the macrocycle.[18] The NH groups form four hydrogen bonds and the aromatic CH group forms the fifth bond with the chloride ion.

4.4. Coordination Number 6

The cyclic hexapeptide **18** (Fig. 4.11), which contains three amide groups, was found to bind halides even in aqueous solution.[19]

The crystal structure of the iodide complex revealed a 2:1 complex $\mathbf{19}_2 \cdot I^-$ in which the iodide ion is sandwiched between the two cyclopeptides. There are two crystallographically independent iodide complexes in the unit cell, both of which have virtually identical structures, indicating that a sandwich complex is the preferred coordination mode in this environment. The two cyclopeptides in both complexes are almost perfectly aligned with each other, so that there is only minor deviation from trigonal-prismatic geometry. The iodide ion is associated with the six amide hydrogen atoms, which point into the cavity.

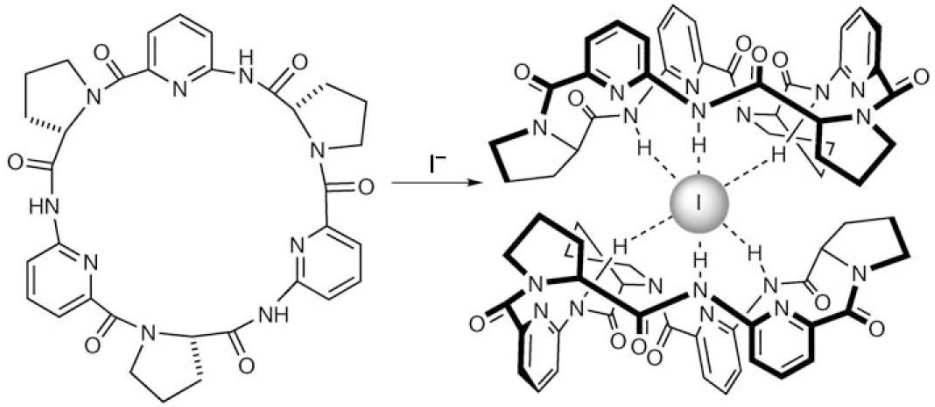

Fig. 4.11

It has been recently reported an example of solvent fixation by the potentially ditopic receptor **19** (Fig. 4.12). The crystal structure of the complex isolated from CH_2Cl_2 revealed that the CH_2Cl_2 had undergone nucleophilic attack by the amine lone pair with the released chloride ion being bound within the cavity to yield $[\mathbf{19}(CH_2Cl)]^+ \cdot Cl^-$.[20] The Cl^- ion is hydrogen bonded to two amide hydrogen atoms; the resulting arrangement of coordination sites is hexagonal planar.

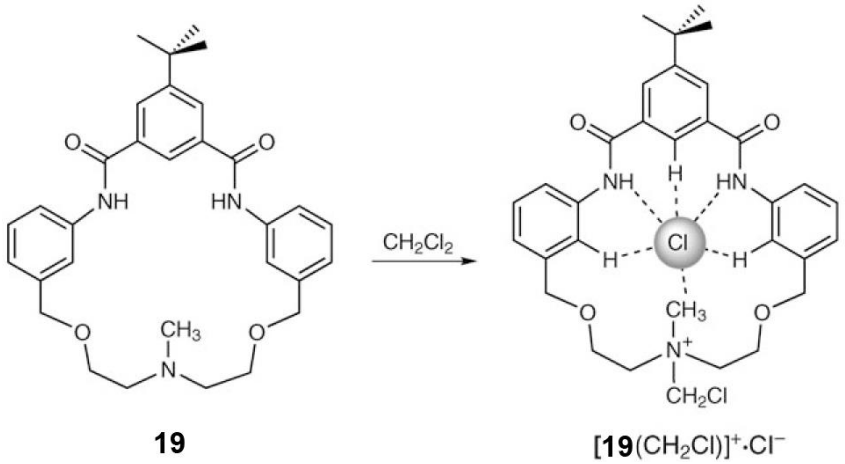

19 **[19(CH$_2$Cl)]$^+$·Cl$^-$**

Fig. 4.12

A bicyclic receptor **20a** (Fig. 4.13) has been reported which was found to be selective for fluoride. All six NH groups are within hydrogen-bonding distances (N···F =2.84-2.89 Å) of the encapsulated fluoride ion.[21]

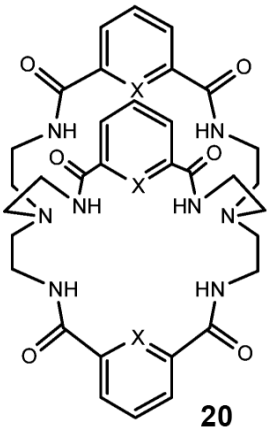

20a, X = N
20b, X = CH

20

Fig. 4.13

The coordination geometry of the fluoride ion is approximately midway between trigonal prismatic and octahedral; the trigonal twist angle is 37°. (Fig. 4.14)

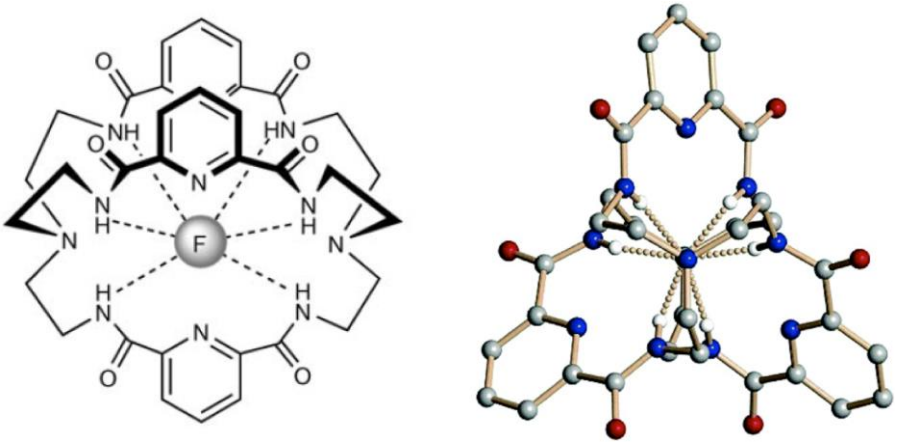

Fig. 4.14 - The fluoride complex **20a**·F^- and his crystal structure.

4.5. Coordination Number 9

What may be the highest coordination number found for the halides with amide-based receptors is observed with the m-xylyl analogue **20**b (Fig 4.15) of the pyridine-containing cryptand **20**a.[22]

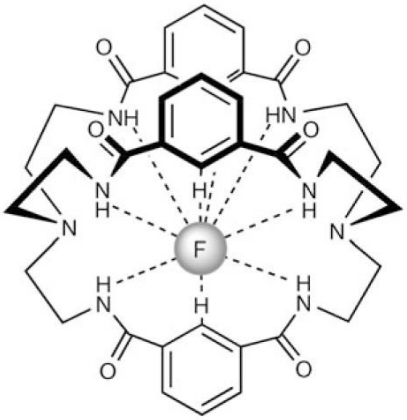

Fig 4.15 - 20b·F^-

The crystal structure of the fluoride complex indicates nine coordination: six bonds to the amide hydrogen atoms and an additional three interactions with the *m*-xylyl CH groups (Fig. 4.16) . The ^{19}F NMR spectra support the existence of all nine hydrogen bonds.

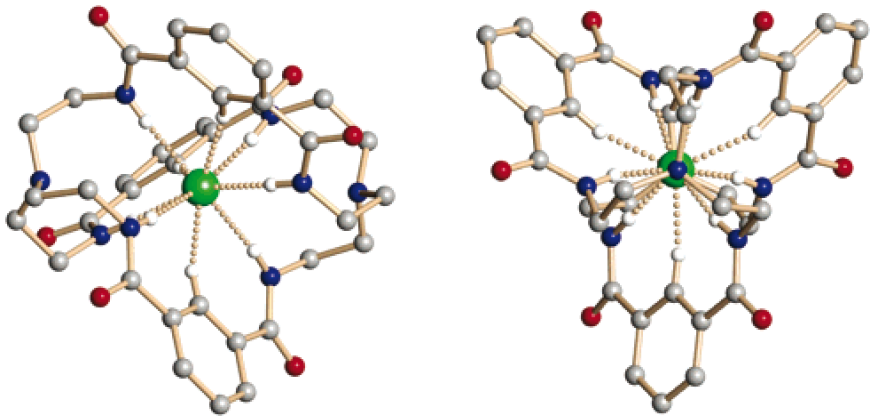

Fig. 4.16 - Perspective views of **20b**·F^-**.** (**A**) Side view. (**B**) End view down the pseudo-three-fold axis.

In the following, geometries other than the spherical one will be reviewed as far as the anions coordinated by amide receptors.

4.6. Linear Anions

Examples of linear anions include azide, thiocyanate, cyanide, and bifluoride. However only one example of a crystallographically characterized linear anion complex with an amide host has been reported to date.[23]

The first inclusion complex of a linear anion was observed by Lehn for azide in an octaazacryptand.[24]

In the crystal structure of azide complex of H_6**21**$^{6+}$·$\mathbf{N_3}^-$ (Fig. 4.17), the seminal example of a linear anion complex, all six of the secondary amine groups are protonated and are hydrogen bonded to the linear N_3^- ion in a C_3-trigonal-prismatic symmetry pattern.

The azide terminal N···N distance is very short (2.32 Å) and the hydrogen-bond distances from the azide terminus to the secondary amines are 2.94 Å.[24]

Although it was envisioned that bifluoride should also bind in these “linear” azacryptand receptors, a selective receptor for bifluoride was only recentlyreported, along with a crystal structure.[23]

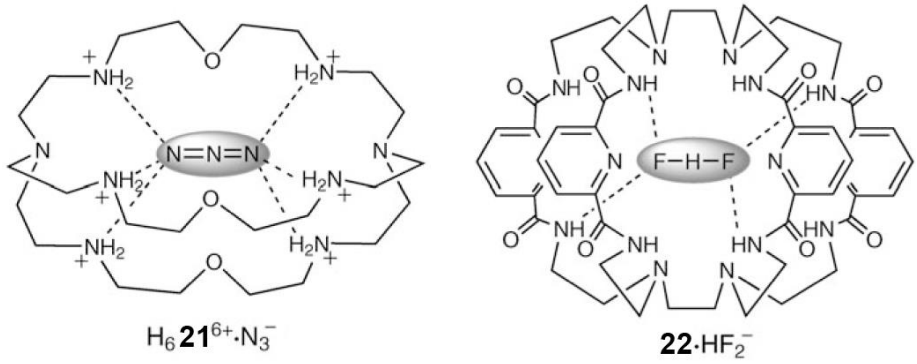

H_6**21**$^{6+}$·N_3^- **22**·HF_2^-

Fig. 4.17

The structurally characterized FHF^- complex of the tricycle **22** (Fig. 4.17) contains a linear FHF^- ion bridging the two macrocyclic caps of the cylindrical tricycle. Although **22**·HF_2^- contains eight amide groups as potential hydrogen-bonding sites, only four are utilized, which results in a tetrahedral four coordinate geometry based on the topology of the four bound NH groups around the anion. The other four amide hydrogen atoms are involved in three-atom hydrogen-bonding networks between the amide hydrogen atoms, and the pyridine and tertiary amine nitrogen lone pairs. The F···F distance in **22**·HF_2^- is 2.47 Å. Binding studies revealed selective binding for FHF^- over other anions.

4.7. V-Shaped Anions

In addition to truly V-shaped anions such as nitrite, simple carboxylates such as acetate and benzoate will also be considered in this section.

Dual-host receptors such as **3**, consisting of crown ethers covalently attached to amide containing straps, bind halides along with their associated cation. This mode of binding also works with other anion shapes, for example, nitrite. **3**·Na^+·NO_2^- (Fig. 4.18) is a relatively rare example of a crystal structure of a nitrite complex, where the nitrite ion may appropriately be considered singly coordinated [25]

The acetate complex of **3** (**3**Na^+·AcO^-) is an example of a two coordinate receptor in which the anion is also chelated by its counterion (K^+), and the acetate ion lies somewhat outside the cavity. Only one of the oxygen atoms is hydrogen bonded to the amide portion of the receptor, but in this case to both

amides (N···O distances of 2.93 and 3.01 Å),[25] which makes this a two-coordinate V-shaped geometry.

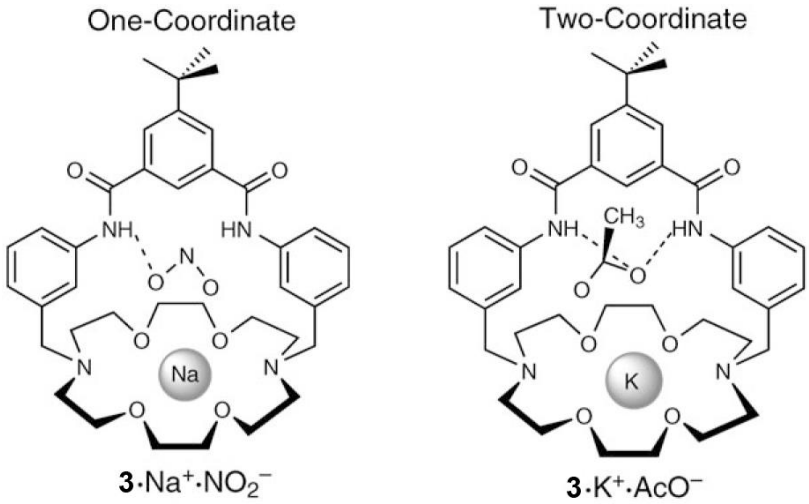

Fig. 4.18

Cheng and co-workers were the first to report **23** (Fig. 4.19) as an anion receptor.[26]

Shortly thereafter, Gale and co-workers reported the crystal structures of the acetate complex of **23** [27] and the benzoate complex of **24**.[28]

Both complexes exhibit three hydrogen-bonding interactions between the anions and the amide and pyrrole hydrogen atoms.

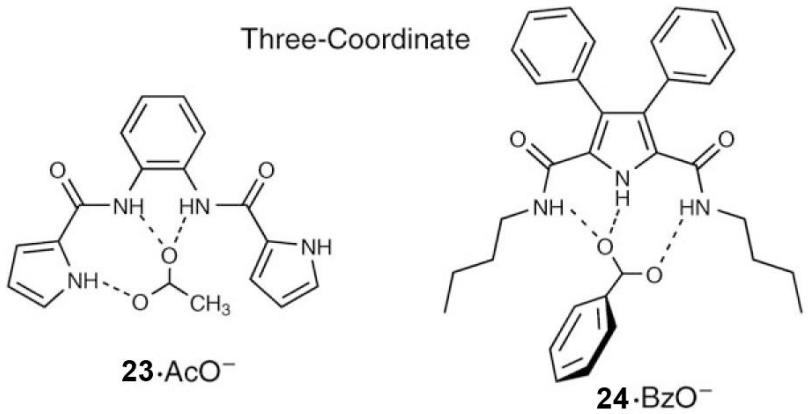

Fig. 4.19

The trigonally symmetric amide-based cyclophane **7** was originally designed to be selective for anions with C_3 symmetry and, as expected, this receptor is selective for the trigonal-planar nitrate ion and for acetate [12]

The crystal structure of the acetate complex **7**·AcO^- (Fig. 4.20) revealed four hydrogen-bonding interactions (two Hydrogen bonds from each oxygen atom to amides of the pyridine-2,6-diamide spacers) and a pyramidal or possibly square-planarlike coordination geometry.

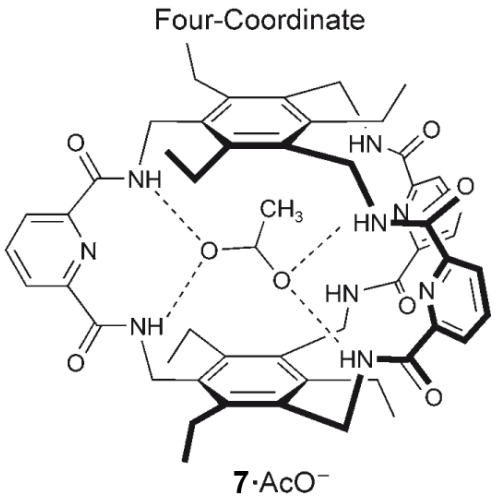

Fig. 4.20

Crystal structures of the acetate complexes of tetraamide macrocycle **16**·AcO^-·H_2O (Fig. 4.21) revealed both 1:1 and 2:1 ligand:anion stoichiometries with five- and eight-coordinate geometries, respectively**.** In the 1:1 complex, grown from tetramethylammonium acetate, one of the acetate oxygen atoms is involved in four hydrogen-bonding interactions with all four amide hydrogen atoms with N···O distances ranging from 2.89 to 3.03 Å. The remaining acetate oxygen atom is hydrogen bonded to an axial water molecule at an O···O distance of 2.70 Å. The result is a square-pyramidal structure.[17]

In contrast, when crystals are grown from tetrabutylammoniumnacetate a sandwichlike structure with $\mathbf{16}_2$.AcO^- is observed. In this case, each acetate oxygen atom is hydrogen bonded to all four amide hydrogen atoms of the adjacent macrocycle (N···O=2.99–3.06 >).[17] The result is octacoordination and a pseudo (tilted) square prismatic geometry.

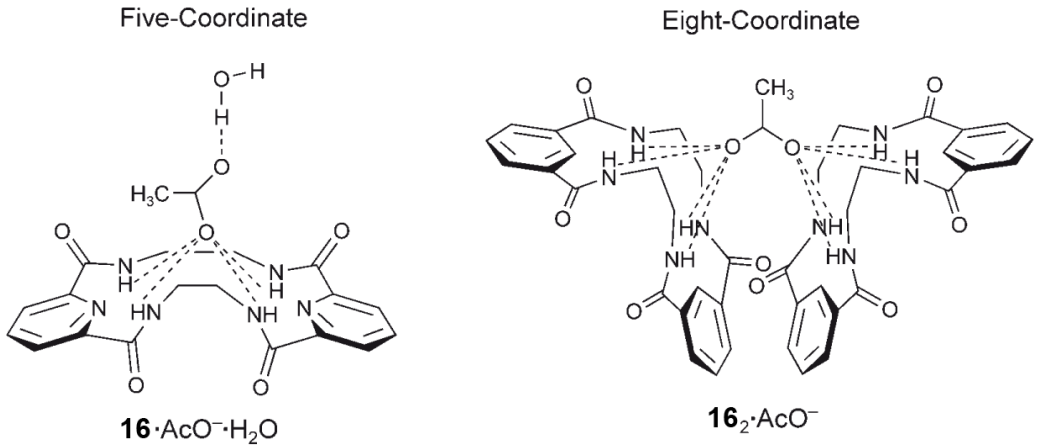

Fig. 4.21

4.8. Trigonal-Planar Anions

One of the classic examples of host–guest binding of a trigonal-planar anion is the nitrate complex of the tren-based amine cryptand system **25** (Fig. 4.22).

Two nitrate ions are encapsulated in **25** in an eclipsed conformation with distances[29] Nnitrate···Nnitrate = 3.34 Å and Nnitrate···Nbridgehead = 3.07 and 3.09 Å. Once again the geometrical complementarity of the host, one of the important factors in a host–guest complex, clearly plays a role in the binding of the trigonal-planar nitrate.

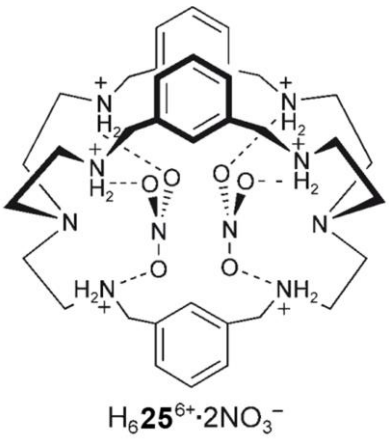

Fig. 4.22

Macrocycle **26** (Fig. 4.23), which possesses oxamido and amine units, is capable of binding anions or metal ions. The crystal structure of the dinitrate complex revealed interesting structural similarities to the dinitrate complex of 27. In $H_4\mathbf{26}^{4+}\cdot 2NO_3^-$, the macrocycle is tetraprotonated and shows only two hydrogen-bonding interactions for each nitrate ion. As with **25**, the two nitrate ions bind in

an eclipsed conformation at an Nnitrate···Nnitrate distance of 3.5 Å and are each about 4 Å from the oxamido caps.[30]

The dual-host receptor **3**, described earlier for encapsulation of halides, acetate, and nitrite, also binds nitrate. Several crystal structures have been obtained with nitrate and three different cations (Li^+, Na^+, and K^+). For both Na^+ and K^+, two of the nitrate oxygen atoms chelate the cation, and the third is hydrogen bonded to the amide part of the ligand. [25]

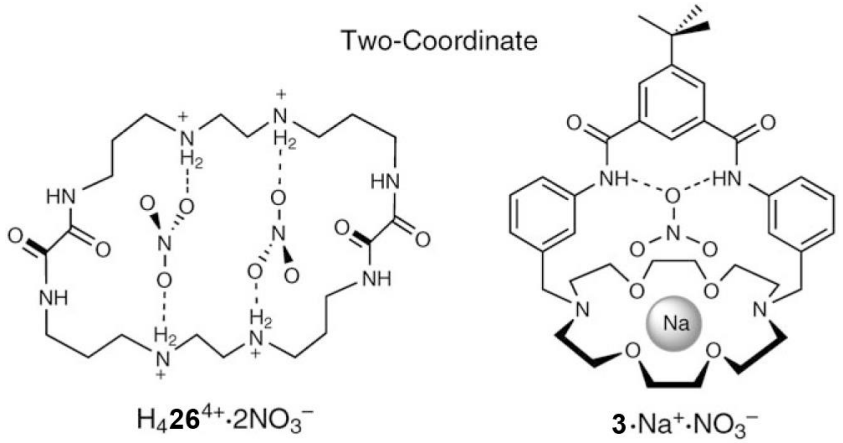

Fig. 4.23

With the smaller Li^+ complex of **3**, however, there is room for an additional guest, in this case water, and, rather than chelating the Li^+, the nitrate is associated with the cation through a water bridge**.**

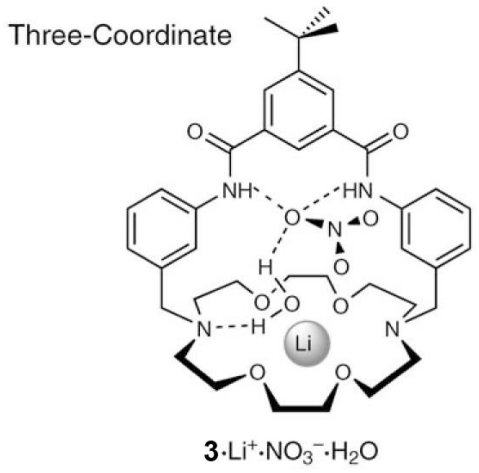

Fig. 4.24

4.9. Tetrahedral anions

Phosphate and sulfate are key anions in biological systems, and the phosphate-binding (**PBP**) and sulfate-binding (**SBP**) proteins provide classic examples of selective receptors for these tetrahedral anions (Fig. 4.25).

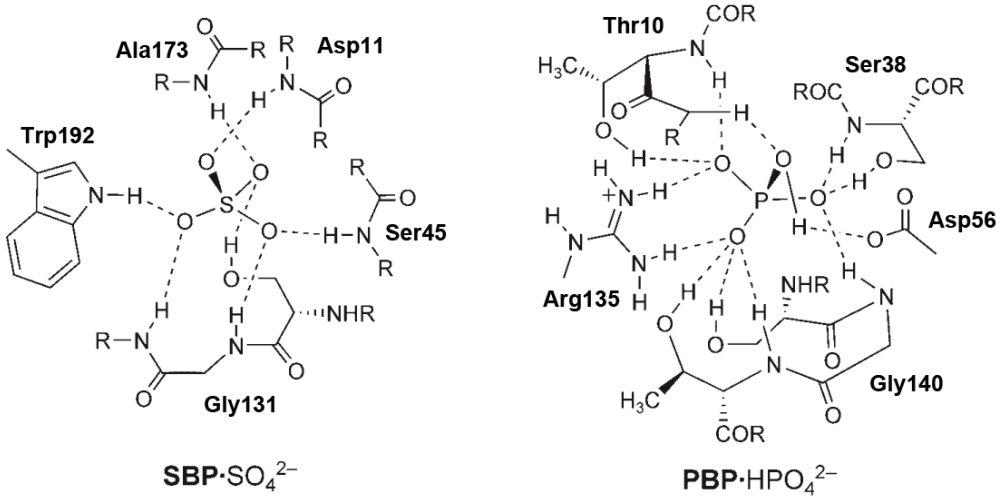

Fig. 4.25

These two proteins are capable of highly selective binding of sulfate and mono-hydrogen phosphate. The crystal structures of both proteins reveal multiple and strong hydrogen bonding through a mixture of functional groups, including amides as well as pyrrole (tryptophan), carboxylate, and guanidinium (arginine) groups. Twelve hydrogen bonds in total hold the mono-hydrogen phosphate in place in the **PBP** and a mere seven hydrogen bonds hold the sulfate in the **SBP**.[31, 32]

Following these crystallographic reports by Quiocho and co-workers of the anion-bound complexes of phosphate and sulfate-binding proteins, researchers have sought to design selective receptors with high affinities for oxoanions by mimicking these natural hosts.

Five structures of amide-based receptors for sulfate, which range in coordination number from six to eight, serve to illustrate sulfate-binding patterns. Three of the five structures are eight-coordinate.

The lowest coordination number for tetrahedral anions (six) was observed in the hybrid amide/pyrrole mixed cyclic receptor **27** (Fig. 4.26).[33]

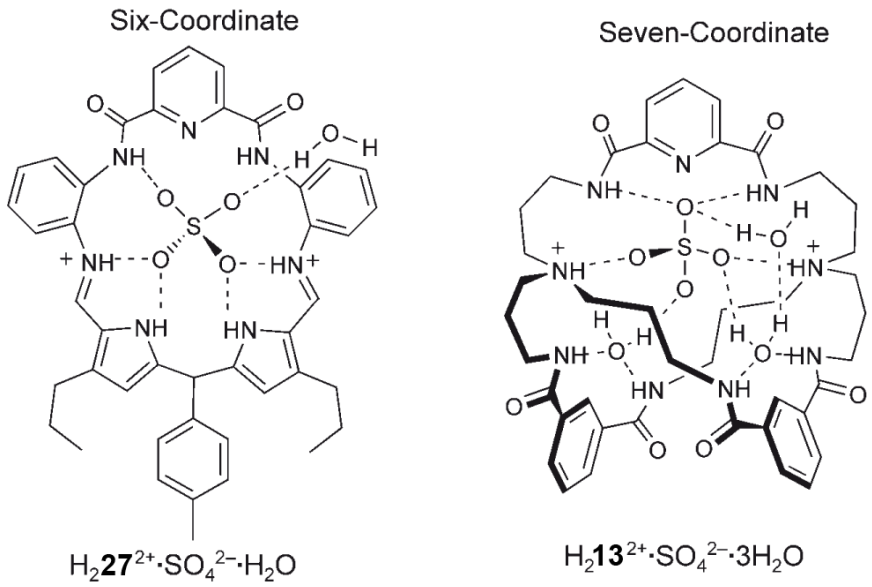

Fig. 4.26

The structure could be considered pseudooctahedral on the basis of the placement of the hydrogen-bond donors.

A seven-coordinate complex was observed for **13**, which is large enough to hold multiple guests.[16] In this case, a sulfate ion and two water molecules are held within the cavity; the sulfate ion acts as a bridge between the two bound water molecules.

The simple tetraamide macrocycle **28** (Fig. 4.27) was found to be selective for tetrahedral oxo acids.[34] The crystal structure of **28** with sulfate revealed a sandwich complex with a dinegatively charged sulfate ion held between two macrocycles.

Each of the sulfate oxygen atoms is held by two amide bonds at N···O distances ranging from 2.86 to 2.98 Å. The two macrocycles are rotated by 908 with respect to each other, which results in a similar coordination mode and accommodates the S_4 symmetry axis of the sulfate ion. The resulting coordination geometry, in which a total of eight amide hydrogen atoms bind to the sulfate ion, is pseudo square prismatic.

An eight-coordinate complex is also observed for the sulfate complex with the bicyclic amido cryptand **20**. All six amide hydrogen atoms and two additional hydrogen atoms on the protonated bridgehead amines are utilized for hydrogen bonding. [35]

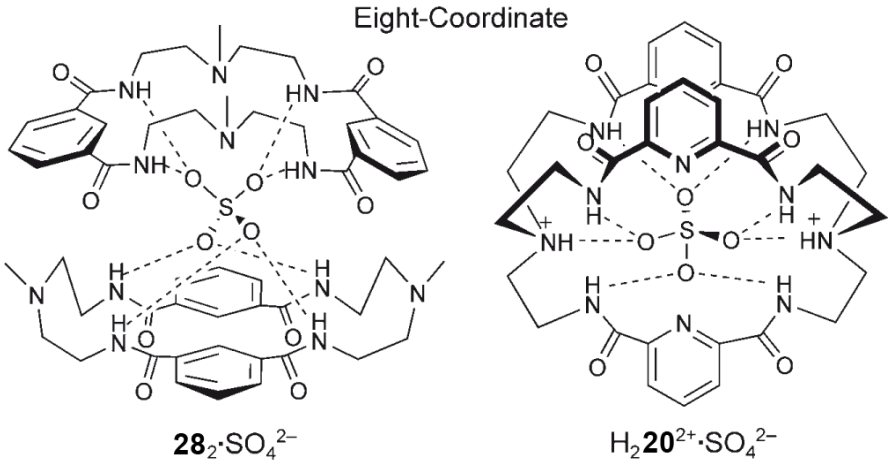

$\mathbf{28}_2 \cdot SO_4^{2-}$ $H_2\mathbf{20}^{2+} \cdot SO_4^{2-}$

Fig. 4.27

Another hybrid receptor, the sulfate complex $H_2\mathbf{29}^{2+} \cdot SO_4^{2-}$ (Fig. 4.28) which is a [3+3]condensation product of bipyrrole and pyridinediamide, was isolated during the crystallization of the [2+2]condensate with sulfate.[36]

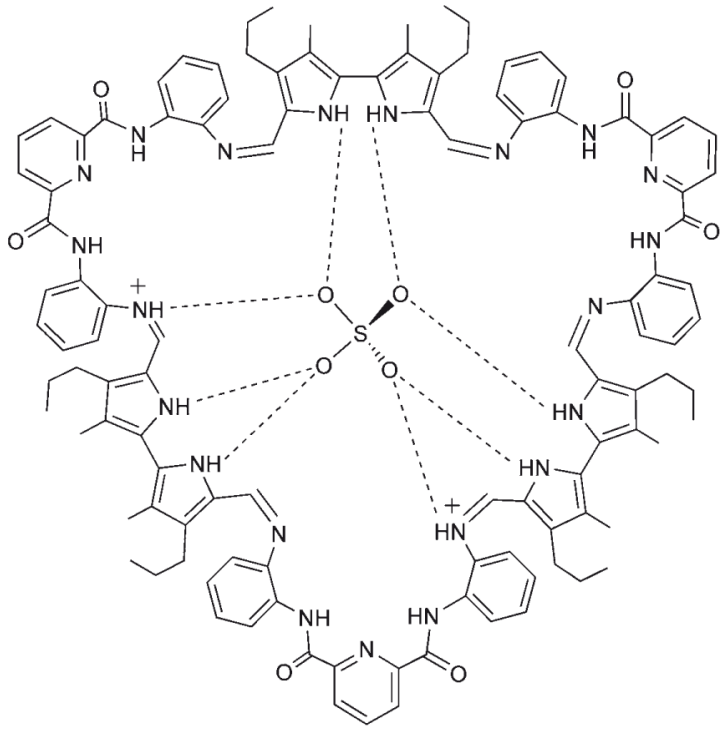

$H_2\mathbf{29}^{2+} \cdot SO_4^{2-}$

Fig. 4.28

The isolation of the higher-order analogue indicates that the anion plays an important role as a template in promoting the formation of the higher-order condensate. In the crystal structure of the sulfate complex, the huge macrocycle is diprotonated and twisted to accommodate the sulfate. There are eight hydrogen bonds to the sulfate ion: six from the three bipyrroles and two from the protonated imines. Although there was some disorder in the sulfate ion, interestingly, the amides do not participate in hydrogen bonding.

References

[1] K. Kavallieratos, S. R. de Gala, D. J. Austin, R. H. Crabtree, *J. Am.Chem. Soc*. **1997**, 119, 2325 – 2326.

[2] M. A. Hossain, S. O. Kang, D. Powell, K. Bowman-James, *Inorg. Chem*. **2003**, 42, 1397 – 1399.

[3] a) M. J. Deetz, M. Shang, B. D. Smith, *J.Am.Chem. Soc*. **2000**, 122, 6201 – 6207; b) J. M. Mahoney, G. U. Nawaratna, A. M. Beatty, P. J. Duggan, B. D. Smith, *Inorg.Chem*. **2004**, 43, 5902 – 5907.

[4] J . M. Mahoney, A. M. Beatty, B. D. Smith, *J.Am. Chem. Soc*. **2001**, 123, 5847 – 5848.

[5] J . M. Mahoney, A. M. Beatty, B. D. Smith, *Inorg.Chem*. **2004**, 43, 7617 – 7621.

[6] J . M. Mahoney, J. P. Davis, A. M. Beatty, B. D. Smith, *J.Org. Chem*. **2003**, 68, 9819 – 9820.

[7] a) P. A. Gale, S. Camiolo, G. J. Tizzard, C. P. Chapman, M. E. Light, S. J. Coles, M. B. Hursthouse, *J.Org.Chem*. **2001**, 66, 7849 – 7853; b) P. A. Gale, S. Camiolo, C. P. Chapman, M. E. Light, M. B. Hursthouse, *Tetrahedron Lett*. **2001**, 42, 5095 – 5097.

[8] T . Zielin´ ski, J. Jurczak, *Tetrahedron* **2005**, 61, 4081 – 4089.

[9] M. E. Light, P. A. Gale, K. Navakhun, *Acta Crystallogr.Sect. E* **2005**, 61, o1300 – o1301.

[10] P . A. Gale, *Chem.Commun* . **2005**, 3761 – 3772.

[11] A. FSrstner, *Angew.Chem*. **2003**, 115, 3706 – 3728; *Angew. Chem.Int. Ed*. **2003**, 42, 3582 – 3603.

[12] A. P. Bisson, V. M. Lynch, M.-K. C. Monahan, E. V. Anslyn, *Angew.Chem*. **1997**, 109, 2435 – 2437; same authors*: Angew.Chem. Int. Ed.Engl*. **1997**, 36, 2340 – 2342.

[13] S . J. Coles, P. A. Gale, M. B. Hursthouse, M. E. Light, C. N. Warriner, *Supramol.Chem*. **2004**, 16, 469 – 486.

[14] M. J. Chmielewski, J. Jurczak, *Chem.Eur . J*. **2005**, 11, 6080 – 6094.

[15] A. Szumna, J. Jurczak, *Helv.Chim. Acta*, **2001**, 84, 3760 – 3765.

[16] S . O. Kang, D. Powell, K. Bowman-James, *J.Am. Chem. Soc*. **2005**, 127, 13478 – 13479.

[17] A. Szumna, J. Jurczak, *Eur.J .Org. Chem*. **2001**, 4031 – 4039.

[18] M. J. Chmielewski, J. Jurczak, *Tetrahedron Lett*. **2005**, 46, 3085 –3088.

[19] a) S . Kubik, R. Goddard, R. Kirchner, D. Nolting, J. Seidel, *Angew. Chem*. **2001**, 113, 2722 – 2725; b) S . Kubik, R. Goddard, R. Kirchner, D. Nolting, J. Seidel, *Angew.Chem*. Int. Ed. **2001**, 40, 2648 – 2651.

[20] J . J. Lee, K. J. Stanger, B. C. Noll, C. Gonzalez, M. Marquez, B. D. Smith, *J.Am.Chem. Soc*. **2005**, 127, 4184 – 4185.

[21] S. O. Kang, J. M. Llinares, D. Powell, D. VanderVelde, K. Bowman-James, *J.Am. Chem. Soc.* **2003**, 125, 10152 – 10153.

[22] S . O. Kang, D. VanderVelde, D. Powell, K. Bowman-James, *J. Am.Chem. Soc*. **2004**, 126, 12272 – 12273

[23] a) S . O. Kang, D. Powell, V.W. Day, K. Bowman-James, *Angew. Chem*. **2006**,118, 1955 – 1959; b) S . O. Kang, D. Powell, V.W. Day, K. Bowman-James, *Angew.Chem. Int. Ed*. **2006**, 45, 1921 – 1925.

[24] J .-M. Lehn, E. Sonveaux, A. K.Willard, *J.Am. Chem. Soc*. **1978**,100, 4914 – 4916.

[25] J . M. Mahoney, K. A. Stucker, J. Jiang, I. Carmichael, N. R. Brinkmann, A. M. Beatty, B. C. Noll, B. D. Smith, *J.Am. Chem. Soc*. **2005**, 127, 2922 – 2928.

[26] Z. Yin, Z. Li, A. Yu, J. He, J. -P. Cheng, *Tetrahedron Lett*. **2004**, 45, 6803 – 6806.

[27] S . J. Brooks, P. A. Gale, M. E. Light, *Chem.Commun*. **2005**, 4696 – 4698.

[28] a) S. Camiolo, P. A. Gale, M. B. Hursthouse, M. E. Light, *Tetrahedron Lett*. **2002**, 43, 6995 – 6996; b) P. A. Gale, S. Camiolo, C. P. Chapman, M. E. Light, M. B. Hursthouse, *Tetrahedron Lett*. **2001**, 42, 5095 – 5097.

[29] S . Mason, T. Clifford, L. Seib, K. Kuczera, K. Bowman-James, *J. Am.Chem. Soc*. **1998**, 120, 8899 – 8900.

[30] L. Cronin, P. A. McGregor, S. Parsons, S. Teat, R. O. Gould, V. A. White, N. J. Long, N. Robertson, *Inorg.Chem*. **2004**, 43, 8023 – 8029.

[31] H. Luecke, F. A. Quiocho, *Nature* **1990**, 347, 402 – 406.

[32] a) J.W. Pflugrath, F. A. Quiocho, *Nature* **1985**, 314, 257 – 260;b) B. L. Jacobson, F. A. Quiocho, *J.Mol.Biol*. **1988**, 204, 783 –787.

[33] J. L. Sessler, E. Katayev, G. D. Pantos, P. Scherbakov, M. D.Reshetova, V. N. Khrustalev, V. M. Lynch, Y. A. Ustynyuk, *J. Am.Chem. Soc*. **2005**, 127, 11442 – 11446.

[34] M. A. Hossain, J. M. Llinares, D. Powell, and K. Bowman-James, *Inorg.Chem*. **2001**, 40, 2936 – 2937.

[35] S . O. Kang,M. A. Hossain, D. Powell, K. Bowman-James, *Chem. Commun*. **2005**, 328 – 330.

[36] E. A. Katayev, G. D. Pantos, M. D. Reshetova, V. N. Khrustalev,V. M. Lynch, Y. A. Ustynyuk, J. L. Sessler, *Angew.Chem*. **2005**, 117, 7552–7556; Same authors: *Angew.Chem.Int.Ed*. **2005**, 44, 7386 – 7390.

5. Urea and Thiourea based anion receptors

Urea represents the junction between organic and inorganic chemistry which, like a sort of aristotelic categories, before of the serendipitous synthesis of Wöhler divided the material substances into two classes, the content of which came from living world, or from the inanimate one. More recently, urea and its N,N'-substituted derivatives assumed a leading role in the field of anion coordination chemistry since when it has been observed that **1** and **2** (Fig. 5.1) were able to interact with phosphonates, sulfates and carboxylates in the poorly polar solvent CH_2Cl_2, forming stable 1:1 complexes held together by two parallel N–H···O hydrogen bonds. [1 ,2]

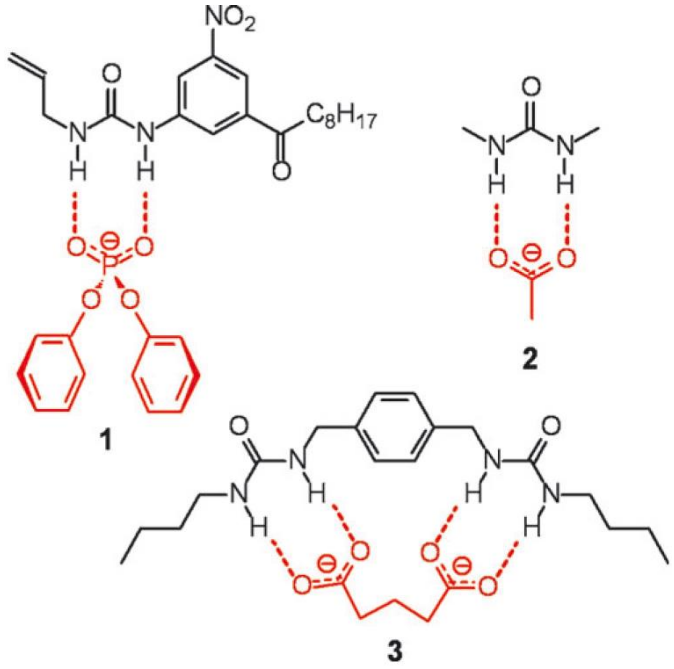

Fig. 5.1

Furthermore, the ditopic receptor **3**, in which two urea subunits are linked together through a 1,4-xylyl spacer, formed a 1:1 complex with the glutarate ion in DMSO.

With respect to the amide group, which can donate a single hydrogen bond, urea can donate two parallel H-bonds, to two oxygen atoms of an oxoanion, possibly displaying geometrical complementarity, forming an eight-membered ring (formula "**a**" in Scheme 5.1), or to a spherical anion in a bifurcate mode, giving rise to a six-membered ring (formula (b) in Scheme 5.1).

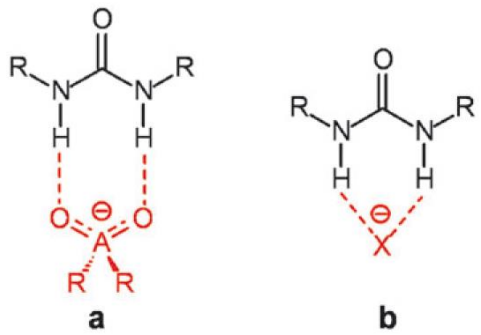

Scheme 5.1 - Urea-based receptors donate two parallel H-bond to oxoanions, forming an eight membered ring (a), and two bifurcate H-bond to a monoatomic anion, forming a six-membered ring.

5.1. Synthesis of N,N'-substituted ureas.

Phosgene (X = X' = Cl; $COCl_2$) appears as the simplest reagent for the synthesis of ureas, following route (i) + (ii) (scheme 5.2), or through the more reactive isocyanate, forming the expected urea, according to route (iii) + (iv).

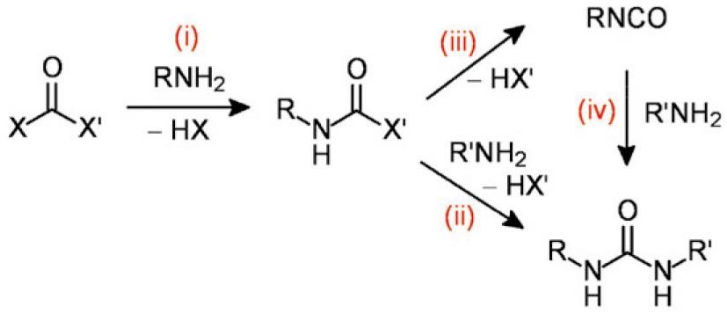

Scheme 5.2 - A general route to N,N'-substituted ureas.

The utilization of plain phosgene in a research laboratory is limited by its high toxicity. However, phosgene can be replaced by a number of safer, milder and easy-to-handle derivatives

An interesting example has been recently reported of the reaction of 4-nitrophenyl chloroformate **(a)** with the dianiline **(b)**, to give the bisurea macrocycle **4** (Scheme 5.3).[3]

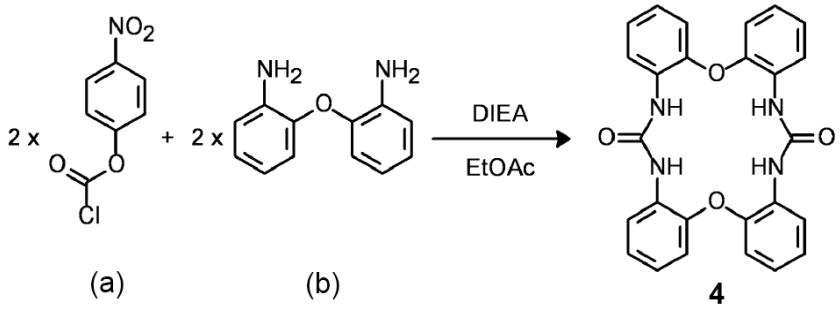

Scheme 5.3 - Synthesis of a bis-urea macrocycle through a 2 + 2 cyclization process (DIEA = diisopropylethylammine).

The crystal structure of the bis-urea macrocycle **4** is shown in Fig. 5.2. The two urea subunits do not lie on the same plane, but they point their N–H fragments to opposite sides of the molecular plane (Fig. 5.2a). In particular, each urea subunit establishes a bifurcate hydrogen bonding interaction with a solvent molecule (DMSO), above and below the plane of the molecule (Fig. 5.2b).

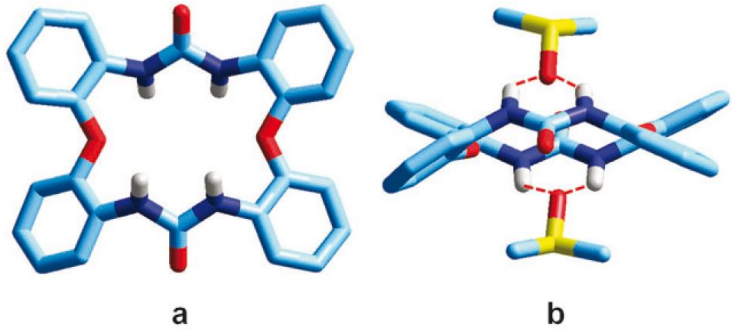

Fig. 5.2 - The molecular structures of the bis-urea macrocycle **4**, as obtained through X-ray diffraction studies [3]: (a) top view; (b) lateral view, showing two H-bonded DMSO molecules.

In the receptor **5** (Fig. 5.3), a urea subunit has been equipped with 4-nitrophenyl substituents. Such an electron withdrawing group further polarizes urea N–H fragments, enhancing the receptor's H-bond donating tendencies.

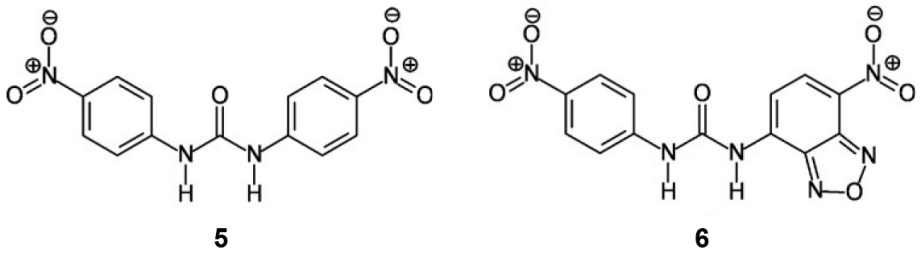

Fig. 5.3

The best way to characterize the receptor–anion complex in its bonding and structural aspects involves growing crystals of the pertinent complex, suitable for X-ray diffraction studies. This was the case of the $[Bu_4N][\mathbf{5}\cdots CH_3COO]$ salt. Figure 5.4 shows the structural arrangement of the $[\mathbf{5}\cdots CH_3COO]^-$ complex.[4]

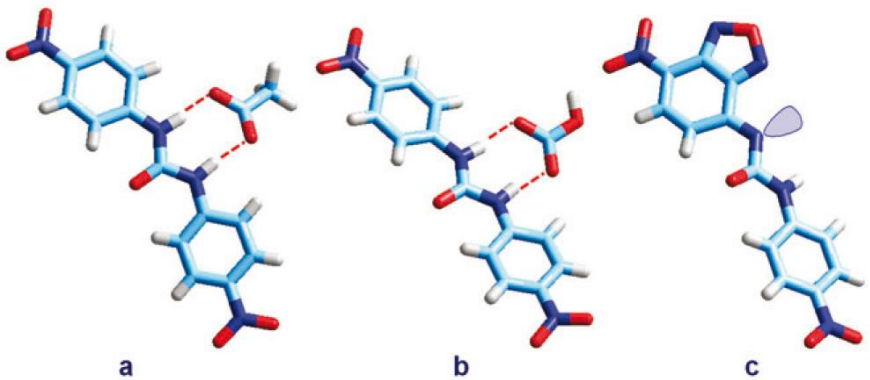

Fig. 5.4 - The molecular structures of urea derivatives, as obtained through X-ray diffraction studies: (**a**) the H-bond complex of receptor **5** with acetate;[4] (**b**) the H-bond complex of **5** with hydrogen carbonate;[4] (**c**) the deprotonated form of receptor **6**.[5] In all cases, the tetrabutylammonium counter-cation has been omitted for clarity.

5.2. Receptors containing more urea subunits

Receptors containing two or more urea subunits, in an open-chain, branched, cyclic or polycyclic arrangement will be here reported. In this sense, the design of anion receptors has progressed in a similar way as observed for the development of multidentate ligands for metal ions, which led to the definition of thechelate, [6] macrocyclic, [7] and cryptate [8] effects (which, in the case of amine ligands, pertained to metal complexes with ethylenediamine, cyclam, and polyamine cages, respectively).

A variety of open-chain receptors containing two or more urea subunits have been synthesised. As an example, receptor **7** possesses two phenylurea fragments linked to a 1,2-phenyl spacer and gives stable 1:1 complexs with carboxylates in a DMSO solution containing 0.5% water.[9]

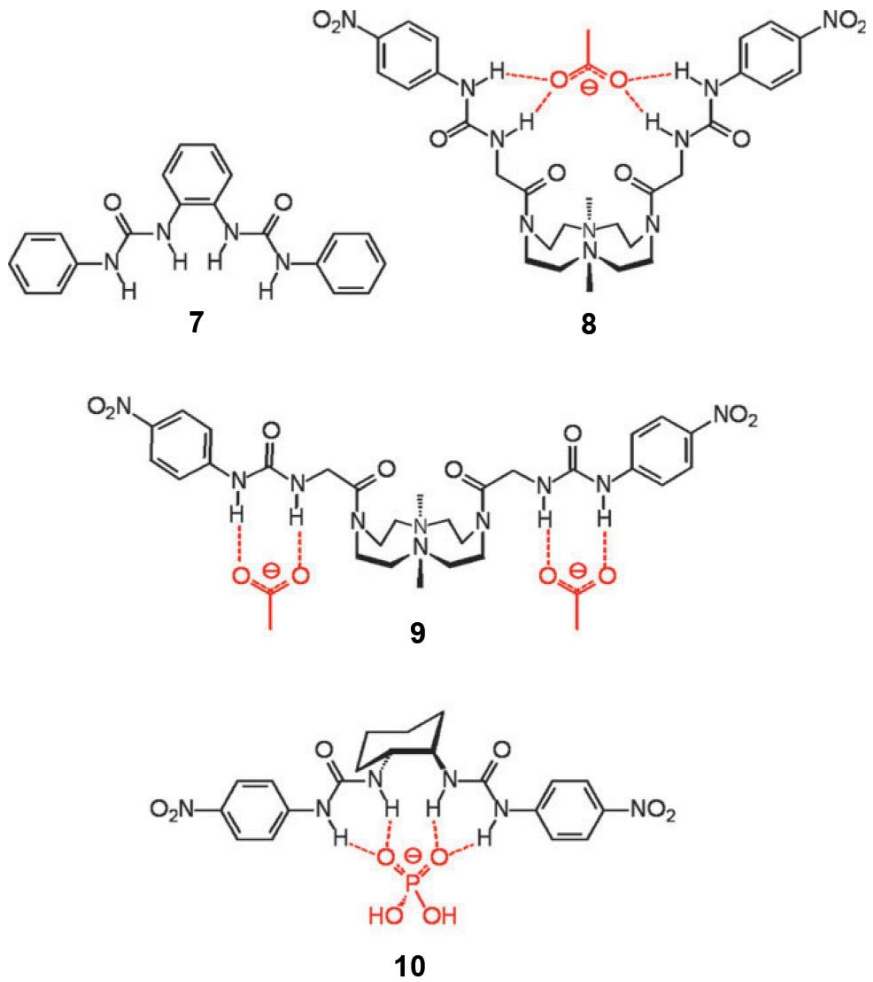

Fig. 5.5

The crystal structure of the benzoate complex, obtained as a tetrabutylammonium salt, showed that each urea subunit donates two H-bonds to one oxygen atom of the carboxylate group, for a total of four (see Fig. 5.6). It is therefore observed that receptor **7** behaves as a chelating agent, with respect to acetate, but a chelate effect cannot be defined because the 2:1 complex in which a CH_3COO^- ion is bound to two distinct urea molecules, required for comparison, has not yet been characterised. It is observed in Fig. 5.6 that the two phenylurea arms of receptor **7** are rotated with respect to the plane of the phenyl spacer, probably in order to place the urea N–H fragments in the right positions and at the correct distances for establishing the four H-bonds with the anion.

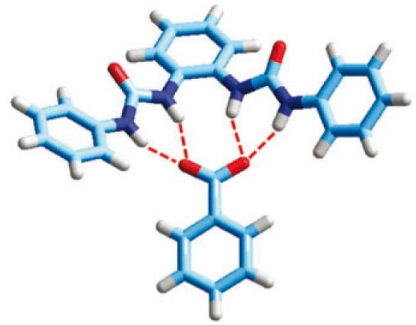

Fig. 5.6 - The crystal structure of the complex between receptor **7** and the benzoate anion.[45] Each carboxylate oxygen atom receives two hydrogen bonds from one urea subunit.

The coordination of one (receptor **8**) and two mole (receptor **9**) of carboxilate for mole of receptor **8** and **9** respectively has been demonstrated by means of measurement of stability constants in solution. [10]

Receptor **10** is similar to receptor **7**, with the main difference that the six-carbon ring acting as a spacer is fully saturated. The conformation of the cyclohexane ring seems to naturally organize the two urea subunits according to a non-coplanar arrangement, which may favour binding of oxoanions.

Spectrophotometric studies in an MeCN solution showed that CH_3COO^- form a 1:1 complex.[11]

Such an unusual behaviour has been explained thanks to the availability of the crystal structure of the $[Bu_4N]_2[H_2PO_4^{-}\cdots\mathbf{10}\cdots H_2PO_4^{-}]$ complex salt, which is shown in Fig. 5.7. It is observed that (i) each $H_2PO_4^-$ ion is bound to a single urea subunit through two N–H···O H bonds and (ii) the two phosphates are bound together through O–H···O hydrogen bonding interactions, each anion acting as both a H-bond donor and a H-bond acceptor.

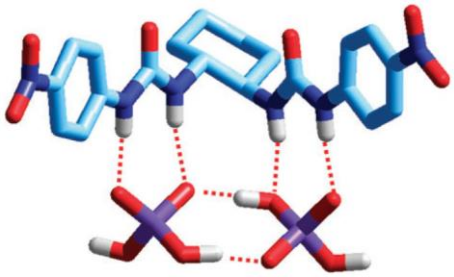

Fig. 5.7 - The crystal structure of the 1:2 complex between receptor **10** and the dihydrogen phosphate anion, $H_2PO_4^-$ [12].

A rather rare example of a bisurea receptor of controllable binding tendencies is represented by system **11**,[13] whose formula is illustrated in Fig. 5.8. The neutral receptor **11** forms with halide ions in MeCN solution 1:1 complexes of moderate stability, as determined through ^{1}H NMR titration experiments.

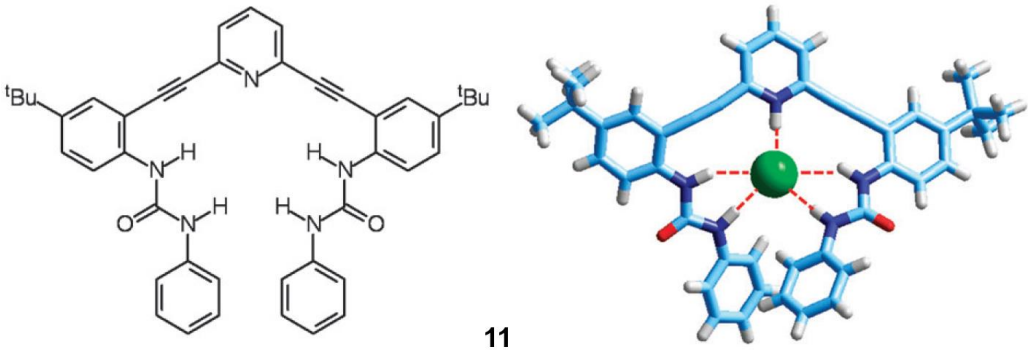

11

Fig. 5.8 - Receptor **11** and the crystal structure of the complex between the protonated form (at the pyridine nitrogen atom) of receptor **11** and the chloride anion.[13]

The crystal structure of the [**11**H]Cl salt, shown in Fig. 5.8, explains why: the chloride ion receives five H-bonds, four from the urea N–H fragments (N···Cl distance: 3.45 ± 0.21 Å) and one, especially strong, from the pyridinium N–H fragment (N···Cl: 3.03 Å).

Böhmer et al. have recently synthesised a class of macrocycles in which three urea subunits are linked by xanthene and/or diphenyl ether spacers.[14] Formulae **12** and **13** (Fig. 5.9) refer to macrocycles containing spacers of the same nature. In particular, the xanthene containing macrocycle **12** is expected to be especially rigid, while macrocycle **13** should exhibit a higher degree of flexibility.

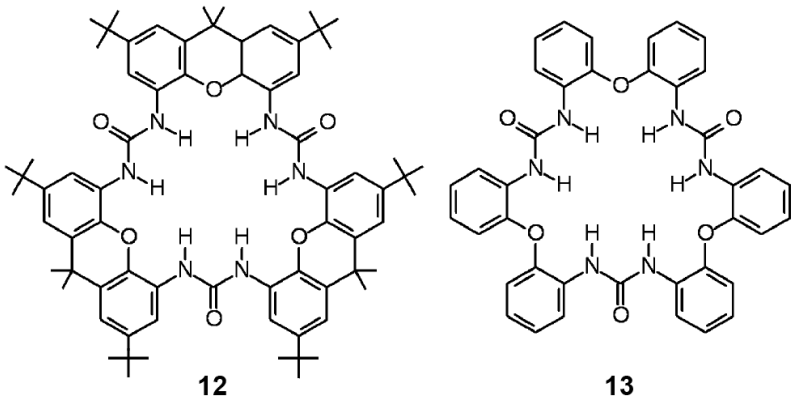

12 **13**

Fig. 5.9

The crystal structure of the $[Bu_4N][\mathbf{13}\cdots Cl]$ complex salt has been determined,[14] and is shown in Fig. 5.10a. It is observed that the chloride ion receives six H-bonds from the three urea subunits, the average N···Cl distance being 3.38 ± 0.15 Å . In Fig. 5.10b and c, urea hydrogen atoms have been linked together, to give an idea of the coordination geometry: it is observed that they do not give rise to a regular polygon (hexagon), but they are arranged in a non-coplanar way, forming a chair.

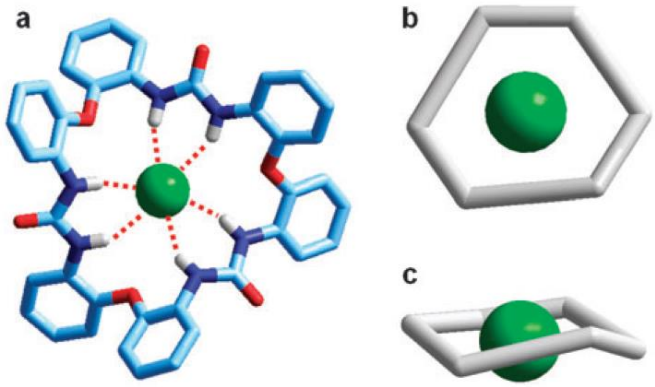

Fig. 5.10 - (**a**) The crystal structure of the complex of receptor **13** with the chloride anion.[51] The tetrabutylammonium counter-cation and the hydrogen atoms of C–H fragments of the receptor have been omitted for clarity; (**b**) top view of the geometrical figure obtained by linking consecutively the hydrogen atoms of the six N–H fragments, showing a distorted hexagonal coordination geometry; (**c**) side view.

In the recently reported tren-based receptor **14**, ureido N–H fragments are polarized by the powerful electron withdrawing substituent $–C_6F_5$.[15]

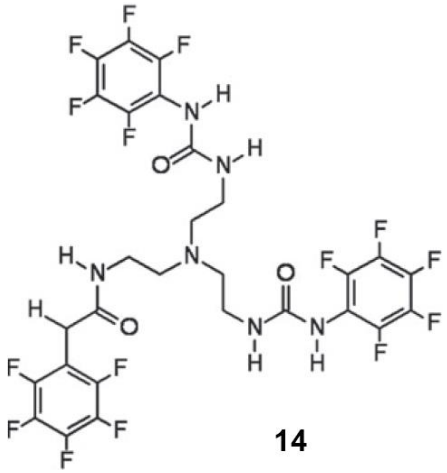

14

Fig. 5.11

The crystal structure of the [Bu_4N][**14**$^{\cdots}$F] salt, shown in Fig. 5.12a, indicates that such a stability results from the capability of the tripodal receptor **14** to establish six hydrogen bonding interactions with the halide ion. Fig. 5.12b and c demonstrate that H-bond coordination is essentially trigonal prismatic, but poorly symmetric. In fact, fluoride is much closer to the plane of the triangle constituted by the hydrogen atoms belonging to the N–H groups linked to the C_6F_5, but N$^{\cdots}$F distances are essentially the same for both triangles.

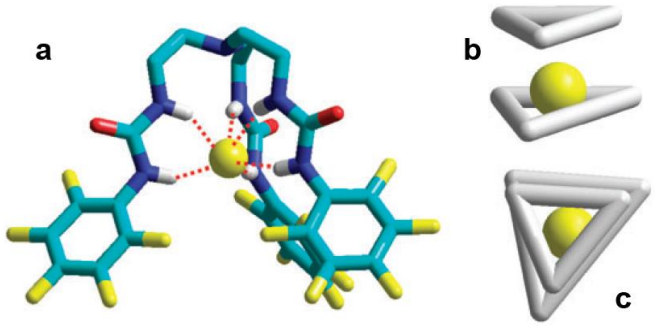

Fig. 5.12 - The crystal structure of the complex of receptor **14** with the fluoride anion.[15] (**b**) Side view of the triangles obtained (i) by linking the hydrogen atoms of the N–H groups bound to the tren framework and (ii) by linking the hydrogen atoms of the N-H groups bound the $–C_6F_5$ substituents, showing a trigonal prismatic coordination geometry. (**c**) Top view.

Convenient scaffolds to generate tetrapodands are calix[4]- arenes and porphyrins. In particular, porphyrins provide a rigid platform for implanting four urea containing arms, to generate a huge cavity. The binding tendencies of the porphyrin based tetra-urea receptor **15** (Fig. 5.13) towards anions in DMSO and in CH_2Cl_2 were investigated, [16,17] disclosing a pronounced solvent effect, whose nature could be explained thanks to the availability of the crystal structures of pertinent tetra-butylammonium complex salts,[16,18] shown in figure 5.14.

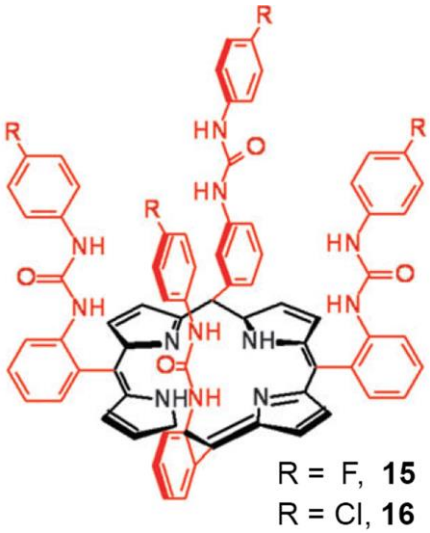

Fig 5.13

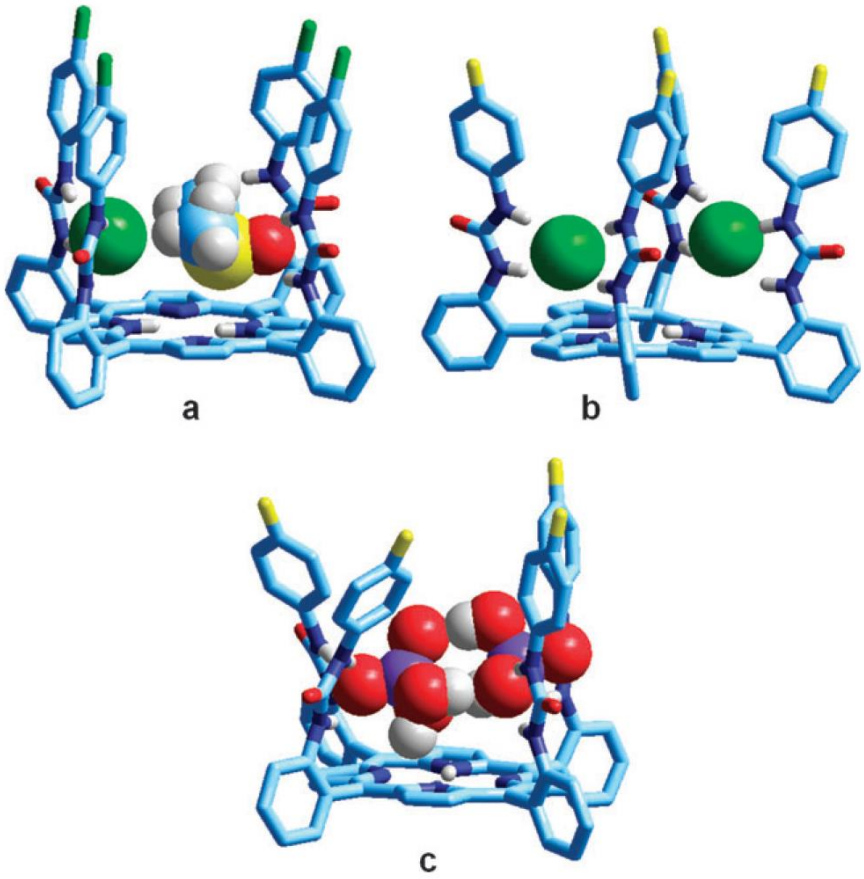

Fig. 5.14 - Crystal structures of the anion complexes with tetra-urea porphyrins. (a) Receptor **16**, whose cavity includes a Cl^- ion and a DMSO molecule.[16] (b) Receptor **15**, including two Cl^- ions. [18] (c) receptor **15** including the H-bond dimer $[H_2PO_4]_2^{2-}$.[18]

5.3. Thiourea based anion receptors

A variety of receptors containing a thiourea subunit have been developed and applied for anion complexation and sensing over the past years.[19,20–24] Therefore, thioureas have been taken as good hydrogen bond donors for the construction of receptors that may bind anions by two hydrogen bonds of the (thio)-ureido–NHs.

In general, the acidity of thioureido –NH protons is higher than that of the ureido–NHs, with pKa of 21.1 and 26.9 for thiourea and urea in DMSO, respectively.[25]

This leads to a stronger hydrogen bonding of an anion with thiourea than with the urea counterpart, an observation that is quite often taken to identify the thiourea anion binding site in the thiourea-based receptors. However, if the –NH protons are acidic enough, in particular when an electron-withdrawing substituent is introduced into the receptor molecule, deprotonation may occur in the presence of a highly basic anion, normally F^-. On the occurrence of –NH deprotonation, dramatic spectral changes with a concomitant solution color change may be observed.

The deprotonation of –NHs by F^- in anion sensing chemistry was first observed by the Gunnlaugsson group[26,27] and the Gale group.[28]

Later, Fabbrizzi et al. carried out a detailed study of the deprotonation of thioureas in the presence anions.[29]

Two step-wise processes are assumed in the deprotonation process, equilibria (1) and (2).

$$LH + X^- \rightleftharpoons [LH\cdots X]^- \qquad (1)$$

$$[LH\cdots X] + X^- \rightleftharpoons L^- + [HX_2]^- \qquad (2)$$

First, a genuine receptor–anion hydrogen bonding complex, $[LH\cdots X]^-$ is formed. Then, on further addition of the anion, one molecule of HX is released from the $[LH\cdots X]$ complex, leading to a self-complex $[HX_2]^-$ and deprotonated receptor L^-. Deprotonation normally occurs at the (thio)ureido-NH proton close to the more electron-withdrawing subunit. It appears that only one of the two (thio)ureido-NHs is deprotonated, if deprotonation occurs. The deprotonation process can be probed by ^1H NMR titrations and, luckily, by X-ray crystallography.

The solution color change following the formation of the urea/thiourea based receptor-anion complex has attracted a great deal of attention, also because this phenomenon may be exploited for the selective detection of anionic species in solution.

The novel colorimetric receptors for selective fluoride ion sensing containing anthraquinone as chromogenic signaling subunit and urea **17** and thiourea **18**

binding sites [30] represents a good example of what said above

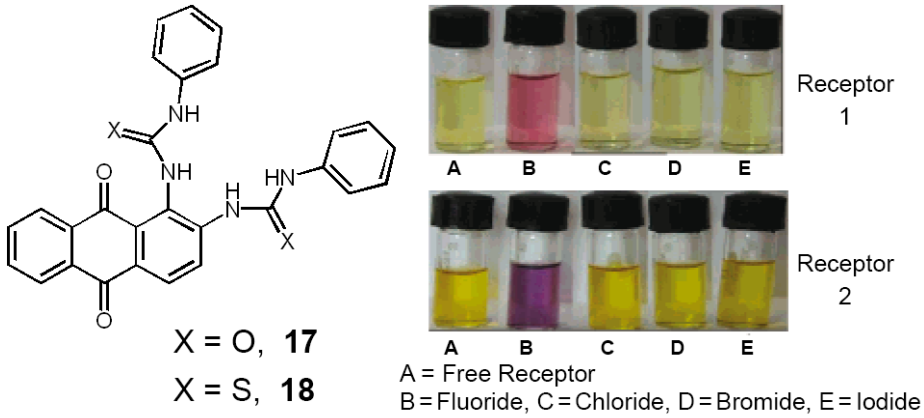

Fig. 5.15

As one can see in figure 5.15, these receptors have shown no affinity for other halide ions (Cl^-, Br^-, and I^- ions). Well-defined color change in the visible region of the spectrum was observed upon addition of fluoride ion in DMSO/CH_3CN solution of the receptors **17** and **18**.

The receptors, effectively and selectively, recognized the biologically important F^- and carboxylate anions from other anions such as Cl^- and Br^- in DMSO.

Other colorimetric anion sensors have been synthesized where 4-nitrophenyl was treated as a signaling unit and urea/thiourea moieties as binding sites. [31] Urea **19** and thiourea **20** were synthesized using the one-step reaction of 4,5-dimethyl-1,2-phenylenediamine and 4-nitrophenyl isocyanate or 4-nitrophenyl isothiocyanate in a reasonably good yield (Scheme 5.4).

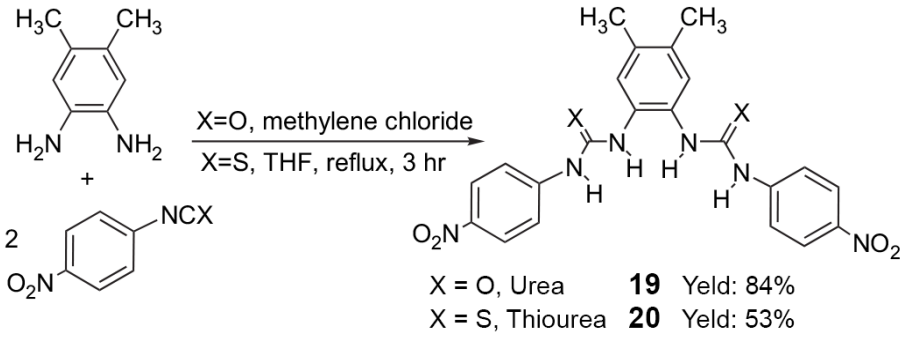

Scheme 5.4 - Synthesis of the receptors **19** and **20** [31].

The anion recognition is also detectable at room temperature with naked eyes as shown in Figure 5.16. Again, Cl^- and Br^- did not give any noticeable color changes in the DMSO solution of urea **19** and thiourea **20**. For urea **19**, only F^- gave significant color changes to reddish orange. Acetate ion made the solution turn pale yellow, but the color change was not noticeable at low concentration with naked eyes. Color change of thiourea **20** was much more sensitive to F^- than urea **19**. One equivalent of F^- was enough to recognize color change from colorless to yellow with naked eyes. More addition of F^- changed the color to reddish orange. In contrast to urea **19**, the solution of thiourea **20** with acetate ion turned yellow at low concentration of acetate ion and reddish orange at high concentration.

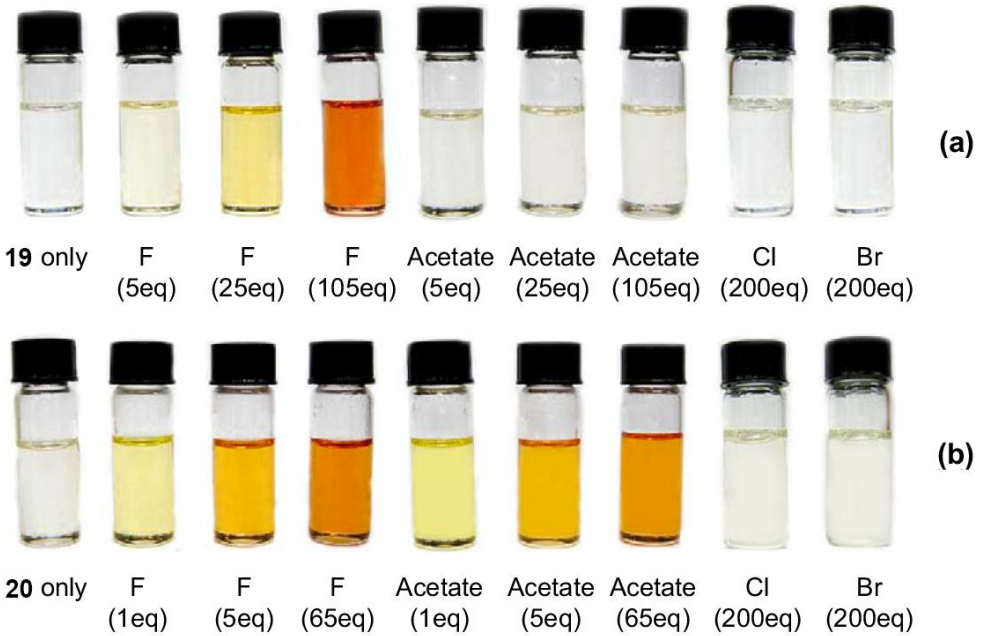

Fig 5.16 - Color changes observed for **19** and **20** in DMSO upon the addition of anions as tetraethylammonium salts at room temperature. (**a**) Urea **19** (2.5×10^{-5} M) and (**b**) thiourea **20** (2.5×10^{-5} M) (number of equivalents in parenthesis).

Other colorimetric chemosensors **21a–d** (Fig. 5.17) for dicarboxylate anions,[32] are based on an anthraquinone skeleton bearing thiourea groups linked through an ethylene spacer.[33]

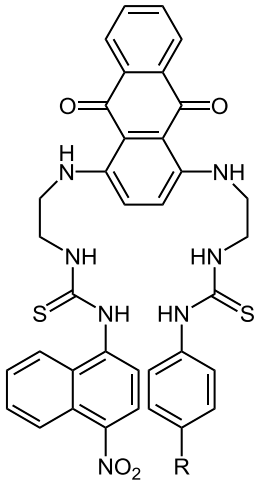

21a, R = CF_3
21b, R = NO_2
21c, R = CN
21d, R = H

Fig. 5.17

A 4-nitronaphthyl group is linked to one of the thiourea moieties, while the other chromophores (4-trifluoromethylphenyl, 4-nitrophenyl, 4-cyanophenyl and phenyl) are appended to the other thiourea group. The colorimetric sensor ability of discriminating maleates versus fumarates of 21a-d was tested by UV-Vis titration techniques. In particular, upon addition of maleate to receptor **21a** (Fig. 5.18a), a color change from dark-blue to dark-red in DMSO was observed which can be detected by the naked eye at part per million concentration (Fig. 5.18b). Similar color changes were observed with the other receptors and have been attributed to deprotonation of the thiourea moiety of the 4-nitronaphthyl chromophore. However, addition of fumarate, caused a change in the color of the solution from dark blue to yellow only for receptor **21a** (Fig. 5.18c), while no changes were observed with the other receptors.

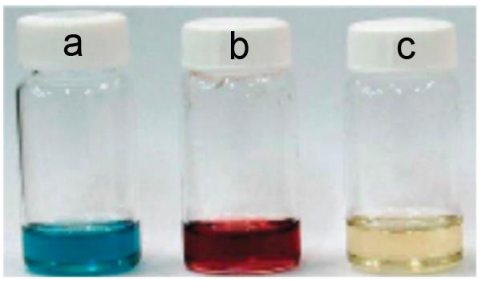

Fig. 5.18 - Color changes of **21a** upon addition of various anions in DMSO: (**a**) **21a** only; (**b**) **21a** + 2.0 equivalents of maleate; (**c**) **21a** +2.0 equivalents of fumarate.

Yet, a new family of [3]polynorbornane frameworks, **22** and **23**, exhibiting conformationally preorganized aromatic thiourea (cleft-like) receptors have been designed and synthesized for anion recognition. [34]

These show excellent affinity for the biologically relevant dihydrogenphosphate ($H_2PO_4^-$) and dihydrogenpyrophosphate ($H_2P_2O_7^{2-}$) anions (among others), which are bound in 1:1 and 2:1 (host-anion) ratio, respectively. Moreover, visually striking color changes accompany guest binding, enabling this family to act as colorimetric anion sensors. A visibly perceptible color change was observed during each titration, which is consistent with the anion hydrogen bonding to the thiourea receptor. This would be expected to affect the efficiency of the ICT (intramolecular charge transfer) character of the resulting receptor-anion complex and lead to these spectral changes. Of the anions tested, the strongest color changes were observed for F^-, which showed a distinctive change from light yellow to red (see Figure 5.19).

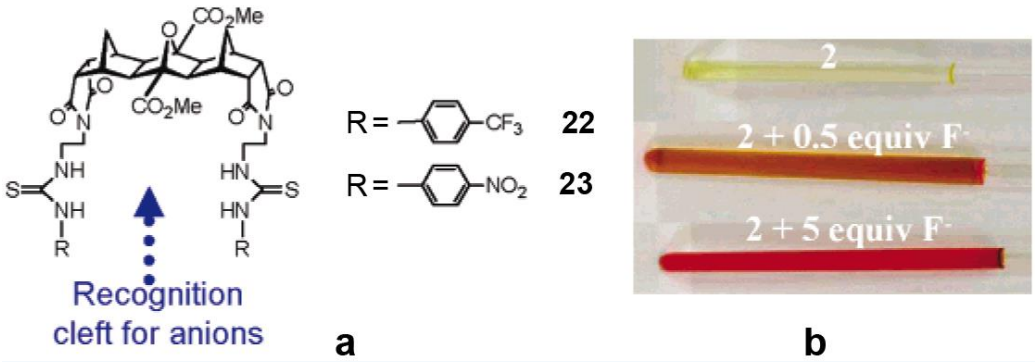

Fig. 5.19 – (**a**) A new family of [3]polynorbornane frameworks, **22** and **23**, exhibiting conformationally preorganized aromatic thiourea (cleft-like) receptors; (**b**) colour change of **23** upon addition of F^-.[34]

This brief survey on selective detection of anionic species in solution will be concluded with a due tribute to professor Fabbrizzi, of whom two examples among a great many will be reported in the following. The first one concerns the anion coordinating properties of the two fluorogenic ureas L^1H and L^2H (Fig. 5.20), containing the 2-anthracenyl and 1-pyrenyl moieties as signaling units [35]

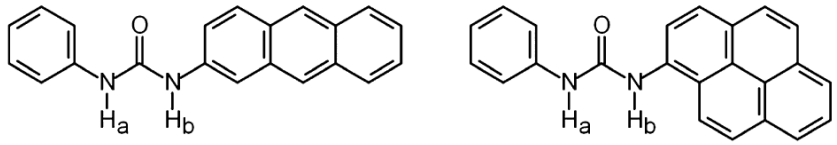

L^1H L^2H

Fig. 5.20

The formation of stable 1:1 receptor-anion H-bond complexes has been confirmed by structural studies on the crystalline $[Bu_4N]$- $[L^1H \cdots Cl]$ and $[Bu_4N][L^2H \cdots CH_3COO]$ salts (Fig. 5.21).

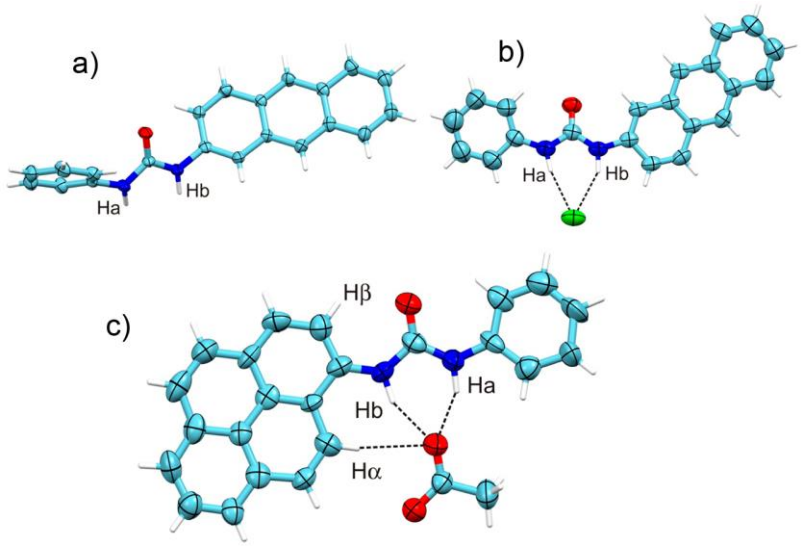

Fig. 5.21 - Molecular structures of: (**a**) L^1H; (**b**) $[L^1H \cdots Cl]^-$;(**c**) $[L^2H \cdots CH_3COO]^-$

Complexation induces significant variations of the emission properties of L^1H and L^2H according to a multifaceted behavior, which depends upon the fluorogenic substituent, the solvent, and the basicity of the anion. Poorly basic anions (Cl^-, Br^-) cause a red shift of the emission band(s). Carboxylates (CH_3COO^-, $C_6H_5COO^-$) induce fluorescence quenching due to the occurrence of an electron transfer process taking place in the locally excited complex $[*L\text{-}H \cdots X]^-$.

However, this excited complex may undergo an intracomplex proton transfer from one urea N−H fragment to the anion, to give the tautomeric excited complex $[L \cdots H{-}X]^-*$, which emits at higher wavelength. F^- displays a unique

behavior: It forms with L^1H a stable $[L{-}H\cdots F]^-$ complex which in the excited state undergoes intracomplex proton transfer, to give the poorly emissive excited tautomer $[L\cdots H{-}F]^-$*. With L^2H, on moderate addition of F^-, the 1:1 H-bond complex forms, and the blue fluorescence of pyrene is quenched. Large excess addition of F^- promotes deprotonation of the ground-state complex, according to the equilibrium $[L^2H\cdots F]^- + F^- \rightleftharpoons [L^2]^- + HF_2^-$. The deprotonated receptor $[L^2]^-$ is distinctly emissive (yellow fluorescence), which generates the fluorimetric response $ON^1{-}OFF{-}ON^2$ of receptor L^2H with respect to F^- (Fig. 5.22).

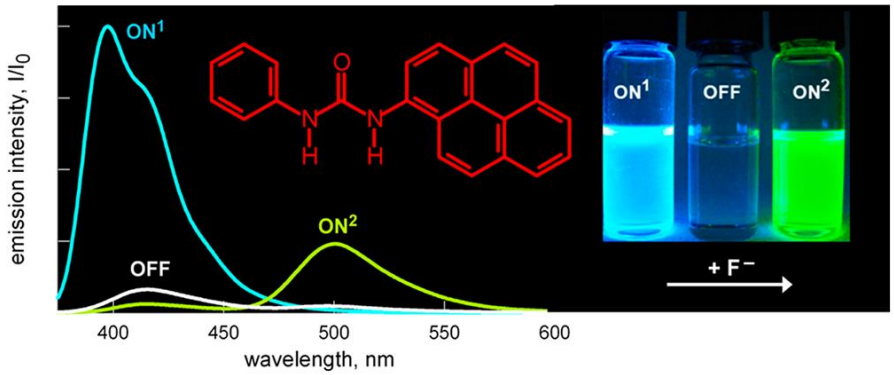

Fig. 5.22. - Emission spectra taken upon addition of $[Bu_4N]F$ to L^2H (0.01 mM) in MeCN. Cyan line is spectrum of the free receptor (L^2H, ON^1); white line is spectrum of L^2H taken upon addition of 75 equiv of $[Bu_4N]F$ (corresponding to $[L^2H\cdots F]^-$, OFF); and yellow line is spectrum taken after the addition of 1000 equiv of $[Bu_4N]F$ (corresponding to $[L^2]^-$, ON^2). Inset: pictures of samples taken in the dark on UV illumination.

The second report among Fabbrizzi's papers concerns Urea-based receptors, containing electron-withdrawing chromogenic substituents. [36]

These compounds in a DMSO solution, in the presence of varying excess of fluoride, do not form H-bond complexes, but undergo stepwise deprotonation of the two N−H fragments, an event which is signaled by the development of vivid colors (Fig. 5.23). Double deprotonation is also observed in the presence of hydroxide. Less basic anions (CH_3COO^-, $H_2PO_4^-$) induce deprotonation of only one N−H.

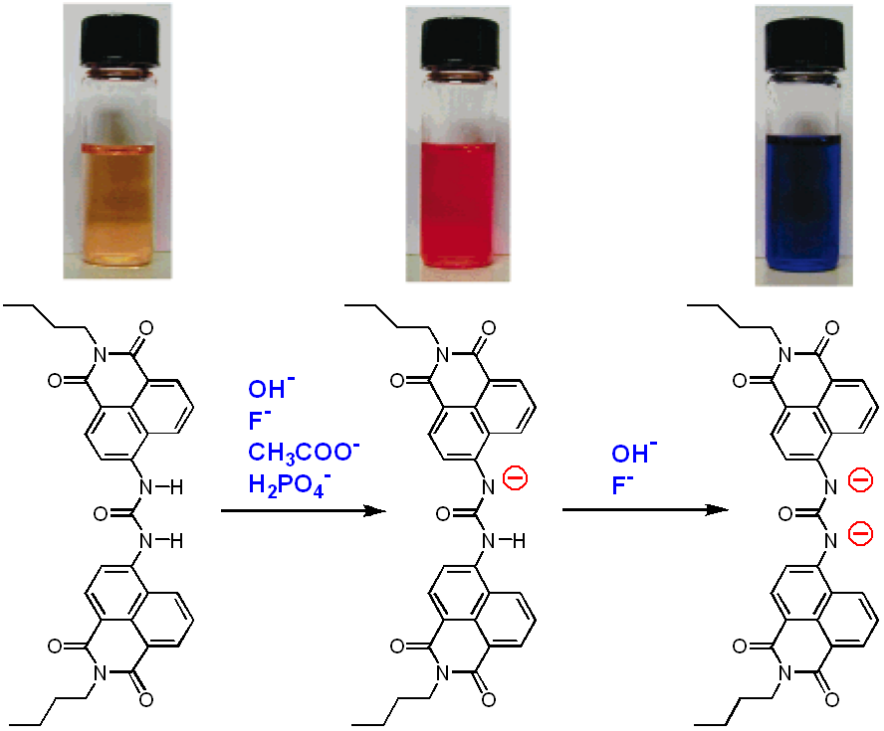

Fig. 5.23

References

[1] P. J. Smith, M. V. Reddington and C. S. Wilcox, *Tetrahedron Lett.*, **1992**, 33, 6085–6088.

[2] E. Fan, S. A. van Arman, S. Kincaid and A. D. Hamilton, *J. Am.Chem. Soc.*, **1993**, 115, 369–370.

[3] D. Meshcheryakov, M. Bolte and V. Boöhmer, *Tetrahedron Lett.*, **2010**, 51, 1202–1204.

[4] M. Boiocchi, L. Del Boca, D. Esteban-Gómez, L. Fabbrizzi, M. Licchelli and E. Monzani, *J. Am. Chem. Soc.*, **2004**, 126, 16507–16514.

[5] M. Boiocchi, L. Del Boca, D. Esteban-Gómez, L. Fabbrizzi, M. Licchelli and E. Monzani, *Chem.–Eur. J.*, **2005**, 11, 3097–3104.

[6] G. Schwarzenbach, *Helv. Chim. Acta*, **1952**, 35, 2344–2359.

[7] D. K. Cabbiness and D. W. Margerum, *J. Am. Chem. Soc.*, **1969**, 91, 6540–6541.

[8] J.-M. Lehn, *Acc. Chem. Res.*, **1978**, 11, 49–57.

[9] S. J. Brooks, P. R. Edwards, P. A. Gale and M. E. Light, *New J. Chem*., **2006**, 30, 65–70.

[10] M. Formica, V. Fusi, E. Macedi, P. Paoli, G. Piersanti, P. Rossi, G. Zappia and P. Orlando, *New J. Chem*., **2008**, 32, 1204–1214.

[11] V. Amendola, M. Boiocchi, D. Esteban-Gómez, L. Fabbrizzi and E. Monzani, *Org. Biomol. Chem*., **2005**, 3, 2632–2639.

[12] M. Formica, V. Fusi, E. Macedi, P. Paoli, G. Piersanti, P. Rossi, G. Zappia and P. Orlando, *New J. Chem*., **2008**, 32, 1204–1214.

[13] C. N. Carroll, O. B. Berryman, C. A. Johnson, L. N. Zakharov, M. M. Haley and D. W. Johnson, *Chem. Commun*., **2009**, 2520–2522.

[14] D. Meshcheryakov, F. Arnaud-Neu, V. Böhmer, M. Bolte, V. Hubscher-Bruder, E. Jobin, I. Thondorf and S. Werner, *Org. Biomol. Chem*., **2008**, 6, 1004–1014.

[15] I. Ravikumar, P. S. Lakshminarayanan, M. Arunachalam, E. Suresh and P. Ghosh, *Dalton Trans*., **2009**, 4160–4168.

[16] R. C. Jagessar, M. Shang, W. R. Scheidt and D. H. Burns, *J. Am. Chem. Soc*., **1998**, 120, 11684–11692.

[17] D. H. Burns, K. Calderon-Kawasaki and S. Kularatne, *J. Org. Chem*., **2005**, 70, 2803–2807.

[18] K. Calderon-Kawasaki, S. Kularatne, Y. H. Li, B. C. Noll, W. R. Scheidt and D. H. Burns, *J. Org. Chem*., **2007**, 72, 9081–9087.

[19] C. Caltagirone and P. A. Gale, *Chem. Soc. Rev*., **2009**, 38, 520–563

[20] P. A. Gale, S. E. Garcia-Garrido and J. Garric, *Chem. Soc. Rev*., **2008**, 37, 151-190.

[21] P. A. Gale, *Acc. Chem. Res*., **2006**, 39, 465–475.

[22] P. A. Gale and R. Quesada, *Coord. Chem. Rev*., **2006**, 250, 3219–3244.

[23] T. Gunnlaugsson, M. Glynn, G. M. Tocci, P. E. Kruger and F. M. Pfeffer, *Coord. Chem. Rev*., **2006**, 250, 3094–3117.

[24] V. Amendola, M. Bonizzoni, D. Esteban-Gómez, L. Fabbrizzi, M. Licchelli, F. Sancenn and A. Taglietti, *Coord. Chem. Rev*., **2006**, 250, 1451–1470.

[25] F. G. Bordwell, *Acc. Chem. Res*., **1988**, 21, 456–463.

[26] T. Gunnlaugsson, P. E. Kruger, T. C. Lee, R. Parkesh, F. M. Pfeffer and G. M. Hussey, *Tetrahedron Lett*., **2003**, 44, 6575–6578.

[27] T. Gunnlaugsson, P. E. Kruger, P. Jensen, F. M. Pfeffer and G. M. Hussey, *Tetrahedron Lett*., **2003**, 44, 8909–8913.

[28] S. Camiolo, P. A. Gale, M. B. Hursthouse and M. E. Light, *Org. Biomol. Chem*., **2003**, 1, 741–744.

[29] V. Amendola, D. Esteban-Gómez, L. Fabbrizzi and M. Licchelli, *Acc. Chem. Res*., **2006**, 39, 343–353.

[30] D. Amilan Jose, D. Krishna Kumar, Bishwajit Ganguly, and Amitava Das *Org. Lett.*, **2004**, 6, 3445-3448

[31] Yeong-Joon Kim, Han Kwak, Se Jin Lee, Je Sin Lee, Hyun Jung Kwon, Sang Ho Nam, Kyoungrim Lee and Cheal Kim. *Tetrahedron* 62 (**2006**) 9635–9640

[32] Y. P. Yen and K. W. Ho, *Tetrahedron Lett*., **2006**, 47, 1193–1196.

[33] Y. P. Tseng, G. M. Tu, C. H. Lin, C. T. Chang, C. Y. Lin and Y. P. Yen, *Org. Biomol. Chem*., **2007**, 5, 3592–3598.

[34] F.M. Pfeffer, T. Gunnlaugsson, P. Jensen, and P. E. Kruger. *Org. Lett*., **2005**, 75357-5360

[35] V. Amendola,. G. Bergamaschi, M. Boiocchi, Luigi Fabbrizzi, L. Mosca. *J. Am. Chem. Soc*. **2013**, 135, 6345−6355

[36] D. Esteban-Gómez, L. Fabbrizzi, and M. Licchelli *J. Org. Chem.*, **2005**, 70 (14), pp 5717–5720

6. Pyrrole based anion receptors

The anion complexation chemistry of the most simple pyrrole systems has recently begun to be explored. For example, tetramethylammonium chloride has been recrystallized from pyrrole yielding a pyrrole–chloride complex (**a**) (Fig. 6.1) that has been crystallographically characterized [1].

Complex (**a**) contains a chloride anion that is bound by hydrogen bonds from two pyrrole rings and a tetramethylammonium cation.

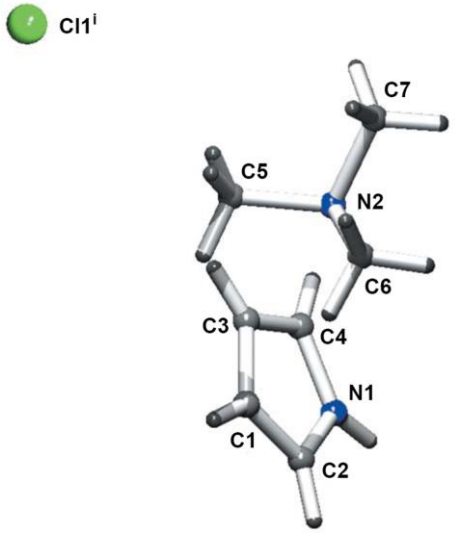

Fig. 6.1 - Asymmetric unit and numbering scheme of complex (**a**).

The asymmetric unit of structure (**a**), shown in figure 6.1, is comprised of a single pyrrole, co-crystallized with half a chloride anion and a partial tetramethyl-ammonium cation situated on the mirror plane of the space group. The supramolecular structure of the crystal depicted in figure 6.2 shows the chloride anion to be hydrogen bonded to two pyrrole heterocycles, in addition to a presumably weaker interaction to the tetramethyl-ammonium cation,

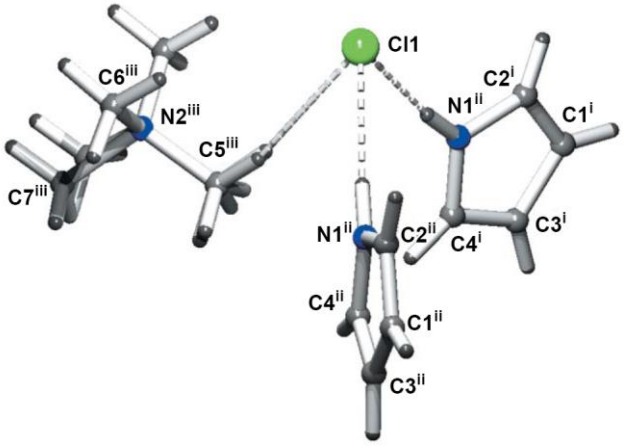

Fig. 6.2 - The supramolecular structure of (**a**)

2,5-Diamidopyrroles **1** and **2** (Fig. 6.3) have been shown. to be oxo-anion selective receptors in DMSOd6/0.5% water and acetonitrile solutions [2,3].

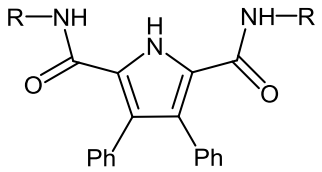

1: R = n-Bu

2: R = Ph

Fig. 6.3

The synthesis and anion binding properties of new acyclic pyrrole receptorsbased that incorporate a central pyridine ring flanked by twopyrroles through 2-aminopyrrole-derived amide bonds have been reported (**3, 4).** Additionally a model system where the central pyridinehas being replaced by a phenyl ring (**5**) was synthesised as well as a receptor in which the configuration of the amide linkages is reversed (**6**) (Fig. 6.4). [4]

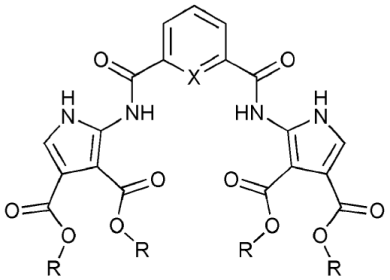

3: R = CH_2CH_3; X = N

4: R = $CH_2CH_2C(CH_3)_3$; X = N

5: R = CH_2CH_3; X = CH

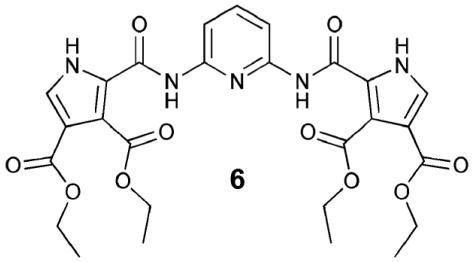

Fig. 6.4

Receptor **4** binds acetate selectively (13900 M^{-1} in dichloroethane), while receptor **5** showed only a weak or no interaction with the anions studied. This data provides further evidence that thepyridine nitrogen atom plays an important role in stabilizing the receptor in a conformation that favours anion complexation. Interestingly receptor **6** in which the amide bonds are reversed has completely different substrate selectivity, being selective for chloride (805 M^{-1} in dichloroethane).

Lastly, as an interesting example of pre-organized receptors, a class of adamantane-dipyrromethane derivatives **7-10** (Fig. 6.5)is here show. In these compounds the bulky adamantane units hinder the rotational mobility of the pyrrole moieties, conferring a higher degree of pre-organisation to the receptors.[5]

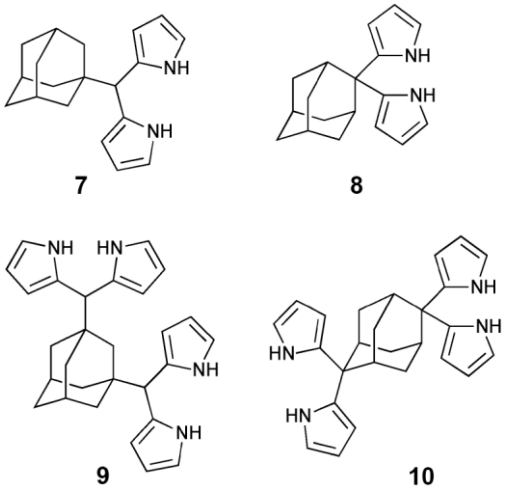

Fig, 6.5

Compounds **7-10** form complexes with chloride, bromide, benzoate, hydrogen sulfate and dihydrogen phosphate characterised by a 1:1 stoichiometry and lower stability constants by 2–3 orders magnitude.

In the following some exsamples some cyclic pyrrole based receptors will be shown. The first ones are three bipyrrole or dipyrromethane based amido-imine hybrid macrocycles, **11-13** (Fig. 6.6), based on substituted pyrrole units. [6]

The three receptors display very high affinities for oxoanions with stability constants determined by UV-Vis titrations in CH_3CN on the order of 107 M^{-1}. Only receptor **11** is able to bind the large perrhenate anion (Ka=124000 M^{-1}), while the most structurally rigid receptor **13** shows a preference for chloride (Ka = 281000 M^{-1}).This unusual preference for a spherical halide was rationalized on the basis of DFT modeling calculations and single-crystal X-ray diffraction studies . It was shown that in the chloride complex all the pyrrole rings and the two amide groups point into the cavity. As a consequence, the size of the cavity is relatively small and only spherical anions such as chloride or bromide can be accommodated in this fashion.

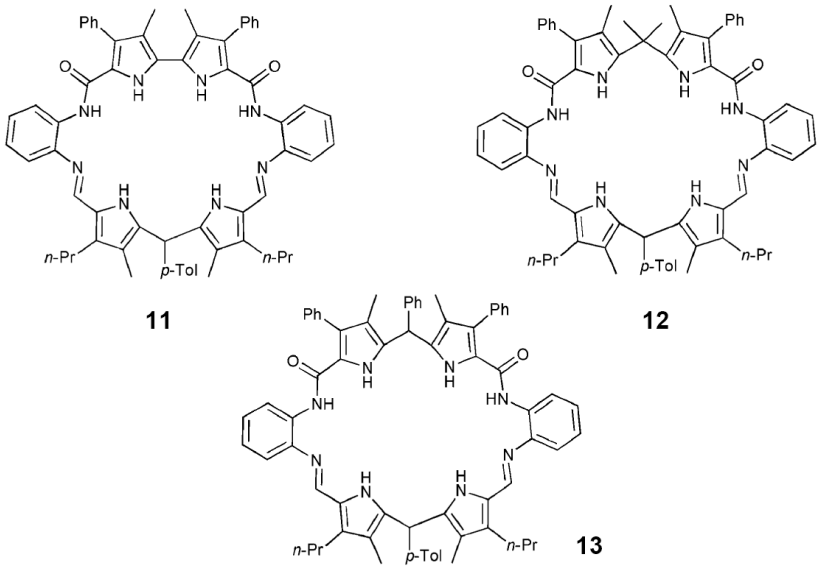

Fig. 6.6

Other large oligopyrrolic macrocycles are here reported,[7] namely compounds **14**, **15** and **16** (fig. 6.7).

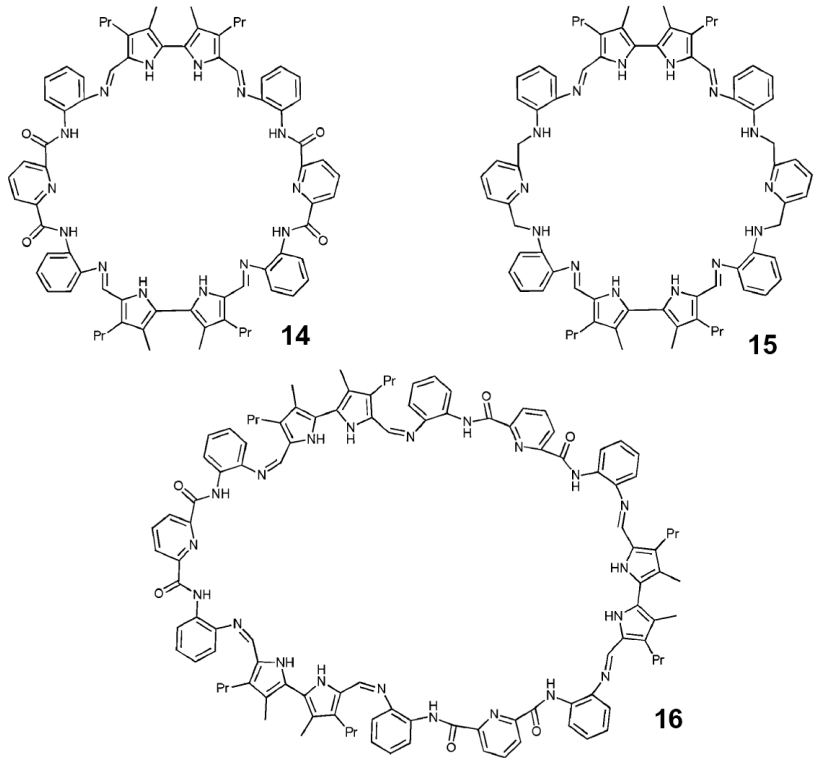

Fig. 6.7

The crystal structure of **16**H^{2+}·HPO_4^{2-} is shown in figure 6.8. The macrocycle twists to encapsulate anion, binding it via 12 hydrogen-bonding interactions.

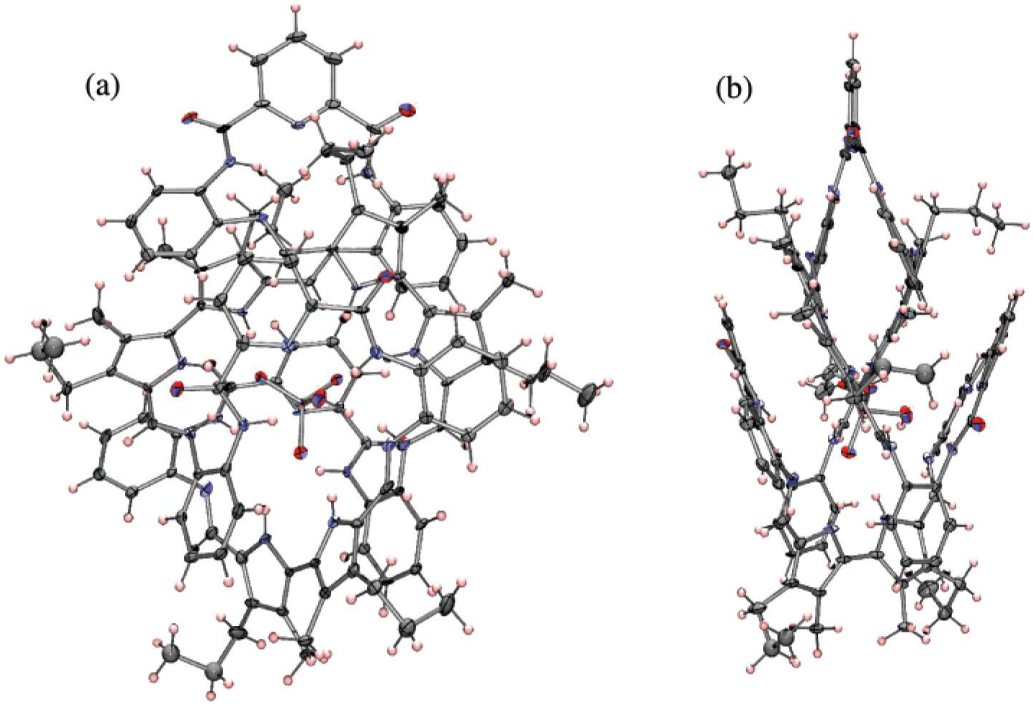

Fig. 6.8 - ORTEP POV-ray rendering of the structure of **16**H^{2+}·HPO_4^{2-} as deduced from a single-crystal X-ray diffraction analysis: (**a**) view along the c-axis and (**b**) view along the a-axis.

The anion binding properties of the three macrocycles have been explored by UV-Vis titrations in CH_3CN at 23 °C with a variety of anions (Cl^-, Br^- , NO_3^-, CH_3COO^-, ClO_4^-, ReO_4^-, HSO_4^- and $H_2PO_4^-$) (Fig. 6.9). All the receptors display a strong preference for HSO_4^- and $H_2PO_4^-$.

Fig. 6.9 - Colors of CH_3CN solutions of receptor **16**:

(**1**) free macrocycle
(**2**) with $(Nbu_4)^+$ Cl^-
(**3**) with 1 equiv. of $(Nbu_4)^+$ HSO_4^-
(**4**) with 1 equiv. of $(Nbu_4)^+$ $H_2PO_4^-$
(**5**) with ≥2 equiv. of $(Nbu_4)^+$ $H_2PO_4^-$

Cyclopyrroles are remarkable structures synthesised by anion templated macrocyclisation procedures and consisting solely of linked pyrrole rings.[8]

Sessler and co-workers have reported the synthesis of new functionalised cyclo[8]pyrrole derivative*s* **17a-c** that have been isolated in the form of their sulfuric acid salts (Fig. 6.10).[9]

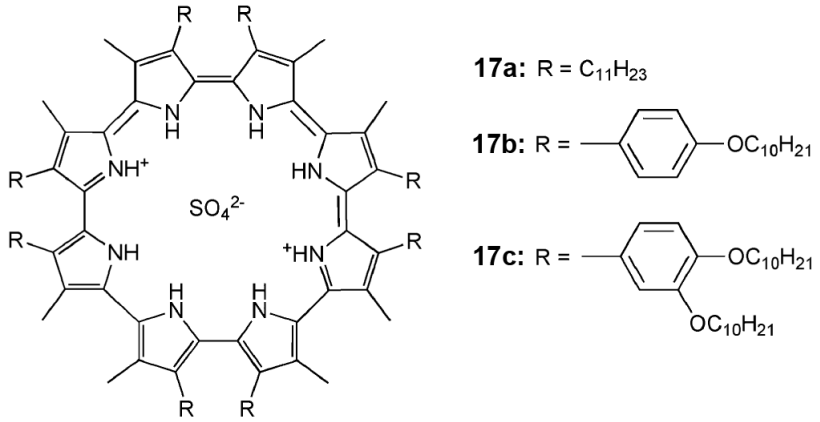

Fig. 6.10

These species possess large p-electron-rich surfaces and form hexagonal columnar mesophases when combined with electrondeficient acceptors, such as trinitrofluorenone, trinitrobenzene, trinitrophenol and trinitrotoluene (Fig. 6.11).

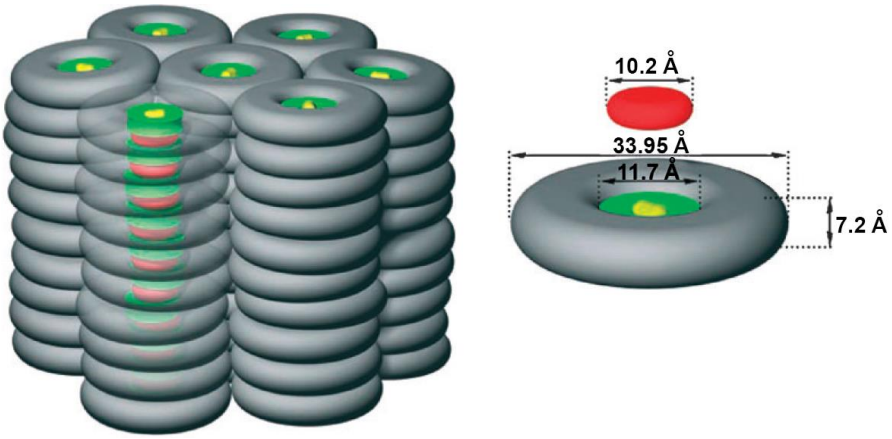

Fig. 6.11 - Idealised packing diagram for the hexagonal columnar liquid crystalline phase of **17c**·trinitrobenzene (TNB) adduct. TNB molecules (red) intercalate into stacks of cyclo[8]pyrrole cores (green; sulfate ions in yellow).

This brief survey on cyclo-pyrrole anion receptor chemistry will be concluded by a focused view on the wide class of calyx[4]pyrroles. Calix[4]pyrroles are macrocyclic compounds consisting of four pyrrole units linked via fully substituted sp^3 hybridized meso carbon atoms (Scheme 6.1). They are effective receptors for Lewis basic anions (e.g., halides) in typical organic media and under certain conditions will recognize ion pairs containing charge diffuse cations, such as a small alkylammonium, imidazolium, or cesium cations. The calix[4]pyrrole framework is further attractive in that it is relatively easy to modify. In particular, functionalization of the β-pyrrolic carbon and meso-carbon atoms with simple crown ethers or calix[4]arene crown ethers can produce heteromultitopic ion pair receptors containing more than two cation binding sites. This allows the interactions between receptors and ions to be manipulated on a higher level than can be achieved using simple ion receptors or heteroditopic ion pair receptors and has made these systems attractive for use in ion transport, recognition, and extraction.

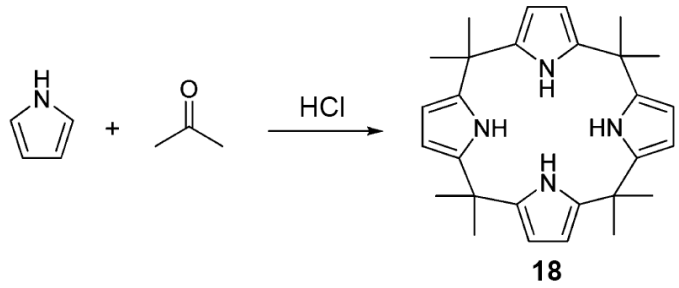

18

Scheme 6.1 - Synthesis of Calix[4]pyrrole **18**

Unsubstituted calix[4]pyrrole **18** can exist in four limiting conformations, namely, the so-called cone, partial cone, 1,2- alternate, and 1,3-alternate conformations.[10−12]

In noncompetitive solvents, these conformations are in fast equilibrium on the NMR time scale at room temperature.[10−12] In contrast, several crystal structures have served to reveal that calix[4]pyrrole **18** adopts the 1,3-alternate conformation favorably in the solid state. In contrast, the cone conformation dominates forthe anion-bound form, both in solution and in the solid state (Fig. 6.12).

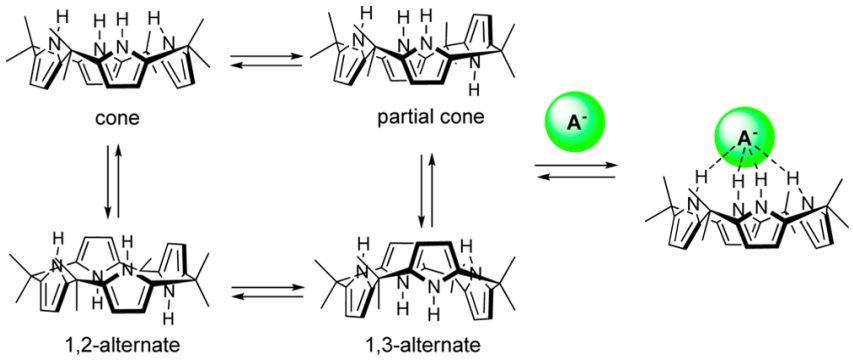

Fig. 6.12 - Four possible conformations of calix[4]pyrrole **18**. These are shown in schematic form, along with the equilibrium that serves to interconvert them in the absence of an anion. The cone conformation dominates for the anion bound form.

Early evidence that calix[4]pyrrole **18** can function as an ion pair receptor came from single crystal X-ray diffraction analyses of complexes containing charge diffuse cations.[13]

The structures of several cesium halide complexes of **1** revealed, for instance, that the halide anions are bound to all four pyrrolic NH protons via hydrogen bonds (Fig. 6.13).

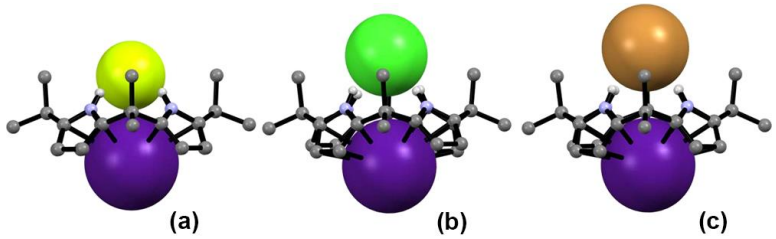

Fig. 6.13 - Single crystal X-ray diffraction structures of (**a**) the CsF, (**b**) CsCl, and (**c**) CsBr complexes of calix[4]pyrrole **18**.

Concurrently, the cesium countercations were found to be encapsulated by the bowl-shaped electron-rich calix[4]pyrrole cavity that is produced when the macrocycle becomes fixed in the cone conformation as a result of anion binding (Fig. 6. 13). Based on the structural parameters, it was inferred that the cesium cation is held in place via a combination of π-cation complexation and dipole interactions.

Two phase liquid−liquid extraction experiments using nitrobenzene and water provided direct support for the proposition that calix[4]pyrrole **18** can act as an effective ion pair receptor.[14]

It was demonstrated by these extraction studies that calix[4]pyrrole **18** is able to extract cesium halide salts, such as CsCl and CsBr, but not $CsNO_3$, from an aqueous phase into a relatively polar organic phase consisting of nitrobenzene. Under conditions of extraction, an ion-paired 1:1:1 cesium/calix[4]pyrrole/halide complex (halide = chloride or bromide) is formed in the nitrobenzene phase. The process of solvent extraction was proposed to take places via three thermochemical steps (Fig. 6.14).

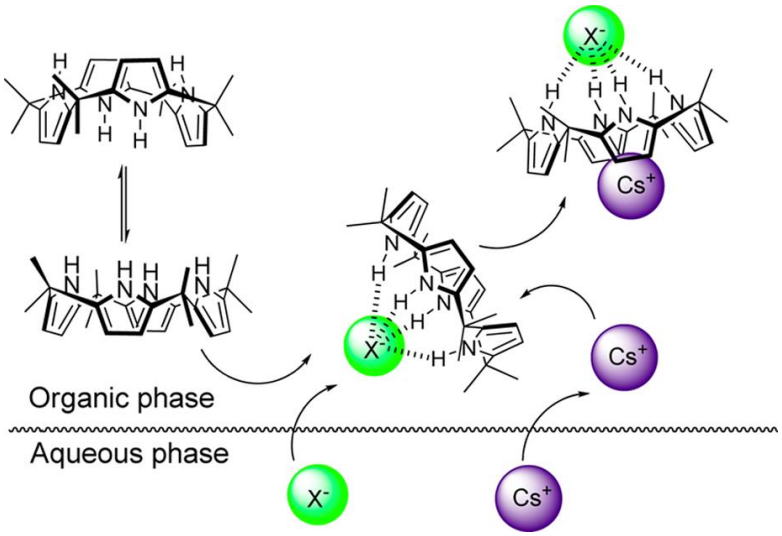

Fig. 6.14

First, the cesium cations and the halide anions partition into the nitrobenzene phase from the water phase. The conformation of calix[4]pyrrole **18** then switches to the cone conformation as the result of halide anion binding. Finally, the cesium cation is encapsulated within the calix[4]-pyrrole cavity formed as a result of the conformational change occurring in the second step.[21]

The anion-bound, cone-shaped calix[4]pyrrole cavity is also capable of interacting with certain organic cations, including imidazoliums, pyridiniums, and tetraalkylammoniums, thereby forming ion pair complexes.[20] This was revealed, for example, by single crystal X-ray structural analyses of the complexes formed between **18** and either 1-butyl-3-methylimidazolium chloride **19** or 1-butyl-3-methylimidazolium bromide **20** (Fig. 6.15); in both cases, the imidazolium cations were found to be included in the cone-shaped calix[4]pyrrole cavity. They are held in place via presumed CH−π interactions involving the acidic CH groups in the 4- and 5-positions of the imidazolium ring and the π-electron clouds of two of the four pyrrole rings that make up the

calix[4]pyrrole cone (Fig. 6.15). [20] Similar binding interactions were observed between calix[4]pyrrole **18** and 1-ethyl-3-methylimidazolium bromide **21**.

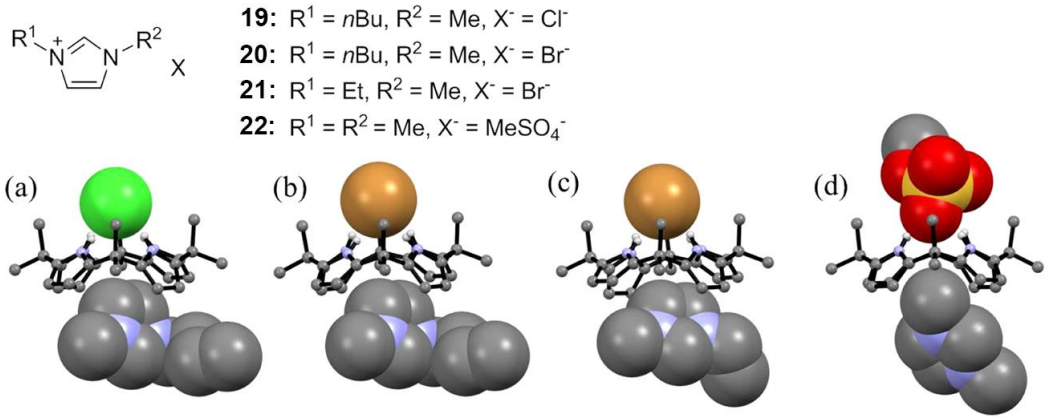

Fig. 6.15 - Single crystal X-ray diffraction structures of complexes (a) (**18·19**), (b) (**18·20**), (c) (**18·21**), and (d) (**18·22**).

One of the more appealing strategies for constructing calix[4]pyrrole-based ion pair receptors is to introduce cation binding sites into β-pyrrolic positions of the parent calix[4]pyrrole **18**.[15]

The first β-octaalkyl substituted calix[4]pyrrole derivative **6** was synthesized by the reaction of *N*-tosylpyrrolidine pyrrole with acetone in the presence of 1.0 equiv of trifluoroacetic acid (TFA) (Scheme 6.2).[15]

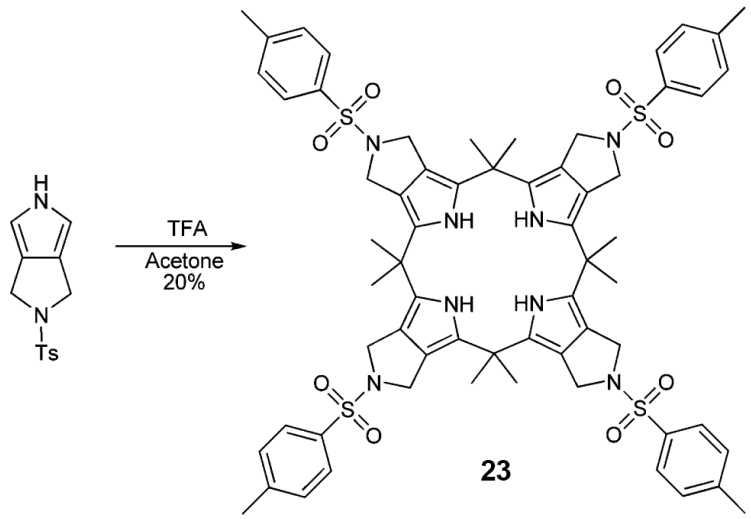

Scheme 6.2

The affinity of calix[4]pyrrole **23** for tetraalkylammonium halide ion pairs were determined by isothermal titration calorimetry (ITC) analyses in chloroform; the resulting values were found to be considerably enhanced relative to what is seen for unsubstituted calix[4]pyrrole **18**.[15] This enhancement is ascribed to the presence of additional stabilizing interactions between the tetraalkylammonium cations and the four tosyl groups as evidenced by the X-ray crystal structure of the $[Nbu_4]Cl$ complex, [**23**·$[Nbu_4]Cl$] (Fig. 6.16). In this case, the tetraalkylammonium cation is encapsulated by the four tosyl groups, which are brought together in proximity as a result of chloride anion binding.[15]

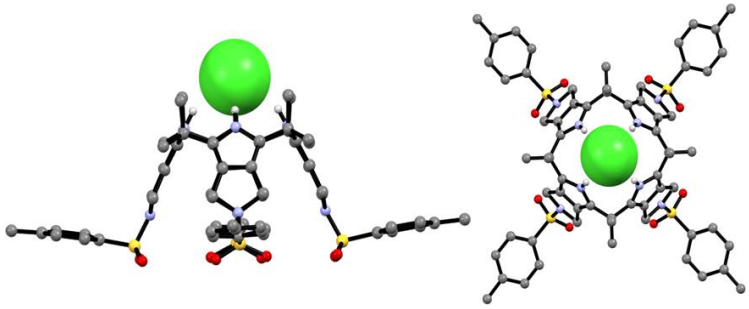

Fig. 6.16 - Two different views of the single crystal structure of **23**·$[Nbu_4]Cl$. Most hydrogen atoms have been removed for clarity. The countercation, $[Nbu_4]^+$, sitting in the cavity formed by four sulfonyl groups, is disordered and is not shown.

In an effort to create ion pair receptors with an improved ion binding property, simple crown ethers of different ring sizes have been linked to the meso-carbon atoms of the calix[4]pyrrole framework. Examples include compounds **24** and **25** (Fig. 6.17).[16,17]

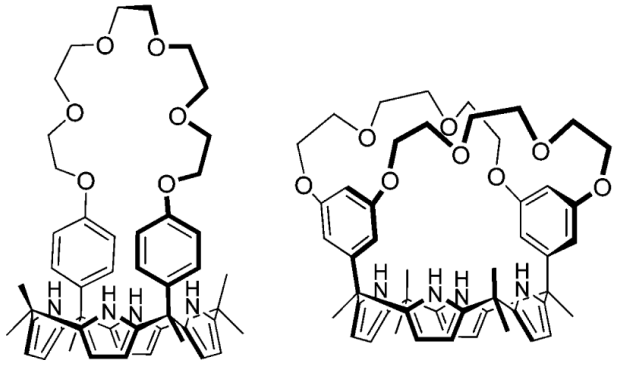

24 **25**

Fig. 6.17

Evidence that receptor **24** acts as an ion pair receptor came from a single crystal X-ray diffraction analysis of the CsCl complex of **24**. The resulting crystal structures revealed that receptor **24** interacts with CsCl in two different binding modes to form a 2:2 ion pair complex (Fig. 6.18). One cesium ion is coordinated by four oxygen atoms of the crown ether ring, as well as by two oxygen atoms from a different molecule. The other cesium ion is sandwiched between two cone shaped calix[4]pyrroles via apparent π–cation interactions. The chloride anions are hydrogen-bonded to the NH protons of the two calix[4]pyrroles that make up theoverall 2:2 complex (Fig. 6.18).[16]

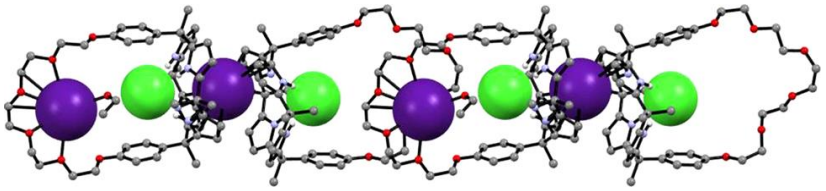

Fig. 6.18 - Single crystal X-ray structure of the cesium chloride complexes of receptor **24**. Most hydrogen atoms have been removed for clarity.

^{1}H NMR spectroscopic analyses in 10% CD_3OD in $CDCl_3$ provided evidence that receptor **24** is also able to bind alkali metal halide salts in solution. When the fluoride and chloride complexes of receptor **24** were treated with alkali metal ions (as their perchlorate salts), varying ion binding behavior, including ion pair complexation and anion decomplexation, was observed.

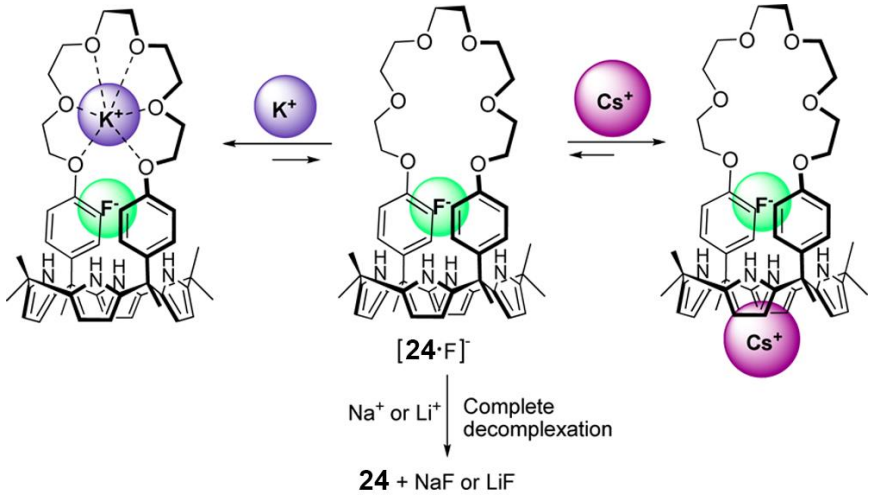

Fig. 6.19 - Schematic representation of the effect of treating complex [**24**·F^-] (tetrabutylammonium salt) with perchlorate salts of various alkali metal cations in 10% CD_3OD in CD_3CN.

In the specific case of fluoride, it was concluded that the cesium cation resides within the cone-shaped calix[4]pyrrole cavity, while the potassium cation is coordinated to the oxygen atoms of the crown ether ring (Fig. 6.19). Finally, it was found that treatment of [**24**·F^-] with either a Li^+ or Na^+ cation source induces decomplexation of the prebound F^- anion; this produces the ion-free receptor **24** and either LiF or NaF.[16]

Different behavior was seen upon the addition of akali metal cations to the chloride anion complex of receptor **24** ([**24**·Cl^-]; tetrabutylammonium salt). In contrast to what was seen with [**24**·F^-], the lithium cation is bound to the crown ether ring present in [**24**·Cl^-], forming an ion pair complex of [**24**·LiCl]. On the other hand, addition of the potassium cation causes partial decomplexation of the bound chloride anion (Fig. 6.20).

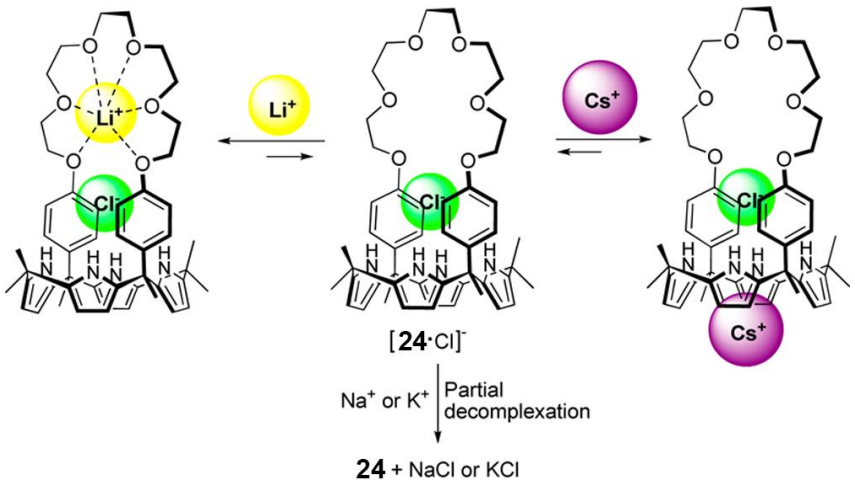

Fig. 6.20 - Schematic representation of the complexation and decomplexation events seen for [**24**·Cl^-] (NBu_4^+ salt) upon exposure to various alkali metal cations (as perchlorate salts) in CD_3CN.

In the case of the ion pair receptor **25**,[17] single crystal X-ray crystal structural analyses served to establish the formation of stable ion pair complexes with CsF and LiCl in the solid state (Fig. 6.21). Two different complexation modes were observed. CsF forms an ion pair complex wherein the cesium cation is held within the cone shaped calix[4]pyrrole cavity. It also interacts with two oxygen atoms of the crown ether ring of a different molecule. In contrast, LiCl

forms a 2:2 ion pair complex with receptor **25** where two lithium cations are sandwiched by the crown ether rings from two different receptor molecules, while the chloride anions are hydrogen bonded to the pyrrolic NH protons. The bound Li^+ cation and Cl^- anion are separated by water molecules. The net result is a solvent-separated ion pair complex.[17]

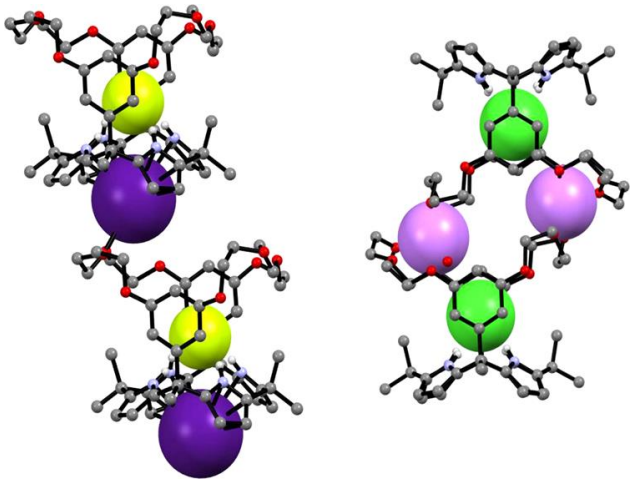

Fig. 6.21 - Single crystal X-ray diffraction structures of the CsF (left and LiCl (right) complexes of receptor **25**

In conclusion, a potentially multitopic ion pair receptor will be showed, whose behavior is a direct consequence of high selectivity and affinity for the Cs^+ cation of an 1,3-alternate calix[4]crown-6 subunit.[18]

The scheme of synthesis of the receptor **26**, is the scheme 6.3. [19]
Initial evidence that receptor **26** forms a stable 1:1 complex with CsF came from a single crystal X-ray diffraction analysis. The resulting crystal structure revealed that the cesium cation is complexed within the calix[4]arene crown-6 ring, while the fluoride anion is hydrogen-bonded to the pyrrole NH protons of the calix[4]pyrrole subunit. There is thus a large separation (ca. 10.92 Å) between the cobound cation (Cs^+) and anion (F^-). A methanol molecule also interacts with the bound fluoride anion (Fig. 6.22).[19]

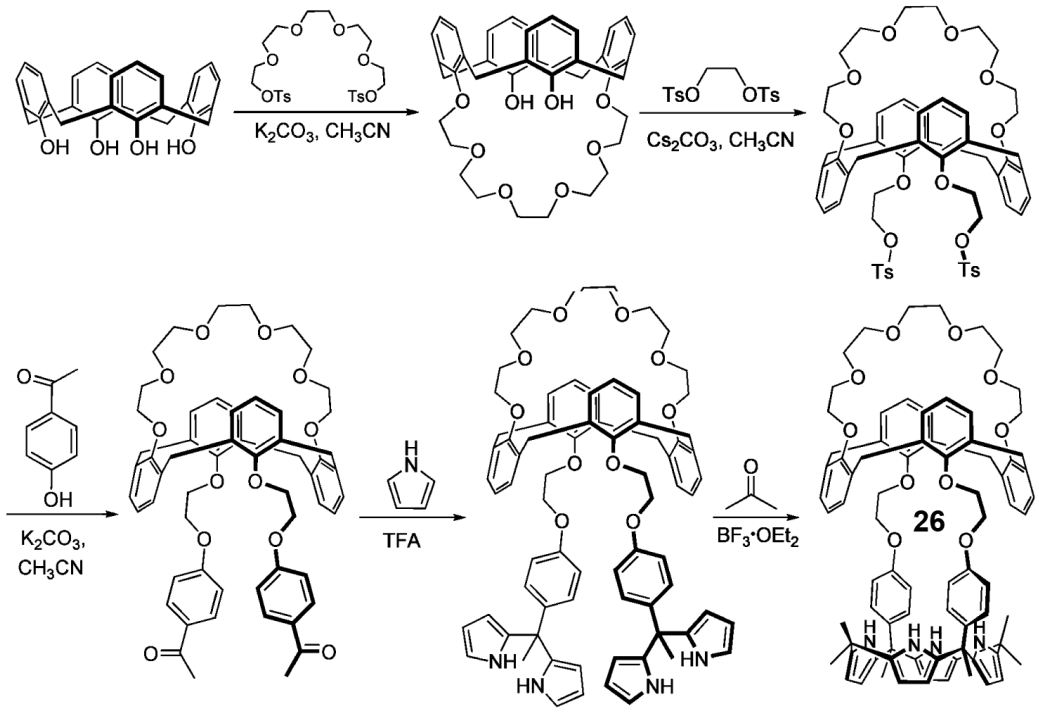

Scheme 6.3 - Synthesis of the Calix[4]crown-6 Strapped Calix[4]pyrrole **26**

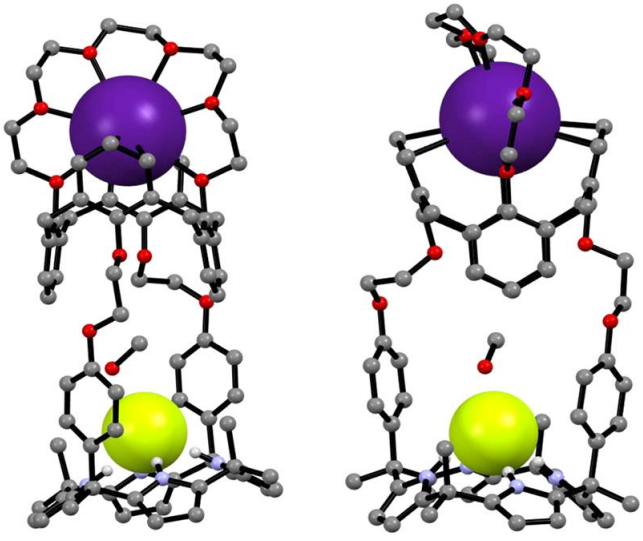

Fig. 6.22 - Two different views of the single crystal X-ray diffraction structure of [**26**·CsF·MeOH].

Conversely, no fluoride binding is seen when Cs^+ is replaced by TBA^+ (Fig. 6.23).[19] This observation is rationalized in terms of the presumption that with the less-coordinating TBA^+ cation, solvation of F^- by the protic solvent (methanol) present in the methanol-d_4/chloroform-*d* (1/9, v/v) mixture outcompetes complexation by the calix[4]pyrrole unit.

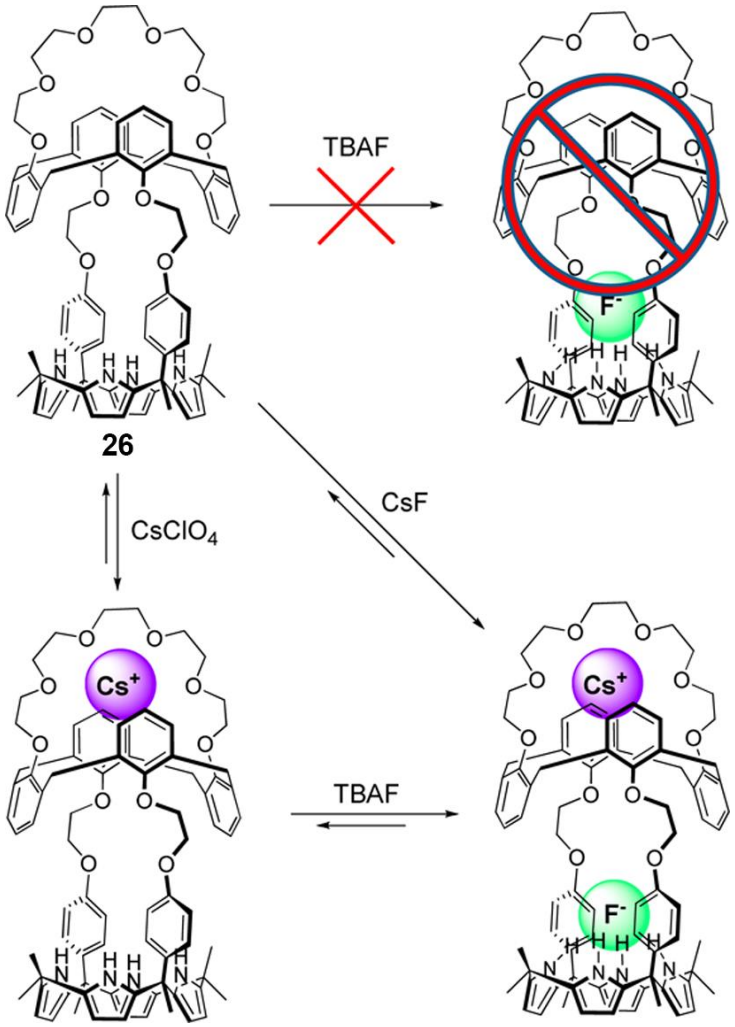

Fig. 6.23 - Binding modes for receptor **26** and various salts of Cs^+ and F^- that are proposed to be operative in methanol-d_4/chloroform-*d* (1/9, v/v). **TBA** = tetrabutylammonium.

The crown-free ion pair receptor **27** was also synthesized. [20]

In contrast to what was seen with **26**, in methanol-d4/chloroform-d (1/9, v/v), receptor **27** (Fig. 6.24) fails to interact appreciably either F^- or Cs^+ when exposed to salts of these ions in the absence of one another. However, in the presence of CsF or a mixture of salts that provide a source of CsF in situ, it binds both Cs^+ and F^- to give rise to a stable 1:1 CsF ion pair complex. This CsF binding behavior thus follows the rules of an **AND** logic gate. Experimental support for this recognition behavior came from ^{1}H NMR spectroscopic analysis carried out in methanol-d_4/chloroform-*d* (1/9, v/v). Chemical shift changes were observed that were consistent with the conclusion that receptor **27** binds both the Cs^+ cation and the F^- anion and that recognition of the two ions occurs concurrently, rather than in the stepwise manner observed in the case of receptor **26**. [20]

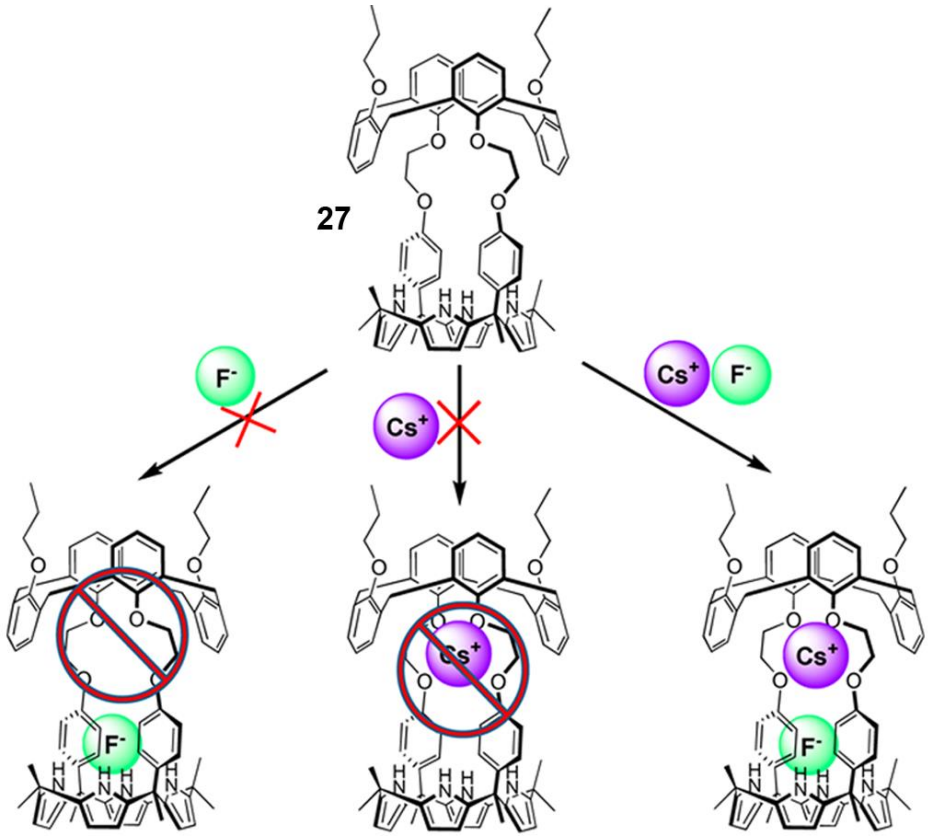

Fig. 6.24 - Proposed **AND** logic gate binding behavior exhibited by receptor **27** when exposed to the cesium cation, fluoride anion, or mixtures thereof in $CD_3OD/CDCl_3$ (1:9, v/v). In addition to CsF, the sources of the ions were TBAF and $CsClO_4$.

The multitopic ion pair receptor **28** was also designed and synthesized in an effort to control cation binding and release by cation metathesis (Fig. 6.25).[11,12]

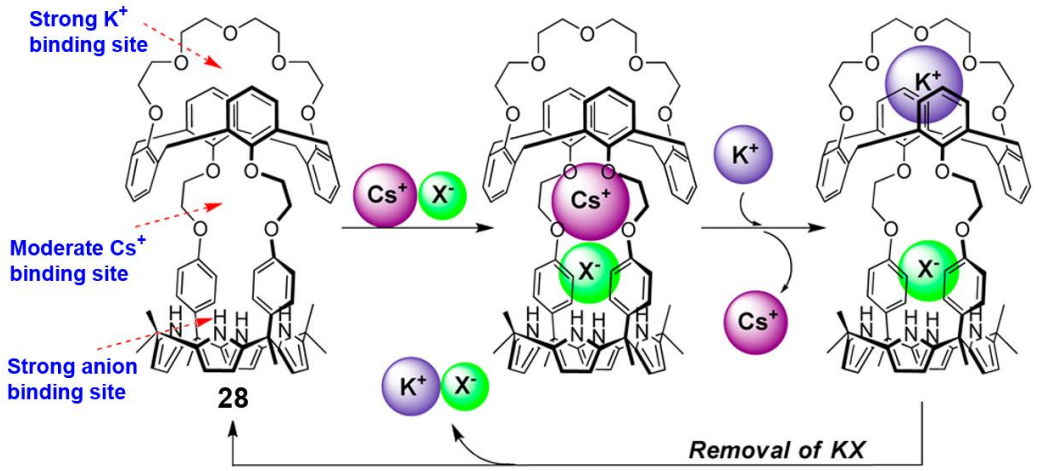

Fig. 6.25 - Design concept underlying ion pair receptor **28**.

This receptor consists of one anion binding site and three cation recognition sites having differing selectivities and affinities for different cations. For example, the 1,3-alternate calix[4]arene crown-5 subunit has an inherently high preference for the K^+ cation relative to the Cs^+ cation. This preference holds for other cation recognition sites within receptor **28**. Therefore, receptor **28** was expected toì complex the Cs^+ cation in the absence of the K^+ cation but to release the Cs^+ cation if subsequently exposed to the K^+ cation (Fig. 6.25).[21,22]

Receptor **28** could be used to extract the Cs^+ cation from aqueous media into a nitrobenzene organic phase. It was found that the Cs^+ cation extracted in this way could be released and recovered by exposure to K^+ as shown schematically in figure 6.26.[21] The actual experiments consisted of exposing receptor **28** in nitrobenzene-d_5 to an aqueous (D_2O) solution of $CsNO_3$ in the presence of excess $NaNO_3$. This exposure led to changes in the ^1H NMR spectrum of the organic phase that were ascribed to the selective extraction of $CsNO_3$ from the aqueous phase and its complexation by receptor **28** within the organic phase. A subsequent washing of the organic phase (containing the $CsNO_3$ complex, [**28**·$CsNO_3$]) with an aqueous D_2O solution of $KClO_4$ leads to release of $CsNO_3$

into the aqueous phase (Fig. 6.26). This produces a new cation complex, [**28**·K^+]NO_3^-, in the organic phase as evidenced by ^{1}H NMR spectroscopy. Contacting the nitrobenzene layer containing this potassium complex with excess chloroform (2×) and D_2O. Binding modes of **28** proposed to exist in the absence and presence of various K^+ and Cs^+ salts as inferred from ^{1}H NMR spectroscopic studies carried out in $CD_3OD/CDCl_3$ (1/9, v/v). serves to regenerate the ion-free form of receptor **28** in the organic phase.[21]

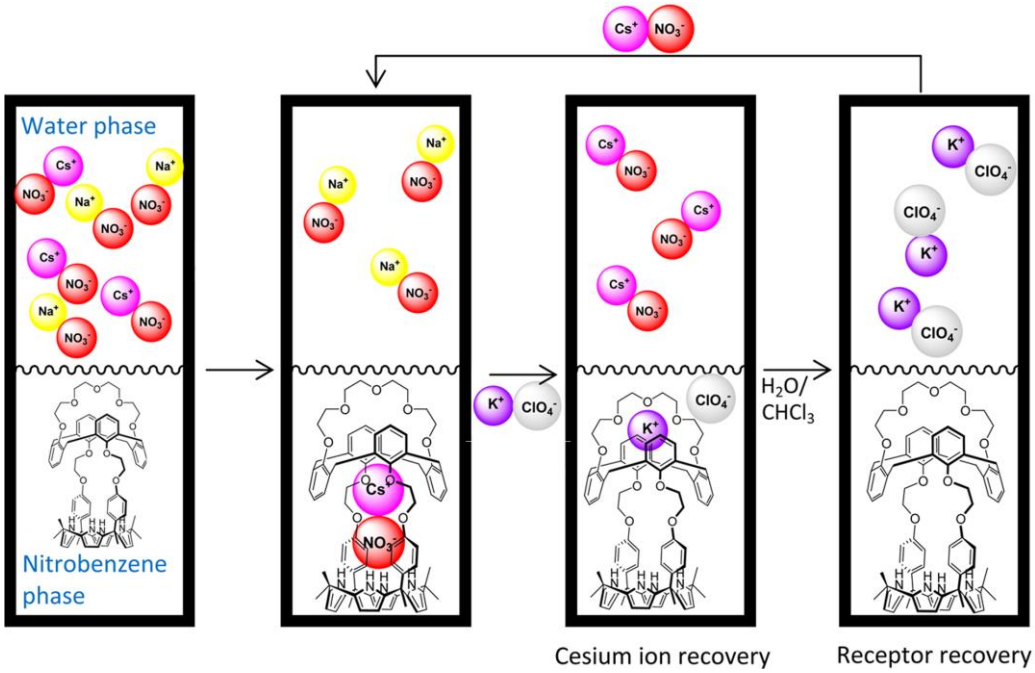

Fig. 6.26 - Schematic representation of a two-phase $CsNO_3$ extraction and recovery process that is based on ion pair receptor **28**. Cation metathesis allows for controlled removal of the cesium cation, while further contacting steps allow recycling of the receptor.

In conclusion, the calix[4]pyrrole framework has emerged as a useful platform for the construction of ion pair receptors. Unsubstituted calix[4]pyrroles (e.g., **18**) can function as ion pair receptors for several cesium salts, as well as ion pairs containing several large, charge diffuse organic cations, including the imidazolium, pyridinium, and tetraalkylammonium cations. Moreover, calix[4]pyrrole **18** is able to transport the CsCl ion pair across phospholipid bilayers selectively and can extract CsCl and CsBr from an

aqueous phase into a nitrobenzene organic phase under two phase liquid−liquid extraction conditions.Furthermore, modification and functionalization of the β-pyrrolic and meso-carbon atoms of the calix[4]pyrrole framework with various cation recognition sites can be used to produce more elaborate ion pair receptors. Strapping the calix[4]pyrrole framework with cation binding motifs that independently bind cations can be used to generate multitopic ion pair receptors. Some of these allow for the metathesis-based control of the underlying cation recognition and release processes.

References

[1] S.J. Coles, P.A. Gale, M.B. Hursthouse, *CrystEngComm*. 53 (**2001**) 1.

[2] P.A. Gale, S. Camiolo, C.P. Chapman, M.E. Light, M.B. Hursthouse, *Tetrahedron Lett.* 42 (**2001**) 5095.

[3] P.A. Gale, S. Camiolo, G.J. Tizzard, C.P. Chapman, M.E. Light, S.J. Coles, M.B. Hursthouse, *J. Org. Chem.* 66 (**2001**) 7849

[4] J. L. Sessler, N. M. Barkey, G. D. Pantos and V. M. Lynch, *New J. Chem*., **2007**, 31, 646–654.

[5] M. Renic, N. Basaric and K. Mlinaric-Majerski, *Tetrahedron Lett*., **2007**, 48, 7873–7877.

[6] E. A. Katayev, N. V. Boev, V. N. Khrustalev, Y. A. Ustynyuk, I. G. Tananaev and J. L. Sessler, *J. Org. Chem*., **2007**, 72, 2886–2896.

[7] E. A. Katayev, J. L. Sessler, V. N. Khrustalev and Y. A. Ustynyuk, *J. Org. Chem*., **2007**, 72, 7244–7252.

[8] J. L. Sessler, D. Seidel and V. Lynch, *Angew. Chem., Int. Ed*., **2002**, 41, 1422–1425.

[9] M. Stepien, B. Donnio and J. L. Sessler, *Angew. Chem., Int. Ed*., **2007**, 46, 1431–1435.

[10] Gale, P. A.; Sessler, J. L.; Král, V. *Chem. Commun*. **1998**, 1−8.

[11] Lee, C.-H.; Miyaji, H.; Yoon, D.-W.; Sessler, J. L. *Chem. Commun*. **2008**, 24−34 and referencestherein.

[12] Gale, P. A.; Lee, C.-H. Top. *Heterocycl. Chem*. **2010**, 24, 39−73.

[13] Custelcean, R.; Delmau, L. H.; Moyer, B. A.; Sessler, J. L.; Cho, W.-S.; Gross, D.; Bates, G. W.; Brooks, S. J.; Light, M. E.; Gale, P. A. *Angew. Chem., Int. Ed*. **2005**, 44, 2537−2542.

[14] Wintergerst, M. P.; Levitskaia, T. G.; Moyer, B. A.; Sessler, J. L.; Delmau, L. H. Calix[4]pyrrole. *J. Am. Chem. Soc*. **2008**, 130, 4129−4139

[15] Kim, S. K.; Gross, D. E.; Cho, D.-G.; Lynch, V. M.; Sessler, J. L. *J. Org. Chem*. **2011**, 76, 1005−1012.

[16] Park, I.-W.; Yoo, J.; Kim, B.; Adhikari, S.; Kim, S. K.; Yeon, Y.; Haynes, C. J. E.; Sutton, J. L.; Tong, C. C.; Lynch, V. M.; Sessler, J. L.; Gale, P. A.; Lee, C.-H. *Chem. Eur. J*. **2012**, 18, 2514−2523.

[17] Park, I.-W.; Yoo, J.; Adhikari, S.; Park, J. S.; Sessler, J. L.; Lee, C.- H. *Chem. Eur. J*. **2012**, 18, 15073−15078.

[18] Casnati, A.; Pochini, A.; Ungaro, R.; Ugozzoli, F.; Arnaud, F.; Fanni, S.; Schwing, M.-J.; Egberink, R. J. M.; de Jong, F.; Reinhoudt, D. N. Synthesis, *J. Am. Chem. Soc*. **1995**, 117, 2767−2777.

[19] Sessler, J. L.; Kim, S. K.; Gross, D. E.; Lee, C.-H; Kim, J. S.; Lynch, V. M *J. Am. Chem. Soc*. **2008**, 130, 13162−13166

[20] Kim, S. K.; Sessler, J. L.; Gross, D. E.; Lee, C.-H.; Kim, J. S.; Lynch, V. M.; Delmau, L. H.; Hay, B. P. *J. Am. Chem. Soc*. **2010**, 132, 5827−5836.

[21] Kim, S. K.; Vargas-Zúñiga, G. I.; Hay, B. P.; Young, N. J.; Delmau, L. H.; Masselin, C.; Lee, C.-H.; Kim, J. S.; Moyer, B. A.; Lynch, V. M.; Sessler, J. L. *J. Am. Chem. Soc*. **2012**, 134, 1782−1792.

[22] Kim, S. K.; Lynch, V. M.; Young, N. J.; Hay, B. P.; Lee, C.-H.; Kim, J. S.; Moyer, B. A.; Sessler, J. L. *J. Am. Chem. Soc*. **2012**, 134, 20837−20843.

7. Metal based anion receptors

In some metal-containing anion receptors the metal acts as a part of redox, luminescent or colorimetric reporter group, or as a component of anion binding solid-state coordination polymer networks, or also as part of the core element of self-assembled coordination complexes based on substitutionally labile metal involving thermodynamic anion templation.

However, the present dissertation focuses on metal-containing anion receptors as:

i) those designed to solely rely on the direct interaction of a cationic metal centre(s) with the target anion; (Fig. 7.1 left) [1]; This is best described as first-sphere, anion recognition since the anion must enter the primary coordination sphere for binding.

ii) those in which a substitutionally inert metal ion plays a structure-organising role. In such a structure selectivity and effective binding of anions is best accomplished by employing the concept of second-sphere coordination; (Fig. 7.1 right). Here the metal ion acts to organise functional groups on separate ligands into a new binding site that takes advantages of the flexibility and directionality inherent in a hydrogen bonding scheme.

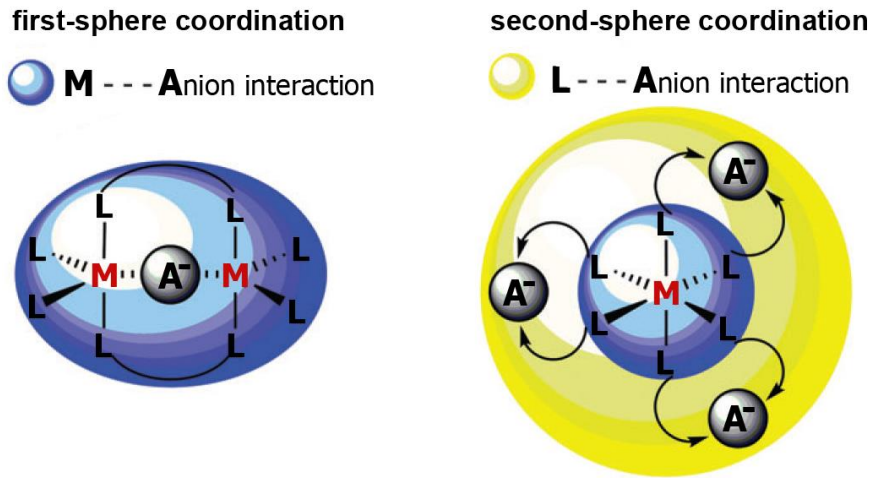

Fig. 7.1 - Schematic representations of the binding of anionic substrates using a metal-based anion receptor design. **Left**: interaction in the firstsphere of coordination. **Right**: interaction in the second-sphere of coordination (first-sphere = blue, second-sphere = yellow).

7.1. Direct interaction of a cationic metal centre(s)

As for receptors which show direct interaction of a cationic metal centre(s) with the target anion, let's start considering an europium compound which is a luminescent sensor selective for hydrogen carbonate. [2]

The role of the europium(III) ion in **1** (Fig. 7.2) is both to complex the HCO_3^- ion as a first-sphere ligand and also to signal its presence by means of sensitised metal-based emission.

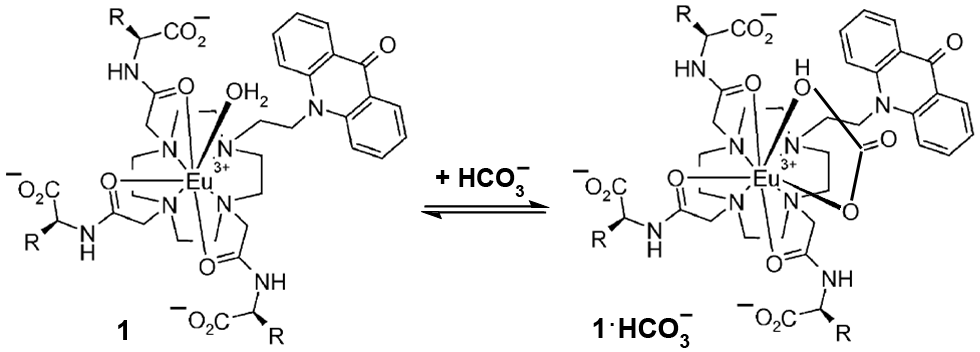

Fig. 7.2

A further elegant link between self-assembly and direct coordination is provided by the metallomacrocycle **2** (Fig. 7.3) reported by Puddephatt and coworkers. [3]

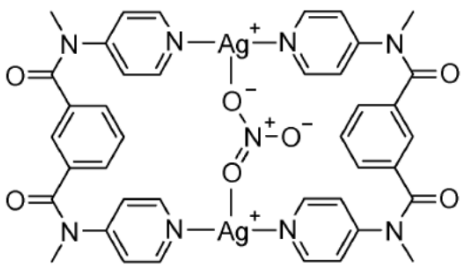

2

Fig 7.3

The bis(amidopyridine) ligands self-assemble to form a 2+2 metallo-macrocycle in the presence of Ag(I) with long (2.53 Å) interactions to a bridging NO_3^- anion in the centre of the cavity that coordinates to each silver(I) centre. The analogous $CF_3CO_2^-$ complex adopts a more collapsed geometry without a central anion.

A wide range of Lewis acidic metals such as Hg(II) and Sn(II) (along with non-metal Lewis acids such as Si(IV) and B(III) [4]) have been used over the years in macrocyclic and macrobicyclic 'anticrown' and 'anti-cryptand' type hosts. Good examples are Newcomb's stannacycles **3-5** (Fig. 7.5) that are related to the original halide-binding katapinands.[5]

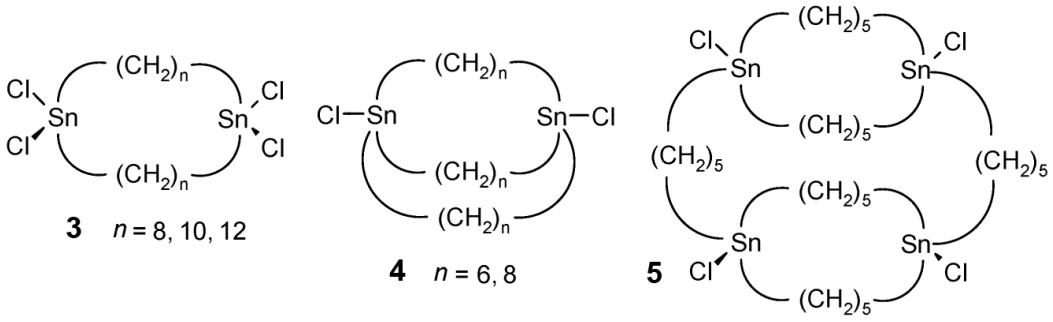

Fig. 7.4

Compound **3** binds chloride in acetonitrile; however, the binding constant is only twice that of open-chain analogues and is independent of ring size, suggesting little cooperativity to the binding. The macrobicyclic compounds **4** are known in crystalline form as the fluoride (n = 6) and chloride (n=8) derivatives. In the former case, the fluoride anion has been shown crystallographically to be approximately symmetrically bridging between the two tin atoms, with Sn–F distances of 2.12 and 2.28 Å (Fig. 7.5a). This host binds strongly to fluoride (log K_s = 4) while chloride is not bound at all. In the Cl^- complex of the larger host, the chloride is coordinated within the macrobicycle to only one tin centre and the cavity is too large for the anion (Fig. 7.5b).

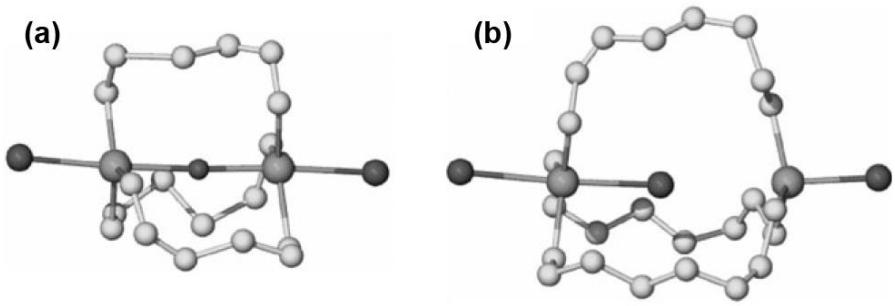

Fig. 7.5 - X-ray crystal structures of (**a**) host **3** (n = 6) with F^- and (**b**) compound **4** (n = 8) with Cl^-.[5]

At -100 °C, in solution the Cl^- anion is dynamic and moves between both metal centres. The halide solution binding affinity is low and comparable to that of a single Sn centre in acyclic systems.

Consistent with the greater number of Sn atoms and the greater organisation of the host in **5**, chloride affinity is significantly higher than in **3** and **4** with a binding constant of 2.7 log units in chloroform.

Other Lewis acidic metal cations supported on various organic scaffolds may be used in similar ways to the 'anticrown' compounds to bind anions. Resorcarene based ligand **6** (Fig. 7.6) forms tetrametallic complexes with Cu(I) and Ag(I) in which the upper rim of the [4]resorcarene bowl is decorated with a phosphine coordinated M_4Cl_4 ring. Anions are bound by long-range lateral interactions with the ostensibly two-coordinate metal centres in a central cavity of extremely rigid, well-defined dimensions. In the case of large anions such as I^- or the larger metal Ag^+, the central anion adopts a symmetric μ_4-bridging coordination-mode interacting approximately equally with all four metal centres. With the smaller Cu^+, chloride is not able to stretch to fill the cavity and adopts an unsymmetrical μ_3-bridging mode.[6]

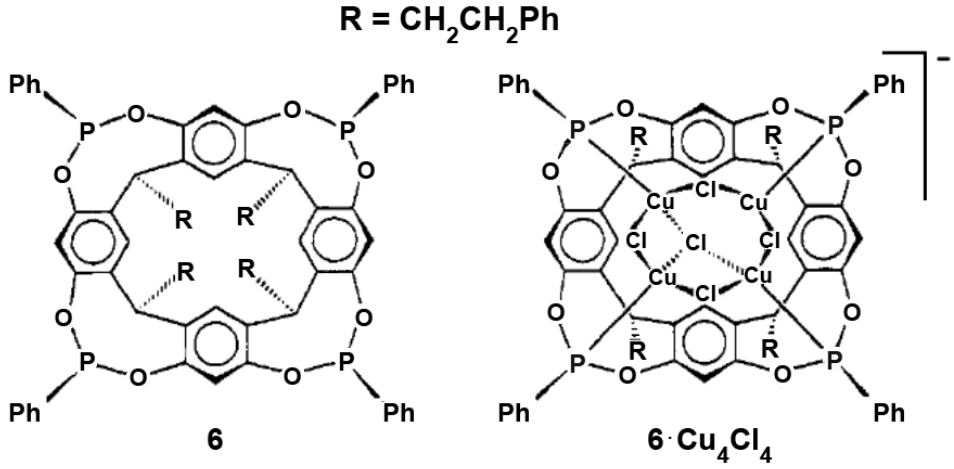

Fig. 7.6

Another relatively classical kind of host involving metal–anion interactions are 'cascade' complexes in which macrocycle-bound metal ions bind to (usually bridging) anions. For example, the macrocycle [24]ane-N_2S_4 is able to coordinate two copper(II) ions, on each tridentate S,N,S-chelate binding domain. Since Cu(II) is typically four- or five-coordinate the remaining coordination sites are available for anion-binding, in this case with the azide

(N_3^-) counter ions. The X-ray crystal structure of the complex shows that two azide anions bridge across the two metal ions while the remaining two bind in a terminal fashion, one to each copper centre (Fig. 7.7). [7]

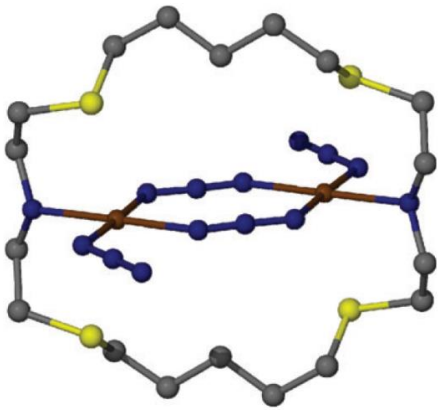

Fig. 7.7 – X-ray structure of the Cu(II) azido cascade complex $[Cu_2([24]ane\text{-}N_2S_4)(\mu\text{-}N_3)_2(N_3)_2]$.[7]

A good example of cryptand-based cascade complexes are bis(tren) derivatives such as the copper(II) complex **7** (Fig. 7.8). [8]

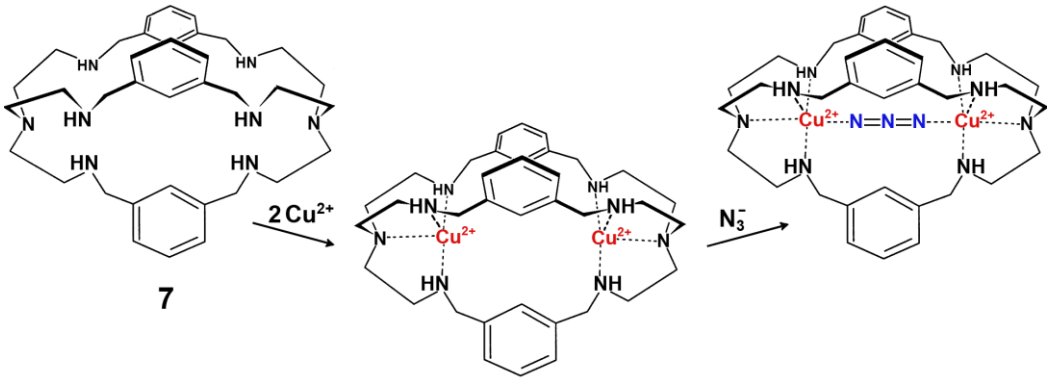

Fig. 7.8

This metallo-receptor binds azide within the space between the two metals resulting in a green colouration arising from an anion-to-metal MLCT absorption at 400 nm. The preference for azide is related to its 'bite length'.[8]

More recently the cascade principle has been adopted by Smith and coworkers to give a large range of bimetallic biological anion receptors such as **8** (Fig. 7.9) capable of sensing pyrophosphate and phosphate-rich membrane surfaces with stabilities of 4–6 log units. [9, 10]

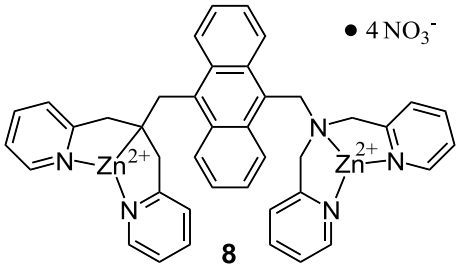

8

Fig. 7.9

Compound **9** is a colorimetric sensor, whereas, compound **10** is a fluorescent sensor (Fig. 7.10). Both receptors are selective for pyrophosphate in water even in the presence of other phosphate-containing compounds anions such as phosphate and ATP. [11]

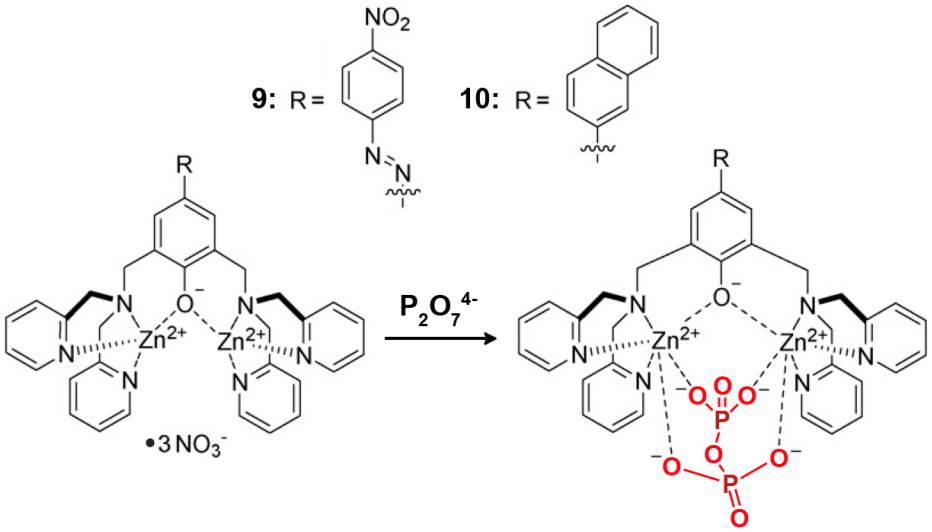

Fig. 7.10

Hydrogen phosphate binding in water is also possible using the cascade complexes **11** and **12** (Fig. 7.11) which are based on tetrahedral copper(II) anion binding sites. Anions are also stabilised by charge-assisted hydrogen bonding to the tripodal peripheral groups. Host **11** is protonated at neutral pH and binds HPO_4^{2-} with log Ks = 4.4 in water. The more rigidly preorganised **12** binds slightly less strongly but is more selective for phosphate. Interestingly, detailed thermodynamic studies show that phosphate binding by **11** is entirely entropically driven, while **12** relies primarily on enthalpy. This difference arises from the lower degree of solvent organisation around the guanidinium groups in **12** in comparison to the more exposed ammonium groups in **11** and hence anion binding in **11** leads to entropically favourable solvent release.[12]

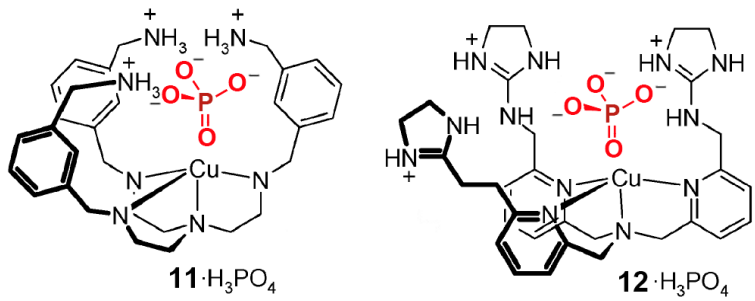

Fig. 7.11

Finally, organo-boron and organo-silicon compounds can act as Lewis acids and as such can behave as anion receptor. In the case of organo-boron derivatives the electron deficient nature of trivalent boron means that strong dative bonds are formed with most Lewis bases. Tetravalent silicon compounds can also interact with anions by expanding their coordination sphere to give five- or even six-coordinate *hypervalent* compounds (compounds formally possessing more than 8 valence electrons in their outer shell [13].

The synthesis of the first boron base anion receptor has been induced by the properties of, 8-bis(dimethylamino)naphthalene (proton sponge Figure 7.12a), known since 1968 as an extremely effective proton chelating agent.

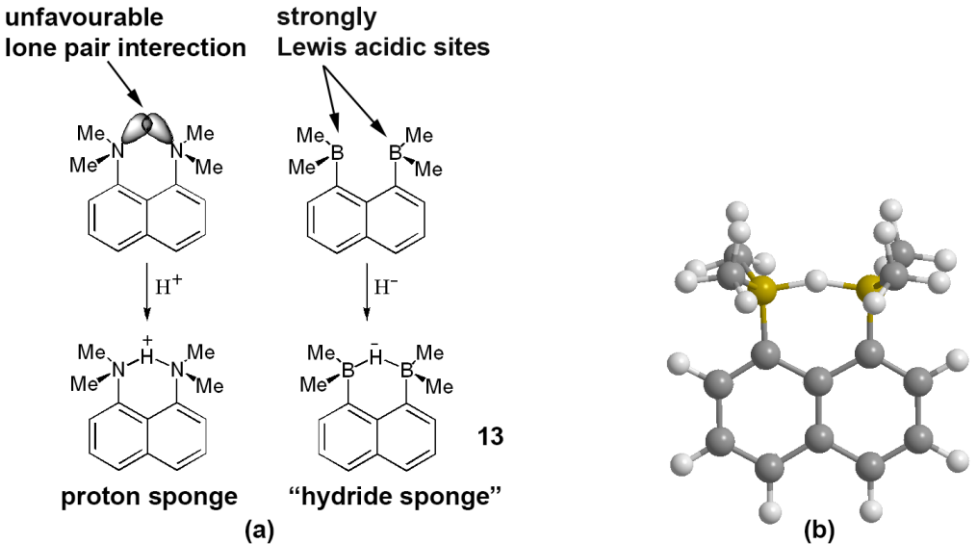

Fig. - 7.12 (**a**) Comparison of 'proton sponge' and 'hydride sponge'. (**b**) X-ray crystal of the anion in the KH complex of hydride sponge **13.**

The protonation of one of the NMe_2 groups serves to significantly reduce the repulsion between the two nitrogen atoms in the free host, and consequently enhances greatly the basicity of the diamine. The $N\cdots H^{+}\cdots N$ hydrogen-bonded bridge is almost symmetrical . If the two amines are replaced by BMe_2, groups a highly electron-deficient anion host, termed 'hydride sponge' **13** is created, which demonstrates a marked ability to abstract hydride from almost all other hydride sources (*e.g.* $HBEt_3^-$).

In fact, the discovery of **13** (and indeed the majority of supramolecular chemistry), was preceded by the observation in 1967 that the much more flexible bidentate Lewis acid $F_2BCH_2CH_2BF_2$ [14] is capable of chelating methoxide ion to give five-membered rings as shown in Scheme 7.1.

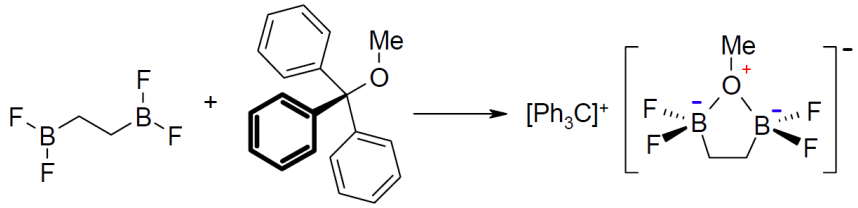

Scheme 7.1 - Anion chelate behaviour.[14]

Following the discovery of hydride sponge by Howard Katz [15] a number of other Lewis acid chelates such as **14**–**18** have been prepared, all of which show a strong affinity for anions (Fig. 7.13).

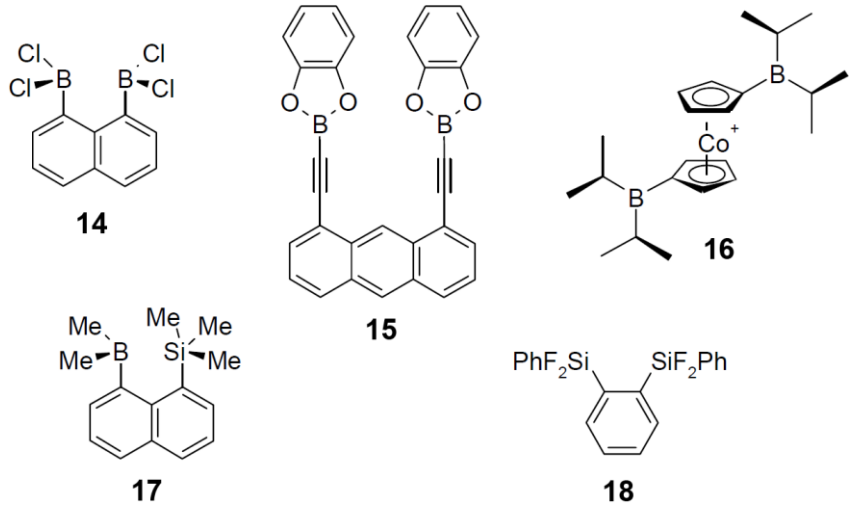

Fig. 7.13

Binding occurs by virtue of the anions Lewis base character and rigid, geometric preorganisation. All of the di-boron and related compounds **14**-**18** form chelate complexes.

Compound **14** chelates Cl^- in a distinctly out-of-plane fashion because of the large size of Cl^- compared to the B···B separation in the rigid napthelenyl system. Despite this mismatch, the chelate effect is evident and the complex is significantly more stable than the model analogue $PhBCl_3^-$. The extended compound **15** was designed to offer a much larger chelate 'bite' angle and displays a distinct chelate coordination to the complementary neutral molecule 5-methylpyrimidine (binding constant 130 M^{-1} compared to 70 M^{-1} with a single boron-containing analogue). The organometallic cation **16** is ideally suited to form a neutral chelate complex with anions, although in the free state it is not preorganised for anion binding since the two $B(isopropyl)_2$ substituents adopt an *anti* conformation. The compound may be obtained anion free (eliminating inter-anion competition effects) by reduction to the neutral Co(II) analogue. Oxidation of this neutral precursor $[Co(C_5H_4B(Pr^i)_2)_2]$ with $[Fe(C_5H_5)_2][PF_6]$, $Cu(OH)_2$ or C_2Cl_6 in non-polar solvents gives a range of complexes of formula **16**·X (X = PF_6, OH or Cl). Only the hydroxy derivative is a chelated compound with the two $B(Pr^i)_2$ substituents rotated into a *syn* conformation. The chloride adduct contains a chloride anion attached to only one boron centre, while the PF_6 complex is a salt. It seems likely that this is a result of the strong Lewis basicity of hydroxide and its small size, which can fit conveniently between the two substituted cyclopentadienyl rings (Fig. 7.14). [16]

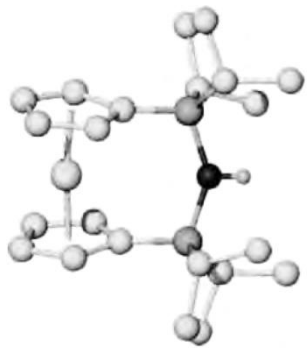

Fig. 7.14 - X-ray structure of **16**·OH showing the symmetric chelation of the hydroxide anion.[16]

Compounds **17** and **18** formally contain tetravalent silicon, which is not electron-deficient. It is, however, a strong Lewis acid, and on reaction with F^-, five-coordinate silicon compounds are obtained. In the case of **17**, the fluoride anion is localised mainly on the boron atom, although it does display dynamic behaviour involving hopping between boron and silicon. Compound **18** as the KF adduct contains two five-coordinate silicon atoms that chelate the F^- anion (Figure 7.15). The coordination sphere of the K^+ counter-ion is completed by a molecule of [18]crown-6.

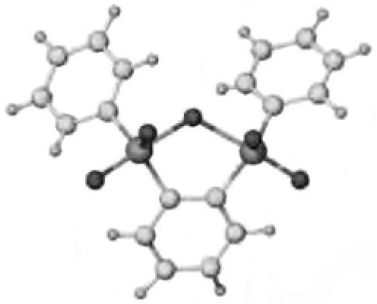

Fig. 7.15 - Structure of the anion in the KF adduct of compound **18**. Bridging Si—F distances are 1.898 and 2.065Å, compared to terminal Si—F distances of 1.60–1.65Å.

Lastly the most remarkable boronic acid derivatives is shown, i.e. the very rigid bis(bora)-*p*-*t*-butylcalix[4]arene derivative **19**. The host binds fluoride very strongly in chloroform with log K_{11} = 6.3. The fluoride is exclusively chelated in between the two boron atoms since fluoride binding to the outside of the host would result in unfavourable steric repulsions between the phenyl groups, (Scheme 7.2). While relatively weak, the fluorescence of the phenyl groups may be used to monitor binding; addition of tetrabutylammonium fluoride almost completely quenches the fluorescence. [17]

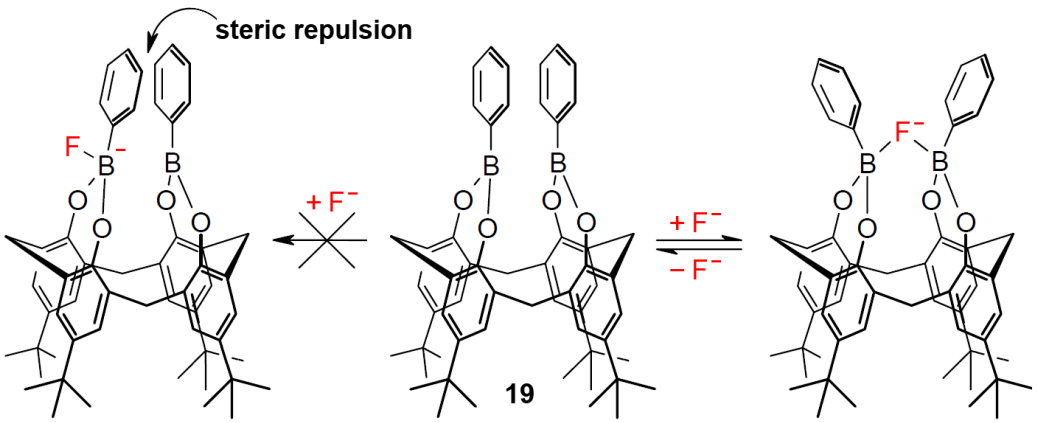

Scheme 7.2 - Fluoride binding by the bis(bora)-*p*-*t*-butylcalix[4]arene derivative **19**.[17]

In the above it has been done a survey of anion receptors in which metal ion Lewis acid (as well non metal Lewis acid) interact with a given anion in a direct way. In other words, in such kinds of receptor, the target anion must enter the primary coordination sphere for binding interaction with metal ions. However, the best metal-based anion receptors combine both the electrostatic attraction of the metal centre and the directional binding effects of appended H-donor functional groups on the ligands. Under these conditions, selectivity and effective binding of anions is best accomplished by employing the concept of second-sphere coordination (Fig. 7.1 right); the metal ion acts to organise functional groups on separate ligands into a new binding site that takes advantages of the flexibility and directionality inherent in a hydrogen bonding scheme.

One of the inherences of supramolecular chemistry is that preorganisation of a binding site leads to enhanced recognition. For metal-based anion receptors, it is coordination of the ligands to the metal centre that acts to preorganise hydrogen bond donor functional groups for anion binding. This preorganisation can take two different forms. **(1)** Metal–ligand coordination can be used to bring together the hydrogen-bond donor groups from individual ligands via complexation, as described by Hamilton et al. in 1995 (Fig. 7.16). [18]

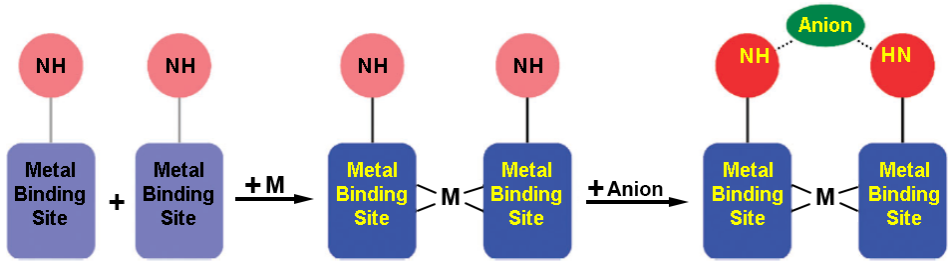

Fig. 7.16 - A schematic representation of Hamilton's original idea for utilising metal-templated self-assembly to arrange functional groups for recognition of anions. From left to right: in the free ligands, neither the metal binding site donors nor hydrogen-bonding donors are used (pale colours). Utilisation of the metal-binding sites (blue) to form a complex organises the hydrogen-bond donor NH groups (red) for anion binding (green).

7.2. Metals that organize ligands to enhance anion binding

More subtly, metal–ligand coordination can be used to induce a conformational change of a single ligand that will result in a beneficial reorganization of hydrogen-bond donor groups. In either case, metal–ligand bonding reduces the entropic cost required to attain the particular conformation needed to bind the guest and any entropic loss associated with rigidifying the system is outweighed by the enthalpic gain accrued by formation of a set of strong M–L bonds.

For a better understanding of what said above, let's consider mono-, bi- and tridentate ligands containing appended functional groups for hydrogen-bonding to anions can be coordinated to a single transition metal ion. This simple form of metal-templated self-assembly results in organising previously independent hydrogen-bonding groups into pockets that can act as efficient anion binding sites. The use of terpyridine, bipyridine and iso-quinoline based ligands **L1**, **L2** and **L3** (see example in Fig. 7.17) to create complexes for anion recognition is now taken into consideration. Each of these ligands can use a different type of hydrogen bond donor functional group, and can shows different selectivity for common anions.

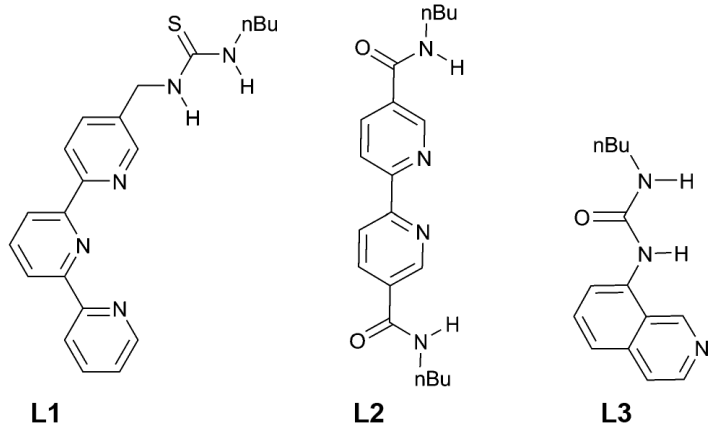

Fig. 7.17 - Terpyridine/thiourea ligand (**L1**), bipyridine/amide ligand (**L2**) and iso-quinoline/urea ligand (**L3**).

In 1995, Hamilton et al. showed that coordinating two equivalents of ligand **L1** to Ru(II) and employing the non coordinating PF_6^- anion created a robust metal complex $[Ru(\mathbf{L1})_2][PF_6]_2$ which could act as an anion receptor in the form of the dicationic complex $[Ru(\mathbf{L1})_2]^{2+}$ (Fig. 7.18). [18,19]

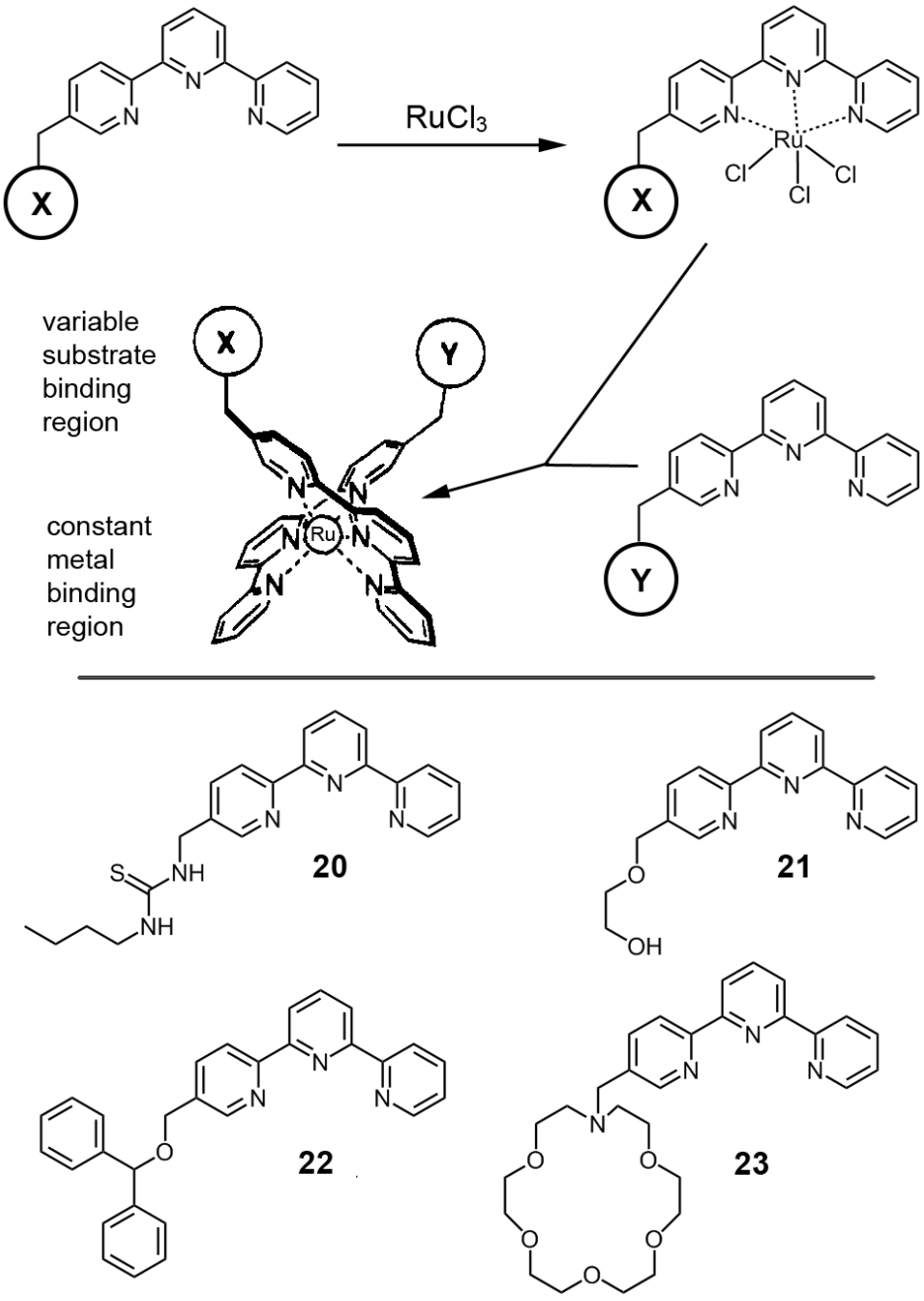

Fig. 7.18 - Metal-templated approach to formation of combinatorial receptor libraries.

This complex was shown to effectively bind dicarboxylate ions through hydrogen bonding to the thiourea groups attached to **L1** (Fig. 7.19).[19]

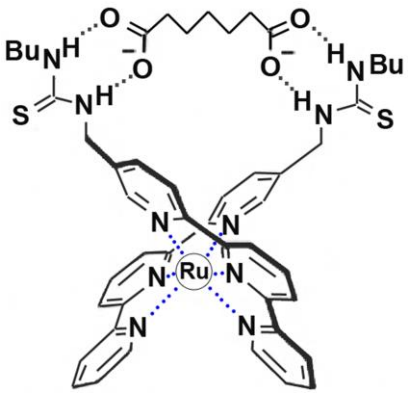

Fig- 7.19 - Proposed structure of complex with receptor **20**·**20**

Thus, two sets of two NH hydrogen-bond donors on different ligands were organised into a single binding site by virtue of their coordination to a metal centre. One of the key design features is the use of an inert metal centre such as Ru(II). This has two distinct advantages. It allows for isolation and characterization of a stable receptor prior to any interaction with a target anion and it eliminates the problem of ligand exchange due to competition between anionic substrates and ligands for coordination sites. Although there is no solid state structural data available for directly probing the thiourea–anion interaction, the strong binding of this receptor with a variety of dicarboxylate anions such as glutarate, adipate, pimelate, iso-phthalate and 1,3-phenylenediacetate led Hamilton to conclude that the binding cavity was relatively flexible. Certainly the presence of a connecting methylene group between the terpyridine ligand and the thiourea groups would facilitate this. A molecular mechanics derived model (MM3) [20] of this receptor clearly shows the presence of a significant binding site between the two terpy ligands (Fig. 7.20) [21]; it can be seen that, in this case, the adipate ion is a good fit and nicely spans the gap between the thiourea groups.

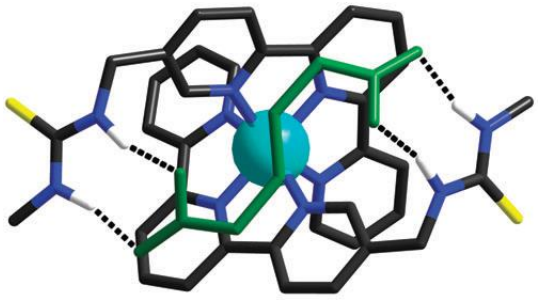

Fig. 7.20 - A molecular mechanics (MM3) derived model [11] of Hamilton's bis-terpyridine receptor binding the adipate anion $[O_2C(CH_2)_4CO2]^{2-}$ (green) by bringing two thiourea groups together in the second-sphere of coordination. The terminal alkyl groups have been shortened to one carbon for ease of visualization.

Beer et al. coordinated three equivalents of the bidentate ligand **L2** to Ru(II) to yield the metal-based anion receptor $[Ru(\mathbf{L2})_3]^{2+}$ (Fig. 7.21).[22]

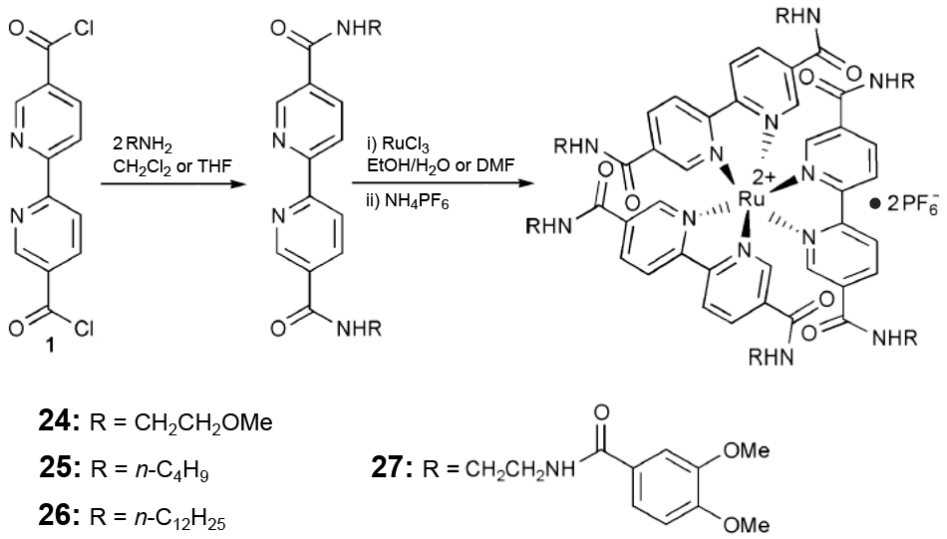

Fig. 7.21

These complexex contain two identical binding sites resulting from the convergence of two sets of three, hydrogen-bond donor, amide NH groups. Since octahedral tris-bipy complexes are chiral, Beer et al. also separated the two enantiomers and investigated the ability of Δ-$[Ru(\mathbf{L2})_3]^{2+}$ to bind chloride, nitrate and acetate ions.[23]

The X-ray structure of the chloride salt $[Ru(\mathbf{L_2})_3]Cl_2$ is shown in figure 7.22. It is clear that the 3-fold symmetry of the complex is superimposed on the binding site which provides for three $NH^{\cdots}Cl^-$ interactions; each from a different molecule of **L2**.

The amido N-atoms define an approximate equilateral triangle that is ~5.7 Å on a side. Given the 3-fold symmetry of the molecule, it is not surprising that this receptor also binds well to the trigonal planar NO_3^- anion.

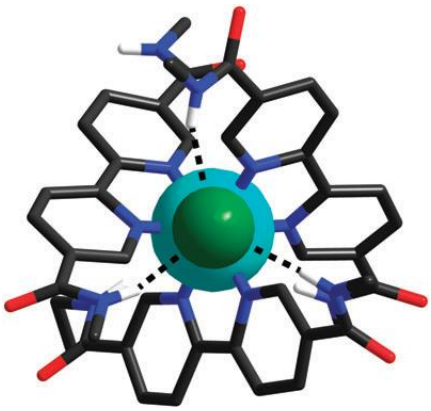

Fig. 7.22 - X-Ray crystal structure of the complex $[Ru(\mathbf{L2})_3]Cl_2$ viewed along the $Cl^{\cdots}Ru$ vector. The three independent amide–anion interactions in the second-sphere of coordination are shown as dashed lines. The terminal alkyl group has been shortened to one carbon for ease of visualisation.

The simple monodentate ligand **L3** is based on an isoquinoline ring system and by coordinating four of these ligands to an inert Pt(II) centre, Loeb and Gale et al. were able to collect together four urea groups into a single binding site.[24] Since rotation about the Pt–N bonds is facile there are four possible geometric isomers based on the relative positioning of the urea groups above or below the square coordination plane. In an analogy to the well studied chemistry of calix[4]-arenes, these isomers were labeled, 1,2-alternate, 1,3-alternate, partial cone and cone for ease of identification (Fig. 7.23). [25,26]

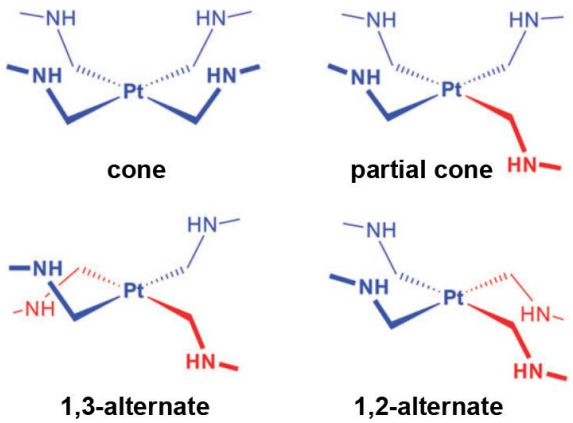

Fig. 7.23 - The four calix[4]arene-like conformations possible for a fourcoordinate square planar Pt(II) complex of **L3**.

Strong 1:1 interactions were observed in solution for halides and symmetrical oxyanions which likely involved surrounding the anion using the cone conformation. This was shown unambiguously by X-ray crystallography for the SO_4^{2-} ion. All eight NH donors from the four urea functional groups are organised so that they are directed at the anion which is nestled into the binding pocket (Fig. 7.24).

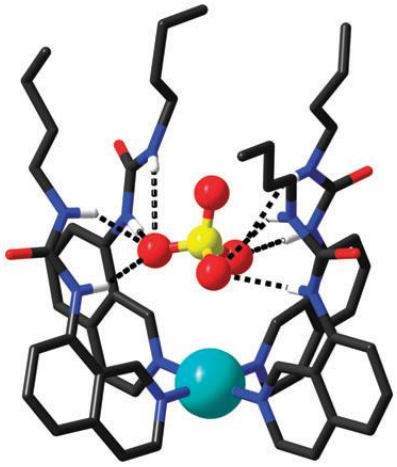

Fig. 7.24 - X-Ray crystal structure of the complex [Pt(**L3**)$_4$]SO_4. The eight independent NH···O urea–anion interactions in the second-sphere of coordination are shown as dashed lines.

It appears that multidentate chelating ligands such as the terpyridine derivative **L1** provide a larger degree of complex stability and a more rigid platform but limit the number of hydrogen-bond donors that can be incorporated. On the other hand, simple monodentate ligands, such as **L3**, are more flexible and allow more functional groups to be incorporated but are more likely to suffer from competition of the anion for ligand coordination sites. The conformational flexibility of [Pt(**L3**)$_4$]$^{2+}$ can be seen as an advantage when looking to bind a variety of different shaped anions with a single receptor but is perhaps a disadvantage when targeting a specific ion and trying to achieve high selectivity in the presence of background competition from other anions.

Let's now consider using metal–ligand coordination to influence the conformation of ligands such that hydrogen-bond donor sites on the same ligand can work together to bind a single anion. Conceptually, this could be anything from a simple, single bond rotation to a fairly substantial conformational

rearrangement that acts to template the formation of an anion binding site. The three ligands to be discussed are **L4**, **L5** and **L6** shown in figure 7.25.

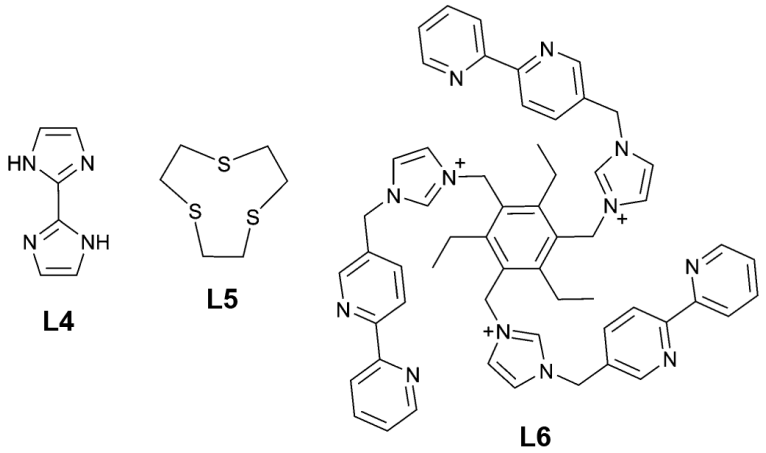

Fig. 7.25

The free ligand 2,2'-biimidazole, **L4**, prefers an anti conformation as shown in figure 7.25. Chelation to a metal centre requires rotation about the single bond linking the rings and adoption of the *syn* conformation which orients both the imidazole NH groups outward where they can participate in a second-sphere interaction with an anion.[27]

This is clearly evident from the X-ray crystal structure depicting the interaction of $[Mo(CO)_2(t\text{BuNC})(\eta^3\text{-allyl})(\mathbf{L4})]$ with a Br^- ion as shown in figure 7.26.[28] In this example, the metal ion does not bring together separate ligands, but acts to organise multiple hydrogen-bond donors on a single ligand by causing a beneficial conformational change.

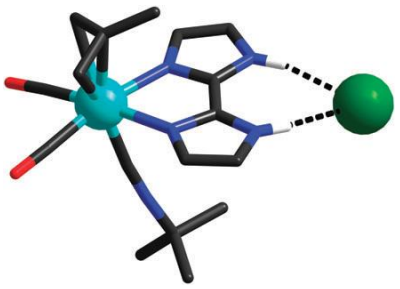

Fig. 7.26 - X-Ray crystal structure of the complex $[Mo(CO)_2(t\text{BuNC})\text{-}(\eta^3\text{-allyl})(\mathbf{L4})]$ with Br^- ion. The two NH···Br interactions in the second-sphere of coordination are shown as dashed lines.

Coordination of the flexible macrocyclic ligand, 1,4,7-trithiacyclononane, 9S3, (**L5**) to palladium requires an endoconformation for the S-donors that results in facial coordination to the metal ion. [29] This simultaneously organises the backbone ethylene groups so that a set of six endo CH bonds can act as hydrogen-bond donors to anions in the second coordination sphere.[30]
No solid-state structure was available for unambiguous verification of this arrangement but molecular mechanics calculations (MM3) [20] yielded the structure shown in figure 7.27 which matches that inferred from the solution data.

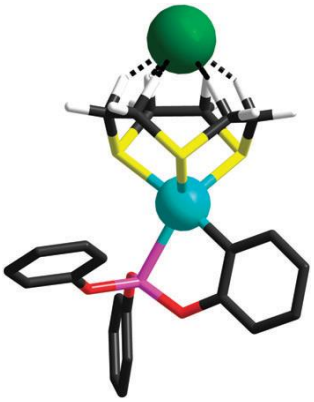

Fig. 7.27 - A molecular mechanics (MM3) derived model [20] of the complex $[Pd(\mathbf{L5})(P(OAr)_3)]^+$ with Cl^- ion. The six $CH\cdots Cl$ interactions in the second-sphere of coordination are shown as dashed lines. The 2,4-*t*Bu groups on the aromatic rings have been removed for ease of visualization

The large and flexible ligand **L6** is a particularly elegant variant on the metal tris(bipyridyl) scaffold. Combining the well-known 1,3,5-triethylbenzene platform with the coordinating ability of the bipyridine units brings together three imidazolium rings which can form a cage around an anion. Complexation with Fe(II) organises the three arms of the ligand to form the $Fe(bipy)_3$ complex. This forms a cage which is the correct size for encapsulating halide ions and the azide ion. ^1H NMR titration experiments showed transfer of electron density on the imidazolium ring suggesting that the anion occupies a position inside the cage and is hydrogen-bonding to three CH bonds from the imidazolium group and three CH bonds from pyridyl rings which now are activated by coordination to the Fe(II) centre. The X-ray structure of the Br^- adduct, shown in Fig. 7.28,

verifies these interactions showing encapsulation of the Br^- ion and six hydrogen-bonds from the two types of CH groups.[31]

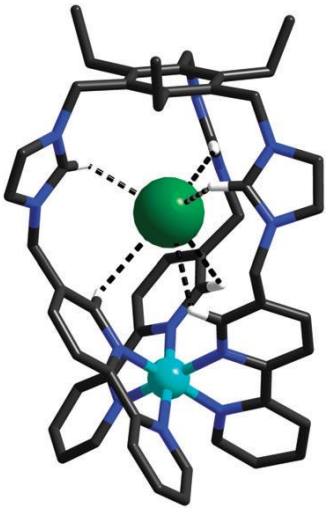

Fig. 7.28

Since this last example requires a fairly labile Fe(II) centre to organise the three bipy groups and create the anion binding cavity, it is important to distinguish this from anion templation. In our example, the anion does not influence the nature of the final assembly. The metal–ligand assembly is stabilized by the chelate effect and the formation of multiple Fe–N bonds making it a robust complex that functions as a molecular receptor for anions.

7.3 Solvent effect

Lastly, some focus on solvent issues seems appropriate since solvent polarity can influence receptor conformation. After all, most of anion receptors are designed to operate in solution and solution binding studies are used to validate receptor designs. For example, when studying the binding of anions to the complex $[Pt(3\text{-}(Pyrrol\text{-}2\text{-}yl)pyridine)_4]^{2+}$,[32] a comparison of the solution binding experiments and the X-ray crystal structure of the methanesulfonate ($CH_3SO_3^-$) complex served to remind that solid state data cannot always be relied upon to predict the structure of complexes in solution. From the X-ray structure of $[Pt(3\text{-}(Pyrrol\text{-}2\text{-}yl)pyridine)_4][CH_3SO_3]_2$ shown in figure 7.29, it is clear that the pyrrole NH group interacts with the anion O-atoms.

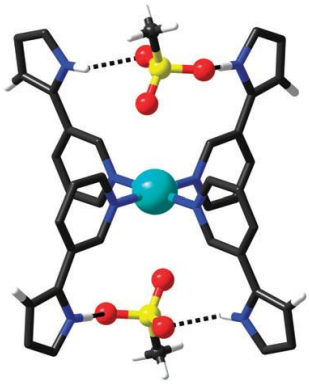

Fig. 7.29 - X-Ray crystal structure of the complex $[Pt(3\text{-}(Pyrrol\text{-}2\text{-}yl)pyridine)_4]^{2+}$ with $CH_3SO_3^-$ ions. The four NH···O interactions in the second-sphere of coordination are shown as dashed lines.

In $MeNO_2$ solution, both the pyrrole NH peak and a-pyridine CH peak shift downfield in the presence of $CH_3SO_3^-$ anions (1.77 and 1.24 ppm respectively). However, in DMSO solution, there is no evidence that the pyrrole NH groups interact with the $CH_3SO_3^-$ anion (0.00 ppm) but rather the pyrrole CH group (0.17 ppm) appears to be involved in a CH···O hydrogen bond with the anion (Fig. 7.30).

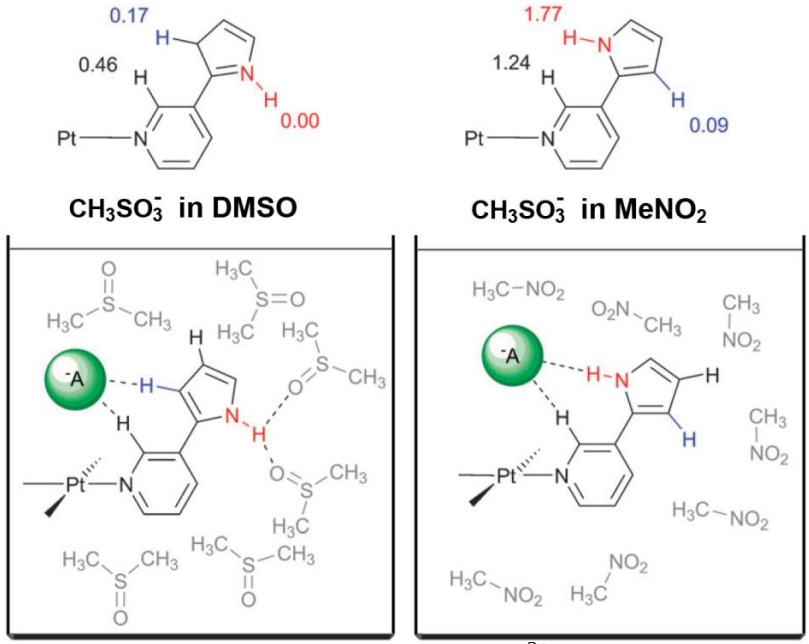

Fig. 7.30 - The receptor $[Pt(3\text{-}(Pyrrol\text{-}2\text{-}yl)pyridine)_4]^{2+}$ is very sensitive to the solvent. Interaction of this receptor with $CH_3SO_3^-$ ions in DMSO or $MeNO_2$ is accomplished via two distinct conformations of the ligand that are driven by solvation and facilitated by a simple rotation about the pyridine pyrrole bond.

These and similar results with other anions allow to conclude that a subtle solvent competition mechanism was responsible. Nitromethane is a notoriously poor hydrogenbond acceptor so when an anion was added to the receptor in this solvent, it bound to the most acidic hydrogen bond donor; the pyrrole NH. However in DMSO, which is a good hydrogen bond acceptor, the anion only bound to the pyrrole NH if it was basic enough (e.g. chloride, acetate). For less basic anions, the pyrrole NH groups actually preferred to orientate themselves into the solvent allowing the formation of hydrogen bonds to the DMSO whilst the anion was involved in weaker hydrogen-bonding with the pyrrole CH group. This rearrangement presumably occurs because it leads to a greater overall stability compared to the NH groups being oriented inwards and the solvent presented with the CH groups of the pyrrole. The profound effect of solvent on the binding mode of this simple anion receptor is an important phenomenon and should be taken into account when designing new receptors containing NH hydrogen bond donor groups.

7.4 Scorpionate effect

To conclude, let's see how coordinatively unsaturated metal complexes might provide cooperative binding with urea- or thiourea based receptors (*scorpionate effect*).[33]

Urea and thiourea can establish H-bond interactions with carboxylates and inorganic oxoanions.[34] Figure 7.31 illustrates the bifurcate binding mode of the urea moiety in the association complex between 1,3-bis(4-nitrophenyl)urea (1) and the acetate anion, as observed in the crystal structure of the corresponding tetra-n-butylammonium salt.[35]

It is observed that each hydrogen atom of the two NH fragments of **1** lies on the straight line joining a nitrogen atom and a carboxylate oxygen atom, indicating an almost perfect geometrical complementarity. However, extended equilibrium studies in non-protic solvents suggested that the stability in solution of the anion-urea H-bond complexes does not depend upon geometrical features, but is solely related to the basicity of the oxygen containing anion.[36]

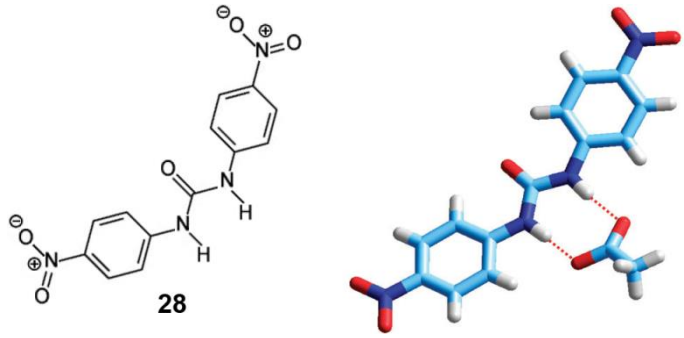

28

Fig. 7.31 - The structure of the 1:1 complex between 1,3-bis(4-nitrophenyl)-urea and acetate, as seen in the crystal structure of the $[Bu_4N][\mathbf{28}\cdot CH_3COO]$ salt.[24] (see fig. 5.4a)

In these circumstances, it seems correct to consider the hydrogen bonding interaction as a frozen proton transfer from the donor (N, in the present case) to the acceptor ($O^{\delta-}$): the more advanced the proton transfer, the stronger the interaction.[37]

In this sense, the presence of electron withdrawing substituents, as the 4-nitrophenyl group, enhances the acidity of the urea subunit, thus favouring complex formation. Ureas form association complexes also with monoatomic anions, like halides, donating two convergent H-bonds. Among halide ions, fluoride represents a very special case. In fact, F can form a genuine 1 : 1 H-bond complex with urea derivatives, in which the small anion interacts with a single N–H fragment of the receptor, as illustrated in figure 7.32. In particular, the interaction takes place at the more acidic N–H fragment, i.e. that closer to the more electron-withdrawing substituent R_1. However, in the presence of powerful electron withdrawing substituents, it may happen that, on addition of a second equiv. of fluoride, the [L–H···F] complex releases an HF molecule, with deprotonation of one of the N–H fragments and formation of the especially stable $[HF_2]^-$ complex.[38]

The two-step equilibrium is illustrated in figure 7.32. Deprotonation of one N–H fragment induces extensive p-delocalization over receptor's framework, which is reflected in a drastic modification of the spectral properties and a dramatic colour change. It is essentially for this reason that the highest number of colorimetric sensors for anions refer to fluoride, but the occurrence of the deprotonation process has been in most cases overlooked.[39]

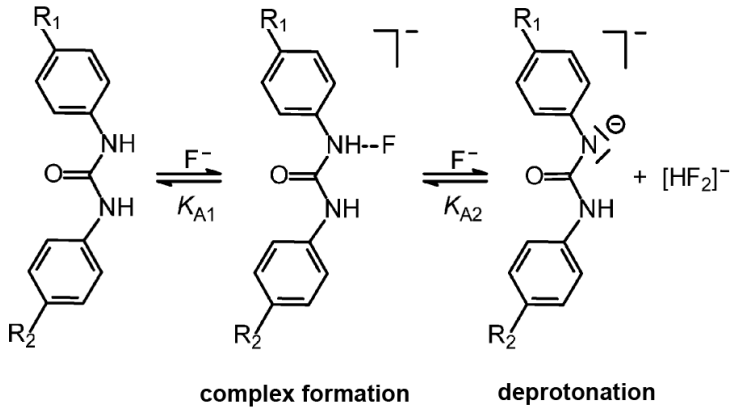

Fig. 7.32 - Stepwise equilibria in the interaction of a urea based receptor with fluoride. Occurrence of second step (deprotonation of one N–H fragment) requires that R_1 and/or R_2 are powerful electron withdrawing substituents (e.g. $–NO_2$).

Deprotonation of one N–H fragment induces extensive p-delocalization over receptor's framework, which is reflected in a drastic modification of the spectral properties and a dramatic colour change. It is essentially for this reason that the highest number of colorimetric sensors for anions refer to fluoride, but the occurrence of the deprotonation process has been in most cases overlooked.[39]

The H-bond donating properties of urea/thiourea subunits can be controlled by a proximate metal centre. As an example, a 15-crown-NS_2O_2 substituent has been appended to a nitrophenylurea/thiourea moiety, to give **29** and **30**, respectively (Fig. 7.33).[40]

The quinquedentate macrocycle can host a variety of metal ions. In particular, due to the presence of two thioethereal sulfur atoms, it firmly encircles a silver(I) metal ion.

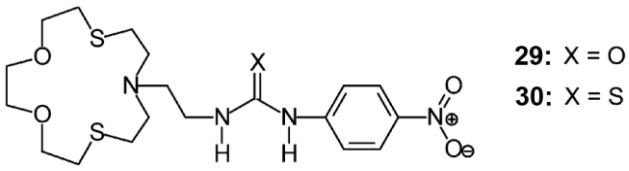

Fig. 7.33

Spectral evidences indicate that when $Ag^ICF_3SO_3$ is added to a MeCN solution 10^{-4} M in the urea derivative **29**, Ag^I cation is definitely encircled by the macrocycle, but it does not interact with the urea containing side chain, as

tentatively sketched in Scheme 7.3, structural formula **31**. Adding $[Bu_4N]CH_3COO$, following the interaction with CH_3COO^-, electron density is transferred on the oxygen atom of the urea carbonyl group, which goes to bind the Ag^I cation.

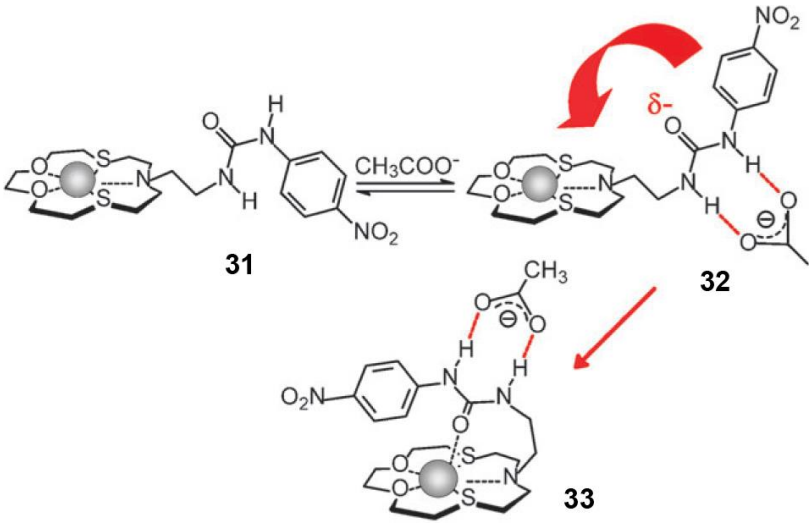

Scheme 7.3

Metal binding of a metal centre by a pendant arm linked to a macrocycle has been defined *scorpionate effect*, [41] a variant of the *chelate effect*. [42]

Scorpionate behaviour is typically associated to deprotonation of ammonium and amide groups present on the pendant arm and has involved Ni^{II}, Cu^{II} and Zn^{II} metal ions encircled by tetra-aza macrocycles.[43] Complex **7** refers to a novel anion driven scorpionate effect.

Occurrence of a scorpionate effect is equally evident in the case of fluoride. Titration of an MeCN solution 1.0×10^{-4} M in **29** (in absence of Ag^I) with a standard solution of $[Bu_4N]F$ induced the simple red shift of the band centred at 350 nm, which corresponded to the formation of the H-bond complex [(**29**···F], with an association constant logK = 4.05 ± 0.01. On the other hand, when the solution contained also 1 equiv. of $AgNO_3$, a more complex behaviour was observed. In particular, addition of the first equivalent of fluoride induced the typical red shift of the band at ca. 350 nm, indicating the formation of the H-bond complex [Ag (HL···F] (HL = **29**), according to equilibrium (1) suggests

again the coordination of the oxygen atom of urea carbonyl group to the metal centre.

$$[Ag^{I}(HL)]^{+} + F^{-} \leftrightarrows [Ag^{I}(HL)\cdots F] \qquad \log K_1 > 6 \qquad (1)$$

$$[Ag^{I}(HL)\cdots F] + F^{-} \leftrightarrows [Ag^{I}(L)] + HF_2^{-} \qquad \log K_2 > 6 \qquad (2)$$

However, a second band at 440 was observed to grow on titration with fluoride, which reached a limiting value on addition of 2 equiv. The absorption at a long wavelength and 1:2 stoichiometry indicate the occurrence of the deprotonation of one of the N–H fragments of the urea subunit and formation of the HF_2^- self-complex. Such a process is described by equilibrium (2) and is pictorially illustrated in Scheme 7.4**a**.

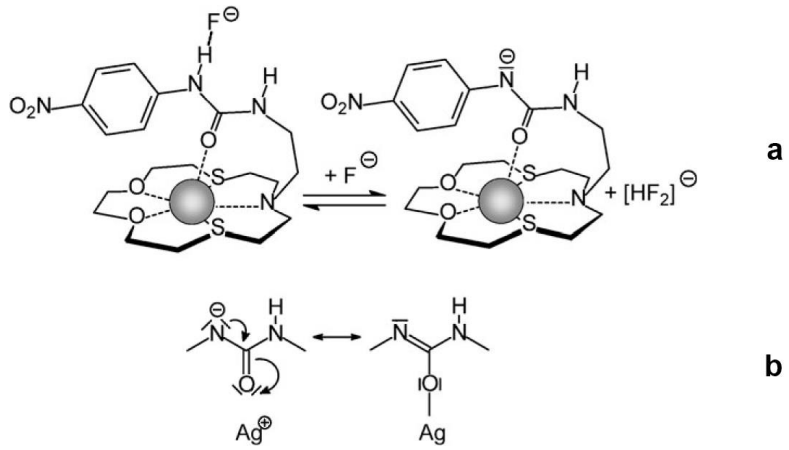

Scheme 7.4

Thus, carbonyl coordination to Ag^{I} enhances the acidity of the urea subunit enough to favour HF release, an event not observed with the plain receptor **29**. In particular, it is suggested that through-bond transfer of electron density from the negatively charged nitrogen atom to the metal centre takes place, as illustrated in Scheme 7.4b, which stabilises the deprotonated form of urea derivative **29**.

Binding behaviour of the thiourea-based receptor **30** towards Ag^{I} is somewhat different. In fact on addition of $Ag^{I}CF_3SO_3$, the absorption band of **30**, centred at 345 nm, undergoes a significant blue shift. The absorption band

originates from a charge transfer from the thiourea subunit (donor) to the $-NO_2$ fragment (acceptor): the reduction of the dipole intensity on Ag^I addition (as demonstrated by the substantial blue shift) suggests the establishing of a coordinative interaction between the metal centre and the thiourea sulfur atom. Titration profiles indicate the formation of a very stable 1:1 complex, whose geometrical structure is sketched in Scheme 7.5, formula **34**.

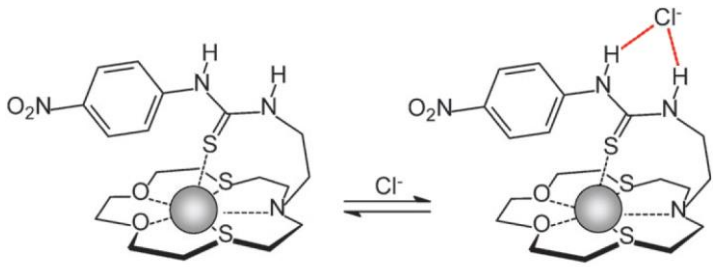

34 **35**

Scheme 7.5

References

[1] V. Amendola, M. Bonizzoni, D. Esteban-Gómez, L. Fabbrizzi, M. Licchelli, F. Sancenón and A. Taglietti, *Coord. Chem. Rev*., **2006**, 250, 1451–1470.

[2] Y. Bretonniere, M. J. Cann, D. Parker and R. Slater, *Org. Biomol. Chem*., **2004**, 2, 1624.

[3] N. L. S. Yue, M. C. Jennings and R. J. Puddephatt, *Inorg. Chem.*, **2005**, 44, 1125.

[4] J. W. Steed and J. L. Atwood, *Supramolecular Chemistry*, 2nd edn, J. Wiley & Sons, Chichester, **2009**.

[5] M. T. Blanda, J. H. Horner and M. Newcomb, *J. Org. Chem*., **1989**, 54, 4626.

[6] W. Xu, J. J. Vital and R. J. Puddephatt, *J. Am. Chem. Soc*., **1993**, 115, 6456.

[7] Y. Agnus, R. Louis and R. Weiss, *J. Am. Chem. Soc*., **1979**, 101, 3381.

[8] L. Fabbrizzi, M. Licchelli, G. Rabaioli and A. Taglietti, *Coord. Chem. Rev*., **2000**, 205, 85

[9] A.V. Koulov, K.A. Stucker, C. Lakshmi, J.P. Robinson, B.D. Smith, *Cell Death Diff.* 10 (**2003**) 1357.

[10] E. J. O'Neil and B. D. Smith, *Coord. Chem. Rev*., **2006**, 250, 3068.

[11] C. Lakshmi, R.G. Hanshaw, B.D. Smith, *Tetrahedron* 60 (**2004**) 11307.

[12] S. L. Tobey and E. V. Anslyn, *J. Am. Chem. Soc*., **2003**, 125, 14807.

[13] McGrady, G. S., Steed, J. W., 'Hypervalent compounds'. in Encyclopedia of Inorganic Chemistry 2, King, R. B., ed. John Wiley & Sons, Ltd: Chichester, **2005**, Vol. 3, pp. 1938–1961.

[14] Shriver, D. F., Biallas, M. J., *J. Am. Chem. Soc*. **1967**, 89, 1078.

[15] Katz, H. E., *J. Org. Chem* **1985**, 50, 5027–5032

[16] Herberich, G. E., Fischer, A., Wiebelhaus, D., Bis(boryl)metallocenes.. *Organometallics* **1996**, 15, 3106–3108.

[17] Arimori, S., Davidson, M. G., Fyles, T. M., Hibbert, T. G., James, T. D., Kociok-Kohn, G. I., *Chem. Commun*. **2004**, 1640–1641.

[18] M. S. Goodman, V. Jubian and A. D. Hamilton, *Tetrahedron Lett*., **1995**, 36, 2551–2554.

[19] M. S. Goodman, V. Jubian, B. Linton and A. D. Hamilton, *J. Am. Chem. Soc*., **1995**, 117, 11610–11611.

[20] Scigress Explorer Software, Biosciences Group, Fujitsu Computer Systems Corp., Westwood MA 02052, **2009**.

[21] DIAMOND, CRYSTAL IMPACT, Postfach 1251, D-53002, Bonn, Germany, **2010**.

[22] L. H. Uppadine, M. G. B. Drew and P. D. Beer, *Chem. Commun*., **2001**, 291–292.

[23] L. H. Uppadine, F. R. Keene and P. D. Beer, *J. Chem. Soc., Dalton Trans*., **2001**, 2188–2198.

[24] C. R. Bondy, P. A. Gale and S. J. Loeb, *J. Am. Chem. Soc*., **2004**, 126, 5030–5031.

[25] C. R. Bondy, S. J. Loeb and P. A. Gale, *Chem. Commun*., **2001**, 729–730.

[26] C. R. Bondy, P. A. Gale and S. J. Loeb, *J. Supramol. Chem*., **2003**, 2, 93–96.

[27] L. Ion, D. Morales, J. Pérez, L. Riera, V. Riera, R. A. Kowenicki and M. McPartlin, *Chem. Commun*., **2006**, 91–93.

[28] L. Ion, D. Morales, S. Nieto, J. Pérez, L. Riera, V. Riera, D. Miguel, R. A. Kowenicki and M. McPartlin, *Inorg. Chem*., **2007**, 46, 2846–2853.

[29] S. R. Cooper, *Acc. Chem. Res*., **1988**, 21, 141–153.

[30] R. B. Bedford, M. Betham, C. P. Butts, S. J. Coles, M. B. Hursthouse, P. N. Scully, J. H. R. Tucker, J. Wilkie and Y. Willener, *Chem. Commun*., **2008**, 2429–2431.

[31] V. Amendola, M. Boiocchi, B. Colasson, L. Fabbrizzi, M.-J. Rodriguez Douton and F. Ugozzoli, *Angew. Chem., Int. Ed*., **2006**, 45, 6920–6924.

[32] I. E. D. Vega, P. A. Gale, M. E. Light and S. J. Loeb, *Chem. Commun*., **2005**, 4913–4915.

[33] V. Amendola, L. Fabbrizzi, *Chem. Commun*. **2009**, 513.

[34] P. J. Smith, M. V. Reddington and C. S. Wilcox, *Tetrahedron Lett*., **1992**, 41, 6085; T. Gunnlaugsson, A. P. Davis and M. Glynn, *Chem. Commun*., **2001**, 2556; S. Sasaki, D. Citterio, S. Ozawa and K. Suzuki, *J. Chem. Soc., Perkin Trans*. 2, **2001**, 23; D. H. Lee, H.

Y. Lee, K. H. Lee and J. L. Hong, *Chem. Commun*., **2001**, 1188; F. Sansone, E. Chierici, A. Casnati and R. Ungaro, *Org. Biomol. Chem*., **2003**, 1, 1802; T. Gunnlaugsson, P. E. Kruger, T. C. Lee, R. Parkesh, F. M. Pfeffer and G. M. Hussey, *Tetrahedron Lett*., **2003**, 44, 6575; T. Gunnlaugsson, A. P. Davis, G. M. Hussey, J. Tierney and M. Glynn, *Org. Biomol. Chem*., **2004**, 2, 1856.

[35] M. Boiocchi, L. Del Boca, D. Esteban-Gómez, L. Fabbrizzi, M. Licchelli and E. Monzani, *J. Am. Chem. Soc*., **2004**, 126, 16507.

[36] V. Amendola, D. Esteban- Gómez, L. Fabbrizzi and M. Licchelli, *Acc. Chem. Res*., **2006**, 39, 343.

[37] T. Steiner, *Angew. Chem., Int. Ed*., **2002**, 41, 48.

[38] M. Boiocchi, L. Del Boca, D. Esteban- Gómez, L. Fabbrizzi, M. Licchelli and E. Monzani, *Chem. Eur. J*., **2005**, 11, 3097.

[39] D. Esteban- Gómez, L. Fabbrizzi and M. Licchelli, *J. Org. Chem*., **2005**, 70, 5717–5720.

[40] V. Amendola, D. Esteban-Gómez, L. Fabbrizzi, M. Licchelli, E. Monzani and F. Sancenón, *Inorg. Chem*., **2005**, 44, 8690.

[41] P. Pallavicini, A. Perotti, A. Poggi, B. Seghi and L. Fabbrizzi, *J. Am. Chem. Soc*., **1987**, 109, 5139.

[42] G. Schwarzenbach, *Helv. Chim. Acta*, **1952**, 35, 2344.

[43] (a) L. Fabbrizzi, M. Licchelli, P. Pallavicini and L. Parodi, *Angew. Chem., Int. Ed*., **1998**, 37, 800; (b) L. Fabbrizzi, F. Foti, M. Licchelli, P. M. Maccarini, D. Sacchi and M. Zema, *Chem. Eur. J*., **2002**, 8, 4965.

8. Platinum(II) dithioxamide complexes based receptors

8.1 The state of art

The first part of the present dissertation has been devoted to show how the most prominent research groups in the field have approached design and synthesis of anion receptors. In particular, much interest has been focused in the choice of synthons containing hydrogen donor groups such as amides, thioureas as well as their sulphur derivatives. For this reason it could seem strange that secondary dithiooxamides, whose structure is strictly similar to that of the aforementioned classes of compounds (Fig. 8.1) have not ever exploited as a synthon to be put into anion receptors properly designed.

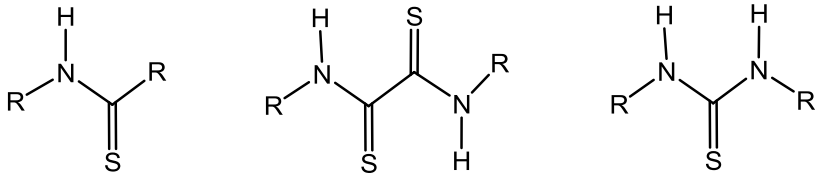

Fig. 8.1

Nevertheless, the hydrogens atoms of secondary dithioxamides, being acidic enough, can be removed to give rubeanates; also, unsubstituted dithiooxamide H_2N-C(S)(S)C-NH_2 is known as rubeanic acid and its hydrogen bond donor properties have been already recognized in the solid state in some binary compounds of dithiooxamide with crown ethers (Fig. 8.2-8.3). [1]

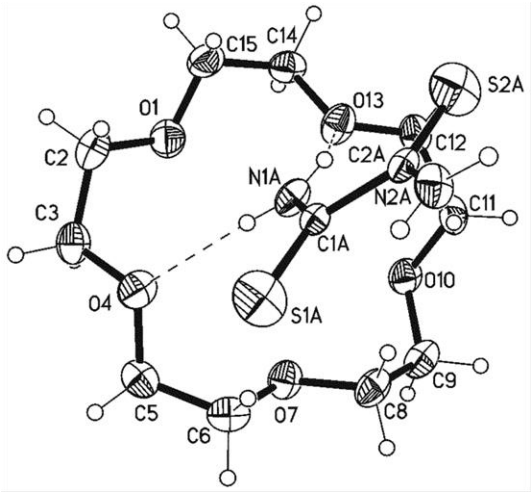

Fig. 8.2 - ORTEP drawing for dithiooxamide with 15-crown-5 complex

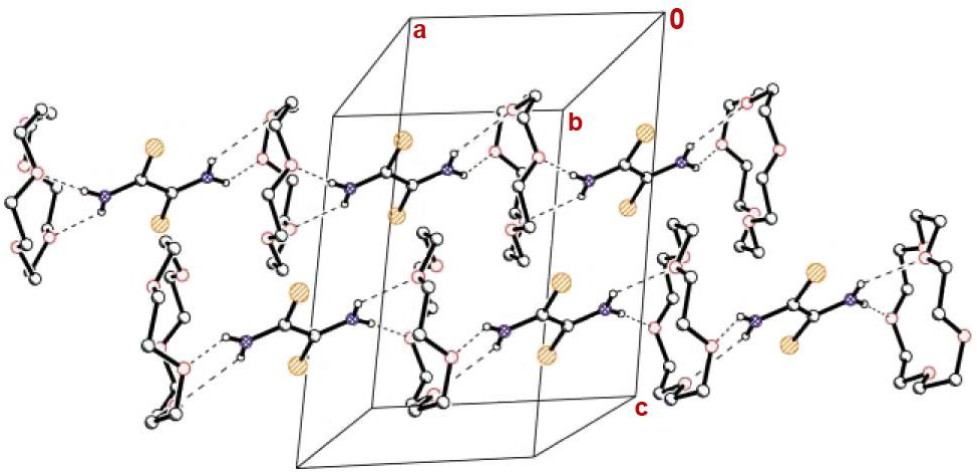

Fig. 8.3 - Arrangement of chains in dithiooxamide with 15-crown-5 complex

Dithiooxamides are polyfunctional molecules which in principle can bind to a given metal ion in a variety of different fashions. They constitute a class of ligands possessing low-lying π* orbitals, long since known [2], and form intensely coloured metal complexes which has a number of applications, including an important imaging process [3], as well as the removal of heavy metals from wastes [4].

The only compounds containing dithiooxamide frames inserted in a cyclic structure, potentially anion receptors, have been reported more than ten years ago [5]

These macrocycles were firstly produces by reaction of unsubstituted dithiooxamide H_2N-C(S)(S)C-NH_2 with primary aliphatic amines *via* elimination of NH_3 (Scheme 8.1).

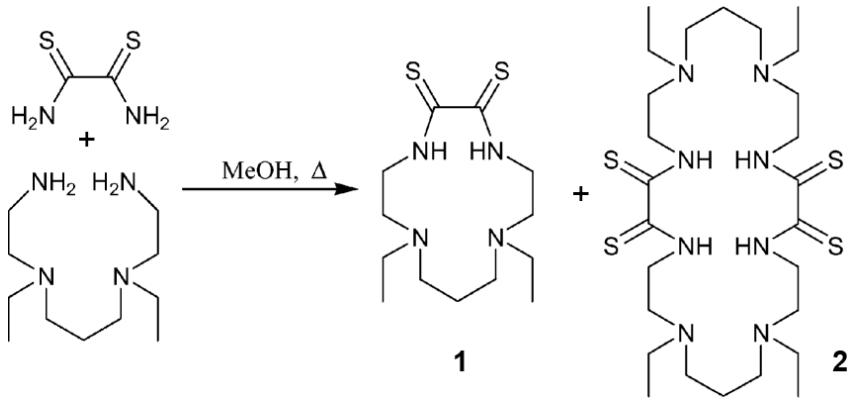

Scheme 8.1

Due to the low yields obtained for **1** and **2** using the cyclisation route above, the synthesis of thioamide macrocycles **1** was better achieved through thionation of the amide macrocycle (scheme 8.2).

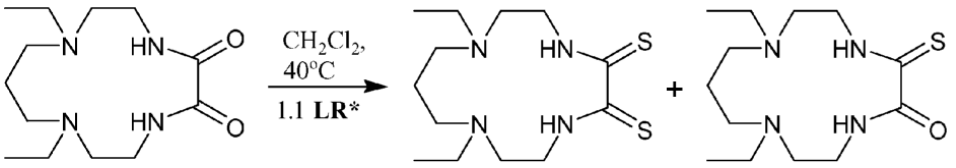

Scheme 8.2 - LR* = Lawesson's reagent [6]

Unfortunately, none of the above macro-cycles has been shown to behave as anion receptor. Nevertheless, a previous report (2003) reported a polythioamide macrocycle series designed as anion receptors and described these as "the first thioamide-based macrocycles",[7] emphasizing the novel nature of such ligands (Fig. 8.4).

4: X = S, Y = CH
5: X = S, Y = N
7: X = O, Y = CH
8: X = O, Y = N

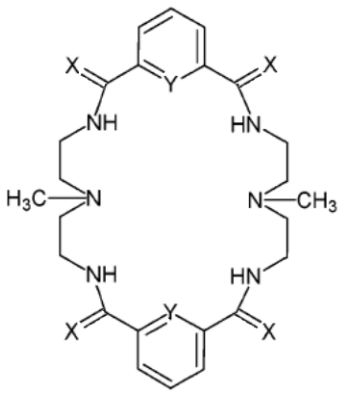

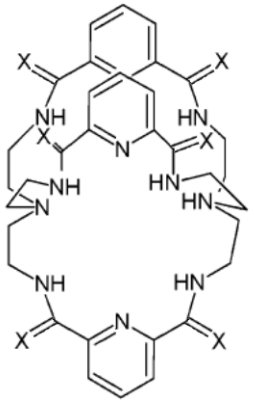

6: X = S
9: X = O

Fig. 8.4

Very similar macrocycles have subsequently been reported. [8,9] These compounds were produced by conversion of their amide-based precursors to thioamides *via* a thionation agent such as Lawesson's reagent.[6] One of them, **5**, is able to host a chloride in its cavity as shown by the X ray structure of [**5**·Cl] (Fig. 8.5).

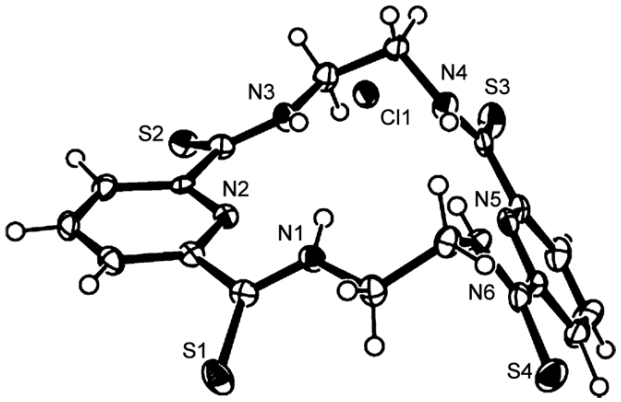

Fig. 8.5 - X-Ray crystal structure of [**5**·Cl^-] complex (obtained as [**5**·Cl]PPh_4)

^{1}H NMR spectroscopy was adopted to study the anion binding ability of **5** in DMSO-d_6. [10,11] Addition of tetrabutylammonium salts (*n*-Bu_4NX; X =F^-, Cl^-, Br^-, I^-, AcO^-, and $H_2PO_4^-$) led to drastic downfield shifts in the N-H resonance as shown in figure 8.6(b). The large downfield shift of the N-H signal is consistent with the presence of a hydrogen-bonding interaction between the inner thioamide protons and the anions. [12]

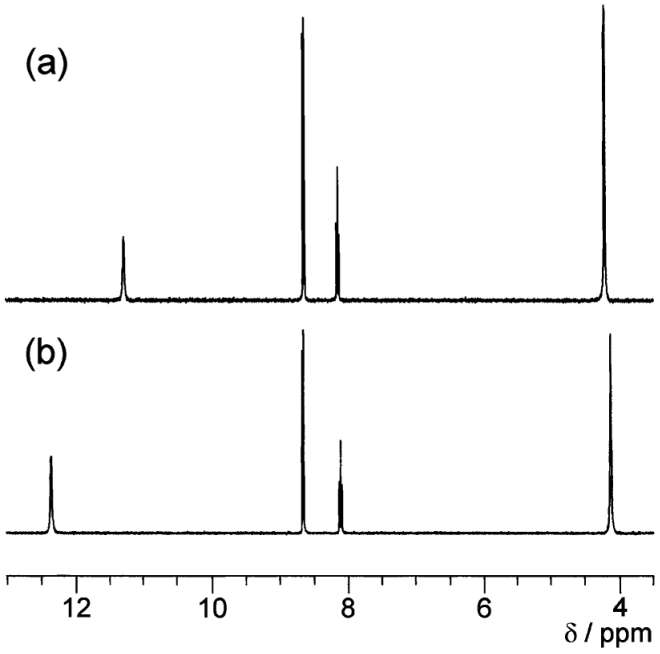

Fig. 8.6

As matter of fact, in thioamide **5** the inner cycle is suitable to host an anion, while **1**, **2**, and **3** arrange amidic hydrogens in such a way that no anion finds a complementary shape. However, in **5** the thioamide groups are not adjacent and thus not positioned for exogenous coordination; therefore future syntheses are expected which provide **1-3** type macrocycles with internal cavities more suitable for anion accommodation.

The laboratories where the experiments of the present dissertation were carried out have a long standing expertice in the coordinating properties of dithiooxamides.

In particular, it has never been observed downfield shift of HN(R)C(S)-C(S)(R)NH protons in the presence of either HCl or tetrabutylammonium chloride in chloroform-*d* and in dimethilsulphoxide-d_6, and this a clear evidence that in solution **HBD** groups of a secondary dithiooxamide do not interact with chloride anion. [9,10,11]

In the free form dithiooxamides exist as E-conformers (Fig. 8.7). [13]

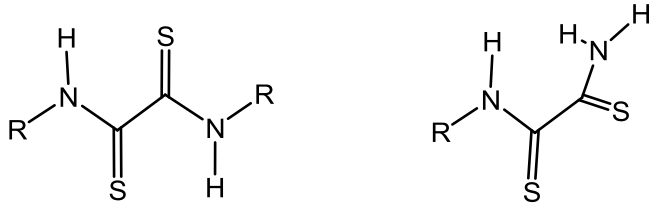

E **Z**

Fig. 8.7

Steric interactions makes the existence of the conformer Z unlikely, and this could explain the observed lack of interaction of a free secondary dithiooxamide with a chloride ion. After all, it has been widely demonstrated in the previous chapters that anion coordination requires a cooperative effect of a number of HBD groups, which sometimes are pre-organized by a suitable metal ion to a more effective anion recognition. In particular, a free secondary dithiooxamide closely resembles the ligand 2,2'-biimidazole which prefers an anti conformation when uncoordinated (see pag. 119). Chelation to a metal centre requires rotation about the single bond linking the rings and adoption of the *syn* conformation which orients both the imidazole NH groups outward where they can participate in a second-sphere interaction with an anion

Actually, when the twofold quantity of a N,N'-di-*n*-butyl-dithiooxamide (H_2-^{n}bu$_2$DTO) is reacted in chloroform with a given amount of cis-[$Pt(Me_2SO)_2Cl_2$] a deep purple compounds is formed which can be isolated in the solid state [14]

The above purple compound shows the following characteristics: i) it is constituted by two moles of H_2-^{n}bu$_2$DTO per mole of $PtCl_2$ unit, i.e. (H_2-^{n}bu$_2$DTO)$_2$·$PtCl_2$; ii) its NH signal in chloroform-*d* is a very broad singlet at 13.65 ppm, which is largely downshifted with the respect to the corresponding resonance of the uncoordinated H_2-^{n}bu$_2$DTO at 10.38 ppm (Fig. 8.8).

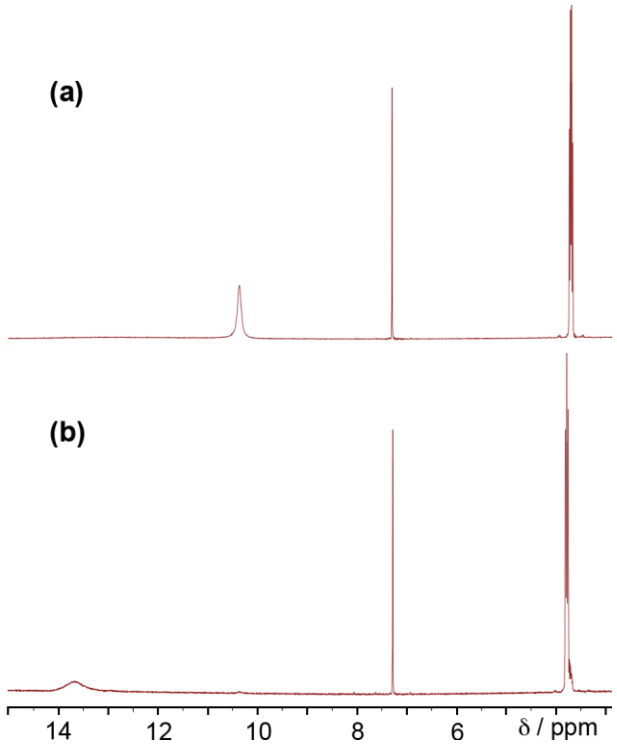

Fig. 8.8

Such an exceedingly large downshift is the result of a strong N-H···Cl interaction [10,11,12], which indicates that chloride ion must be in the outer platinum(II) coordination sphere and, consequently, that the inner platinum coordination sphere must occupied by the S,S chelating system of the dithioxamide. In other words, platinum(II) is engaged in a PtS_4 coordination; iii) its proton spectrum shows only one *n*-butyl pattern, which however features

the NH-CH_2- methylene protons as a triplet, while in the uncoordinated H_2-$^{n}bu_2$DTO the same protons appeared as a quartet ; iv) its electronic spectrum holds the Beer's law also at high dilution. On the basis of the above points, the platinum dithiooxamide purple complex may be formulated as the tight-contact ion pair represented in the figure 8.9.

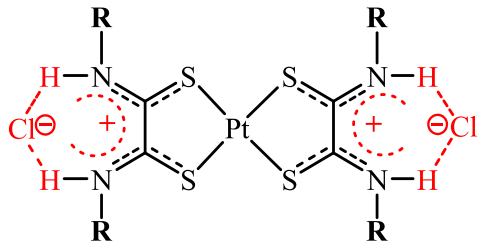

11: R = *n*-butyl

Fig. 8.9 - Molecular formula of the tight ion pair [Pt(H_2R_2DTO κ-S,S Pt)$_2$][Cl]$_2$

It is unlikely that the individual (and planar) thioamide groups are nearly coplanar in the [Pt(H_2R_2DTO κ-S,S Pt)$_2$][Cl]$_2$ species; such a coplanarity in the neutral ligand would require a non-bonded H···H distance of *ca.* 1.40 Å between the amide protons. It may be emphasized that extremely short non-bonded H···H distances have been reported in the range 1.71-1.75 Å.[15]

Hence, a S,S'-geometry in neutral dithio-oxamides requires a torsional motion about the C-C bond between the thioamide moieties in [Pt(H_2R_2DTO κ-S,S Pt)$_2$][Cl]$_2$. A pair of papers dealing with the tilted array of metal complexes containing S,S chelated neutral dithioxamides reports the X-ray structures of [Cu(H_2Bn_2DTO)$_2$][ClO_4]$_2$, [Zn(H_2Me_2DTO)Cl_2], $SnBr_4$(H_2bu_2DTO) and $BiCl_3$(H_2Et_2DTO)$_2$ (Fig 8.10). [16]

The torsional angle, which ranges in them all between 36° and 40° *ca*) seems to be independent of the central metal (Zn, Cu, Sn, and Bi) and coordination geometry (square planar, tetrahedral, octahedral, bipyramidal), and therefore it is probably a structural feature of neutral chelating dithiooxamides.

However, in chloroform solution the molecular plane of [Pt(H_2-$^{n}bu_2$DTO k-S,S Pt)$_2$][Cl]$_2$ appears to be symmetrical, since the N-CH_2- protons of *n*-butyl groups are featured by a sharp triplet, despite the chiral torsion around the C-C bond of the coordinated dithioxamide.

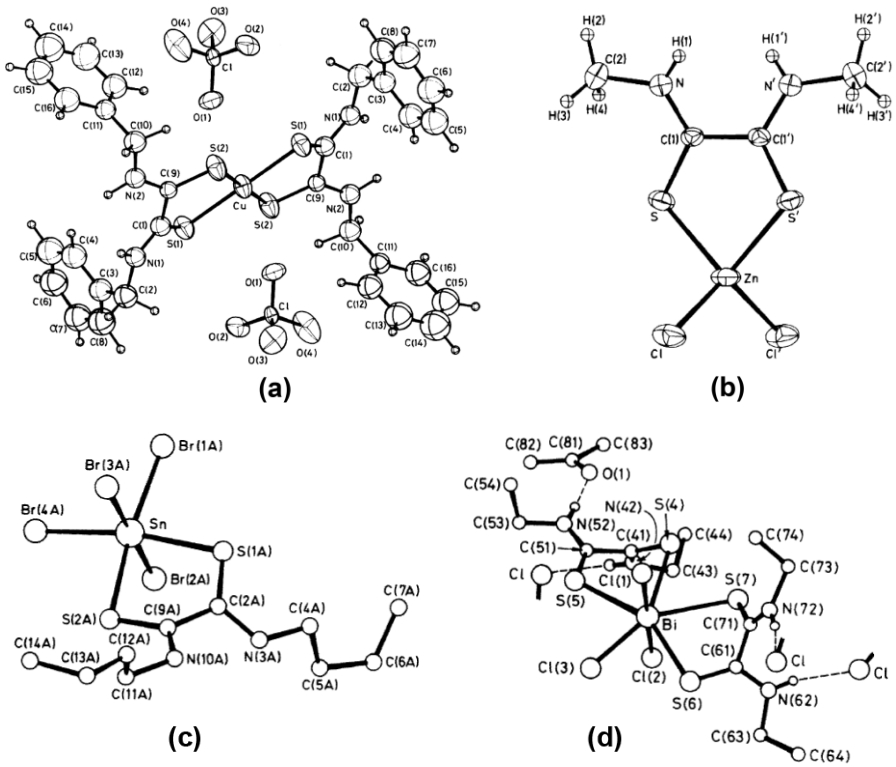

Fig. 8.10 - (a) ORTEP view of $[Cu(H_2Bn_2DTO)_2][ClO_4]_2$ showing the atom-labelling scheme and thermal motion ellipsoids at the *50%* level. **(b)** ORTEP view of $[Zn(H_2Me_2DTO)Cl_2]$**.** Primed atoms are related to unprimed by a two-fold axis through the Zn atom and bisecting the S-Zn-S' angle. **(c)** The molecular structure of $SnBr_4(H_2bu_2DTO)$. **(d)** The molecular structure of $BiCl_3(H_2Et_2DTO)_2$

It should be remembered that a high energy barrier chiral torsion is a chiral axis and, in such a case, the α prochiral N-CH_2-CH_2- protons should have appeared in the spectrum as an ABX_2 spin system. Moreover, the further simplification of N-CH_2-signals on going from the free H_2-^{n}bu_2DTO (a quartet) to the S,S coordinated Pt(H_2-^{n}bu_2DTO k-S,S Pt) moiety (a triplet) could be attributed to the lack of magnetic coupling between N-CH_2- and N-H protons because of probable fast exchange of the N-H protons. The above spectral findings are a clear sign that the symmetrization of the molecular plane requires the movement of HCl, which, leaving from and re-entering in the coordinated dithioxamide very fastly, produces the rapid (in the NMR time scale) δ ⇌ λ isomerization of the seven membered $C_2N_2H_2Cl$ ring and hence the symmetrization of the mean plane of such a ring (vide infra).

It is possible to remove hydrochloric acid from [Pt(H_2-^{n}bu$_2$DTO k-S,S Pt)$_2$][Cl]$_2$ in a variety of ways. Among these, the most simple is to add sodium bicarbonate under stirring to a chloroform solution of the purple ion pair, whose colour turns soon from purple to red. From the red solution the solid bicarbonate is filtered off. The red dehydroalogenated compound [Pt(H-^{n}bu$_2$DTO k-S,S Pt)$_2$] ,**12,** can be formulated as in figure 8.11.

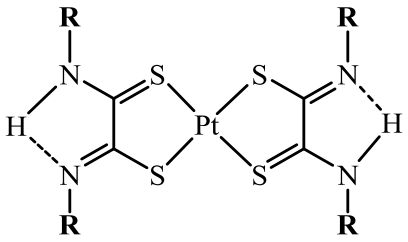

12: R = *n*-butyl

Fig. 8.11 – Structural formula of [Pt(H-^{n}bu$_2$DTO k-S,S Pt)$_2$] ,**12**.

Upon concentration, red crystals of **12** were obtained whose crystal structure was determined by a crystallographic analysis (Fig 8.12) [14]

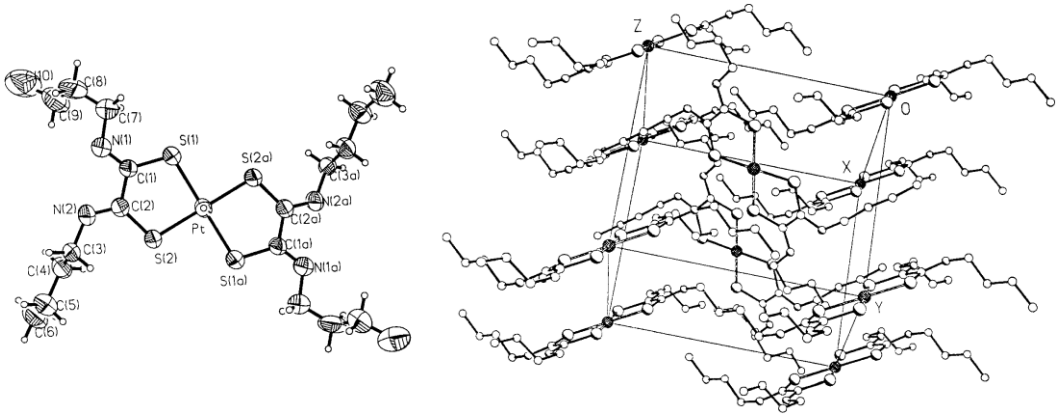

Fig. 8.12 - Molecular structure and packing of [Pt(H-^{n}bu$_2$DTO)$_2$]

By bubbling gaseous HCl into a chloroform solution of **12** the tight ion pair **11** is restored. The same result is obtained by shaking a chloroform solution of **12** against concentrated aqueous solution of HCl.

The mono-chlorohydrate [(H-^{n}bu$_2$DTO k-S,S Pt)Pt(H_2-^{n}bu$_2$DTO k-S,S Pt)][Cl] ,**13**, (Fig. 8.13) can be prepared as a pure compound through the following process:

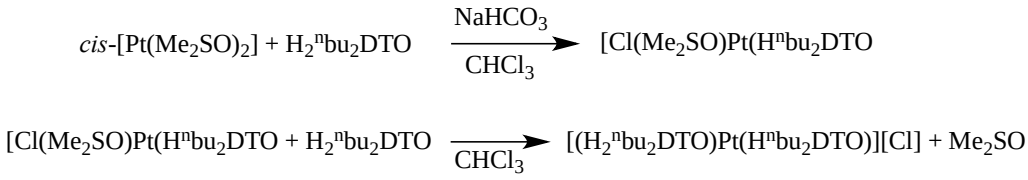

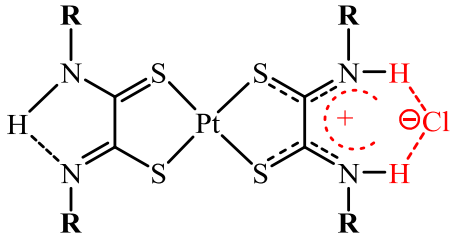

13: R = *n*-butyl

Fig. 8.13 – Structural formula of mono-chlorhydrate [(H-^{n}bu$_2$DTO k-S,S Pt) Pt(H$_2$-^{n}bu$_2$DTO k-S,S Pt)][Cl] , **13.**

The proton spectrum of mono-chlorhydrate ion pair **13** displays the same spectral pattern of the di-chlorhydrate ion pair **11**, *i.e.*, only one group of signals for either the N-H resonance (13.00 ppm) or the methylene and methyl protons of the butyl chain. This means that HCl cannot be localized in one of the two S,S chelated rubeanate frame, (alkyl substituents experience the same chemical environment) but it is rapidly exchanged between the two N-H$^{\cdots}$N sites of both rubeanate frames in such a way that the chemical environment become the same for the four alkyl substituents at least in the NMR time scale. After all, the rapid exchange of the N-H protons has been suggested by the apparent symmetry of the molecular plane in **11**. Proton spectra of **13** recorded at temperature as low as 210 K produced only a broadening of the N-CH$_2$- triplet together with a sharpening of the very broad N-H singlet at 13.00 ppm. However, low temperature NMR spectra of the mono-chlorhydrate [(H(R-2-phenylethyl)$_2$)DTO κ-S,S Pt)Pt(H$_2$(R-2-phenylethyl)$_2$ κ-S,S Pt)][Cl], **14**, (Fig. 8.15) gave more reasonable results, probably because the more encumbered 2-phenylethyl groups slow down the HCl scrambling between basic sites. A similar dependence of the exchange rate from the steric congestion of the (R)N-H$^{\cdots}$N(R) site has also been observed in a Rh(III) dithiooxamide complex[17]. In the figure 8.14 the variable temperature spectra of [(H(R-2-phenylethyl)$_2$) DTO κ-S,S Pt)Pt(H$_2$(R-2-phenylethyl)$_2$ κ-S,S Pt)][Cl] species are shown.

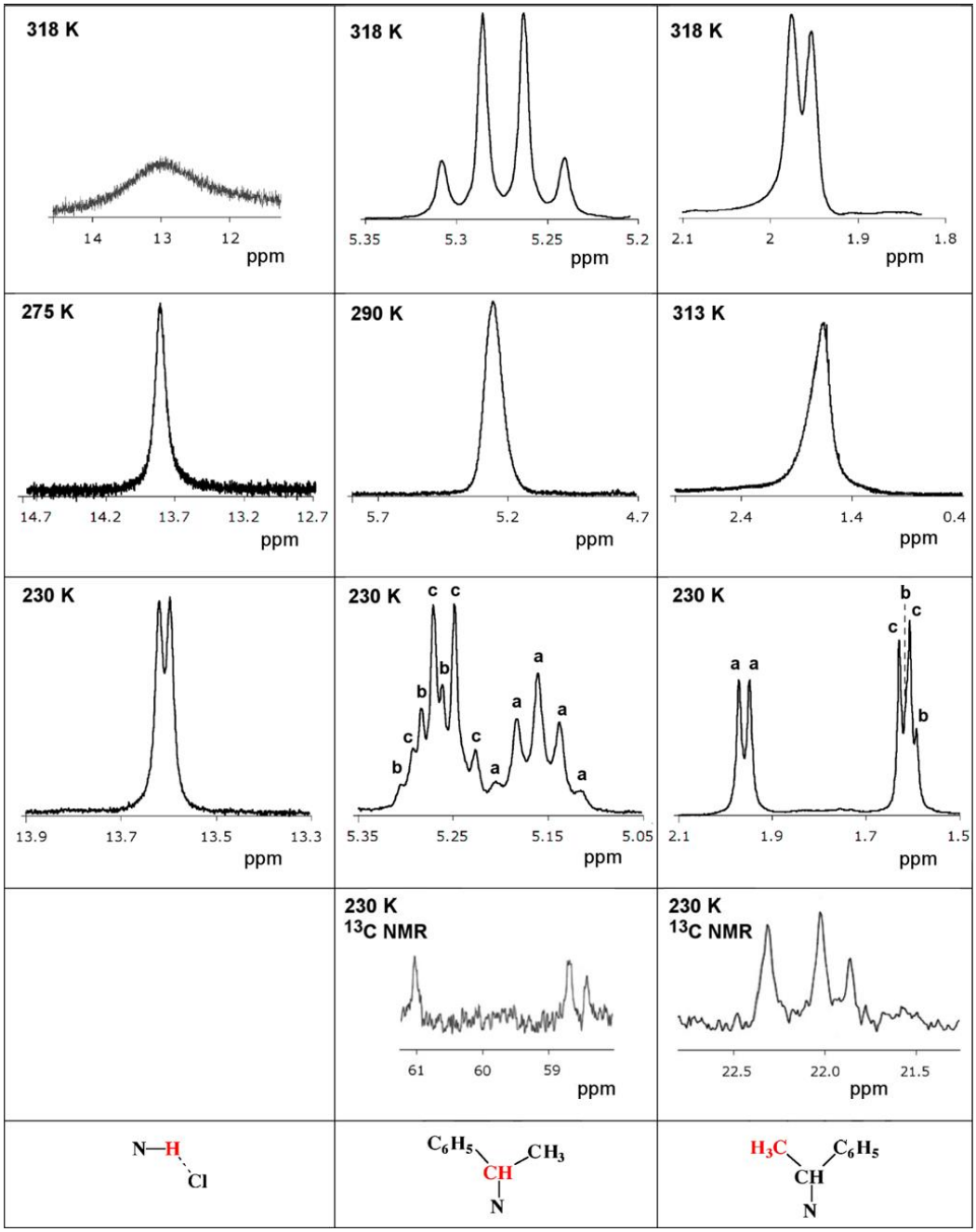

Fig. 8.14 - Spectral signals of NHCl group (left column), methine (central column) and methyl protons (right column) of the [(H(R-2-phenylethyl)$_2$) DTO k-S,S Pt)Pt(H$_2$(R-2-phenylethyl)$_2$ κ-S,S Pt)][Cl] in chloroform at 318 K (first row), at coalescence temperatures (second row) and at 230 K (third row). ^{13}C NMR signals of both methine and methyl groups are reported in the fourth row.

The CH and CH_3 signals at 230 K are labelled by the letters "**a**", "**b**" and "**c**". Peaks labelled as "**a**" (five lines corresponding to two quartets plus a doublet at higher fields) refer to the fully hydrohalogenated species **16** (see figure 8.15). Peaks labelled as "**b**" (five lines, of whom two are obscured by a superimposed quartet) refer to the hydrohalogenated half moiety of **14**. Finally, peaks indicated as "**c**" refer to two coincident quartets featuring CH of **14** and **15** (Fig. 15), and to two coincident doublets featuring CH_3 of the dehydrohalogenated half moiety of the species **14** as well as to both halves of the totally dehydrohalogenated species **15**. NHCl signal at 230 K features the amide protons of both **14** and **16**.

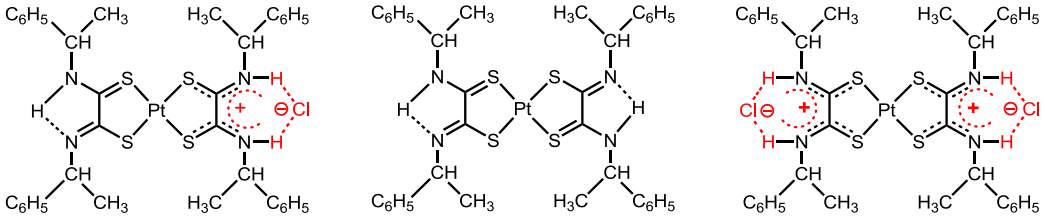

Fig. 8.15 - Structural formulae of the species **14**, **15** and **16** mentioned in figure 8.14. The compounds are the various hydrohalogenated forms of compound [(R-dithiooxamidate)Pt(H-R-dithiooxamide)][Cl] (formally, compound **14** in figure), in which R stands for the {S}-1-phenylethyl group.

The data in figure 8.14 demonstrate that in a chloroform solution of the compound **14**, formally made of a hydrohalogenated dithiooxamide moiety and a dithiooxamidate moiety, undergoes a rapid equilibrium with **15** and **16** species, as a consequence of fast HCl transfer.

Actually, the reported spectra indicate that at high temperature the HCl very rapidly jumps among the two nitrogen N-H···N sites of the molecule. In fact, the two halves of the species **A** yield only one group of signals in the NMR spectra (see first row). In particular, because of the rapid motion of HCl, NH···Cl proton appears in the spectrum as a very broad singlet, while CH methine protons of the dithiooxamide groups are featured by a quartet, since such protons cannot couple with the mobile NH protons. On cooling, after coalescence (second row) the methyl doublet tends to split into two groups of signals, until three doublets appear in the proton spectrum at 230 K (third row). The spectrum does not change anymore on further cooling. The corresponding ^{13}C NMR spectra in the

methyl region show the same behaviour: the single methyl signal at 318 K (not shown) splits into three signals at 230 K (fourth row, third column).

As for the dithiooxamide CH protons, the sharp quartet at 318 K (first row, second column) coalesces at 290 K (second row, second column); then, it splits into two groups of signals which at 230 K appear as two groups of five lines and a quartet which is superimposed to one of them (third row, second column). The five line patterns feature CH groups near to the coordinated HCl in **14** and **16** species. In fact, the CH quartet is split by the near amide proton, which is fixed on the amide nitrogen at low temperature, at least on the NMR time scale. Three signals feature the CH system also in the ^{13}C NMR spectrum (fourth row, second column). Finally, the very broad singlet, featuring NHCl at high temperatures, becomes a sharp doublet at 230 K, since the fixed NH proton is split by the near methine hydrogen. It should be stressed that the above data also indicate that species **14** is not a single compound in chloroform at room temperature, but is a mixture including also the parent **15** and **16** species.

A further interesting example of HCl motion within a Pt-S,S chelated neutral dithioxamide is provided by $[(Me_2SO)(CH_3)Pt(H_2\text{-}Bn_2\text{-}DTO)][Cl]$ (Fig. 8.16).[18]

This compound has been prepared by reacting trans-$[Pt(Me_2SO)_2(CH_3)Cl]$ with the equimolar quantity of H_2-Bn_2-DTO. Actually, the chelating dithioxamide replaces one of the two coordinated sulphoxide trans to each other; then, the other sulfur tooth of the ligand forms the chelate ring by removing the chloride ion from the inner coordination sphere of platinum(II); the leaving chloride however remains as a guest in the outer coordination sphere of the complex, held by the electrostatic interaction of the two thioamidic HBD N-H groups. As a result, the ion pair depicted in the figure 8.16 is formed:

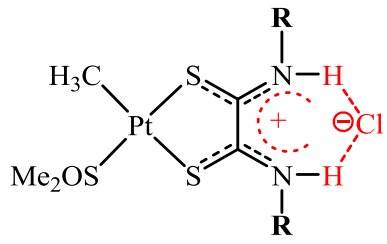

17: R = benzyl

Fig. 8.16 - Structural formula of the ion pair $[(Me_2SO)(CH_3)Pt(H_2\text{-}Bn_2\text{-}DTO)][Cl]$.

The complex showed in figure 8.16 represents the $[(Me_2SO)(CH_3)Pt(H_2\text{-}Bn_2\text{-}DTO)]^+$ as a anion binding receptor, which hold a chloride ion in a tight ion pair

through its HBD N-H groups. In the above ion pair the N-H protons, as well as the chloride related to them, are mobile; this is clearly demonstrated by the fact that when $[(Me_2SO)(CH_3)Pt(H_2\text{-}Bn_2\text{-}DTO)][Cl]$ is left to stand in solution, an electrophilic attack by HCl to Pt-CH_3 bond happens, according to a well known mechanism [19]

The figure 8.17 shows the NMR monitoring of the protonolisis process:

$$[(Me_2SO)(CH_3)Pt(H_2\text{-}R_2\text{-}DTO)][Cl] \longrightarrow [(Me_2SO)ClPt(H\text{-}R_2\text{-}DTO)] + CH_4$$

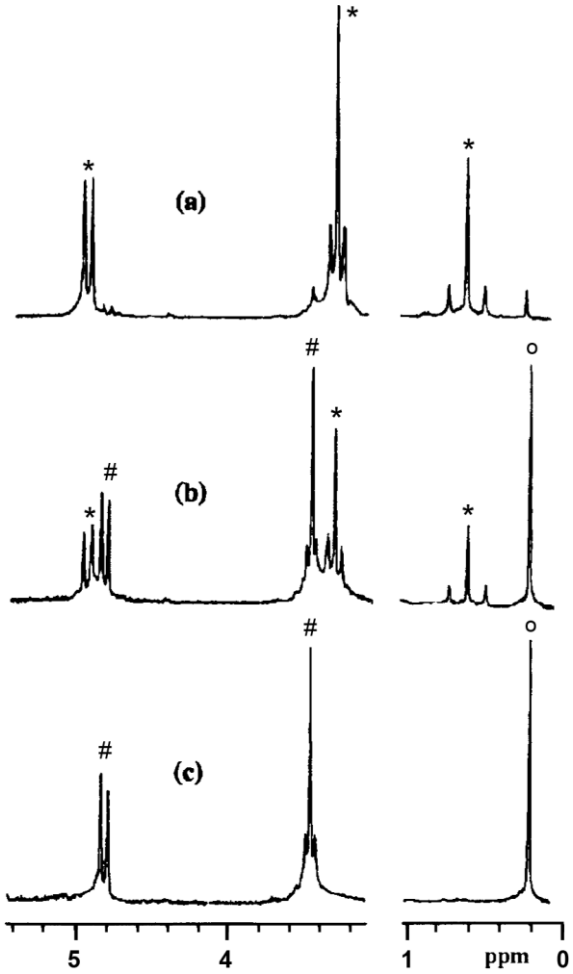

Fig. 8.17 - ^1H NMR spectral monitoring of the reaction trans- $[Pt(Me_2SO)_2MeCl]$ + $H_2\text{-}Bn_2\text{-}DTO$. (**a**) Spectrum recorded immediately after the mixing of the reagents; (**b**) after 30 min.; (**c**) at the end of the reaction. Signals labeled with * refer to $[(Me_2SO)(CH_3)Pt(H_2\text{-}Bn_2\text{-}DTO)][Cl]$, those labeled with # refer to $[(Me_2SO)ClPt(H\text{-}Bn_2\text{-}DTO)]$, and finally the singlet indicated with ° refers to metane.

Variable temperature ^{1}H NMR experiments in $CD_2Cl_2/CDCl_3$ mixture 30/70 are important to elucidate the structure of $[(Me_2SO)(CH_3)Pt(H_2\text{-}Bn_2\text{-}DTO)][Cl]$. As shown in figure 8.18, the two singlets at 4.96 and 4.90 ppm, which are sharp and well resolved at r.t., change into broad peaks at low temperature, but unfortunately they do not decoalesce at temperatures as low as 180 K. As for this dynamic process (Fig. 8.18a), it is reasonable to assume that the rapid flipping of the thioamidic NCS moieties around the C(S)-C(S) axis becomes slower at low temperature; thus, the broadened N-CH,- singlets should give rise to two sets of four AB lines at inaccessible temperatures. At the same time, the N-H resonances at about 13 ppm, which appear as two broad, partially superimposed peaks at room temperature, tend to coalesce as the temperature rises (Fig. 8.18b). Unfortunately, a temperature high enough to see a single sharp peak for both N-H groups has not been reached. On the contrary, temperature lowering produces in the N-H region of the spectrum a fairly good separation and sharpening of the two N-H signals. This result clearly indicates that at high temperatures a rapid exchange of the amidic proton does occur.

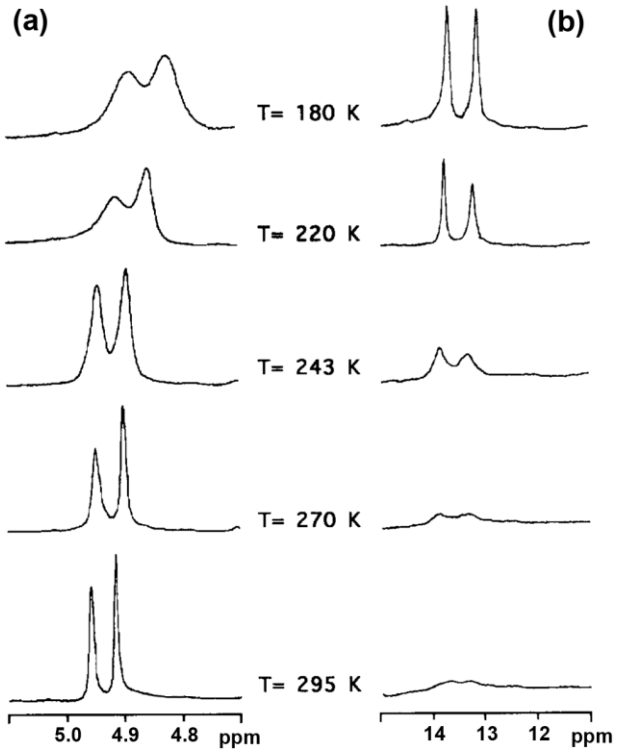

Fig. 8.18 - Temperature dependencies of benzyl (**a**) and N-H (**b**) resonances of $[(Me_2SO)(CH_3)Pt(H_2\text{-}Bn_2\text{-}DTO)][Cl]$.

Variable temperature ^{1}H NMR experiments performed on both [(H-^{n}bu$_2$DTO κ-S,S Pt)Pt(H$_2$-^{n}bu$_2$DTO κ-S,S Pt)][Cl] and [(Me$_2$SO)(CH$_3$)Pt(H$_2$-Bn$_2$-DTO)][Cl] ion pairs clearly indicate that the neutral S,S coordinated dithioxamide planes in the moieties 〰Pt(H$_2$-Bn$_2$-DTO κ-S,S Pt)[Cl], in which the chelate ligand is forced in a chiral torsion around the pivot C-C bond, become symmetrical because of the fast scrambling of HCl between the solvent and the N-H···N basic sites, according to the following mechanism (Scheme 8.3):

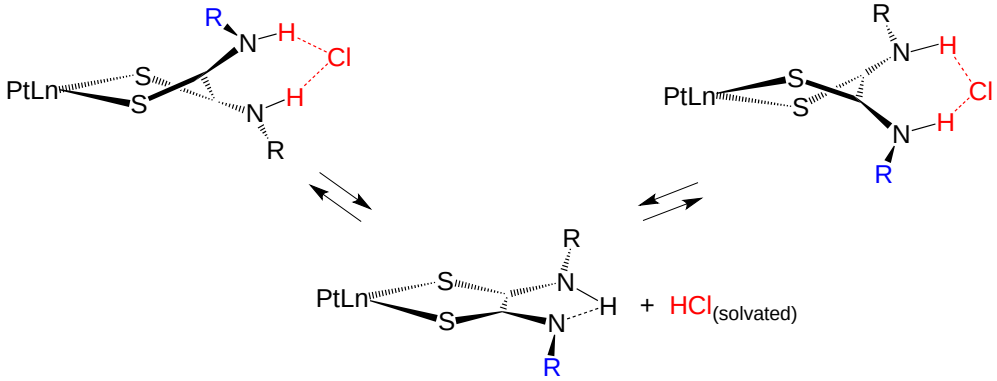

Scheme 8.3 - Proposed mechanism for the δ ⇌ λ conformational change of the PtSCCS plane.

The role of the solvent in such a process will be examined in the following (See section 10.2) in a detailed way; at this stage it is possible only say that this peculiar molecular motion plays a crucial role in ruling the behavior of platinum-DTO based anion receptors as sensors, molecular carriers and acid-base titrators.

8.2. Pt(II)-dithiooxamide κ-S,S Pt based anion receptors as sensors.

8.2.1 Sensing in the fluid phase: [Pt(H$_2$R$_2$DTO)$_2$]X$_2$ and [Pt(HR$_2$DTO)$_2$] as sensors.

[Pt(H$_2$R$_2$DTO)$_2$]X$_2$ species (R = methyl, X = Cl, **1**; R = buthyl, X = Cl, **2**; R = benzyl, X = Cl, **3**; R = cyclohexyl, X = Cl, **4**; R = cyclohexyl, X = Br, **5**; R = cyclohexyl, I = Cl, **6**) are luminescent at room temperature (**1**-**4**) and at

77 K (**1-6**). Their absorption (λ_{max} and molar absorption coefficient ε) and luminescent properties are reported in table 8.1.

Table 8.1- Absorption Spectra and Luminescence Properties of Compounds 17,11,16,18,19,20[a].

compd	formula	absorption 298 K λ_{max}, nm (ϵ, 10^{-3} M^{-1} cm^{-1})	luminescence[b] 298 K λ_{max}, nm	τ, ns	Φ	77 K λ_{max}, nm	τ, ns
17	$\{Pt(H_2-Me_2-dto)_2^{2+},(Cl^-)_2\}$	507 (10.0)	700	20	9×10^{-4}	640	485
11	$\{Pt(H_2-Bu_2-dto)_2^{2+},(Cl^-)_2\}$	513 (12.0)	716	25	10×10^{-4}	640	425
16	$\{Pt(H_2-Bz_2-dto)_2^{2+},(Cl^-)_2\}$	518 (13.0)	620[c]	60[c]	2×10^{-4}	645	345
			720	23			
18	$\{Pt(H_2-Cy_2-dto)_2^{2+},(Cl^-)_2\}$	520 (12.8)	610[c]	*d*[c]	8×10^{-4}	650	510
			725	18			
19	$\{Pt(H_2-Cy_2-dto)_2^{2+},(Br^-)_2\}$	520 (12.5)	620[c]	*d*[c]		645	480
			730	20			
20	$\{Pt(H_2-Cy_2-dto)_2^{2+},(I^-)_2\}$	520 (13.8)	730	18		645	490

[a]Solvent used: dichloromethane (room temperature) or butyronitrile (77 K). For the absorption spectra, only visible maxima are reported. [b]Excitation wavelength 500 nm except as otherwise noted. [c]Excitation wavelength 450 nm. [d]Luminescence too low to measure lifetime.

On the contrary, the dehydrohalogenated form $[Pt(HR_2DTO)_2]$ of complexes, are not light emitting in the same experimental conditions.

What said above has been effectively sketched in the figure 8.19.

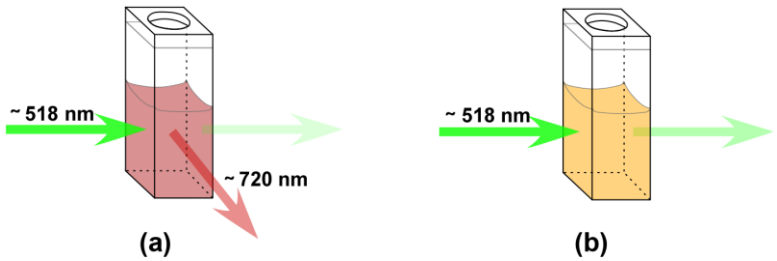

Fig 8.19 - Sketch showing the photo-physical properties of CH_2Cl_2 solutions of $[Pt(H_2R_2DTO)_2]X_2$ (a), and $[Pt(HR_2DTO)_2]$ (b) species.

Even a careless glance at figure 8.19 leads to the conclusion that $[Pt(H_2R_2DTO)_2]X_2$ allows the detection of bases such as pyridines or amines, while $[Pt(HR_2DTO)_2]$ can be used as sensors to detect halogen acids in chlorinated solvents.

Figure 8.20 shows absorption spectra of **17** and **18** in dichloromethane solution, figure 8.21 show luminescence spectra of **17** and **11** at room-temperature, figure 8.22 shows emission spectra of **16** at two different excitation wavelengths, and luminescence spectra (at room-temperature) of **18-20** are shown in Figure 8.23.

Absorption spectra of **17-18** in dichloromethane (Fig. 8.20) are dominated by moderately intense bands in the visible region, with a maximum in the 500-530 nm range (ε in the range 104-105 M^{-1} cm^{-1}) and by an absorption feature lower in intensity at about 350 nm (ε in the range 103-104 M^{-1} cm^{-1}). More intense absorption bands appear at much higher energies. The Lambert-Beer law holds for all the compounds studied in dichloromethane within the concentration range investigated ($2\times10^{-5} \div 2\times10^{-4}$ M), indicating that no aggregation (e.g., dimerization) occurs in this concentration range.

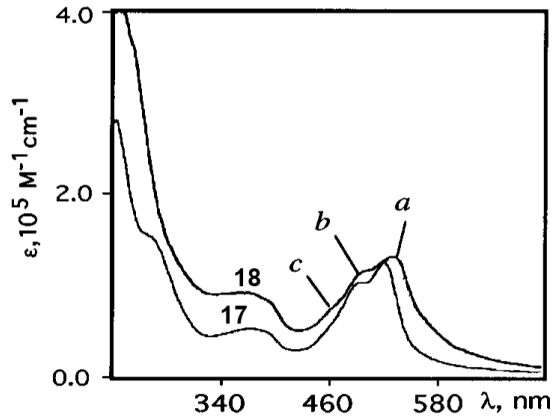

Fig. 8.20 - Absorption spectra of compounds **17** and **18** in dichloromethane solution. The visible maxima or shoulders labeled as *a*, *b*, and *c* are discussed in the text.

All of the compounds exhibit luminescence both at 77 K in a rigid matrix and at room-temperature in fluid solution (Table 8.1)

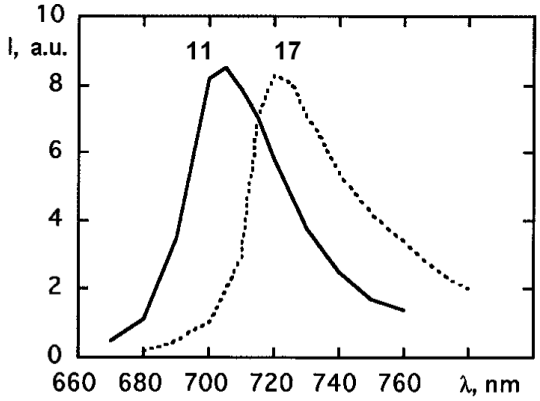

Fig. 8.21 - Room-temperature luminescence spectra of compounds **11** and **17** in dichloromethane solution. Excitation wavelength: 500 nm.

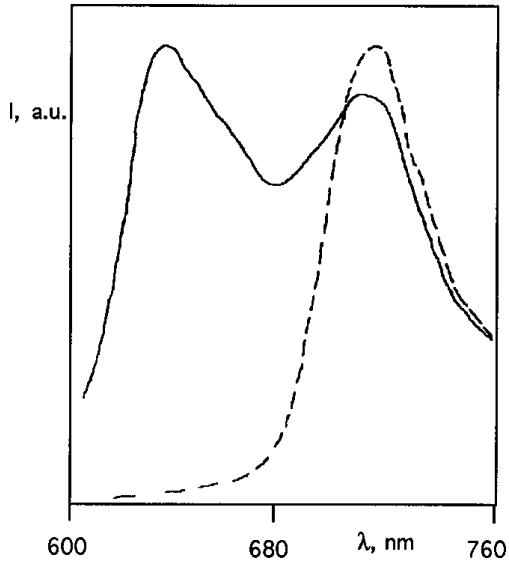

Fig. 8.22 - Room-temperature luminescence spectra of compound **16** in dichloromethane solution: solid line, excitation wavelength 450 nm; dashed line, excitation wavelength 500 nm.

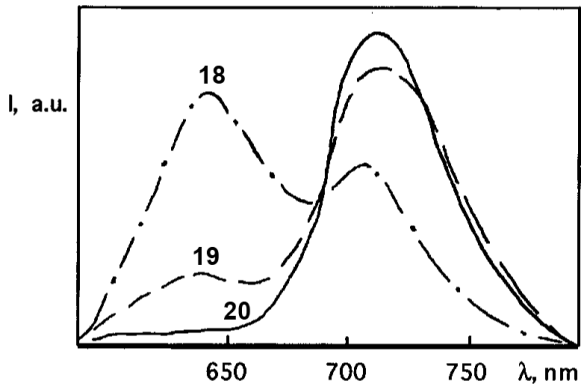

Fig. 8.23 - Room-temperature luminescence spectra of compounds **4**, **5** and **6** in dichloromethane solution. Excitation wavelength is 450 nm in all cases.

All of the compounds exhibit luminescence both at 77 K in a rigid matrix and at room-temperature in fluid solution (Table 8.1). Room-temperature luminescence spectra are unstructured and centered at about 720 nm. Their shapes do not depend on concentration of the compounds within the concentration range investigated. For the chloride-containing compounds, the emission energy decreases in the series **17**, **11**, **16**, and **18**.

Compounds **19** and **20** exhibit very similar luminescences at slightly lower energies. Compounds **16-19** also exhibit a second luminescence band at higher energies. Emission spectra are independent of excitation wavelength for **17** and **11** whereas they are dependent on the wavelength of the excitation light for **16-19**. In particular, excitation at 500 nm (the maximum of the absorption spectra in the visible region) maximizes low-energy emission, while excitation at 450 nm (corresponding to a shoulder at the blue side of the main absorption band; see later) maximizes high-energy emission. Luminescence lifetimes are on the 10-8-10-7 s time scale. At 77 K in a rigid matrix, only one luminescence band is found for all the complexes, for each excitation wavelength; 77 K luminescence lifetimes are on the 10-7-10-6 s time scale.

In absorption spectra the strong bands in the visible region exhibited by all the complexes (Table 8.1, Fig. 8.20) to Pt(dπ)/S(p)$\rightarrow$dithiooxamide (π^*) CT transitions (this transition, and the corresponding excited state, will be hereafter named Pt/S$\rightarrow$ DTO (CT), on the basis of (i) the sensitivity of the absorption band energy to the substituents of the dithiooxamide moieties (Table 8.1), (ii) the extinction coefficients of the bands (Table 8.1), (iii) the absence of any absorption feature in the visible region in the absorption spectra of the free ligands, and (iv) the structural and electronic similarities between the Pt(II)-dithiolate complexes [20,21] and the Pt(II)-dithiooxamide compounds. The visible absorption maximum is in any case followed by a shoulder at slightly higher energy (e.g., see figure 8.20 for **18**, where the dominant visible maximum *a* is followed by the shoulder *b*; ΔE between the maxima $\cong$1300 cm^{-1}). This higher energy shoulder could be attributed to another Pt/S$\rightarrow$DTO CT transition or to the vibrational progression of the main band. The energy difference is equivalent to the C=N and C=C stretching frequency, so that if the latter hypothesis is true, this frequency mode would be the dominant vibrational progression of the Pt/S$\rightarrow$DTO CT excited state of **11**,**17**-**20**. It can be recalled that C=C and C=N stretching modes are the dominant vibrational modes of the ground and excited states of polypyridine metal complexes.[22,23]

The fact that the same vibrational modes could also be the dominant modes in these complexes would suggest an interesting similitude between dithiooxamide and polypyridine metal compounds. The Pt/S$\rightarrow$DTO CT transition warrants further comments: the Pt(II) metal ion provides a large electronic coupling between the two chelating sulfur-containing ligands, as demonstrated in square-planar d^8 complexes of Ni(II), Pd(II), and Pt(II).[24,25]

The HOMO in the series of complexes **11**,**17-20** is therefore probably well described as delocalized on both the ligands, receiving contribution from the Pt(dð) and all the S(p) orbitals. On the other hand, depending on the electronic coupling between the ligands, the molecular LUMO will be centered on the amidic moiety of a single DTO ligand or delocalized on the entire molecule (nevertheless, mainly centered on the amidic moieties of both the ligands). A definitive preference for one of the two hypotheses is impossible with the experimental data in our hands: however, due to the very small solvent sensitivity of the absorption band (solvents used: dichloromethane, chloroform, benzene), we believe that a π^* LUMO delocalized on the two DTO ligands is more likely.[26]

In this case, this electronic transition (and the excited state) should not have a net CT contribution, in that the overall electric dipole of the molecule does not change. However, because of the redistribution of the density of charge upon excitation (an electron is shifted from the center of the molecule, where the HOMO is essentially located, to the periphery, where the LUMO is centered), sensitivity to the environment (for example to the nature of the ion-paired anions; see later) is expected. From this discussion, it appears that the electronic transition under study is a particular type of CT transition. We will continue to call it (and the corresponding excited state) as Pt/S→CT for the sake of simplicity. Another electronic transition contributes to the strong absorption at about 500 nm, and it can be noticed in the blue side of the main band, clearly visible as a shoulder at 460 nm for **18** (figure 8.20, shoulder *c*). Because of its intensity, this shoulder cannot be attributed to MC transitions, so that MLCT or LC transitions should be responsible for it. Similar absorption bands (λ_{max} at about 450 nm) are present in the spectra of the neutral parent compounds [Pt(H-R-DTO)$_2$]. As a consequence, a LC assignment seems to be most likely. MLCT transitions, in fact, should be more sensitive to the different charge densities on the DTO ligands in neutral [Pt(H-R-DTO)$_2$] and ion-paired [Pt(H$_2$-R-DTO)$_2$][X]$_2$ species (the possibility that the absorption shoulder *c* is a vibrational component of the main band (*a*+ *b*) or that it is due to partial contamination of **11**,**17-20** owing to the presence of the parent neutral species can be excluded on the basis of the photophysical properties; see later).

It is interesting to note that, on the basis of the electron donor power of the R substituents, the Pt/S→DTO CT bands could be expected to move to higher energies in the order **17** < **16** e **11** < **18** (**19** and **20** are left aside for simplicity).

This order is not found in the absorption properties (see Table 8.1). The experimental order for the absorption band energies **18** < **16** < **11** < **17** is the reverse order of the steric hindrance of the R substituents. Such a result can be explained when one considers that, in tight ion pairs like the ones studied here, also CT interactions (and states) involving the paired ions (outer-sphere CT) may play important roles.[27]

In **11**,**16-18** compounds, CT interactions between the chloride anions and DTO can destabilize the π^* orbital of the DTO ligands. These interactions depend on the proximity of chloride to DTO, which in its turn can be governed by steric hindrance. Bulky substituents can prevent or diminish ion-pair interactions, leading to decreased electron density on the DTO ligands and moving the Pt/S→CT transition to lower energies. The effect of the substituents of the DTO nitrogens on the absorption (and emission; see later) energy should be therefore a consequence of the different steric hindrance. The following alternative explanation could also be taken into account: It should be noted that substituents on nitrogen are essentially σ-donor groups. Donor ability could be transferred across the *ó*-backbone of the DTO ligands to the Pt/S region, and its main effect would be destabilization of the HOMO. Destabilization of the LUMO (DTO-centered π^* orbitals) could be less important. As a consequence, Pt/S → CT transitions should move to lower energy with increased σ-donor ability of R, according to the experimental results. Nevertheless, a slight (although not definitive) preference for the former explanation is suggested from the differences in the LC shoulder intensity in the series **18,16,11,17.** In fact, intensity of the LC shoulder at about 460 nm decreases in the series **18,16,11,17**. This can be explained by considering that strong interactions between the ions in the tight contact ion pairs could lead to an increased distortion of the DTO backbone, yielding different intensities of DTO-centered transitions. This confirms that interpenetration of the ion pairs significantly modifies the electronic properties of the compounds under study.

The luminescence of all complexes at ~720 nm at room-temperature and at ~ 640 nm at 77 K to triplet Pt/S→CT levels, on the basis of the following arguments: (i) matrix sensitivity of the emission energy (which tends to rule out LC and MC assignments); (ii) energy maximum dependence on the R substituents of the DTO ligands; (iii) luminescence lifetimes, which are on the same time scale as luminescence lifetimes for Pt(II)-dithiolate emission, already assigned to Pt/S→π^*(thiolate) CT levels.[28]

The effect of the R substituents on excited state energy can be explained with the same arguments used to discuss absorption spectra (see above). The second emission exhibited by **16**-**20** at room-temperature has the absorption counterpart in the absorption feature at ~450 nm, as clearly demonstrated by excitation spectroscopy (not shown), and is therefore assigned to excited states centered in the DTO ligands.

Further support for such an assignment comes from the luminescence at 620 nm of the somewhat similar compound Zn(tdt)2 (tdt^{2-} = 3,4-toluenedithiolate),[29] a *bona fide* LC emitter.

An interesting point to be discussed here is the double emission exhibited by some of the complexes at room temperature (Table 8.1). Multiple emission in mononuclear metal complexes is rare and usually occurs at low temperature.[30,31,32 ,33]

A different situation is the case of multiple emissions in multinuclear metal complexes. In such multinuclear systems, in fact, multiple emissions can originate from inefficient energy transfer among the chromophores.[33]

In most of the cases, multiple emission originates from two closely-lying excited states which can equilibrate at room-temperature, while they are essentially independent at 77 K in rigid matrices. Inefficiency of direct conversion between excited states is attributed to high nuclear barriers. The behavior of compounds **16**-**20** is somewhat surprising, in that double emission is only found at room-temperature (Table 8.1). This somewhat puzzling behavior can be rationalized as follows.

The experimental results (Table 8.1) indicate that high-energy emission becomes more and more important on passing from **17** and **11** (for which high-energy 640 nm emission is totally absent) to **16** and **18**. This suggests that emission at 640 nm becomes dominant over the 720 nm emission when the steric hindrance of the R substituents increases (i.e., with decreased close proximity of the ions in the tight ion pairs). Therefore, a role of the halide counterions in promoting conversion between LC and Pt/S f CT states can be envisaged. This role could be the efficient participation of a high-lying X→CT level in mediating excited state conversion.

It can be pointed out that conversion of a DTO-centered ($\pi \rightarrow \pi^*$) level into a Pt/S→CT state corresponds to electron transfer from a Pt/S σ-bond orbital to a π orbital of DTO. Significant distortions within the molecule structure are

expected for such an electron transfer, due to the reduced strength of the Pt-S bond, so that nuclear barriers are indeed possible. Due to the tight contact ion pair nature of the compounds, the DTO-centered level could be easily converted into a higher-lying X→CT level (this would be a thermally activated process), which in its turn would afford the final Pt/S→CT state by Pt/S to halide electron transfer. Significant distortions are also expected for this electron transfer, but the higher driving force could overcome the nuclear barriers. The above mentioned hypothesis is almost equivalent to considering that excited state conversion from LC and Pt/S f CT levels can be promoted by mixing between LC and X→CT levels. In this case, however, effective production of the X→CT state is not necessary. The conclusion that can be inferred from both viewpoints is that the more the halides approach the DTO ligands (e.g., in **17** and **11**), the more efficient would be the X→CT level in promoting conversion between LC and Pt/S→CT excited states. At 77 K, the rate constants of the direct deactivations to the ground state of the LC level decrease, so that conversion to the Pt/SfCT level can efficiently compete with luminescence from LC levels even for **16** and **18**. The proposed mechanisms could be confirmed by the results obtained for **19** and **20**, compared to **18**. In compounds **19** and **20**, in fact, we used bromide and iodide instead of chloride, respectively, to form tight contact ion pairs. Br → and I → CT levels are lower in energy than the Cl→CT state, and the X→CT level is expected to be more efficient in promoting interconversion between LC and Pt/S→CT levels in **19** and **20** than in **18**. The fact that the ratio between LC and Pt/S→CT emissions decreases in the series **18**, **19**, and **20** (Fig. 8.23) is in full agreement with the proposed role for the X→CT level. It should be noted that, on the basis of the above considerations, one might expect a larger difference in the λ_{max} in the absorption and emission spectra of **18**-**20**, as also pointed out by one of the reviewers. However, it has been suggested that highlying excited states can influence excited state dynamics without significantly affecting spectroscopic properties.[34] This seems also to be the case for the compounds studied here.

8.2.2. Sensing in the fluid phase: [(dppf)ClPt(HR_2DTO)]Cl *and* [(dppf)$_6$Cl$_6$P$_6$(HR_2DTO)$_6$][Cl]$_6$ *as sensors.*

The photo-physical properties of the tight ion pairs **11**,**16-20** significantly depend on the fast scrambling of HCl with the solvent (see scheme 8.3) which is influenced by the nature of R substituents on nitrogen atoms; then, the possibility to functionalize such R substituents with desired substrates and to construct supramolecular assemblies may open the way to more versatile luminescent compounds. Besides this, it seems useful to explore the behavior of different dithioxamide containing complexes, like ones containing only one dithioxamide chelate to platinum(II) through sulfur.[35]

In this path, it has been found interesting investigate on the ionic complexes [(dppf)ClPt(HR_2DTO)]Cl (R = alkyl, dppf = 2,2'-diphenylphosphinoferrocene), obtained according to the scheme 8.4.

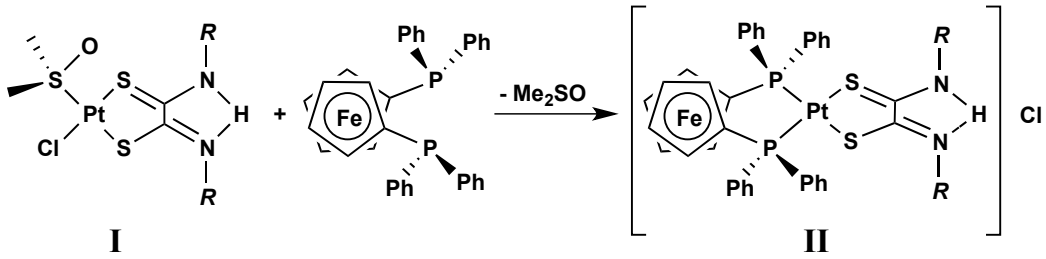

I **II**

II:

21: R = methyl	**25:** R = *n*-decyl
22: R = ethtyl	**26:** R = isopropyl
23: R = propyl	**27:** R = {R}-(1-phenyl)ethyl
24: R = *n*-butyl	**28:** R = {S}-(2-hydroxy)propyl

Scheme 8.4

The NMR spectra of bimetallic Pt/Fe species **II** show a dppf unit chelated through the phosphorus atoms to a Pt–HR_2DTO κ-S,S Pt moiety, which is consistent with the overall structures possessing *σh* and *σv* symmetry planes, with a C_2 axis passing through the two metal centers. Dppf is a versatile ligand, which is known to adopt various modes of coordination depending on the specific stereoelectronic requirements around a given molecule. The majority of transition-metal complexes with dppf are mononuclear species bearing a single or two chelating dppf ligands; polynuclear complexes containing bridging dppf are less common, albeit, adequately reported in the literature.[36]

Similarly, the unidentate η^1-mode has been observed in $[M(\eta^1\text{-dppf})(CO)_5]$ (M = Fe,[37] or Cr, Mo, W[38a,b]) and $[Co_2(\eta^1\text{-dppf})(\mu^2\text{-}(MeO_2C)_2C_2)(CO)_5]$. The latter compound has been structurally characterized.[38c]

Finally, a further type of known coordination mode for dppf and related diphosphine ferrocenyl ligands has been reported (especially with Pt and Pd centers), in which the ligand prefers a *trans* coordination with a weak dative bond from Fe to the Pt or Pd centers.[39]

In this case, a sort of η^3 coordination mode of a dppf-type ligand is operating. The examples cited above clearly indicate that a dppf ligand can adapt its structure to fit various coordination requirements, such as suitable bite angles for chelation, yielding quite stable compounds with various geometries.

8.2.3. Spontaneous Assembly and Characterization of the Hexameric Macrocycles

The complexes type **II** were found to be indefinitely stable both in the solid state and in solution provided that bulky alkyl substituents are attached to the nitrogen atoms of the DTO moieties, that is, **26**–**28** (Scheme 8.4). Conversely, when R is a linear alkyl group, the behavior of the corresponding bimetallic complexes (i.e., **21**–**25**, Scheme 8.4) is somewhat more complex. In particular, the yellow microcrystalline powders of **21**–**25** begin to show the presence of some greenish microcrystals within a couple of weeks. The number of these greenish microcrystals increases with time. According to NMR spectroscopic analysis, the bulk of the powder, however, predominantly contains the original Fe/Pt complex even after several months; thus, indicating that in the solid state, the process generating the greenish microcrystals from **21**–**25** is low-yielding and slow. Conversely, methanol solutions of **21**–**25** (in the concentration range 0.01–0.001 m) turn green within a few hours and then become deep blue within two days. Likewise, chloroform or dichloromethane solutions of **21**–**25** turn yellow–green within a few hours and become deep greenish within two weeks. The dramatic color change is clearly mirrored by tangible changes in the absorption spectra (Fig. 8.24).

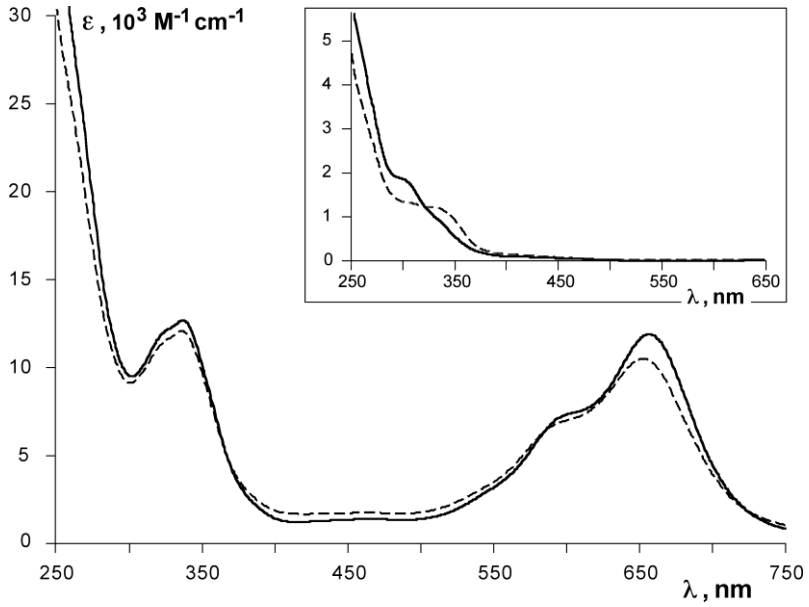

Fig. 8.24 - Absorption spectra of the "blue" compound (later characterized as the self-assembled hexameric macrocycles $\mathbf{21_6}$, see below; molar absorption is calculated by assuming a hexamer has formed), produced from **21** upon standing in methanol (dashed) and chloroform (solid line) solutions. The corresponding absorption spectra of the starting complex **21** are shown in the inset.

Based on the NMR spectroscopic analysis, each methanol solution of **21**–**25** that turned deep-blue upon standing contained a single species, whereas, the greenish chloroform solutions of the same compounds consisted of a mixture of two species. Chromatographic separation (on Al_2O_3) of these mixtures gave, in all instances, a yellow- and a blue-colored solid material consistent with the corresponding unaltered/starting bimetallic complex and a newly formed compound, respectively; the latter being identical (UV/Vis and NMR spectroscopy) to the one obtained separately upon direct solubilization and standing of the precursor in methanol. These findings indicate that **21**–**25**, bearing linear alkyl substituents (Scheme 8.4), spontaneously evolve into different species in solution (i.e., $\mathbf{21_6}$–$\mathbf{25_6}$; Scheme 8.5) with rates and yields that depend on the reaction medium. Interestingly, once isolated, the "blue" species type **III (**Scheme 8.5) gave the same elementary analysis as the corresponding starting species type **II.**

The new compounds $\mathbf{21_6}$–$\mathbf{25_6}$ were characterized by NMR spectroscopy. ^{1}H and ^{31}P spectra of the "blue" dimethylthiooxamide $\mathbf{21_6}$ show diagnostic signals at

different frequencies than those of the corresponding "yellow" precursor **21**, albeit, featuring similar patterns – consistent with one dppf unit coordinated through the phosphorus atoms to a $[Pt(HMe_2DTO\ \kappa\text{-}S,S\ Pt)]^+$ moiety – and the same elemental analysis. Different and more complex patterns are observed in the cases of **22**–**25** and $\mathbf{22_6}$–$\mathbf{25_6}$ on the other hand. Each of these compounds contains *N*-CH_2R geminal protons which, in the ^1H NMR spectra of **22**–**25**, give rise to an A_2Xn spin pattern, as a clear consequence of the fact that the H–C–H angle is bisected by a symmetry plane. However, in the case of $\mathbf{22_6}$–$\mathbf{25_6}$, the same geminal protons display a typical ABX_n (n = 2 or 3) spin pattern, suggesting that the H–C–H angle is no longer bisected by a symmetry plane. These spectral features indicate that the dppf ligand has changed coordination mode on going from **21**–**25** to $\mathbf{21_6}$–$\mathbf{25_6}$: it is chelated to a single platinum center in the bimetallic "yellow" precursors **21**–**26** (the same is true for **26**–**28**), whereas is acting as a bridging ligand – coordinating two different platinum centers, each one with a single coordination site – in $\mathbf{21_6}$–$\mathbf{25_6}$. A dppf unit can indeed coordinate two square-planar platinum moieties as depicted in figure 8.25. Clearly, the two platinum planes shown in figure 8.25 do not possess σh symmetry and as a result the *N*-CH_2R geminal protons display ABX_n spin patterns in the ^1H NMR spectra.

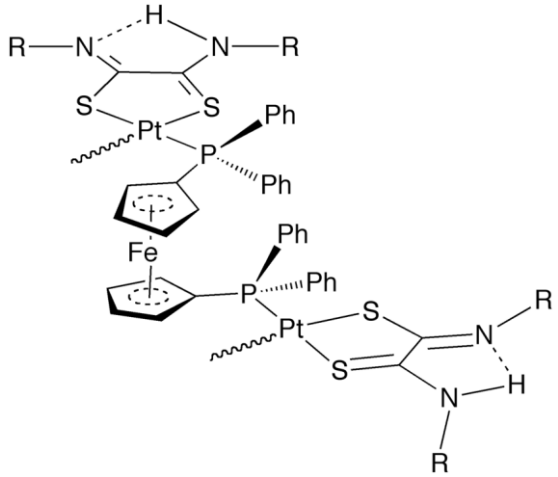

Fig. 8.25.- Suggested bridging coordination mode of the dppf ligand in compounds $\mathbf{21_6}$–$\mathbf{25_6}$.

Furthermore, the ^{31}P spectra of $\mathbf{21_6}$–$\mathbf{25_6}$ show a single Pt–P signal, implying that all phosphorus atoms in these compounds must be symmetrically arranged in a

cyclic structure containing an even number of platinum fragments connected by an equal number of dppf units acting as bridging ligands. The spontaneous reaction leading to **21$_6$**–**25$_6$** from the corresponding bimetallic complexes **21**–**25** in solution can therefore be depicted as in Scheme 8.5.

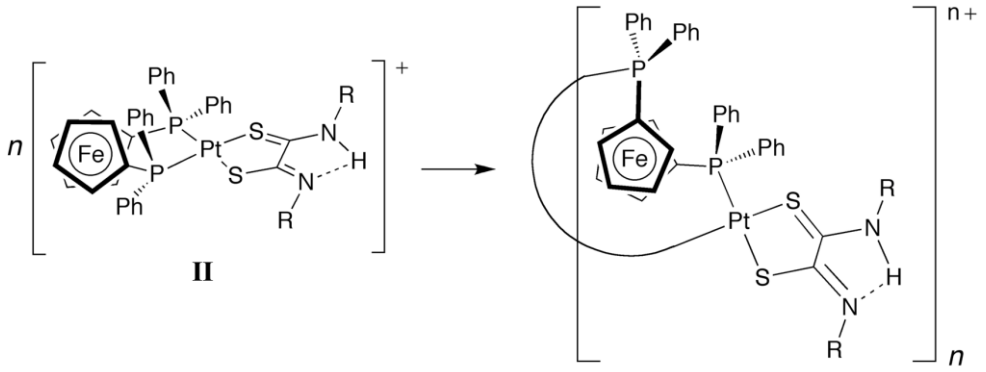

II **III**

III: **21$_6$:** R = methyl
22$_6$: R = ethyll
23$_6$: R = *n*-propyl
24$_6$: R = *n*-butyl
25$_6$: R = *n*-decyl

Scheme 8.5

Efforts to grow X-ray-grade crystals to assess the molecular structure and, therefore, the nuclearity of the cyclic self-assembled oligomers **21$_6$**–**25$_6$**, were to no avail. Diffractometric analysis performed on their powders did not provide any useful information either. Mass spectra were equally uninformative, as they produced neither reproducible fragmentation patterns, nor reliable molecular peaks.

However, diffusion-ordered NMR spectroscopy (DOSY) experiments, in strong connection with other NMR results (see below), allowed to determine the hexameric nature of the "blue" compounds **21$_6$**–**25$_6$**. The DOSY NMR technique[40] has been used recently to unambiguously prove the formation of discrete hexameric supramolecular aggregates,[41a] linear multinuclear metal complexes,[41b] and self-assembled coordination metallomacrocycles. [42]

The DOSY spectra of mixtures of "yellow" compounds **21**–**25** and the corresponding "blue" ones **21$_6$**–**25$_6$**, consistently show the presence of two species with differenttranslational mobilities (see figure 8.25 for **22** and **22$_6$**): a faster moving one, which corresponds to monomers type **II** (dashed black line),

and a slower one consistent with the presence of the corresponding self-assembled species type **III** (dashed red line).

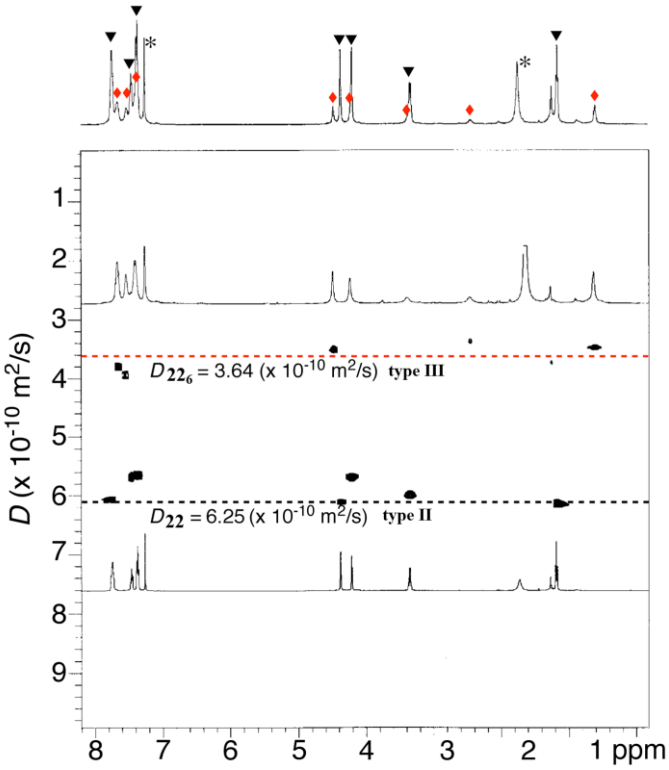

Fig. 8.25 - DOSY spectrum (500 MHz, CDCl3, 298 K) of a mixture of compounds **22** and **22_6**. The asterisks indicate residual solvent peaks.

Self-diffusion coefficients of monomers type **II** (D_{II}) and oligomers type **III** (D_{III}) were measured by only using sets of well-separated signals. The data in Table 8.2 show that the D_{II} and D_{III} values slightly decrease along the **21**–**25** series, in line with the corresponding increase in the molecular masses. By using Equation (1) and assuming a spherical shape for both monomers and oligomers, self-diffusion coefficients of the "yellow" (D_{II}) and "blue" (D_{III}) compounds (determined in a single diffusion experiment) consistently indicated that the molecular mass of a given "blue" compound (M_{III}) was roughly 5–6 times that of the corresponding "yellow" precursor (M_{II}), in all cases under examination (Table 8.2).[43]

$$D_{II}/D_{III} = (M_{III}/M_{II})[1/3] \quad (1)$$

Table 8.2 - Self-diffusion coefficients and calculated hydrodynamic radii for **21**–**25**, **28** and $\mathbf{21_6}$–$\mathbf{25_6}$.[a]

Type II			Type III			M_{III}/M_{II}
	D_{II} ($\times 10^{-10}$ m^2 s^{-1})	R_h (Å)		D_{III} ($\times 10^{-10}$ m^2 s^{-1})	R_h (Å)	
21	6.25 ± 0.04	6.42 ± 0.04	$\mathbf{21_6}$	3.64 ± 0.04	11.03 ± 0.12	5.06
22	6.08 ± 0.02	6.60 ± 0.02	$\mathbf{22_6}$	3.28 ± 0.01	12.24 ± 0.04	6.34
23	5.78 ± 0.03	6.95 ± 0.03	$\mathbf{23_6}$	3.27 ± 0.02	12.28 ± 0.07	5.42
24	5.59 ± 0.05	7.18 ± 0.06	$\mathbf{24_6}$	3.27 ± 0.04	12.28 ± 0.15	4.99
25	5.40 ± 0.02	7.43 ± 0.03	$\mathbf{25_6}$	2.91 ± 0.06	14.70 ± 0.62	6.39
28	6.03 ± 0.03	6.66 ± 0.03				

[a] D_{II} and D_{III} values were obtained from DOSY NMR spectroscopy, and *R*h values were calculated from the Stokes–Einstein equation (see text). Compound **28** does not self-assemble.

The hydrodynamic radius (*R*h) of **28** (6.66_0.03 Å, Table 8.2), calculated by the Stokes–Einstein equation, is in excellent agreement with the radius value (ca. 6.5 Å) experimentally determined by single-crystal X-ray analysis (Fig. 8.28). The radius approximated from Xray analysis was averaged for the dimensions along the *x*, *y*, and *z* axes of a single molecule). In general, the *R*h values of $\mathbf{21_6}$–$\mathbf{25_6}$ were found to be approximately twice the size of those determined for the corresponding building blocks **21**–**25**, suggesting that, overall, spherical objects are formed as a result of the self-assembly process.

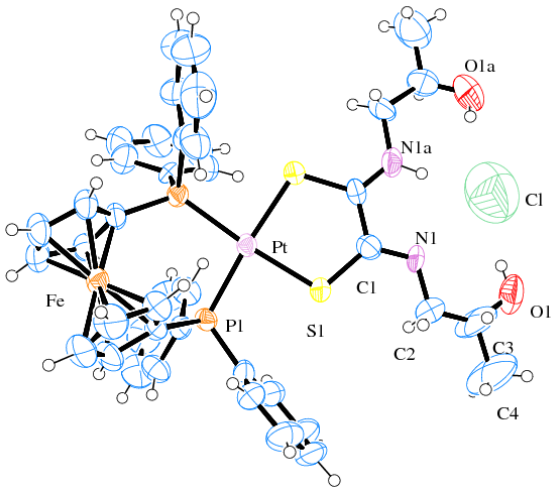

Fig. 8.26 - The X-ray structure of compound **28** [(dppf κ-*P*,*P* Pt) Pt((*S*)-2-hydroxypropyl-DTO κ-*S*,*S* Pt)][Cl].

To rule out any influence of the concentration on the size of the observed macrocycles, a set of DOSY experiments (Fig. 8.27) was performed by adding increasing amounts of $\mathbf{21_6}$ to a 1 mm solution of **21** (acting as an internal standard). The self-diffusion coefficient values of the aggregates present in solution hardly changed in the 0.02–2.0 mM concentration range [$D\mathbf{21_6}$ = $3.60\pm0.14\times10^{-10}$ m^2 s^{-1}, Fig. 8.27, (b)–(d)], suggesting that the size of $\mathbf{21_6}$ is concentration independent.

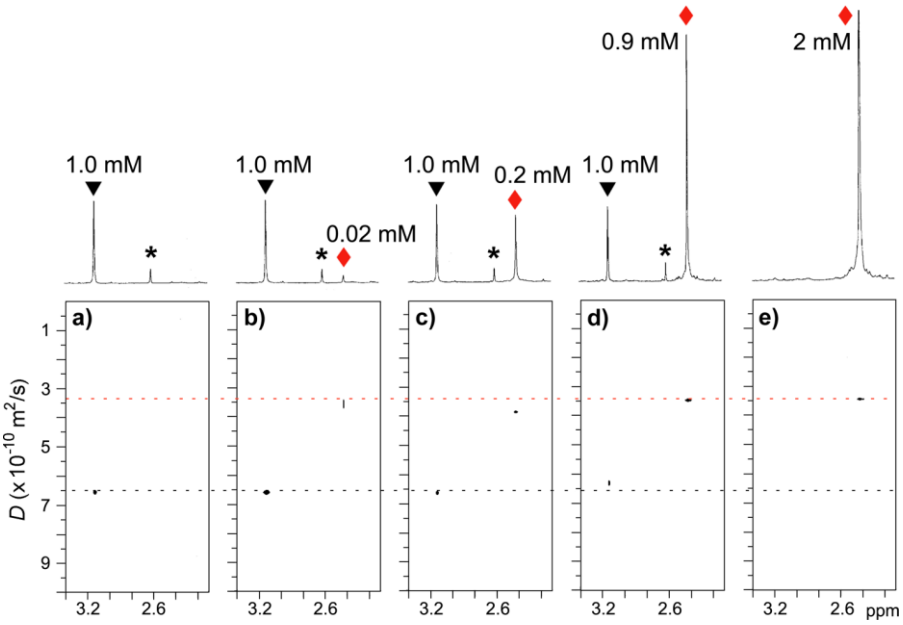

Fig. 8.27 - Selected regions of the DOSY spectra (500 MHz, $CDCl_3$, 298 K) of: (**a**) **21**; (**b**)–(**d**) mixtures of **21** and $\mathbf{21_6}$; (**e**) $\mathbf{21_6}$. The asterisks indicate residual DMSO peaks. Monomer and hexamer concentrations are indicated next to the pertinent ^{1}H NMR signals.

Symmetry considerations (see above) along with ^{1}H and ^{31}P NMR spectra as well as DOSY data, when taken together, strongly suggest that the structures of $\mathbf{21_6}$–$\mathbf{25_6}$ are best described as oligomeric macrocycles resulting from the selfassembly of six corresponding **21**–**25** subunits (Fig. 8.28). The data are fully consistent with a structure in which the six dppf molecules are placed in the inner part of the cyclic hexamer and act as bridging ligands between the subunits. Each dppf ligand links two platinum atoms, and each platinum atom adopts a coplanar arrangement with the cyclopentadienyl ring bearing the phosphorus-linked atom. Thus, platinum square planes alternate with respect to each other in such a way that three of them are coplanar to one set of

cyclopentadienyl rings, whereas the other three lie, together with the second set of cyclopentadienyl rings, on a plane parallel to the first one (Fig. 8.28b).

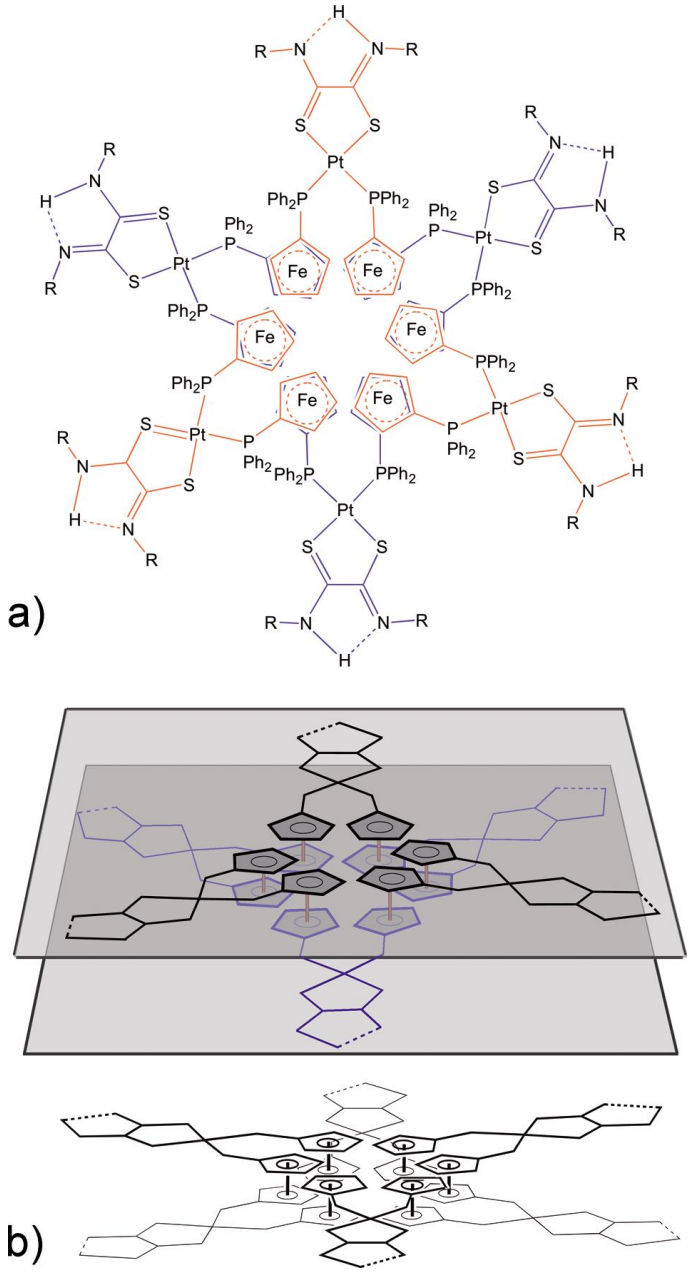

Fig. 8.28 - (**a**) Suggested structure of the cyclic hexamers $\mathbf{21_6}$–$\mathbf{25_6}$; the red- and black-colored molecular frames lie in parallel – but different – planes. Dppf ligands act, at the same time, as reels/spacers between the two planes and as bridging units between the **21**–**26** monomers. (**b**) Perspective views of the sketched structures $\mathbf{21_6}$–$\mathbf{25_6}$ showing the spacing between the two parallel planes present in the macrocycles.

The proposed cyclic structure of hexamers $\mathbf{21_6}$–$\mathbf{25_6}$ is corroborated by the 2D ROESY spectrum of $\mathbf{21_6}$. This shows the presence of a diagnostic close-contact between the methyl group of the DTO ligands and the phenyl moiety of the dppf spacers (Fig. 8.29). Given that no such interaction was observed for any of the monomer precursors **II** (including **28** where X-ray analysis showed a favorable spatial arrangement between the (*S*)-2-hydroxypropyl and the phenyl moieties, Fig. 8.28), it is reasonable to assume that the spatial proximity between the Me and Ph moieties, giving rise to the ROE cross-peak, occurs as a result of a change in the coordination mode of the dppf ligand. This takes place spontaneously upon self-assembly of monomers **21**–**25** into cyclic hexamers $\mathbf{21_6}$–$\mathbf{25_6}$. According to our data, congestion from bulky R groups on the nitrogen atoms of the DTO ligands likely hampers the coordination change, ultimately preventing the macrocyclization of monomers **26**–**28**.

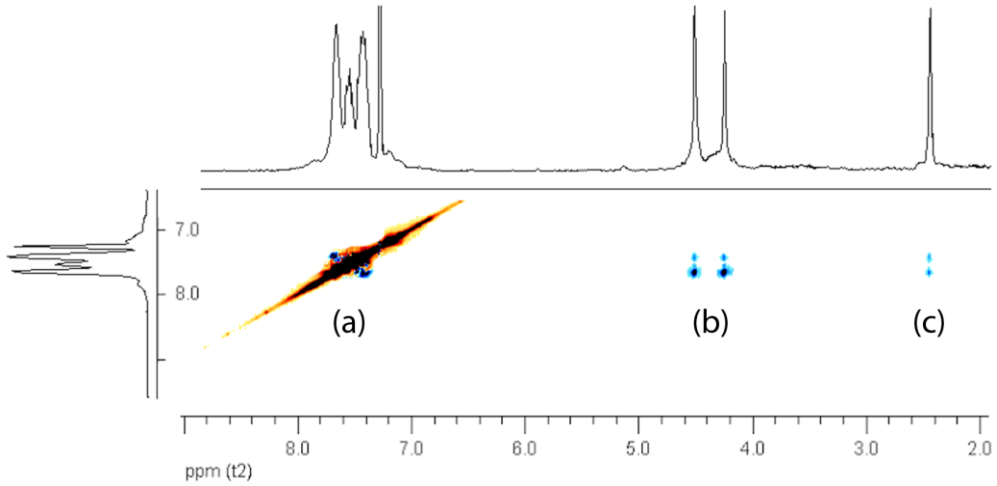

Fig. 8.29 - Section of the ROESY spectrum of $\mathbf{21_6}$ showing the close proximity of the phenyl (**a**) to the cyclopentadienyl (**b**) and methyl (**c**) protons.

To summarize, the cyclic hexameric nature of $\mathbf{21_6}$–$\mathbf{25_6}$ has been inferred by combining the information gained from the following experiments: (i) ^{1}H and ^{31}P NMR spectra indicate that in $\mathbf{21_6}$–$\mathbf{25_6}$ the type **II** subunits are symmetrically arranged in a cyclic structure containing an even number of platinum fragments, connected by an equal number of dppf units acting as bridging ligands; (ii) in agreement with point (i), 2D ROESY results confirm that the coordination mode of the dppf ligands changes on passing from type **II** to type **III** compounds; (iii) DOSY data indicate, through calculation of the hydrodynamic radius, that the

molecular mass of a given type **III** species is roughly 5–6 times that of the corresponding type **II** precursor.

8.2.4. Properties of the Hexameric Macrocycles

Conductivity measurements in organic solvents[44] have been extensively used to determine the structures of coordination compounds:[45] molar conductivity, Λ_M, is expected to be linearly dependent on the square root of the molar concentration, if the nature of the conductive species remains unchanged in the concentration range studied.

"Yellow" precursors **II** show molar conductivity values typical of 1:1 electrolytes in methanol. When the cationic part of such electrolytes self-assembles into cyclic hexamers **III**, it should provide a 6+ charged species, which must be counter-balanced by six chloride anions. However, the molar conductivity of hexamers **III** (Fig. 8.30; data for $\mathbf{22_6}$ are illustrated as an example) shows that such oligomers behave as 1:2 electrolytes.

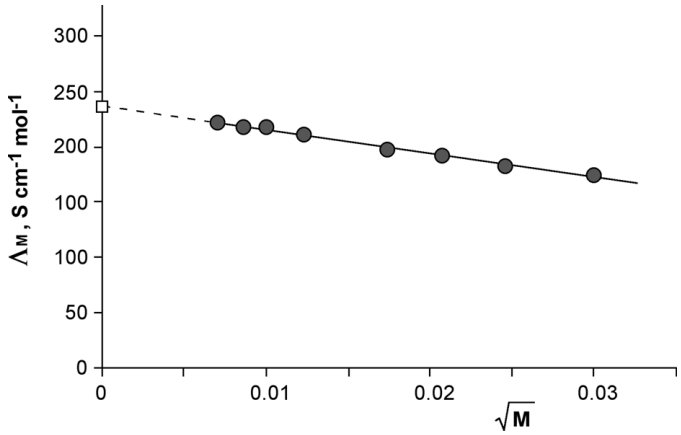

Fig. 8.30 - Molar conductivity (S cm^{-1} mol^{-1}) versus the square root of the molar concentration of $\mathbf{22_6}$ in methanol.

This means that in the case of $\mathbf{22_6}$, taken as a representative example, only two chloride ions per hexamer behave as counterions, while the other four are tightly ion-paired to the cationic hexamers, even at concentration as low as 10^{-4} M. This is probably due to the fact that a (relatively small) cyclic molecule with a large number of positive charges would otherwise be unstable and, as a result, disassemble into the corresponding precursors. Furthermore, this

observation suggests that chloride ions may play a role as templating agents in the self-assembly of the "blue" compounds. In this regard, examples where chloride ions act as templating agents in the self-assembly of cyclic oligomers have already been reported.[46,47,47b]

The circumstance that in solution four chloride ions are strongly held in the hexameric macrocycle allow to classify the hexameric species type III as anion receptors. As a tentative hypothesis, chloride ion could be receipted between two alternate platinum planes, held by two hydrogen atom of two alternate cyclopentadienyl rings (Fig. 8.31).

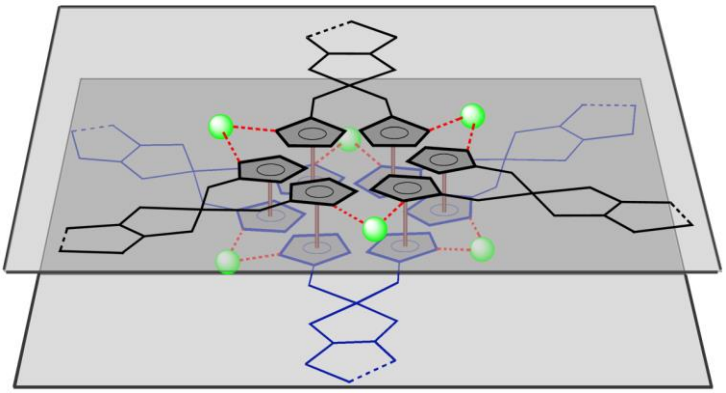

Fig. 8.31 - Possible reception sites for chloride anion in type **III** complexes.

Obviously, in absence of structural data, this is only a speculative conjecture; anyway, NMR data (Fig. 8.25) show pentadienyl protons in **III** significantly downshifted and quite broadened with respect to the corresponding signals in **II**. This could indicate a weak interaction as C-H···Cl. It is worthy of note that a C-H···F interaction between fluorine and a low acidic C-H of a thiophene ring (see pag. 41) has been already reported (Fig. 8.32). [48]

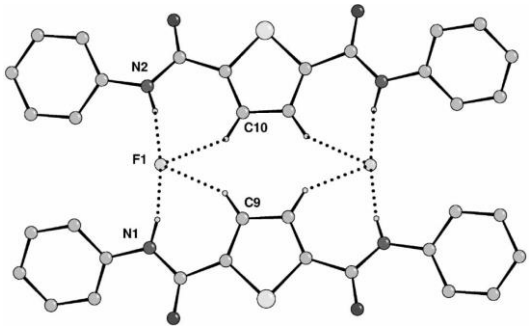

Fig. 8.32 - Coordination environment of two fluoride anions [48]

It is curious to consider that in figure 8.31 chloride ions are mutually arranged like metal cations in a celebrated Stoddart's supramolecular compound, the Borromean Ring **BR**$^{12+}$ (Fig. 8.33). [49] In the third superstructural representation (C) in figure 8.33, one can see an octahedron associated with the six Zn^{+2} ions; such a geometrical array may be also presented by the six chloride anions in fig 8.33. Obviously, this analogy is only formal, but is useful to understand how many work still needs to be done in the field of the coordination chemistry of anions.

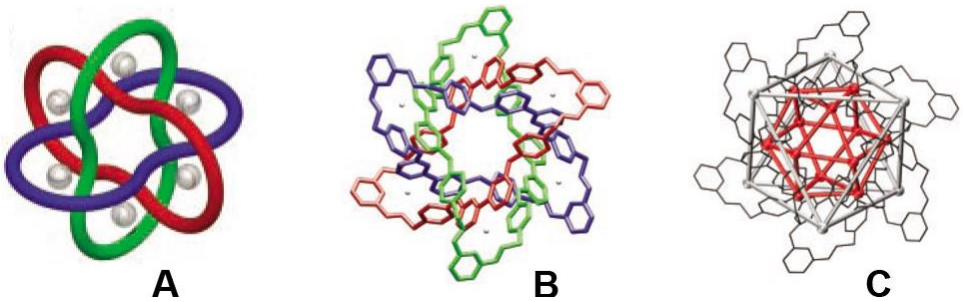

Fig. 8.33 - (ex 3). Different structural and superstructural representations of the **BR**$^{12+}$ dodecacation(s) in the solid state as deduced from x-ray crystallography carried out on single crystals of **BR**-12TFA. In the case of the illustrations of the single **BR**$^{12+}$ dodecacation the three equivalent macrocycles are featured, as tubular and space-filling representations, in the three primary colors, green, red, and blue. The six Zn(II) ions are depicted in silver.

The dramatic color change observed upon oligomerization of Pt–Fe **II** suggests a lower HOMO–LUMO energy gap in the "blue" hexamers **III** compared with the "yellow" bimetallic precursors **II**. Indeed, an electron redistribution involving all the assembled subunits is expected. In particular, the lone pairs of the N–H···N moieties of **III** are likely to display a less basic, as well as a less nucleophilic character after self-assembly. The N–H···N moieties of precursors **21**–**25** and hexamers $\mathbf{21_6}$–$\mathbf{25_6}$ react with electrophilic metals of chloro-bridge dimers in different ways. We have already observed that [(dppf κ-*P*,*P* Pt)Pt(*n*Bu_2DTO κ-*S*,*S* Pt)]Cl (**24**) reacts with a half molar quantity of [Ru(η^6-*p*-cymene)Cl_2] in $CHCl_3$/MeOH (95:5, v/v) in a relatively short time (1 h) and at moderate temperature (50 °C), giving rise to the hetero-trimetallic [(dppf κ-*P*,*P* Pt)Pt(μ-*n*Bu_2DTO κ-*S*,*S* Pt κ-*N*,*N* Ru)Ru(η^6- *p*-cymene)Cl]Cl in high yield.[50]

It have also been shown that the abovementioned reaction can be regarded as a general method for the synthesis of hetero-trimetallic complexes of formula [(dppf κ-*P*,*P* Pt)Pt(μ-R_2-DTO κ-*S*,*S* Pt κ-*N*,*N* Pd)- ML*n*]Cl, in which the ML*n*

subunit is a molecular frame where Mn^+ is a metal ion and Ln is a set of neutral or anionic ligands with an overall negative charge of (n–1). These anticipations are confirmed here, where reaction of [(dppf κ-*P*,*P* Pt)Pt(H-Me$_2$-DTO κ-*S*,*S* Pt)]Cl (**21**) with a series of chloro-bridged dimers [MLnCl]$_2$ {MLn = [(η^3-allyl)Pd]$^+$, [(η^6-*p*-cymene)RuCl]$^+$, [Ir(ppy)$_2$]$^{2+}$ (ppy = *C*,*N*-chelating 2-phenylpiridine), [Rh(ppy)$_2$]$^{2+}$, [Rh(COD)]$^+$ (COD = 1,5- cyclooctadiene)}, under the same conditions described earlier,[50] gave **IV** in 63–71% yields (Scheme 8.6).

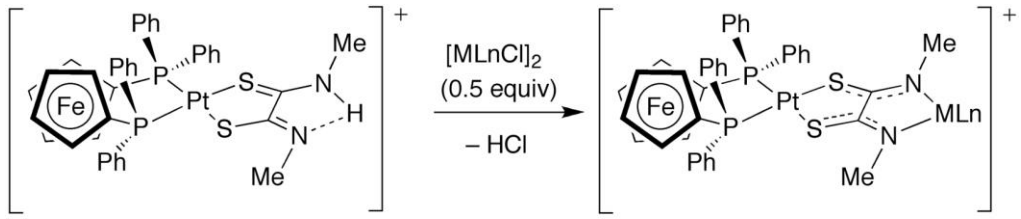

21 **IV**

IV: **29:** MLn$^+$ = [(η^3-allyl)Pd]$^+$
30: MLn$^+$ = [Rh(COD)]$^+$
31: MLn$^+$ = [Ru(η^6-*p*-cymene)Cl]$^+$
32: MLn$^+$ = [Rh(2-phenylpyridine)$_2$]$^+$
33: MLn$^+$ = [Ir(2-phenylpyridine)$_2$]$^+$

Scheme 8.6

The reactions of **21** with the abovementioned electrophiles were straightforward, whereas those of **21$_6$**, taken as a typical example of the type **III** series, with the same [ML$_n$Cl]$_2$ dimers were much more complex. In particular, the reaction of **21** with an equimolar quantity of [(η^3-allyl)PdCl$_2$]$_2$ gave unexpected results. No reaction was observed, even under more severe experimental conditions. That is, keeping the reaction mixture in CHCl$_3$/MeOH, 70:30 (v/v) for two days with heating at reflux (compared with a few hours heating as in the case of precursors **II**). After this time, **21$_6$** was recovered substantially unreacted. Moreover, **21$_6$** did not react with a half-molar quantity of [Rh(COD)Cl]$_2$ under the same experimental conditions. Similarly, a large excess of either Pd or Rh dimers under the same experimental conditions left the starting material unchanged. These results suggest that, as consequence of the cyclization process, the lone pair electrons of the N–H···N frames are withdrawn toward the inner part of hexamers **21$_6$**–**25$_6$**, in such a way that the N–H···N chelating systems becomes chemically harder in the cyclic assemblies.[51] As a result such a nucleophilic array of nitrogen atoms is no

longer available to chelate the soft {$Pd^{II}(\eta^3$-allyl)} or {Rh^{I}(COD)} metal fragments, because of the unfavorable hard–soft interaction.[51]

Thus, **21_6** has been reacted with a half-molar quantity of [Ru(η^6-*p*-cymene)Cl_2]$_2$ in an attempt to gain a better match between the hard N–H···N moiety of the former and the borderline "hard–soft" (according to the Pearson scale)[51] Ru(II) atom of the latter. After about eight hours with heating at reflux, the trimetallic complex [(dppf κ-*P*,*P* Pt)Pt(μ-HMe_2DTO κ-*S*,*S* Pt, κ-*N*,*N* Ru)Ru(η^6-*p*cymene)] Cl (**31**, Scheme 8.6) was recovered together with a large quantity of unreacted **21_6** (about 80% of the weighed amount). Based on these observations, a given quantity of **21_6** was treated with [Ru(η^6-*p*-cymene)Cl_2]$_2$ in a 1:3 molar ratio (in $CHCl_3$), with the aim of disassembling the hexamer. Surprisingly, this reaction gave, after eight hours with heating at reflux, an unexpected result, which could be macroscopically visualized through a color change from blue to yellow–green. Column chromatography of the mixture provided a significant quantity of the known dimer [{Ru-(η^6-*p*-cymene)Cl}$_2$(μ-MeDTO κ-*N*,*S* Ru κ-*N*,*S* Ru)][52] together with a large amount of [(dppf κ-*P*,*P* Pt)Pt-(μ-HMe_2DTO κ-*S*,*S* Pt, κ-*N*,*N* Ru)Ru(η^6-*p*-cymene)]Cl (**31**, Scheme 8.6).

Finally, the "blue" compound **21_6** was also reacted with [Ir$(ppy)_2$Cl]$_2$ and [Rh$(ppy)_2$Cl]$_2$ under the same experimental conditions, yielding only minute quantities of unidentified products in addition to unreacted material. The conclusions drawn after these experiments are as follows: the N–H···N frames in the "blue" compounds **21_6**–**25_6** are poorly reactive toward nucleophilic addition, even under harsh experimental conditions. However, when the reaction takes place, it results in an uncontrolled disassembling of hexamers **21_6**–**25_6**. In other words, a single hexamer cannot add an ML*n* unit while keeping the hexameric structure intact. This finding seems also to match with the fact that π electrons of the bridging dithiooxamide, when engaged in a C_2N_2M metalloaromatic cycle,[53] prevent the formation of "blue" oligomers.

The oxidation behavior of **II** and **III** was investigated in1,2-dichloroethane solution by using cyclic voltammetry(CV) and differential pulse voltammetry (DPV). The cyclic voltammograms of **II** exhibit an oxidation process in the potential range +1.00 to +1.20V versus a saturated calomel electrode (SCE). In most cases, these oxidations are irreversible, but become partially reversible at relatively fast scan rates (e.g., 600 mV s^{-1}). Interestingly, the cyclic

voltammogram of [(dppe)Pt(HR_2DTO κ-*S*,*S* Pt)]Cl (dppe = 1,2-diphenylphosphino ethane; R = isopropyl), under the same experimental conditions, exhibits a quasi-reversible process at +1.15 V versus SCE, which is very similar to that of the corresponding complex with the dppf ligand instead of the dppe one, that is, compound **23** (*E*1/2 at +1.16 V). The oxidation process of [(dppe)Pt(HR2DTO κ-*S*,*S* Pt)]Cl is straightforwardly assigned to the Pt(II)/Pt(III) oxidation, and,by analogy, the same is true for **23** and all the other compounds of type **II**.[29]

It is noted that the free dppf ligand undergoes a quasi-reversible oxidation process at +0.67 V versus SCE under identical experimental conditions.[50] The absence of a dppf-based oxidation at potentials less positive than +1.10 V is attributed, in the case of **II**, to the strong electron-withdrawing ability of the dithiooxamide ligands, which drain electronic charge from the dppf ligands through the Pt(II) center.

The cyclic voltammograms of $\mathbf{21_6}$–$\mathbf{25_6}$ are all qualitatively very similar, showing a quasi-reversible oxidation process in the +0.38 to +0.45V potential range, followed by a second, irreversible process – which in most cases becomes quasi-reversible by using fast scan rates – in the +1.05 to +1.20 V potential range (Table 8.3). The intensity ratio between the potential peaks corresponding to the first and second oxidation processes in CV and DPV (when reversible or quasi-reversible processes are seen) is 1:2, indicating that the number of electrons exchanged in the second process (at more positive potentials) is twice the number of those exchanged in the first process (at less positive potentials).

Table 8.3. Oxidation data in 1,2-dichloroethane.

compound	$E_{1/2}$/V *vs* SCE		**compound**	$E_{1/2}$/V *vs* SCE	
21	-	+1.08[b]	21_6	+0.45[a]	+1.10[b]
22	-	+1.06[b]	22_6	+0.42[a]	+1.07[b]
23	-	+1.16[a]	23_6	+0.39[a]	+1.18[a]
24	-	+1.12[b]	24_6	+0.38[a]	+1.17[b]
25	-	+1.05[b]	25_6	+0.45[a]	+1.08[b]

a) Reversible process; b) quasi-reversible process at scan a rate > 600mV/s

The redox behavior of $\mathbf{24_6}$ has already been reported,[50] and the oxidation at +0.38 V versus SCE exhibited by such species has been assigned to a

delocalized orbital involving several dppf subunits. This assignment was based on the consideration that bridging Pt(II) centers may allow good electronic interaction between redox-active groups. This is the case for the complex *trans*-[Pt(ethynylferrocene)$_2$-(PPh$_3$)$_2$], for which the two ferrocene-centered oxidations are split by 260 mV.[54]

The interpretation invoked for **24$_6$** is considered to be valid for all the other type **III** compounds studied here. Although the Pt(II) centers of the type **III** species are quite different from that of trans-[Pt(ethynylferrocene)$_2$(PPh$_3$)$_2$], it is assumed that two nearby dppf subunits can be significantly coupled through the Pt(II) centers (through space interaction). As all the dppf subunits of a given type **III** compound are identical to one another (as shown by NMR spectroscopy), the coupling can be reasonably extended to all the dppf subunits present in each cyclic multinuclear array. As a consequence, the six dppf subunits of a single hexamer can give rise to delocalized orbitals that, compared with the dppf centered orbitals of the "isolated" subunits, are either stabilized or destabilized (lower or higher in energy, respectively). The destabilized orbitals present in the type **III** cyclic hexamers are expected to undergo oxidation relatively easy and, therefore, are most likely the one(s) involved in the oxidation process observed in the +0.35 to +0.45 V potential range. Such a peculiar redox behavior of the hexamers is, therefore, one of the properties that results from the formation of the molecular assemblies from monomers **II**. Clearly, a destabilized (with respect to the orbitals of the isolated monomers), delocalized orbital extending over the six dppf units of the cyclic hexamers **III** would also be the HOMO involved in the low-lying transition responsible for the absorption peaking around 660 nm of these species (Fig. 8.24), thereby justifying the color changes on passing from type **II** to **III** compounds.

A characteristic feature of adaptive chemistry is the reversibility of self-assembly processes, as reversibility of a self-assembled species may allow different geometries and structural arrangements to be explored upon changes of the "environmental" conditions employed. The results described above indicate that the reaction of macrocyclic hexamers **III** with hard metal centers leads to hexamer disassembly. Disassembly processes generally yield unpredictable species in a non-reversible fashion. However, it is known that Pt(II) dithiooxamide compounds similar to **II** may easily react with HCl to form luminescent, tight contact ion pairs in a reversible fashion (reversibility is obtained upon base addition). This property has been explored in the context of

gas sensor preparation, as well as fast HCl transporters across organic phases (*vide infra*). Indeed, HCl addition to a solution of any of the hexamers **III** readily leads to a distinct color change; solutions suddenly turning yellow from blue. The NMR spectra of the new species thus obtained are identical to those resulting from any freshly prepared solution of compounds **II** upon HCl addition (Fig. 8.34).

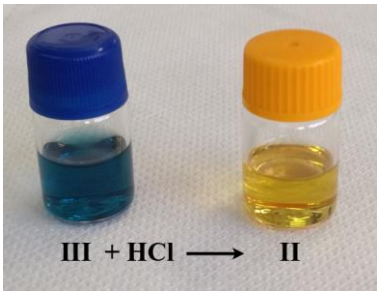

Fig. 8.34

Notably, once reacted with HCl, the whole series of **II** (including **21**–**25**, which spontaneously self-assemble to form $\mathbf{21_6}$–$\mathbf{25_6}$) does not undergo hexamer formation anymore, as indicated by the fact that their absorption spectra remain unaltered. This demonstrates that HCl addition disassembles the hexameric macrocycles, producing stable/unreactive monomers. Interestingly, addition of sodium hydrogen carbonate to $\mathbf{21_6}$–$\mathbf{25_6}$ previously reacted with HCl regenerates the macrocycle, as indicated by the absorption spectra changes; thus, demonstrating the reversibility of the HCl-promoted process. The disassembly/assembly process is sketched in figure 8.35.

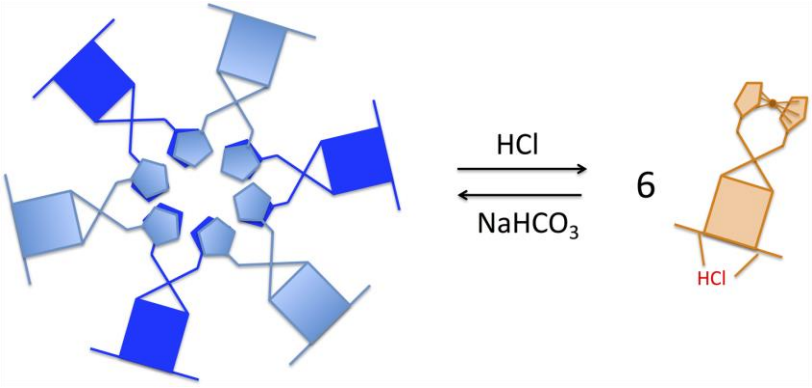

Fig. 8.35 - Sketch of the disassembly/assembly process of $\mathbf{21_6}$–$\mathbf{25_6}$ upon HCl/$NaHCO_3$ addition.

In the disassembled state, HCl is incorporated into the isolated building blocks. In the isolated building blocks (orange), each dppf unit chelates a single Pt(II) center. In the assembled hexamers (blue), each dppf unit coordinates two different Pt(II) centers. The blue and dark-blue colors are used to differentiate the two different, parallel planes in which the molecular fragments lie (see also Figure 8.28). From a different perspective, HCl addition to **21–25** can be seen as a method to freeze the system in a "separate/unreactive" state, in which the dimetallic platinum/ferrocene building blocks are stable once HCl has been incorporated in their structure. Removal of HCl from the solution, on the other hand, re-activates the self-assembly. In this respect, base addition is the external input that triggers the self-assembly process, as well as HCl addition is as the switch-off input, preventing the macrocyclization process.

8.2.5. Sensing in the solid phase.

In the solid state, non-luminescent platinum(II) dithiooxamide species $[Pt(HR_2DTO)_2]$ adsorb gaseous HCl, yielding a tight ion pair species which exhibits photoluminescence; the process is quantitatively reversed on heating or by exposing the sample to ammonia vapors (Fig. 8.36) [55].

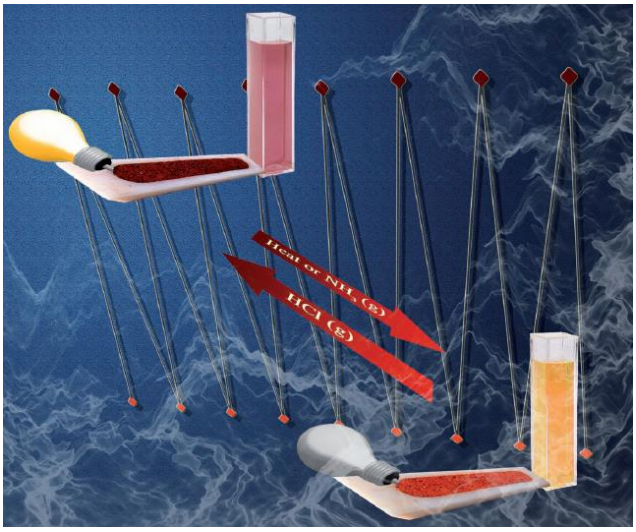

Fig. 8.36 - Sketch of the luminescence reversible switching of $[Pt(HR_2DTO)_2]$ and $[Pt(H_2R_2DTO)_2][Cl]_2$ on exposition to HCl and NH_3 vapor exposure both in the solid state and in solution. The figure is the front cover of [55].

Molecular systems capable of exhibiting on/off switching of luminescence in the presence of suitable substrates or under specific conditions are being extensively investigated since they are of interest in various applicative and fundamental research fields, such as sensors and molecular logic gates and machines.[56]

However, whereas luminescence switching in solution is very well documented, luminescence switching in the solid state, related to coordination of gases to switchable molecular species, i.e. as a consequence of site-specific interactions at the molecular level, is far less common. A noticeable exception is the extensively studied field of luminescent oxygen sensors, where anyway the interaction is not site-specific. [57]

A recent interesting example is the luminescence switching exhibited by crystals of a dinuclear (bipyridine)platinum(II) complex bridged by pyridine-2-thiolate ions, in the presence of organic vapors of acetonitrile or ethanol.[58]

Herein is reported the solid-state switching of the luminescence of a Pt(II) complex based on [Pt(H-R_2-DTO)$_2$] (DTO = dithiooxamide; R = *n*-butyl. See Fig. 8.37), in the presence of gaseous HCl. The solid-state luminescence switching can be reversed by heating the complex powder or in the presence of ammonia vapors.

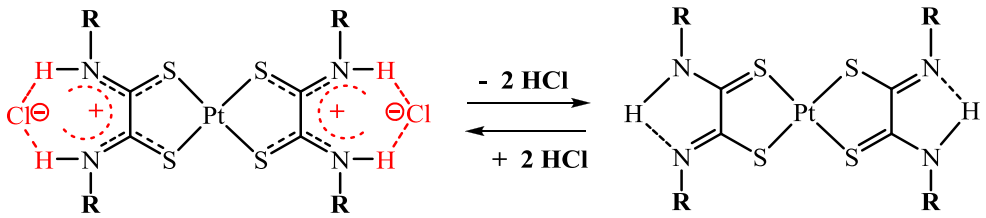

11 **12**

Fig. 8.37 - Structural formulas of **11** and **22** and their conversion scheme. R is *n*-butyl.

The {[Pt(H_2R_2DTO)$_2$][X]$_2$ ion pairs (X = Cl, Br, I) emit from a charge transfer excited state (namely, a Pt/S A DTO CT triplet state), whereas the [Pt(HR_2DTO)$_2$] species (‘‘unprotonated’’, for simplicity) are not luminescent.[59]

The absorption spectra of the tight ion pairs and their ‘‘unprotonated’’ homologous species are also notably different from one another, with the ion pairs absorbing at significantly lower energy than the corresponding

‘‘unprotonated’’ ones. This process was investigated in detail in solution [59] (section *8.2.1*)

when it was also shown that it is common to a series of Pt(II) species carrying various amide substituents (including the compounds **11** and **12** reported here); it is not limited to HCl, but can also involve HBr and HI and therefore, in principle, any HX species (X = pseudohalogen group).

On the basis of the known solution behavior, the solidstate luminescence properties of the Pt(II) dithiooxamide complexes has been tested, having seen that the different photophysical properties for the tight ion pairs and the ‘‘unprotonated’’ species are also retained in these conditions.

Indeed, in the solid state **11** exhibits photoluminescence quite similar to that reported in solution (see Fig. 8.38), so a Pt/S A dto CT attribution still holds, whereas the excited state of compound **12** only decays by radiationless processes.

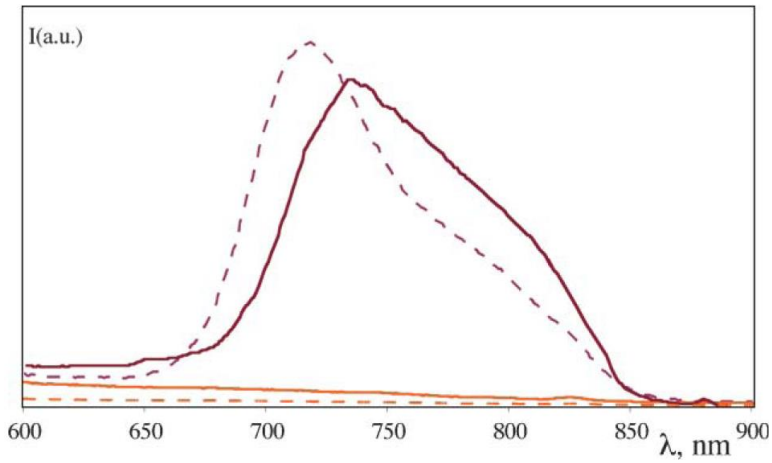

Fig. 8.38 - Luminescence spectra of **11 (**tight ion pairs**)** in the solid state (solid purple) and in dichloromethane solution (dashed purple). Orange curves are the emission responses of **11** under the same conditions. Excitation wavelength is 464 nm. Lifetime of **11** emission in the solid state is 28 ns, comparable with the solution lifetime (25 ns).[59] Excitation wavelength for emission lifetimes, 408 nm.

The transition from **12** to **11** is easily obtained in the solid state: when **12** is exposed to HCl vapors for a few seconds, the color of the solid changes, passing from an initial orange-red to purple-brown (see Fig. 8.39), indicating formation of **11**.

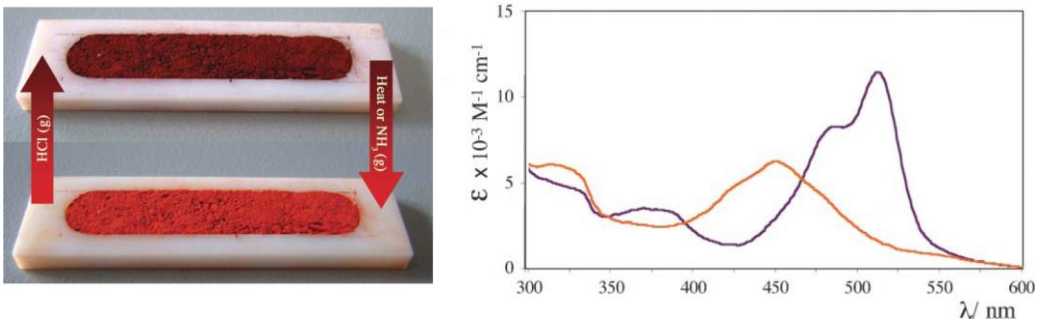

Fig. 8.39 - Color changes obtained by converting solid **11** (the purple-brown species) to **12** (the orange-red species). For comparison, in the right panel the absorption spectra of **11** (purple) and **12** (orange) in dichloromethane are shown.

The experiment shown in figure 8.39 has been realized according to the following procedure: 36 mg of **12** were anchored on a Teflon substrate and the plate was exposed to HCl vapors for 5 seconds. Then a representative sample (8 mg) was dissolved in $CDCl_3$ (0.5 mL). NMR spectra were identical to those of **11**.

At the same time, photoluminescence takes place. The so-formed **11** is identical to that independently prepared in solution, and is very stable at room temperature, as demonstrated by the constancy of its optical properties after several days.

However, **11** can be quantitatively converted into **12** by heating the powder in an oven at 80 °C for 10 min. Several cycles have been performed, and no substantial degradation of the starting material has been noted, at least for 8 cycles. Figure 8.40 shows some of these cycles, followed by luminescence. The procedure can obviously be started from **11**. In this case, the first step is heating to prepare the non-luminescent compound **12**.

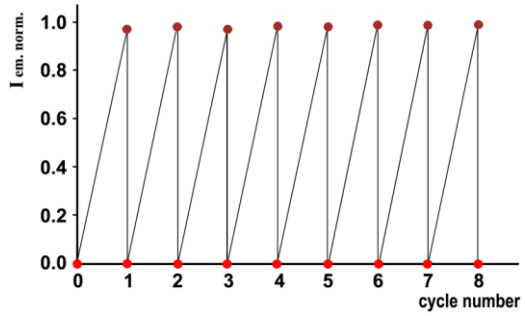

Fig. 8.40 - Values of I_{em} (λ_{exc} = 464 nm, isosbestic point) for solid sample of **12** (orange) exposed to HCl vapors to yield **11** (purple) and heated to restore **12** vs. cycle number.

The solid-state **11** → **12** transition has also been evaluated by temperature programmed techniques, by using TA Instruments Q-100 and DSC-2950. A sample of 2.4 mg of 1 was placed in a sealed sample pan (120 *m*L) to be studied in a differential scanning calorimeter apparatus. On increasing the temperature by 2.5 °C min^{-1} in the range 30–250 °C, two thermal transitions of similar extent take place in the very small temperature range of 155–165 °C (see Fig. 8.41).

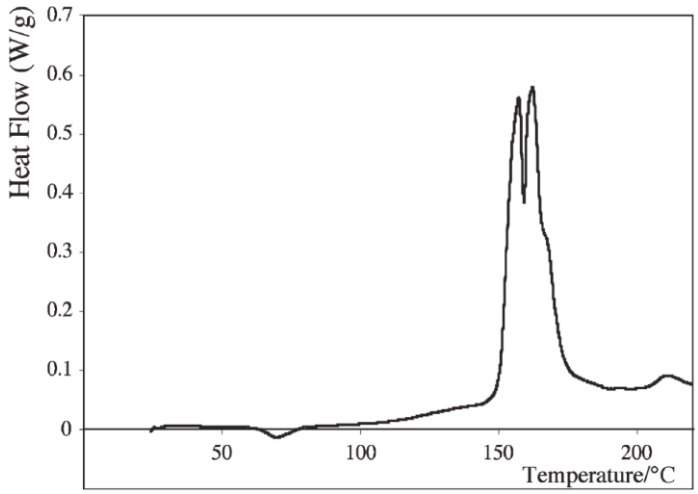

Fig. 8.41 - Differential scanning calorimetry of **11**. Temperature increase rate, 2.5 °C min^{-1}.

This phenomenon is attributed to the sequential loss of the two HCl molecules linked to **11**. The overall thermal exchange measured in these conditions is 186.8 J g^{-1}. In thermal experiments, peak temperatures and relative ratio, as well as the overall thermal exchange, depend on various factors, including the temperature increase rate. For example, the overall thermal exchange increases to 198.7 J g^{-1} for a 10°C min^{-1} temperature increase rate, and in these conditions the two processes coalesce. Thermal inertness is responsible for such an effect.

Moreover, an analogous experiment carried out in a thermogravimetric analysis apparatus with an open pan made it possible to estimate the related weight loss to be close to 10%. This percentage is in fair agreement with the loss of two HCl molecules from **11**.

An interesting variation is that the solid-state 11→12 transition is obtained at room temperature by exposing **11** to NH_3 vapors. In these conditions, after several cycles NH_4Cl is clearly formed and can be analyzed by standard methods. Even in this case, no damage or degradation of the starting material is observed after at least 10 cycles.

In conclusion, we report the potential of Pt(II) dithiooxamide complexes to exhibit luminescence switching in the presence of HCl vapors. The luminescence switching can be reversed by heating or by NH_3 vapors. These results are appealing in view of the interest in searching for hydrogen halide and hydrogen pseudohalide gas sensors. [60]

The sensitivity of the luminescence of the title species to amines may also open up interesting potential applications, since molecules that exhibit useful optoelectronic responses when exposed to amines could be used to detect compounds used in the manufacture of drugs, pesticides, dyes, preservatives and disinfectants, as well as in the food industry.[61]

References

[1] Yurii A. Simonov, Marina S. Fonari, Michael J. Zaworotko, Heba Abourahma, Janusz Lipkowski, Edward V. Ganin and Arkadii A. Yavolovskii, *Org. Biomol. Chem*., **2003**, 1, 2922–2929

[2] R. N. Hurd, G. DeLa Mater, G. C. MC Elheny and L. V. Peiffer, J. *Am. Chem. Sot., 82* (**1960**) *4454.*

[3] (a) C. S. Miller and B. L. Clark, US Patent No. 2 663 656, **1953**; (b) D. A. Ostlie, US Patent No. 4 334 *015, **1982**; Chem. Abstr., 71 (1969) 72167; (c)* D. R. Yarian, US Patent No4334 015, **1982**; *Chem. Abstr., 97 (**1982**) 101744;* (d) W. J. Fraser, US *Patent No. 422 466, **1981**; Chem. Abstr., 94* (**1981**) *165742; (e)* H. C. Heas, *US Patent No. 3 287 154, **1966**; Gem. Abstr., 66 (**1967**) 47524; (f)* Ditto, Inc. Br. *Putent No. 802 170, **1958**.*

[4] A.O. Jorgettoa, R.I.V. Silva a, M.M. Longoa, M.J. Saekia, P.M. Padilhaa, M.A.U. Martinesb, B.P. Rochaa, G.R. Castroa,∗ *Applied Surface Science 264 (**2013**) 368– 374* and references therein.

[5] Vivienne A. White, Nicholas J. Longa and Neil Robertson, *Org. Biomol. Chem*., **2005** , **3**, 4268–4273

[6] S. O. Lawesson, S. Scheibye and J. Kristensen, *Tetrahedron*, 1979, 35,1339.

[7] M.A. Hossain, S.O.Kang, J.M.Llinares,D. Powell and K. Bowman-James, *Inorg. Chem.*, **2003**, 42, 5043

[8] Y. Inoue, T. Kanbara and T. Yamamoto, *Tetrahedron Lett.*, **2003**, 44, 5167.

[9] Y. Inoue, T. Kanbara and T. Yamamoto, *Tetrahedron Lett.*, **2004**, 45, 4603.

[10] (a) Bisson, A. P.; Lynch, V. M.; Monahan, M.-K. C.; Anslyn, E. V. *Angew. Chem., Int. Ed. Engl.* **1997**, 36, 2340–2342; (b) Kim, Y. H.; Calabrese, J.; McEwen, C. *J. Am. Chem.*

Soc. **1996**, 118, 1545–1546; (c) Szumna, A.; Jurczak, J. *Eur*. *J*. *Org*. *Chem*. **2001**, 4031–4039; (d) Choi, K.; Hamilton, A. D. *J*. *Am*. *Chem*. *Soc*. **2001**, 123, 2456–2457; (e) Jagessar, R. C.; Burns, D. H. *Chem*. *Commun*. **1997**, 1685–1686; (f) Gale, P. A.; Camiolo, S.; Tizzard, G. J.; Chapman, C. P.; Light, M. E.; Coles, S. J.; Hursthouse, M. B. *J*. *Org*. *Chem*. **2001**, 66, 7849–7853; (g) Navakhun, K.; Gale, P. A.; Camiolo, S.; Light, M. E.; Hursthouse, M. B. *Chem*. *Commun*. **2002**, 2084–2085; (h) Kubik, S.;Kirchner, R.;Dolting, D.; Seidel, J. *J*.*Am*. *Chem*. *Soc*. **2002**, 124, 12752–12760.

[11] It is known that the association constant of thiourea to oxoanion is higher than that of the corresponding urea derivative; see (a) Linton, B. R.; Goodman, M. S.; Fan, E.; van Arman, S. A.; Hamilton, A. D. *J*. *Org*. *Chem*. **2001**, 66, 7313–7319; (b) Ayling, A. J.; Pe´rez-Paya´n, M. N.;Davis, A. P. *J*.*Am*. *Chem*. *Soc*. **2001**,123, 12716–12717; (c) Herges, R.; Dikmans, A.; Jana, U.; Ko¨ hler, F.; Jones, P. G.; Dix, I.; Fricke, T.;Ko¨ nig, B. *Eur*. *J*. *Org*.*Chem*. **2002**, 3004–3014.

[12] J. Emsley, *Chem. Soc. Rev., 9 (1980)* 91.

[13] A. Giannetto, S. Lanza, G. Bruno, Giuseppe A. Saccà, HA Rudbari, *Acta Crystallographica Section E-Crystallographyc Communication*, 71 (**2015**) O67; G. Bruno, A. Rotondo, F. Nicolo, S. Lanza, *Crystallographica Section E-Structure Reports Online*, 63 (**2007**) O3595-U4306; G. Bruno, S. Lanza, F. Nicolo, G. Tresoldi, G. Rosace *Acta Crystallographica Section C-Crystal Structure Communication* 58 (**2002**) O608-O609.

[14] G. Rosace, Gi. Bruno, L. M. Scolaro, F. Nicolo', S. Sergi , S. Lanza *Inorganica Chimica Acta*, 208 (**1993**) 59-65

[15] 0. Ermer and S. A. Mason, J. *Chem. Soc., Chem. Commun***., 1983**, 53.

[16] (a) L. Antolini, A. C. Fabretti, G. Franchini, L. Menabue, G. C. Pellacani, H. 0. Desseyn, R. Dommisse and H. C. Hofhnans, J. *Chem. Sot., Dalton Trans., **(1987)*** 1921; (b) G. B. Drew, J.M. Kisenyi ,G.R. Willey.

[17] S. Lanza, A. Giannetto, G. Bruno, F. Nicolò and G. Tresoldi, *Eur. J. Inorg. Chem*., **2009**, 2647.

[18] S. Lanza, L. M. Scolaro, G. Rosace, *Inorganica Chimica Acta*, 227 (**1994**) 63-69

[19] R. Romeo, D. Minniti, S. Lanza, P. Uguagliati, U. Belluco, *Inorganic Chemistry*, **17, 1978**, 2813-2818 and references therein.

[20] (a) Tossi, A. B.; Kelly, J. M. *Photochem. Photobiol.* **1989**, *49*, 545. (b) Friedman, A. E.; Chambron, J.-C.; Sauvage, J.-P.; Turro, N. J.; Barton, J. K. *J. Am. Chem. Soc.* **1990**, *112*, 2695.

[21] Pt(II)-dithiolate compounds exhibit typical Pt/S f DTO CT absorption bands peaking at wavelengths longer than 500 nm (_ in the range104-105 M-1 cm-1). (a) Zuleta, J. A.; Chesta, C. A.; Eisenberg, R. *J. Am. Chem. Soc.* **1989**, *111*, 8916. (b) Zuleta, J. A.; Bevilacqua, J. M.; Eisenberg, R. *Coord. Chem. Re*V. **1991**, *111*, 237. (c) Zuleta, J. A.; Bevilacqua, J. M.; Proserpio, D. M.; Harvey, P. D.; Eisenberg, R. *Inorg. Chem.* **1992**, *31*, 2396. (d) Bevilacqua, J. M.; Eisenberg, R. *Inorg. Chem.* **1994**, *33*, 2913. (e) Cummings, S. D.; Eisenberg, R. *Inorg. Chem.* **1995**, *34*, 2007.

[22] Meyer, T. J. *Pure Appl Chem.* **1986**, *58*, 1193.

[23] (a) Juris, A.; Balzani, V.; Barigelletti, F.; Campagna, S.; Belser, P.; von Zelewsky, A. *Coord. Chem. Re*V. **1988**, *84*, 85. (b) Kalyanasundaram, K. *Photochemistry of Polypyridine and Porphyrin Complexes;* Academic Press: London, **1992**.

[24] Vogler, A.; Kunkely, H. *Comments Inorg. Chem.* **1989**, *9*, 201.

[25] (a) McCleverty, J. A. *Prog. Inorg. Chem.* **1968**, 10, 49. (b) Schrauzer, G. N. *Acc. Chem. Res.* **1969**, *2*, 72. (c) Burns, R. P.; McAuliffe *Adv. Inorg. Chem. Radiochem.* **1979**, *22*, 303.

[26] A complete study of the solvent sensitivity of the band is hampered because of the instability of the compounds in polar solvents.

[27] (a) Sexton, D. A.; Curtis, J. C.; Cohen, H.; Ford, P. C. *Inorg. Chem.* **1984**, *23*, 49. (b) Pina, F.; Maestri, M.; Ballardini, R.; Mulazzani, Q. G.; D'Angelantonio, M.; Balzani, V. *Inorg. Chem.* **1986**, *25*, 4249. (c) Billing, R.; Rehorek, D.; Hennig, H. *Top. Curr. Chem.* **1990**, *158*, 151.

[28] Zuleta, J. A.; Bevilacqua, J. M.; Eisenberg, R. *Coord. Chem. Re*V. **1991**, *111*, 237.

[29] Benedix, R.; Hennig, H.; Kunkely, H.; Vogler, A. *Chem. Phys. Lett.* **1990**, *175*, 483.

[30] Maestri, M.; Balzani,V.; Deuschel-Cornioley, C.; von Zelewsky, A. *Ad*V. *Photochem.* **1992**, *17*, 1 and references therein.

[31] (a) Didier, P.; Ortmans, L.; Kirsch-De Mesmaeker, A.; Watts, R. J. *Inorg. Chem.* **1993**, *32*, 5239. (b) Ortmans, L.; Didier, P.; Kirsch-DeMesmaeker, A. *Inorg. Chem.* **1995**, *34*, 5239.

[32] Colombo, M.; Hauser, A.; Gu¨del, H. U. *Top. Curr. Chem.* **1994**, *171*, 143.

[33] Balzani, V.; Juris, A.; Venturi, M.; Campagna, S.; Serroni, S. *Chem. Rev.* **1996**, *96*, 759.

[34] Guglielmo, G.; Ricevuto, V.; Giannetto, A.; Campagna, S. *Gazz. Chim. Ital.* **1989**, *119*, 457.

[35] A. Giannetto, F. Puntoriero, A. Notti, M. F. Parisi, I. Ielo, F. Nastasi, G. Bruno, S. Campagna, S.Lanza, *Eur. J. Inorg. Chem.* **2015**, 5730–5742

[36] (a) G. Bandoli, A. Dolmella, *Coord. Chem. Rev.* **2000**, *209*, 161; (b) F. Canales, M. C. Gimeno, A. Laguna, P. G. Jones, *Organometallics* **1996**, *15*, 3412; (c) J. Diez, M. P. Gamasa, J. Gimeno, A. Aguirre, S. Garcia-Granda, J. Holubova, L. R. Falvello, *Organometallics* **1999**, *18*, 662; (d) P. M. N. Low, A. L. Tan, T. S. A. Hor, Y. S. Wen, L.-K. Liu, *Organometallics* **1996**, *15*, 2595.

[37] T.-J. Kim, K.-H. Kwon, J.-O. Baeg, S.-C. Shim, *J. Organomet.Chem.* **1990**, *389*, 205.

[38] (a) H. S. O. Chan, T. S. A. Hor, L.-T. Phang, K. L. Tan, *J. Organomet. Chem.* **1991**, *407*, 353; (b) L.-T. Phang, S. C. F. Au-Yeung, T. S. A. Hor, S. B. Khoo, Z.-Y. Zhou, T. C. W. Mak, *J. Chem. Soc., Dalton Trans.* **1993**, 165; (c) C. J. McAdam, N. W. Duffy, B. H. Robinson, J. Simpson, *J. Organomet. Chem.* **1997**, *527*, 179.

[39] a) M. Sato, M. Sekino, S. Akabori, *J. Organomet. Chem.* **1988**, *344*, C31; b) M. Sato, H. Shigeta, M. Sekino, S. Akabori, *J. Organomet. Chem.* **1993**, *458*, 199.

[40] a) Y. Cohen, L. Avram, L. Frish, *Angew. Chem. Int. Ed.* **2005**, *44*, 520; *Angew. Chem.* **2005**, *117*, 524; (b) C. S. Johnson Jr., *Prog. Nucl. Magn. Reson. Spectrosc.* **1999**, *34*, 203.

[41] (a) G. Schaeffer, O. Fuhr, D. Fenske, J.-M. Lehn, *Chem. Eur. J.* **2014**, *20*, 179; (b) A.-M. Stadler, F. Puntoriero, F. Nastasi, S. Campagna, J.-M. Lehn, *Chem. Eur. J.* **2010**, *16*, 5645.

[42] (a) A. Kaloudi-Chantzea, N. Karakostas, F. Pitterl, C. P. Raptopoulou, N. Glezosa, G. Pistolis, *Chem. Commun.* **2012**, *48*, 12213; (b) S. Perera, X. Li, M. Guo, C. Wesdemiotis, C. N. Moorefield, G. R. Newkome, *Chem. Commun.* **2011**, *47*, 4658; (c) S. Perera, X. Li, M. Soler, A. Schultz, C. Wesdemiotis, C. N. Moorefield, G. R. Newkome, *Angew. Chem. Int. Ed.* **2010**, *49*, 6539; *Angew. Chem.* **2010**, *122*, 6689.

[43] A. R. Waldeck, P. W. Kuchel, A. J. Lennon, B. E. Chapman, *Prog. Nucl. Magn. Reson. Spectrosc.* **1997**, *30*, 39.

[44] (a) P. Debye, E. Hückel, *Phys. Z.* **1932**, *24*, 311; (b) L. Onsager, *Phys. Z.* **1926**, *27*, 388; (c) R. D. Feltham, R. G. Haiter, *J. Chem. Soc.* **1964**, 4587; d) R. K. Bogges, D. A. Zatko, *J. Chem. Educ.* **1975**, *52*, 649.

[45] See, for example: (a) T. R. Weaver, T. J. Meyer, S. A. Adeyemi, G. M. Brown, R. P. Eckberg, W. E. Hatfield, E. C. Johnson, R. W. Murray, D. J. Untereker, *J. Am. Chem. Soc.* **1975**, *97*, 3039; (b) D. P. Rillema, R. W. Callahan, K. B. Mack, *Inorg. Chem.* **1982**, *21*, 2589; (c) C. A. Bignozzi, S. Roffia, C. Chiorboli, J. Davilla, M. T. Indelli, F. Scandola, *Inorg. Chem.* **1989**, *28*, 4350; (d) S. Campagna, A. Giannetto, S. Serroni, G. Denti, S. Trusso, F. Mallamace, N. Micali, *J. Am. Chem. Soc.* **1995**, *117*, 1757.

[46] B. Hasenknopf, J.-M. Lehn, B. O. Kneisel, G. Baum, D. Fenske, *Angew. Chem. Int. Ed. Engl.* **1996**, *35*, 1838; *Angew. Chem.* **1996**, *108*, 1987.

[47] (a) J. F. Ayme, J. E. Beves, D. A. Leigh, R. T. McBurney, K. Rissanen, *Nature Chem.* **2012**, *4*, 15. (b) For a review see: M. D. Lankshear, P.D. Beer *Acc. Chem. Res.*, **2007**, *40* (8), 657–668.

[48] S. J. Coles, P. A. Gale, M. B. Hursthouse, M. E. Light, C. N. Warriner, *Supramol.Chem.* **2004**, 16, 469 – 486

[49] K. S. Chichak, S.J. Cantrill, A.R. Pease, Sheng-Hsien Chiu, G. W. V. Cave, J. L. Atwood, J. F. Stoddart *SCIENCE* 304 (**2004**) 1308-1312

[50] S. Lanza, F. Loiseau, G. Tresoldi, S. Serroni, S. Campagna, *Inorg. Chim. Acta* **2007**, *360*, 1929.

[51] (a) R. G. Pearson, *J. Am. Chem. Soc.* **1963**, *85*, 3533; (b) R. G. Pearson, *Acc. Chem. Res.* **1993**, *26*, 250; (c) R. G. Pearson, *J. Chem. Educ.* **1999**, *76*, 267.

[52] S. Lanza, G. Bruno, F. Nicolò, A. Rotondo, G. Tresoldi, *Eur. J. Inorg. Chem.* **2002**, *1*, 65.

[53] (a) M. K. Milćić, B. D. Ostojić, S. D. Zarić, *Inorg. Chem.* **2007**, *46*, 7109; (b) Y. Wang, H. R. Gregory, *Organometallics* **2007**, *26*, 21; (c) J. J. Torres-Vega, A. Vásquez-Espinal, J. Caballero, M. L. Valenzuela, L. Alvarez-Thon, E. Osorio, W. Tiznado, *Inorg. Chem.* **2014**, *53*, 3579; (d) H. Masui, *Coord. Chem. Rev.* **2001**, *219–221*, 957.

[54] D. Osella, L. Milone, C. Nervi, M. Ravera, *J. Organomet.Chem.* **1995**, *488*, 1.

[55] F, Nastasi, F, Puntoriero, N. Palmeri, S. Cavallaro, S. Campagna, S. Lanza, *Chem. Commun*., **2007**, 4740–4742

[56] See for example: (a) A. P. De Silva, H. Q. N. Gunaratne, T. Gunnlaugsson, A. J. M. Huxley, C. P. McCoy, J. T. Rademacher and T. E. Rice, Chem. Rev., **1997**, 97, 1515; (b) Molecular Switches, ed. B. L. Feringa, Wiley-VCH, Weinheim, **2001**; (c) V. Balzani, A. Credi and M. Venturi, Molecular Devices and Machines, Wiley-VCH, Weinheim, **2003**; (d) L. Prodi, New J. Chem., **2005**, 29, 20.

[57] See for example: (a) W. Su, R. Schmidt, M. Whaley, J. N. Demas, B. A. DeGraff, E. K. Karikari and B. L. Farmer, Anal. Chem., **1995**, 67, 3172; (b) F. N. Castellano and J. R. Lakowicz, Photochem. Photobiol., **1998**, 67, 179; (c) G. Di Marco, M. Lanza, A. Mamo, I. Stefio, C. Di Pietro, G. Romeo and S. Campagna, Anal. Chem., **1998**, 23, 5019; (d) B. A. DeGraff and J. N. Demas, in Reviews in Fluorescence, ed. C. Geddes and J. R. Lakowitz, Springer, Netherlands, **2005**, vol. 2,p. 125.

[58] M. Kato, A. Omura, A. Toshikawa, S. Kishi and Y. Sigimoto, Angew. Chem., Int. Ed., **2002**, 41, 3183. For other examples of Pt(II) complexes exhibiting vapochromism and vapoluminescence in the solid state, see also: T. J. Wadas, Q. M. Wang, K. J. Kim, C. Flaschenreim, T. N. Blanton and R. Eisenberg, J. Am. Chem. Soc., **2004**, 126, 16841; W. Lu, M. C.W. Chan, N. Zhu, C.-M. Che, Z. He and K.-Y. Wong, *Chem.–Eur. J*., **2003**, 9, 6155 and refs. therein.

[59] G. Rosace, G. Giuffrida, G. Guglielmo, S. Campagna,S. Lanza, Inorg. Chem., **1996**, 35, 6816. Formation of the tight ion pair moves the inherently emitting Pt/S A DTO CT level to lower energy compared to the ‘‘unprotonated’’ species. This makes the radiative transition an effective decay process by decreasing the CT mixing with upper, nonluminescent excited states.

[60] M. Pantsar-Kallio and P. K. G.Manninen, *Anal. Chim. Acta*, **1998**, 360,161.

[61] P. L. McGrier, K. M. Solntsev, J. Schonhaber, S. M. Brombosz, L. M. Tolbert and U. H. F. Bunz, Chem. Commun., **2007**, 2127.

9. Pt(II)-dithiooxamide κ-S,S Pt based anion receptors as molecular carriers

9.1 Transfer of HCl from acqueous fase to chloroform solution containing platinum dithiooxamide complexes.

When in a chloroform solution of a **C** species, [Pt($HR_2DTO)_2$], put in a spectrophotometric cuvette, a 2M solution of HCl in water is carefully stratified, the spectrum starts to change giving rise to the orange series of the spectra in figure 9.1 (process 1 orange spectral series). The last spectrum of the orange series is the same of an authentic sample of a **C-(HCl)** species independently prepared. This means that HCl has crossed the interface to react with the basic sites of **C**. Then a second process starts which gives rise to the purple series of spectra; the last spectrum of this series is coincident with that of an authentic sample of **C-(2HCl)** independently prepared (process 2). The figure 9.1 also shows the colour change observed in the spectrophotometric cuvette on going from **C** to **C-(HCl)**, and from **C-(HCl)** to **C-(2HCl).**

The scheme 9.1 indicate the chemical processes associated with the two spectral series

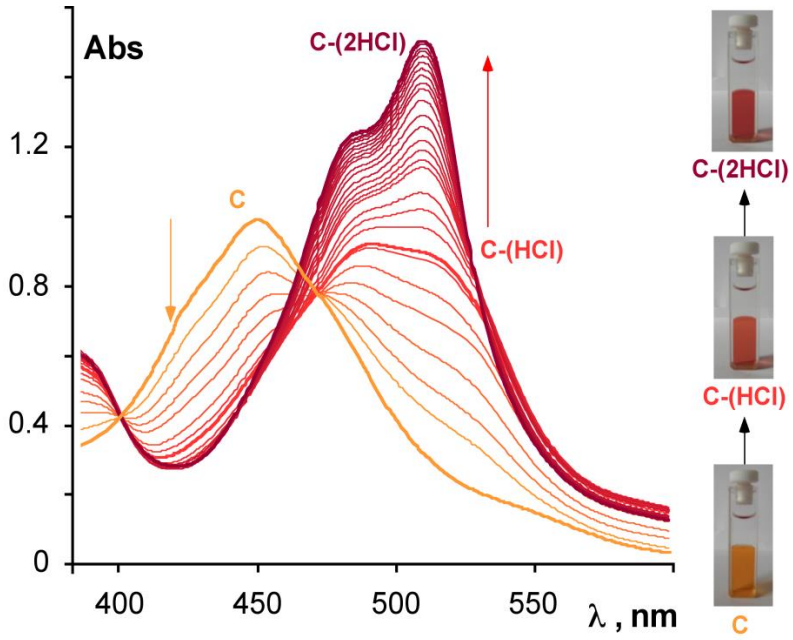

Fig. 9.1

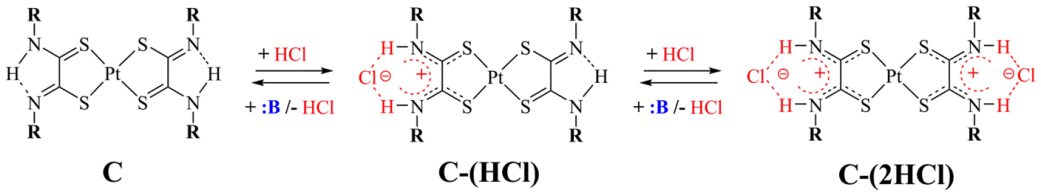

C **C-(HCl)** **C-(2HCl)**

Scheme 9.1

The spectrophotometric monitoring has been done below the middle point in the chloroform region of the cuvette. The spectral trend has been obtained without agitation in none of the two fases.

Any chemical reaction paired with interface hydrodynamic processes should imply both mass transfer and kinetic processes which generally produce curious geometrical motifs since instabilities due to superficial tension. This is what one should have expected to see in the above experiment. However in the organic phase none of the above phenomena has been observed, as if the organic phase were been under agitation.

This strange process has never been observed before. This was confirmed by carefully search in the scientific literature.

The two spectral series obey first order kinetics. This fact is troubling since, if the slow step of the process had been HCl diffusion through the interface, it should not have obeyed first order kinetics. Furthermore it is not understandable how a first order kinetic process could happen without mixing reagents.

Most of the kinetic experiments have been performed by starting processes with $[Pt(HR_2DTO)_2] = 1\times10^{-4}$M. When HCl in the aqueous phase was 0.8÷2 M, the two process are consecutive and quantitative. When HCl concentration was 0.5÷0.8 M the first process was quantitative while the second one did not go to completion. By using [HCl] = 0.5 M the first reaction went to completion and the second one did not start. Obviously 1×10^{-4} M solutions of $[Pt(HR_2DTO)(H_2R_2DTO)][Cl]$ put in contact with aqueous HCl 0.5 M did not gave rise to any process. When the HCl used is less concentrated than 0.5 M, not even the first process went to completion.

Anyway the two kinetic run, when complete, have specific velocity 0.032 min^{-1} and 0.01 min^{-1} respectively (Fig. 9.2). For both processes the relative kinetic constants are independent of HCl concentration obviously when [HCl]> 0.8 M.

The measurement of the rate constants has been performed by recording spectral changes a few mm below the interface and 1.5 cm below the interface, in different sets of experiments. In both cases, the results were totally identical.

It is not obvious that the spectral changes in the chloroform phase observed near the chloroform/water interface and 1.5 cm below the interface give identical results. The independence of spectrophotometric analysis on changing distances from the interface indicates that the whole chloroform solution remains largely homogeneous during the HCl transfer process and suggests that the rate limiting step of the overall process is the interfacial transfer, with an extremely fast diffusion of HCl within the chloroform phase. In fact, since the unidirectional macroscopic diffusion coefficient of a solute in fluid solution is of the order of 10^{-9} m^2 s^{-1},[1] it would take about 10^5 s (i.e., about one day) for a solute (e.g., HCl immobilized on the receptor, like **C-HCl**) to effectively travel over a distance of 1 cm, in the absence of solution stirring. Therefore, HCl is spontaneously transported within a chloroform solution when **C** is present, at rates that exceed the unidirectional macroscopic diffusion coefficient.

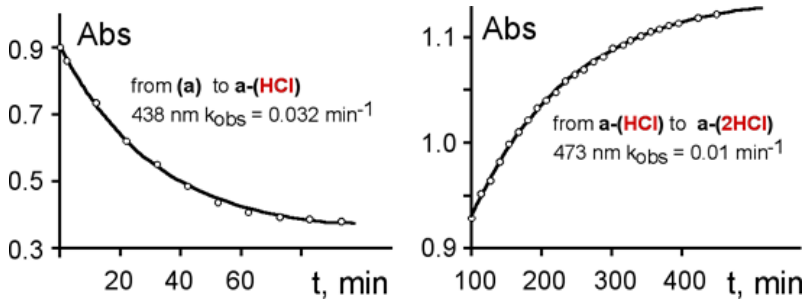

Fig. 9.2

When in a chloroform solution of a **C-(2HCl)** species, $[Pt(H_2R_2DTO)_2][Cl]_2$, put in a spectrophotometric cuvette, distilled water is carefully stratified, the spectrum starts to change giving rise to the orange series of the spectra in Fig. 9.1 (process 1 purple spectral series). The last spectrum of the purple series is the same of an authentic sample of a **C-(HCl)** species independently prepared.

The experiments shown in Fig. 9.3 allow to investigate the rate of release of HCl from a chloroform solution of **C-(2HCl)** (1×10^{-4}M) to water, by taking advantage of the changes in the absorption spectrum of the chloroform solution, which clearly indicate formation of **C** from **C-(2HCl)**. The HCl transfer from the chloroform solution to the aqueous phase is also confirmed by quantitative

conductivity experiments as well as by qualitative chloride determination (via $AgNO_3$ addition), performed in the aqueous solution at the end of the experiment.

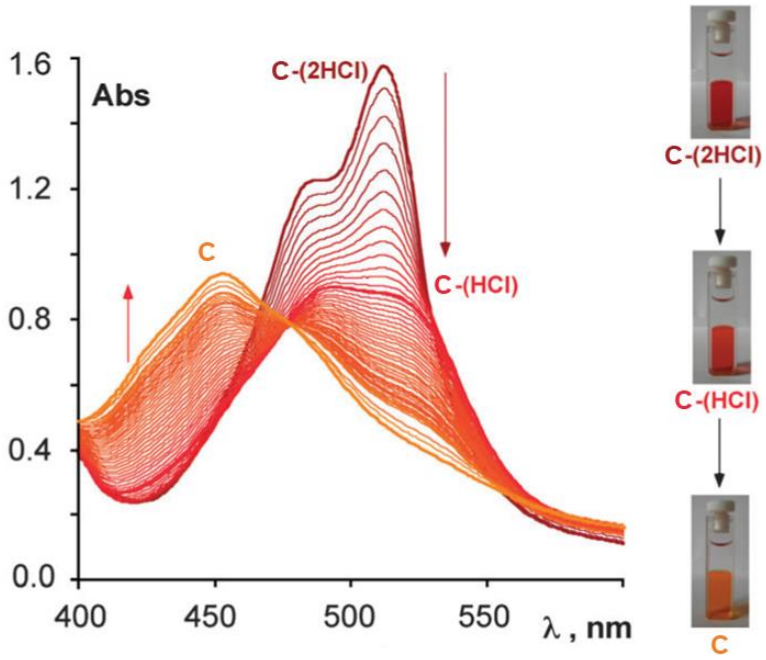

Fig. 9.3

The two kinetic run have specific velocity 0.028 min^{-1} and 0.01 min^{-1} respectively (Fig. 9.4). Also in this case the measurement of the rate constants has been performed by recording spectral changes a few mm below the interface and 1.5 cm below the interface, in different sets of experiments and yet, in both cases, the results were totally identical.

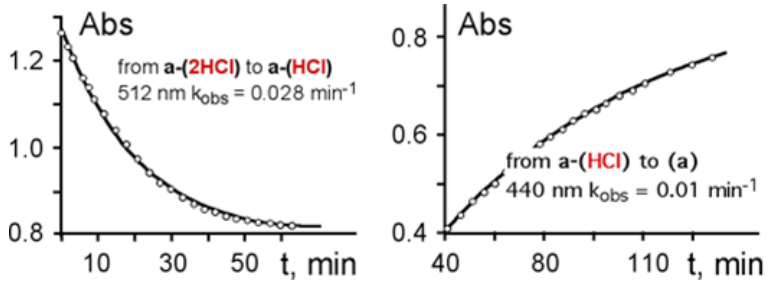

Fig. 9.4

Once again the organic phase remains homogeneous without mechanical agitation, but at this it is need to add the problem of the homogeneity of HCl concentration in the overlying aqueous phase. In fact the accumulation of HCl in

a narrow region adjacent to the interface could stop the transfer of HCl toward the aqueous phase. In the actual experimental condition the amount of HCl that can be accumulated in close proximity of the interface, cannot exceed 2×10^{-2} M which is far from the value for which the stopping of the HCl transfer has been verified (0.5 M). In fact, the diffusion time is large enough to ensure a proper diffusion of HCl (as it can be argued from Fig. 9.5)

In the figure 9.5a mean distances of diffusion fronts of a species whose diffusion coefficient are shown in two time ranges; these mean distances are compared with those of the H+ in water

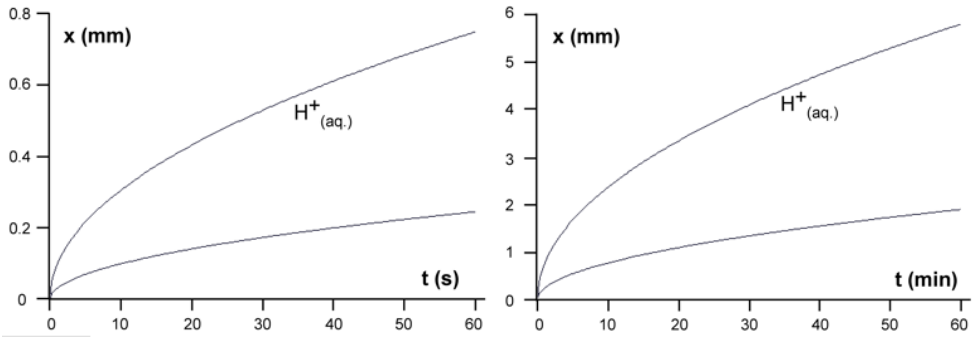

Fig. 9.5 - Comparison between distances gone through by the diffusion front of the proton (a) and of a typical substance with diffusion coefficient 1.0×10^{-9} m^2 sec^{-1} (b)

Rate constant of the HCl transfer from water to Chloroform and *vice versa* do not seem to be dependent on temperature at least in the 16-30 °C range.

However such transfer rate noticeably depends on the interface extension. This has been verified by measuring the rate transfer in two cuvettes whose type is depicted in fig. 9.6

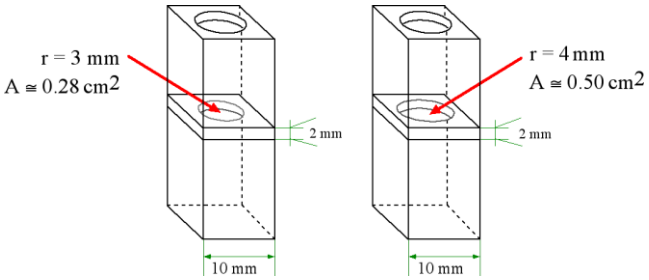

Fig. 9.6 - type of cuvettes used to measure the effect of interface extension on the HCl transfer rate between water and chloroform (and *vice versa*)

The result obtained by using two different cuvettes like those depicted in fig. 9.6 are reported in Table 9.1. From these results is evident that the transfer rate depend on the interface extension.

Table 9.1 – Transfer rate constants obtained using special UV-vis cuvette

	k_{obs} **(r = 3 mm)** min^{-1}	k_{obs} **(r = 4 mm)** min^{-1}
HCl from water to chloroform phase		
C + HCl(aq) → C-(1HCl)	0.0068	0.013
C-(1HCl) + HCl(aq) → C-(2HCl)	0.0025	0.0044
HCl from chloroform to water		
C-(2HCl) → C-(1HCl) + HCl(aq.)	0.0078	0.014
C-(1HCl) → C + HCl(aq.)	0.0023	0.0038

The two spectral series obey first order kinetics.The first order kinetics dependence suggests that the transfer rate depends of the number of carrier molecule per surface unit which, on turn, depends on the carrier concentration in the bulk organic solvent).

The rate of transfer process obviously is almost instantaneous when the interface extension becomes very large; this happens when the two phases are vigorously shaken

9.2 Transfer of HCl from acqueous fase to other chlorinated solvents containing platinum dithiooxamide complexes.

When the HCl is transfers through the interface from concentrated aqueous solutions to a 1×10^{-4} M dichloromethane solution of **C**, a less surprising phenomenon is observed. In fact the transport of HCl through the interface H_2O/CH_2Cl_2, which is an acid-base process, has the typical trend of a processes which implies mass transfer: the propagation of the reaction front is non a definite surface but is a confused, shadowed zone due of the geometrical motifs produced by the instability of the superficial tension at the interface.

What happens is better explained by the sequence of images in Fig. 9.7 were the transfer experiment $H_2O\rightarrow CHCl_3$ (left) is compared with that $H_2O\rightarrow CH_2Cl_2$ (right).

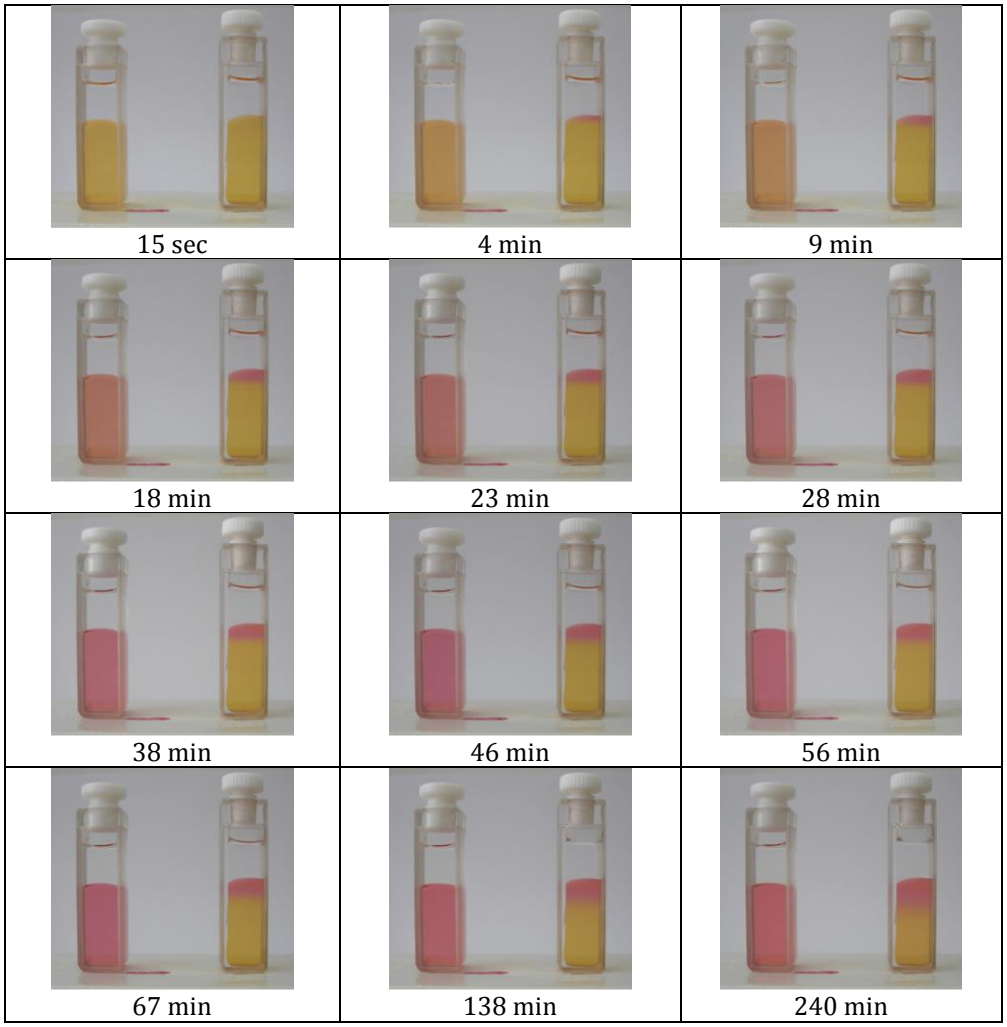

Fig. 9.7 - HCl transfer experiment (see text)

The Figure 9.7 show that HCl in CH_2Cl_2 (right cuvette) diffuses according to Fick's law; as a matter of fact, the mechanism of diffusion of HCl in the presence of the carrier metal-complexes dramatically changes on going from chloroform to methylene chloride.

In other chlorinate solvents like 1,1,2,2-Tetrachloroethane the above phenomenon happens just like in CH_2Cl_2.

As previously observed when a 2 M aqueous HCl is put into contact with a chloroform solution of **C**, a twofold molar quantity of HCl (with respect to **C**) in transferred from water to chloroform; on turn, when a chloroform solution of

C-2HCl is put into contact with distilled water, all hydrochloric acid of the ion pair **C-2HCl** leaves the chloroform and moves into water.

9.3 Transfer of HCl between two aqueous phases through bulk organic membranes.

The obvious conclusion which can be drawn from the above experiments is that a chloroform solution of **C** species placed in a U-tube in order to separate a 2M aqueous HCl from distilled water (i.e. a bulk organic membrane) should allow the transfer of HCl from the acidic aqueous solution into distilled water. This is what really happens. Chloroform by itself is not able to do that, so that one can conclude that **C** species behaves as HCl transporter through a bulk organic membrane [2]

The Figure 9.8 shows how a transport experiment appears to an observer: the donating phase (2 M aqueous HCl, left hand side of the tube) is in contact with a more coloured part of the chloroform membrane, while the receiving phase (distilled water, right hand side of the tube) touches the less intense coloured part of the membrane. Unexpectedly, a third interface is formed which separates two region of different colour within the membrane, but no explanation has been found for this unusual phenomenon.

In other words [Pt(H-R_2-dithiooxamidate)$_2$] plays the role of a HCl symporter, allowing fast HCl transport over macroscopic distances (cm scale) across a hydrophobic layer made of a chloroform solution, without any stirring.

Transport of ions and small molecules plays a crucial role in biological systems as well as in many potential applications. In particular, transport of chloride anions across lipid bilayers, regulated in Nature by transmembrane ion channels,[3] has attracted much attention, as malfunctioning of chloride transport has been associated to various diseases, including nephrolithiasis and cystic fibrosis.[3a,4] Boosted by the aim to shine light on the factors that influence anion and smallmolecule transport, the field of the design of synthetic receptors has attained a prominent role in chemistry.[5–8]

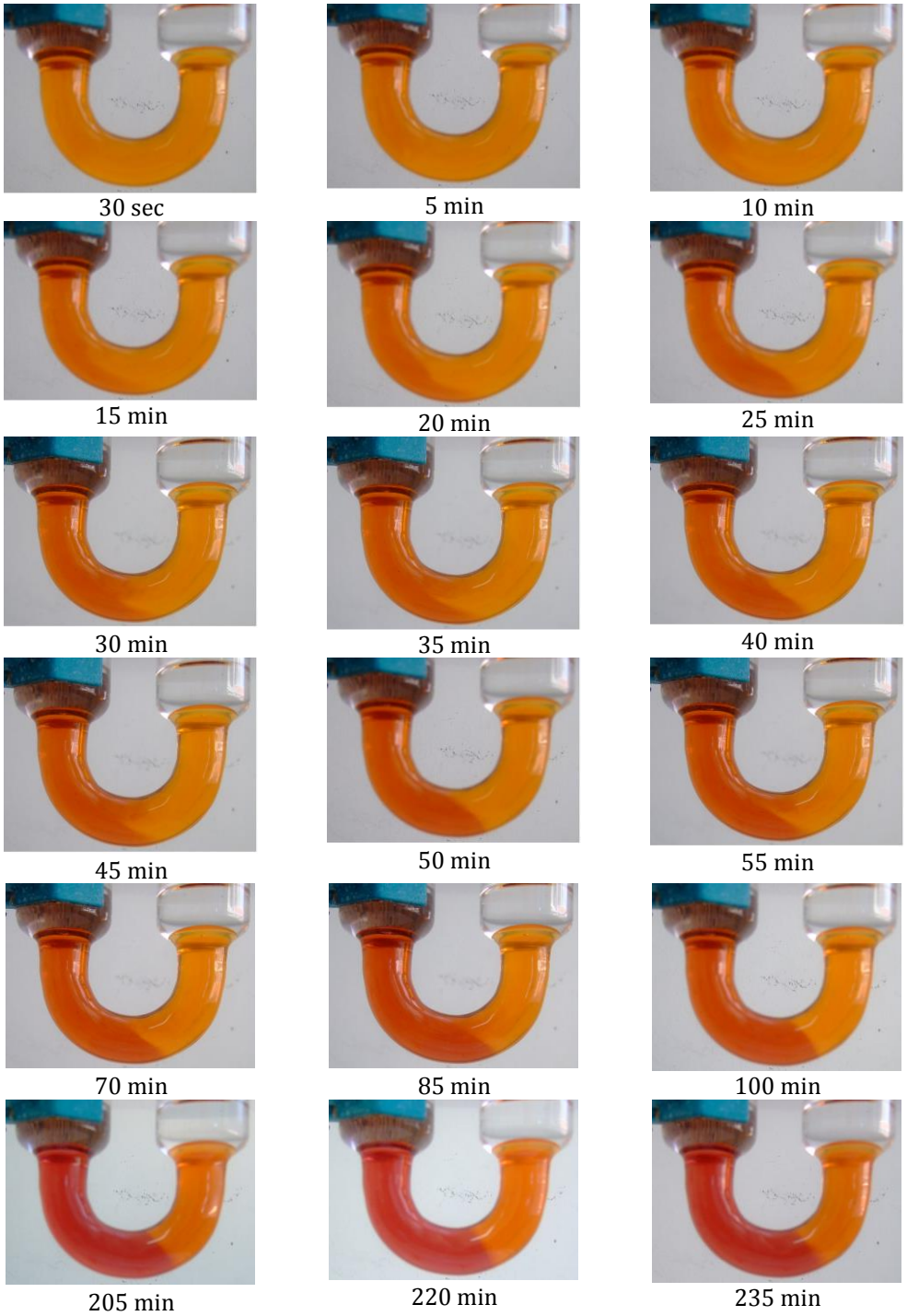
30 sec
5 min
10 min
15 min
20 min
25 min
30 min
35 min
40 min
45 min
50 min
55 min
70 min
85 min
100 min
205 min
220 min
235 min

Fig. 9.8

Fast chloride carriers recently reported in the literature include pre-organized squaramides,[9] amide-functionalized derivatives of the 'tren' scaffold (''tren'' is tris(2-aminoethyl)amine),[10] steroid-based cholapods,[11] and amphiphilic catechols and monoacylglycerols.[12] In practically all the cases the macroscopic, unidirectional diffusion limit remains far to be reached (in fact, the reported transport experiments are usually performed under stirring), with noticeably few exceptions, such as some rigid-rod compounds featuring anion–p interactions, capable of exhibiting a cooperative multi-ion hopping mechanism.[13]

Here we report on the HCl transport properties of a Pt(II) compound (**C**, general formula [Pt(H-R_2-dithiooxamidate)$_2$], where R is an ethyl substituent; scheme. 9.1).[14] **C** acts as a H^+/Cl^- symporter, capable of transporting HCl over large distances (several cm, in a U-tube experiment) across a hydrophobic environment, a chloroform solution, without any stirring, therefore bypassing the diffusion limit. The formation of tight-contact ion pairs between **C** and HCl is the key point for such a transport. Noticeably, this is the first time that a transition metal compound is used as a HCl carrier.

Generally principal methods used in the studies of anion transmembrane transport involve the preincorporation of the carrier in the vesicle membranes, and the subsequent detection of inward-transported anion. [15,16]

However such kind of studies in some cases are performed by using U-tubes[17,18,19].

The ability of **C** to transport HCl across a $CHCl_3$ solution has been tested via U-tube experiments. In a typical experiment, 35 mL of 1 (1.8×10^{-4} M) in $CHCl_3$ was placed at the base of a U-tube (diameter = 2 cm), 15 mL of aqueous HCl (1.5 M) was added into the left-hand-arm and 15 mL of pure water was added into the right-hand-arm of the tube (Fig. 9.9).

The organic phase was not stirred, in contrast to other similar experiments reported in the literature.[4,10] The transport of HCl was monitored by following the conductivity in the right-hand-arm. In the absence of **C**, conductivity is constant over one day (i.e., no HCl transport occurs), but the presence of **C** in the chloroform phase allows the transport of HCl in few hours. Formation of the tight-contact ion pairs **C-HCl** and **C-(2HCl)** in the organic phase during the HCl transport process is also evidenced by color changes in the chloroform solution.

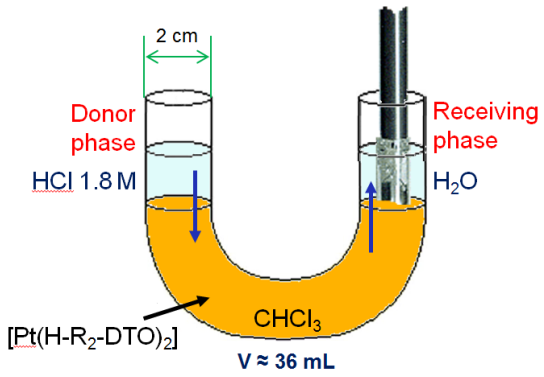

Fig. 9.9

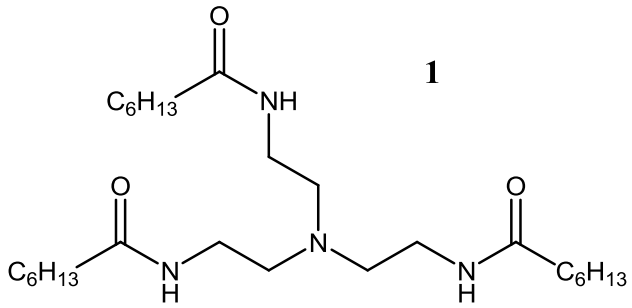

Fig. 9.10

As a control test, an analogous U-tube experiment was performed by using a well-known HCl transporter, **1** (Fig. 9.10), also capable of coordinating two HCl moieties, like **C**, although by using different coordination sites,[4,10] under the conditions used for the experiment whose results are shown in figure 9.11.

The results indicate that **C** is largely more effective than **1** as a HCl transporter. In particular, the lag time for the appearance of HCl in the receiving phase (measured in close-contact with the chloroform/water interface) is 2.5 min for **C** and 60 min for **1**. As the lag time is related to the rate of HCl transport within the chloroform phase, this result definitely indicates that **C** is a faster HCl transporter than **1**. Arguments based on the flow rates lead to similar conclusions. The transition metal complex **C** transports HCl over large, hydrophobic barriers with a speed that can exceed the unidirectional, macroscopic diffusion coefficient, by promoting fast and efficient HCl transfer at the water/chloroform interface and driving an extremely high HCl mobility within the hydrophobic phase. The mobility of the HCl ‘‘packet’’ in tight-

contact ion pairs formed by **C** and HCl, possibly supported by solvent-mediated HCl hopping, is probably the basis of the excellent HCl transport ability of **C**.

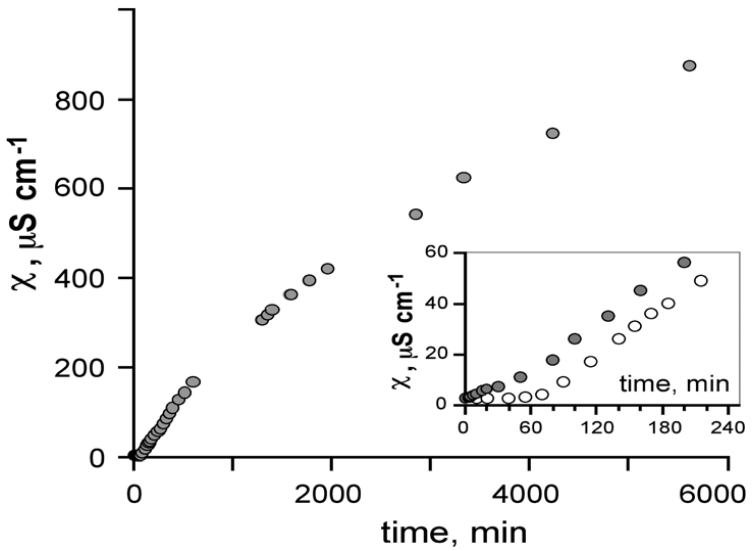

Fig. 9.11 - Increased conductivity of the aqueous solution in the right-hand-arm of a U-tube, as a consequence of the HCl transferred to the aqueous solution in the right-hand-arm (the receiving phase) from a 1.5 M HCl solution in the left-hand-arm (the donating phase), across a 35 mL chloroform phase containing **C** (1.8×10^{-4} M), in the absence of stirring. The experiment is performed by measuring the conductivity 3 mm above the chloroform/water interface in the right-hand-arm. A lag time of ca. 60 min is present (inset, open circles), probably partly due to the slow diffusion of HCl in the 3 mm of the aqueous receiving phase. When the conductivity is measured in close contact with the chloroform/water interface (inset, solid circles), the lag time is reduced to 2.5 min.

The lag time is probably the more interesting parameter: it is mainly related to the rate of HCl transport in the chloroform phase and appears that **C** is about 25 times faster than **1** as HCl transporter. The difference between **C** and **1** is smaller as far as the flow rate is concerned: in fact, the HCl flow rate mainly depends on the interface transfer rates, so leveling off the differences between **C** and **1**. It can also be noted that **1**, although slower than **C** as HCl transporter, is still a quite good HCl transporter, even in the absence of stirring.

Finally, we also performed similar U-tube experiments with stirring the chloroform phase: in these conditions, lag time was about 1 min for both **C** and **1**, as expected since diffusion of HCl receptors within the organic phase is extremely increased by stirring; HCl transport flow rate also increases for both

C and **1** (32 μS/h and 17 μS/h, respectively), also in agreement with the expectations. It is interesting to note that the flow rate of **C** in the absence of stirring is practically equivalent to the flow rate of **1** with stirring.

Taking advantage from the fact that **C**, **C-HCl and C-2HCl** can be detected by electronic spectroscopy, even when they are simultaneously present in the same solution, it has been possible to put into evidence what species, among the three, is implied as carrier. hence Vis spectra of the solution, during the transport experiment, have been recorded in different point of the U-tube by exploiting a optical fiber apparatus connected to the spectrophotometer.

Results recorded in point "1" of the U-tube are shown in figure 9.12.

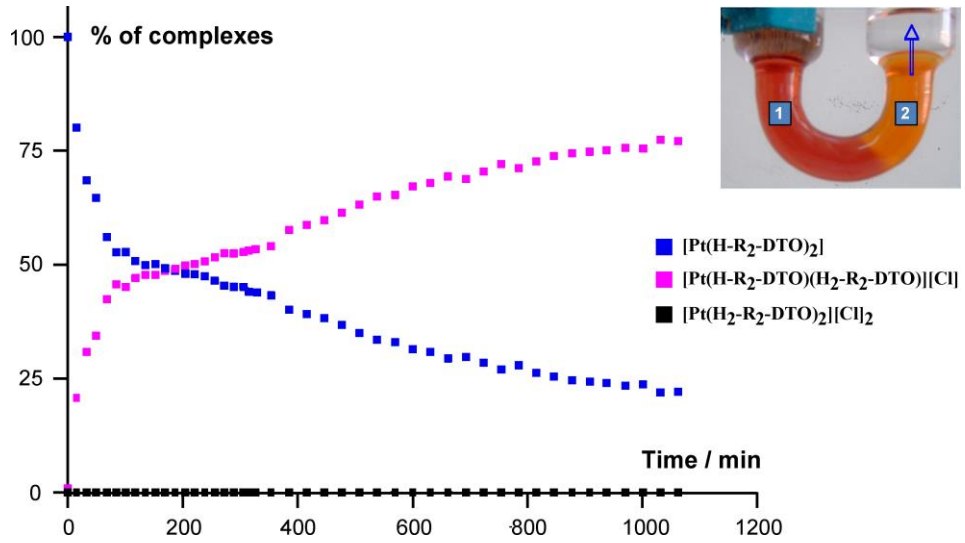

Fig. 9.12 - Changed in % of **C** (blu), **C-HCl** (magenta), **C-2HCl** (black) recorded in point "1" of the U-tube during transfer experiment.

As one can see concentration of **C** decreases during the time of the experiment; at the same time **C-HCl** species show an increasing trend. The **C-2HCl** is not detectable.

A new experiment has been performed by recording spectral changes in the point "2" of U-tube. During the experiment only species **C** is detectable. As matter of fact, HCl is transferred in the receiving phase: this mean that **C-HCl** concentration is too small to be detectable, and keeps itself constant. Probably a stable interface is formed as a consequence of such a stationary flow.

U-tube experiment has been performed by exploiting CH_2Cl_2 as bulk organic membrane, using the same concentration of carrier. This solvent dramatically influences the lag time (Fig. 9.13).

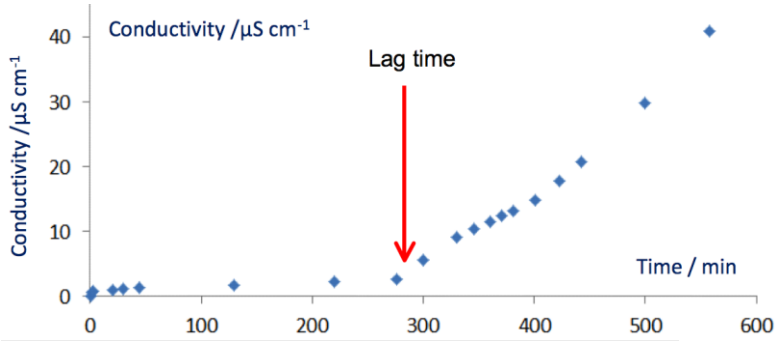

Fig. 9.13 - Changes of Specific conductance in receiving phase (CH_2Cl_2 as Bulk membrane)

Obviously is possible to exploit various $CH_2Cl_2/CHCl_3$ mixtures in order to change the lag time (Fig. 9.14)

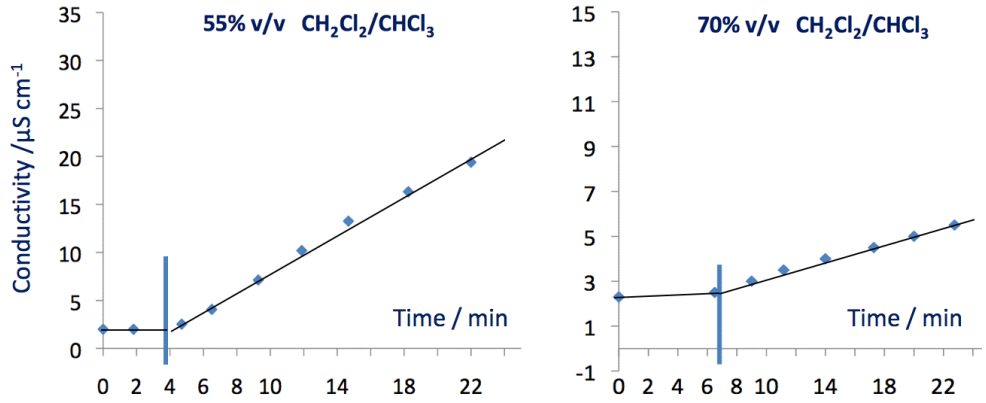

Fig. 9.14 - Changes of Specific Conductivity in receiving phase (CH_2Cl_2 / $CHCl_3$) mixture as Bulk membrane)

In the transport experiments performed up here, the only **C** carrier in which R= ethyl has been taken into consideration. Hence it has been appropriate to extend the transport studies to the same kinds of carrier (C) having alkyl substituents other than ethyl group. Moreover, further information has been obtained from carriers containing metal-dithiooxamide complexes having only one N H···N basic site.

In order to realize what said above the complex in figure 9.15 have been tested.

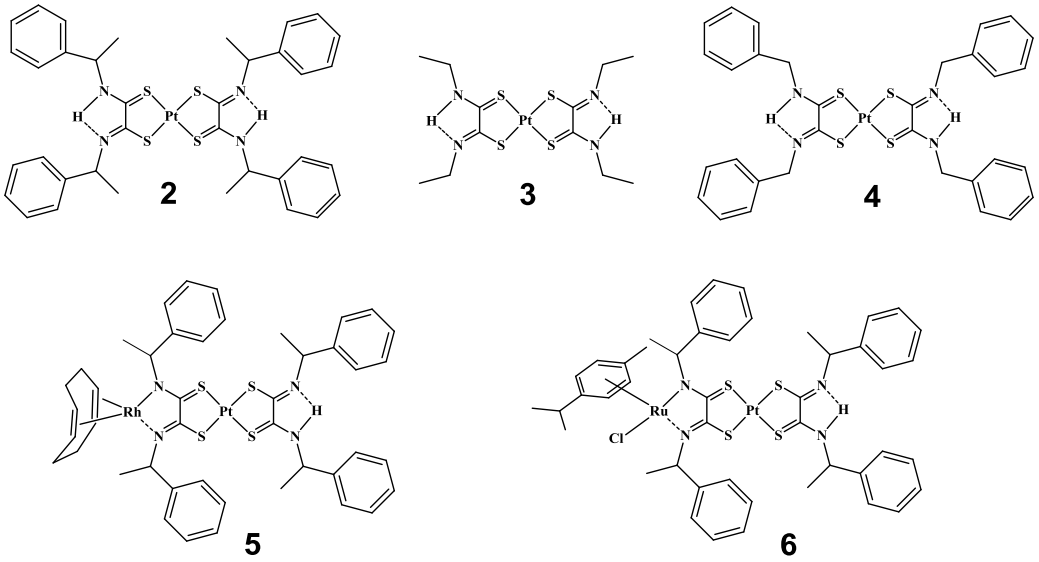

Fig. 9.15

The plots of specific conductance vs. time (Fig. 9.16) show the obtained result.

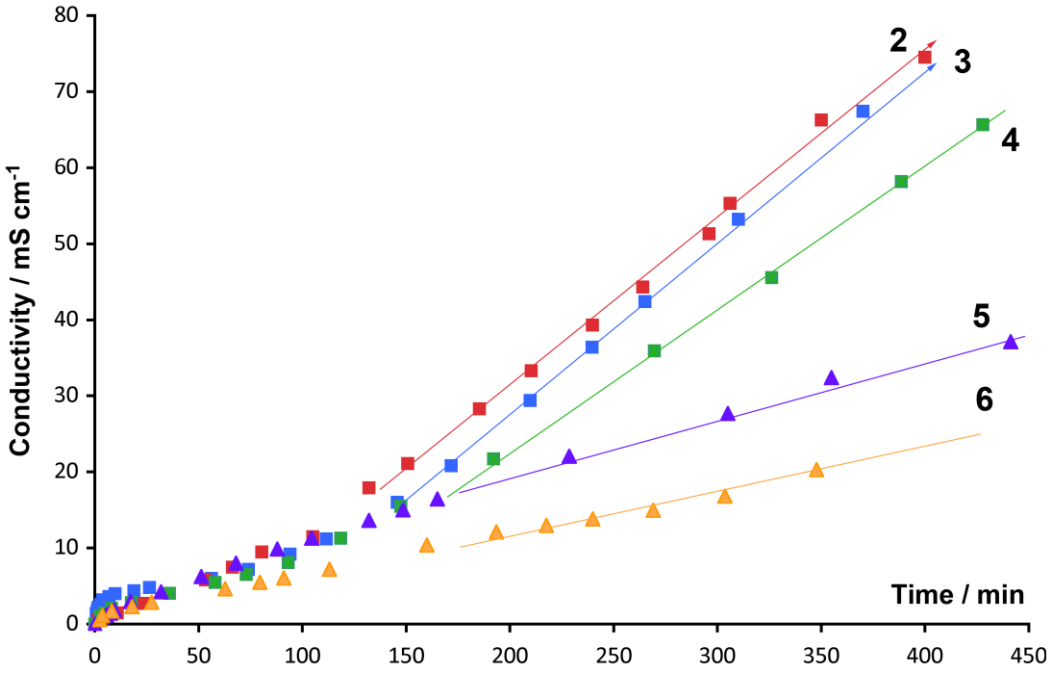

Fig. 9.16 – Trend of specific conductance vs. time using different complexes**.** Red squares (**2**); blue square (**3**); green square (**4**); purple triangles (**5**); orange triangles (**6**). All carriers were 1.5×10^{-4} M

The lag time is the same for all carriers. The flow of HCl become constant after about 100 minutes when the carriers contains two N H···N basic sites (numeri curve) while it become constant after about 50 minutes for carriers contains one N H···N site. For these latter the transport flow rate is about ¼ of that of those containing two basic sites (**5**,**6**).

The results obtained by studing either Transfer of HCl from aqueous phase to chloroform solution and *vice versa* or the transport of HCl through a bulk organic membrane confirm that in these phenomena the peculiar motion of HCl between the solvent and the basic sites of the carrier plays a crucial role. For this reason the hopping mechanism shown in figure 9.17 can be proposed for HCl transportation .

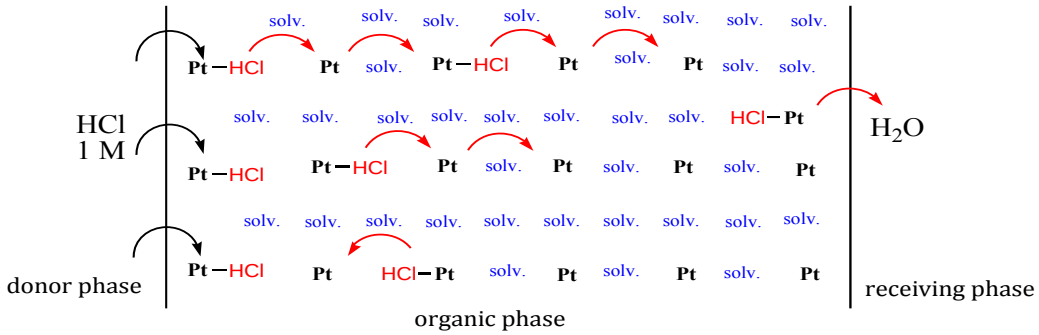

Fig. 9.17 –Hopping mechanism proposed for the transfer of HCl between two aqueous phases through bulk organic membranes.

References

[1] J. Benitez, Principles and Modern Applications of Mass Transfer Operations, Wiley and Son Ltd, Chichester, 2nd edn, **2009**.

[2] A. Giannetto, S. Lanza, F. Puntoriero, M. Cordaro, S. Campagna, *Chem. Commun*. 49 (**2013**) 7611-7613

[3] (a) F. M. Ashcroft, Ion Channels and Disease, Academic Press, San Diego, **2000**; (b) C. Higgins, *Nature*, **1992**, 358, 536; (c) J. Y. Choi, D. Muallem, K. Kiselyov, M. G. Lee, P. J. Thomas and S. Muallem, *Nature*, **2001**, 410, 94.

[4] S. J. Moore, C. J. E. Haynes, J. González, J. L. Sutton, S. J. Brooks, M. E. Light, J.Herniman, G. J. Langley, V. Soto-Cerrato, R. Pérez-Tomás, I. Marques, P. J. Costa, V. Félix and P. A. Gale, *Chem. Sci*., *2013*, 4, 103.

[5] (a) J. L. Sessler, P. A. Gale and W.-S. Cho, *Anion Receptor Chemistry*, RSC, Cambridge, **2006**; (b) A. Frontera, J. Morey, A. Oliver, M. N. Pinˇa, D. Quinodero, A. Costa, P. Ballester, P. M. Deyá and E. V. Anslyn, *J. Org. Chem*., **2006**, 71, 7185.

[6] (a) A. P. Davis, D. N. Sheppard and B. D. Smith, *Chem. Soc. Rev*., **2007**, 36, 348; (b) P. R. Brotherhood and A. P. Davis, *Chem. Soc. Rev*., **2010**, 39, 3633.

[7] (a) J. T. Davis, P. A. Gale,O. A.Okunola, P. Prados, J. C. Iglesias-Sánchez, T. Torroba and R. Quesada, *Nat. Chem*., **2009**, 1, 138; (b) J. T. Davis, O. Okunola and R. Quesada, *Chem. Soc. Rev*., **2010**, 39, 3843.

[8] (a) P. A. Gale, *Chem. Soc. Rev*., **2010**, 39, 3746; (b) P. A. Gale, *Acc. Chem. Res*., **2011**, 44, 216; (c) S. Matile, A. Vargas Jentzsch, J. Montenegro and A. Fin, *Chem. Soc. Rev*., **2011**, 40, 2453.

[9] N. Busschaert, I. L. Kirby, S. Young, S. J. Coles, P. N. Horton, M. E. Light and P. A. Gale, *Angew. Chem*., Int. Ed., **2012**, 51, 4426.

[10] K. J.Winstanley, S. J. Allen andD.K. Smith, *Chem. Commun*., **2009**, 4299.

[11] B. A. McNally, A. V. Koulov, T. N. Lambert, B. D. Smith, J.-B. Joos, A. L. Sisson, J. P. Clare, V. Sgarlata, L. W. Judd, G. Magro and A. P. Davis, *Chem.–Eur. J*., **2008**, 14, 9599.

[12] S. Bahmanjah, N. Zhang and J. T. Davis, *Chem. Commun*., **2012**, 48, 4432.

[13] (a) J. Mareda and S. Matile, *Chem.–Eur. J*., **2009**, 15, 28; (b) R. E. Dawson, A. Hennig, D. P. Weimann, D. Emery, V. Ravikumar, J. Montenegro, T. Takeuchi, S. Gabutti, M. Mayor, J. Mareda, C. A. Schalley and S. Matile, *Nat. Chem*., **2010**, 2, 533.

[14] G. Rosace, G. Giuffrida, G. Guglielmo, S. Campagna and S. Lanza, *Inorg. Chem*., **1996**, 35, 6816, and references therein.

[15] Smith, B. D. & Lambert, T. N. *Chem. Commun*. 2261 (**2003**).

[16] Koulov, A. V et al. *Angew. Chem*. Int. Ed. Engl. 42, 4931–3 (**2003**).

[17] Mary Pinkerton, L.K. Steinrauf, Phillip Dawkins, *Biochemical and Biophysical Research Communications* 35, **1969**, 512-518

[18] Seiji Shinkai, Takahiro Nakaji, Toshiyuki Ogawa, Kazuyoshi Shigematsu, and Osamu Manab *J. Am. Chem. SOC*. **1981**,103, 111-115

[19] Beatriz Baragaña ,Adrian G. Blackburn, Perla Breccia, Anthony P. Davis, Javier de Mendoza, José M. Padrón-Carrillo, Pilar Prados, Jens Riedner, Johannes G. de Vries, *Chem. Eur. J*. **2002**, 8, No. 13 2931

10. Acid base behavior of Pt(II)-dithiooxamide based anion receptors

10.1. acid-base reactions between hydrohalogenated ion-paired complexes and pyridine

Tight-contact ion pairs (TCIPs) play key roles in anion and ion-pair receptor chemistry, [1,2] and in general in the functional behavior of most cofactors and substrates involved in biological transformations and/or processes, which are usually anionic in nature. [3,4]

The formation of TCIP also plays important roles on processes involving artificial systems, like the stabilization of some diacids [5] and the anion-templated assembly of catenanes and pseudorotaxanes.[6] However, in spite of the importance of TCIPs in the above-mentioned fields, detailed investigations on the parameters which determine TCIP formation and stability are quite rare, in particular when multiple TCIP equilibria are involved.

It has been demonstrated that the ability of [Pt(H-R_2-dithiooxamidate)$_2$] complexes (R=alkyl groups) to form TCIPs of general formula {[Pt(H_2-R_2-dithiooxamide)$_2$][Cl]$_2$ (see Figure 10.1) by addition of HCl,[7,8] where ion-pair formation is driven byH-bonding. The process is common to HXspecies,where X is a halogen or a pseudo-halogen anion.[9]

To gain information on the equilibrium between TCIPs containing HCl "moieties" and parent dehydrohalogenated systems in Pt(II) bis(R-dithiooxamide/amidate) complexes, the properties which govern the following equilibrium have been systematically investigated:

$$[Pt(H\text{-}R_2\text{-}DTO)_2] + 2\ HCl \rightleftharpoons [Pt(H_2\text{-}R_2\text{-}DTO)_2][Cl]_2$$

In particular, here we investigate the equilibrium constants between [Pt(H_2-R_2-dithiooxamide)$_2$][Cl]$_2$ and pyridine in chloroform solution. Indeed, pyridine can compete with [Pt(H_2-R_2-dithiooxamide)$_2$][Cl]$_2$ species for protons, so driving formation of the neutral parent complexes from the tight ion pairs.

The reactions studied are shown in eqs 1 and 2 in the Scheme 10.1

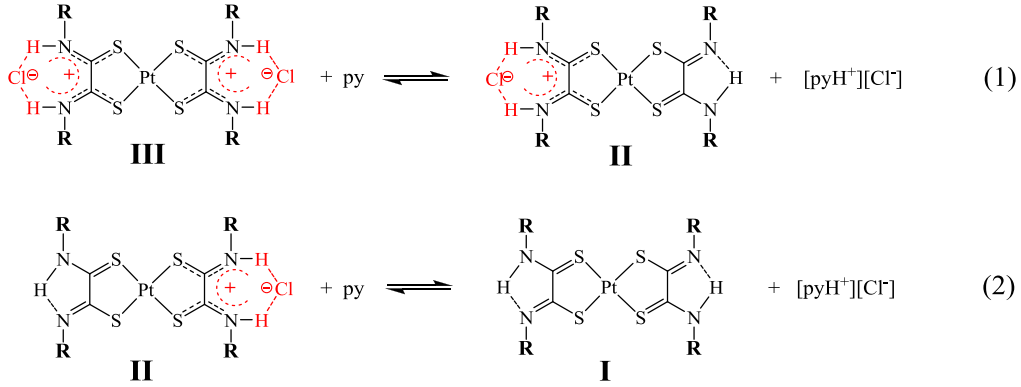

Scheme 10.1

By comparing the equilibrium constants for such reactions in the various compounds, we have been able to (i) obtain information on the relative stability of the TCIP, and, by taking advantage of the difference between the two equilibrium constants involving sequential titration of the two HCl moieties in each compound, (ii) gain knowledge on the electronic interaction between the two basic sites of the Pt(II) bis-dithiooxamide complexes, mediated by the metal center. The complexes exploited for studing equilibria (1) and (2) are those depicted in Figure 10.1

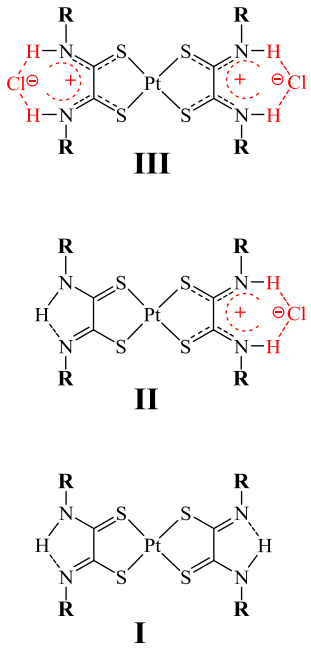

1_{III}, 1_{II} , 1_{I} : R = methyl

2_{III}, 2_{II} , 2_{I} : R = ethyl

3_{III}, 3_{II} , 3_{II} : R = *n*-propyl

4_{III}, 4_{II} , 4_{I} : R = isopropyl

5_{III}, 5_{II} ,5_{I} : R = *n*-butyl

6_{III}, 6_{II} , 6_{I} : R = cyclohexyl

7_{III}, 7_{II} , 7_{I} : R = benzyl

8_{III}, 8_{II} , 8_{I} : R = β-phenylethyl

9_{III}, 9_{II} , 9_{I} : R = allyl

Fig. 10.1

Complexex $\mathbf{1_{III}}$-$\mathbf{9_{III}}$ can be easily obtained in very high yields, using chloroform as solvent, according to the processes described in the Scheme 10.2.[8,9]

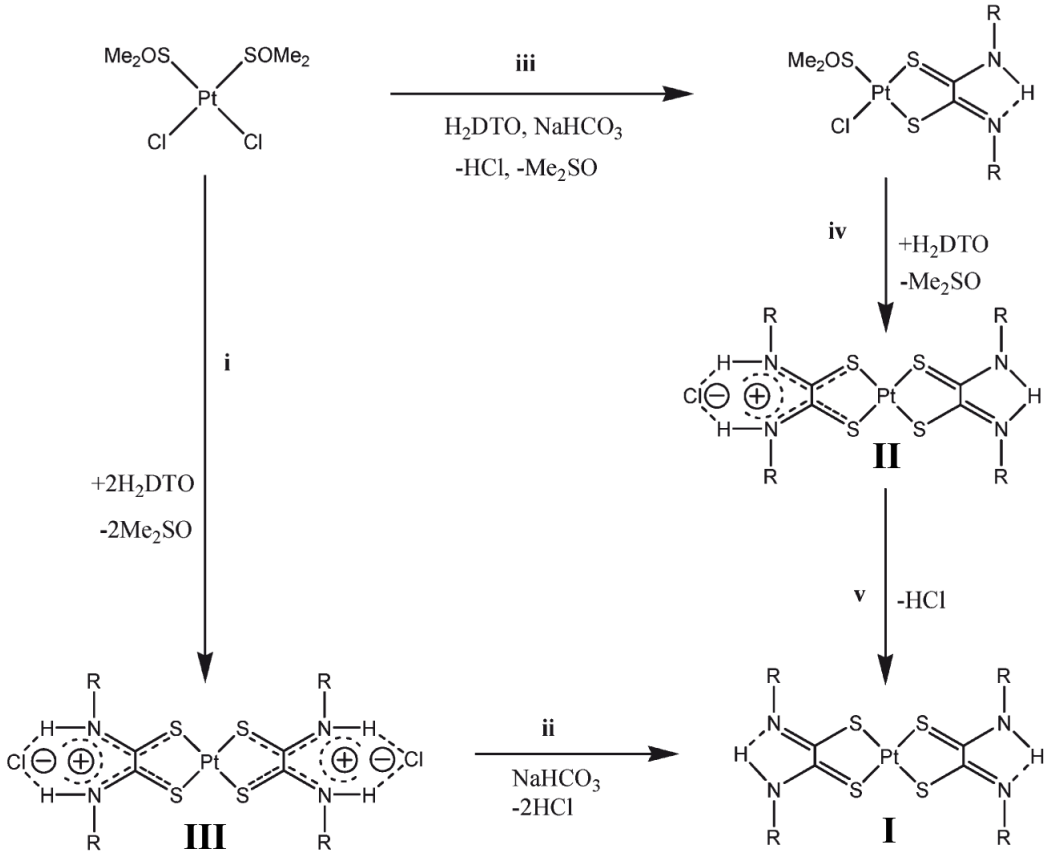

Scheme 10.2

Pyridine has been successfully used to study proton transfer.[9] Since proton transfer is the first requisite for the occurrence of the equilibria shown in eqs (1) and (2), we performed titration of such equilibria by using pyridine as the titration agent for the $[Pt(H_2\text{-R-DTO})_2][CL]_2$ complexes ($\mathbf{1_{III}}$-$\mathbf{9_{III}}$) in chloroform, by following the evolution of the process spectrophotometrically. A typical experiment is shown in Figure 10.2, reporting the changes of the absorption spectrum of $[Pt(H_2\text{-(isopropyl)}_2\text{-DTO})_2][CL]_2$ ($\mathbf{4_{III}}$) upon pyridine addition.

All the **III**-type complexes exhibit similar absorption spectrum changes and titration behavior, which corresponds to sequential HCl transfer from the Pt(II) complexes to pyridines (Fig. 10.2a) . This assignment is confirmed by comparison of the spectra obtained upon first and second titration steps of the

III-type compounds with those of the corresponding **II**-type and **I**-type compounds, independently prepared (Fig. 10.2b-c)

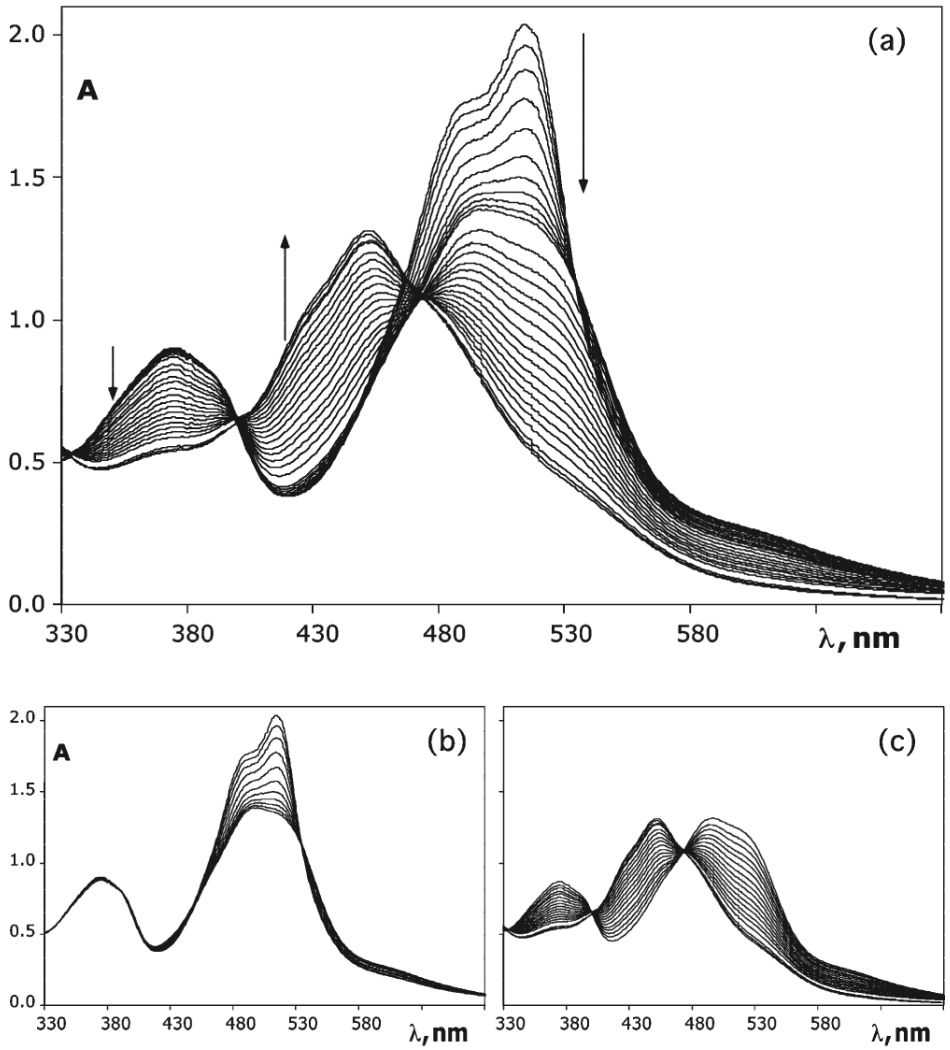

Fig. 10.2 - Changes of the absorption spectrum of $\mathbf{4_{III}}$ (1.39×10^{-4} M) upon successive pyridine addition in chloroform. Panel (a) shows the overall process, and panels (b) and (c) show the separate two successive processes. See text for details.

Figure 10.3 shows the titration curves connected with the experiment in Figure 10.2.

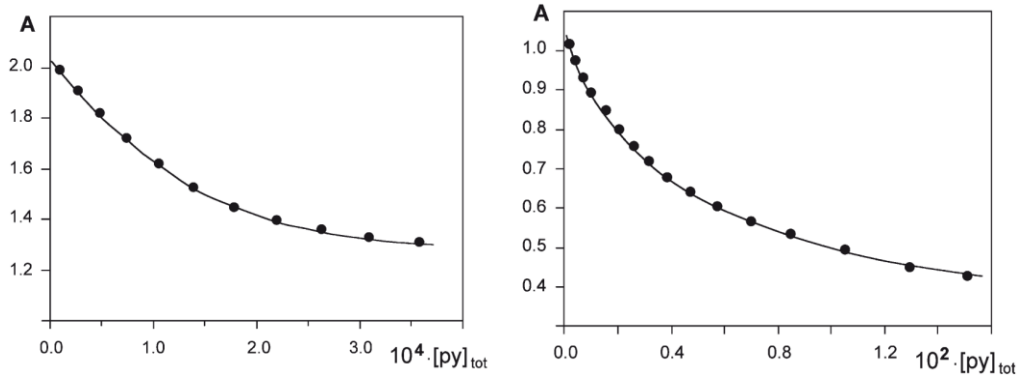

Fig. 10.3 - Titration curves relative to the experiments in Figure 10.2(b) (top) and Figure 10.2(c) (bottom). [complex] =1.39×10^{-4} M. Top: absorption values monitored at λ=513 nm; bottom: absorption values monitored at λ=534 nm. [py] stands for molar concentration of added pyridine.

The equilibrium constants Kc are collected in Table 10.1.

Table 10.1 - Equilibrium Constants and σ-Taft Values[a]

com-pound	R substi-tuent	Kc1	Kc2	Σσ*	pKc1	pKc2
1$_{III}$	methyl	4.1 (±0.4)	0.066 (±0.004)	−0.98	−0.613	1.180
2$_{III}$	ethyl	2.3 (±0.4)	0.039 (±0.003)	−0.88	−0.362	1.409
3$_{III}$	*n*-propyl	2.2 (±0.3)	0.077 (±0.05)	−0.86	−0.342	1.113
4$_{III}$	iso-propyl	1.7 (±0.2)	0.028 (±0.003)	−0.79	−0.230	1.796
5$_{III}$	cyclohexyl	2.6 (±0.3)	0.024 (±0.002)	−0.83	−0.415	1.620
6$_{III}$	*n*-butile	2.1 (±0.3)	0.062 (±0.004)	−0.85	−0.322	1.208
7$_{III}$	benzyl	7.2 (±0.5)	1.280 (±0.05)	−1.20	−0.857	−0.107
8$_{III}$	*β*-phenyl-ethyl	4.9 (±0.5)	0.250 (±0.05)	−1.06	−0.690	0.602
9$_{III}$	allyl	6.1 (±0.5)	1.40 (±0.05)	−1.11	−0.785	−0.146

[a] Data are in chloroform solution at 298 K. *Σ*σ* values are taken from ref 10b, and refer to the value derived from the amine species used to prepare the **III**-type compounds (see ref 11). The Kc2 values of the **III**-type compounds are identical, within experimental uncertainty, to the single Kc value obtained for the corresponding **II**-type compounds.

The different Kc constants (Kc1 and Kc2, related to equilibria in eqs (1) and (2), respectively) of the two titration equilibria for each compound indicate that significant electronic interaction takes place between the two sites involved in equilibrium reactions. The equilibrium in eq (2) has also been investigated by using the independently prepared and characterized [Pt(H-R_2-DTO)(H_2-R_2-DTO)][Cl] **II**-type species.

A very good linear correlation is found between the pKc values and the so-called σ-Taft value (Σσ*)[16,17] of the amine substituents of the DTO ligands (Fig. 10.4).

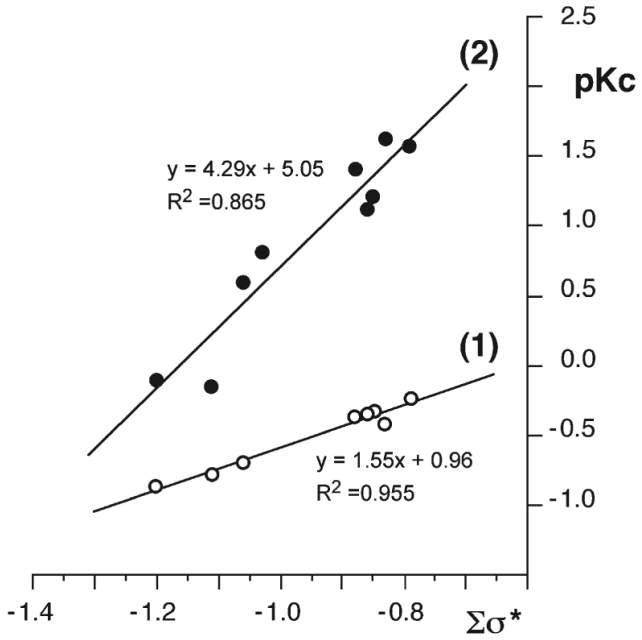

Fig. 10.4 - Plots of pKc vs Σσ* values given in Table 10.1; (**1**) and (**2**) refer to pKc1 and pKc2, respectively.

The σ-Taft value for an amine is a constant which expresses the polar effect of the substituents, taking also into account for steric effects on the nitrogen atom, so determining its basicity. In other words, the σ-Taft value reflects the effective electron density on the nitrogen atom. In our case, it expresses the ability of the DTO ligands to coordinate protons (and, via hydrogen bonding, the HCl "moiety"). It is therefore not unexpected that the linear correlation in Figure 10.4 is found, with less negative Σσ* values corresponding to higher effective electron density on the nitrogen and as a consequence to lower pKc values, that is, relatively more stable TCIPs. The second equilibrium constants Kc2 values

span a much larger range for the series of compounds under study, compared to the first equilibrium constants Kc1 values (Table 10.1, Figure 10.4), although the linear correlation between Kc2 and the Taft constant is still kept. Differences between Kc1 and Kc2 for each species are related to the electronic interaction between the two active sites. Apparently, the difference in Kc1 and Kc2 increases with the electronic density on the nitrogen of the amine substituents of the DTO, as indicated by the Taft constant. Such a behavior can be rationalized by considering that upon the first step of the titration (that is, once **II**-type species are formed from **III**-type compounds), the electron density on the already titrated nitrogen, which is not engaged in hydrogen bonding anymore, is now available to be partially transferred, via the Pt(II) complex molecular framework, to the other half of the molecule where the hydrogen bonding is still present, reinforcing the still existing TCIP. Such a reinforcement effect is therefore more effective (so leading to a larger splitting in the Kc values) for R substituents inducing more effective electron density on their nitrogens, according to the σ-Taft values. The situation is reminiscent of the oxidation splitting occurring in symmetric dinuclear metal complexes where the metal centers, which undergo oxidation, are connected by bridging ligands.[12]

In these latter species, oxidation of the first metal center causes a shift of electron density, via bridging ligand orbitals, making second metal oxidation more difficult. When the bridging ligand is kept constant, the metal-centered oxidation splitting depends on the effective electron density which is located on each metal center (in other words, from the energy level of the metal-centered occupied orbitals), on its turn a function of the nature of the peripheral ligands. For strongly electron acceptors peripheral ligands, leaving less electron density on the metal centers (i.e., strongly stabilizing the metal orbitals, which have to couple with the lowest unoccupied molecular orbital (LUMO) centered in the bridging ligands, in the super-exchange electron-transfer mechanism mediating the metal-metal coupling), oxidation splitting can not occur.[13,14] In this similitude, oxidation splitting is here represented by Kc1 and Kc2 splitting and the electronic factors, governed in bridged dinuclear metal complexes by peripheral ligands, are here determined by the σ-Taft values of the nitrogen substituents of the dithiooxamide ligands. As a matter of fact, Kc1 and Kc2 tend to become closer and closer with decreasing σ-Taft values, and can be predicted that for nitrogen substituents yielding σ-Taft values of about -1.45, a single titration process, corresponding to simultaneous transfer of the two HCl moieties of a $[Pt(H_2\text{-}R_2\text{-}DTO)_2][Cl]_2$ species to pyridines, can take place.

In conclusion the above date represent an approach for investigating the stability of TCIPs and demonstrates that the equilibrium constants in the formation of multiple TCIP systems can be significantly interconnected one another and governed by parameters which can be easily tuned, such as electron density on ion pairing sites.

10.2. acid-base reactions between hydrohalogenated ion-paired complexes and pyridines of different pKa: a study of thermodynamic parameters governing noncovalent interactions

With the aim to explore other factors affecting acid-base equilibria of tight ion pairs $[Pt(H_2R_2DTO)_2][Cl]_2$ and $[Pt(HR_2DTO)(H_2R_2DTO)][Cl]$ as well as of their neutral counterpart $[Pt(HR_2DTO)_2]$ the reaction in the Scheme 10.3 has been studied.

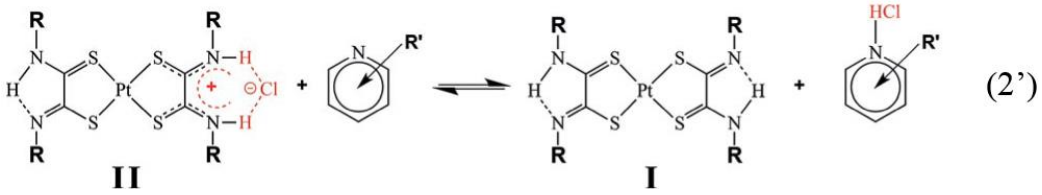

Scheme 10.3 - Acid‑base reaction between **II** and a series of substituted pyridines. For **IIa**: R = ethyl; R′ = 3-chloro, 5-bromo-2-methyl, 2-phenyl, H, 3- methyl, 4-methyl, 2-methyl, 3,5-dimethyl, 3,4-dimethyl, 2,4-dimethyl, 2,6-dimethyl For **IIb**: R = benzyl; R′ = 3-chloro, 5-bromo-2-methyl, H, 2,6-dimethyl

The reactions:- $[Pt(H_2R_2DTO)_2][Cl]_2$ + Substituted pyridine $\rightleftharpoons$ $[Pt(HR_2DTO)(H_2R_2DTO)][Cl]$ + Substituted pyridinium chloride - has not been taken into consideration since they are shifted too much towards the products and thus provide equilibrium constant values with very high experimental errors.

The experimental conditions of reaction (2′) allow us to explore a number of pyridines covering a wide range of basicity. Substituents R, ethyl and benzyl, in process (2′) have been chosen to evaluate the effect of the basicity of the N-H···N moiety of complexes **II** on the thermodynamic parameters. Results obtained for process (2′) are reported in Tables 10.2 and 10.3.

Table 10.2 - Equilibrium constant values for reactions (2′) in which **R** = ethyl (compounds **IIa**), determined at various temperatures and relative thermodynamic parameters.

Pyridine	**pKa**	**Kc**					***ΔH°***	***ΔG°***	***ΔS°***
		10°C	15°C	20°C	25°C	30°C	kJ/mol	kJ/mol	J/(K mol)
3-chloro	2.90	2.43×10^{-4}	2.41×10^{-4}	2.65×10^{-4}	2.71×10^{-4}	2.33×10^{-4}	0.56±3.1	20.4±0.3	-66.4±1.4
5-Bromo-2-methyl	3.86	1.18×10^{-3}	1.08×10^{-3}	1.19×10^{-3}	9.80×10^{-4}	1.15×10^{-3}	-2.17±4.0	17.2±0.4	-64.9±3.5
2-phenyl	5.27	0.0163	0.0161	0.0171	0.0166	0.0168	1.31±1.0	10.1±0.4	-29.7±3.5
H	5.17	0.0413	0.0410	0.0395	0.0408	0.0391	-1.6±0.9	7.9±0.1	-32.0±3.3
3-methyl	5.63	0.165	0.161	0.163	0.151	0.154	-2.9±1.0	4.6±0.1	-25.4±3.7
4-methyl	6.05	0.336	0.331	0.338	0.345	0.326	-0.3 ± 1.1	2.6±0.1	-9.7±0.6
2-methyl	5.96	0.583	0.588	0.581	0.562	0.564	-1.6±0.5	1.4±0.1	-10.1±1.9
3,5-dimethyl	6.15	0.748	0.762	0.734	0.702	0.732	-1.8±1.2	0.88±0.1	-8.9±4.1
3,4-dimethyl	6.56	2.45	2.37	2.52	2.29	2.41	-0.95±1.2	-2.5±0.2	+3.7±4.0
2,4-dimethyl	6.79	6.31	6.41	6.39	6.07	6.11	-1.7±0.9	-4.5±0.2	+9.4±3.0
2,6-dimethyl	6.65	10.43	10.68	10.12	10.83	10.31	0.12±1.4	-5.9±0.2	+19.3±4.7

Table 10.3 - Equilibrium constant values for reactions (2′) in which **R** = benzyl (compounds **IIb**), determined at various temperatures and relative thermodynamic parameters.

Pyridine	**pKa**	**Kc**				***ΔH°***	***ΔG°***	***ΔS°***
		15°C	20°C	25°C	30°C	kJ/mol	kJ/mol	J/(K mol)
3-chloro	2.90	0.0231	0.0222	0.0177	0.0186	-9.4±2.7	9.9±0.2	-65.0±9.1
H	5.17	2.83	2.61	2.16	2.22	-9.6±2	1.9±0.2	-38.6±6.7
3-methyl	5.63	10.10	9.35	9.18	9.15	-4.6±2	-5.5±0.3	3.0±5.5
2,6-dimethyl	6.65	564	588	498	496	-6.0±2	-14.8±0.2	29.6±7.4

The *K*c values in Table 10.3 seem to depend very little on temperature. Furthermore, p*K*c values are linearly dependent on p*K*a values of pyridines, once the temperature is held constant. As a consequence, the plots of p*K*c vs. p*K*a obtained at the explored temperatures provide almost coinciding straight lines whose experimental points appear grouped with a low scattering within each group (Fig. 10.5).

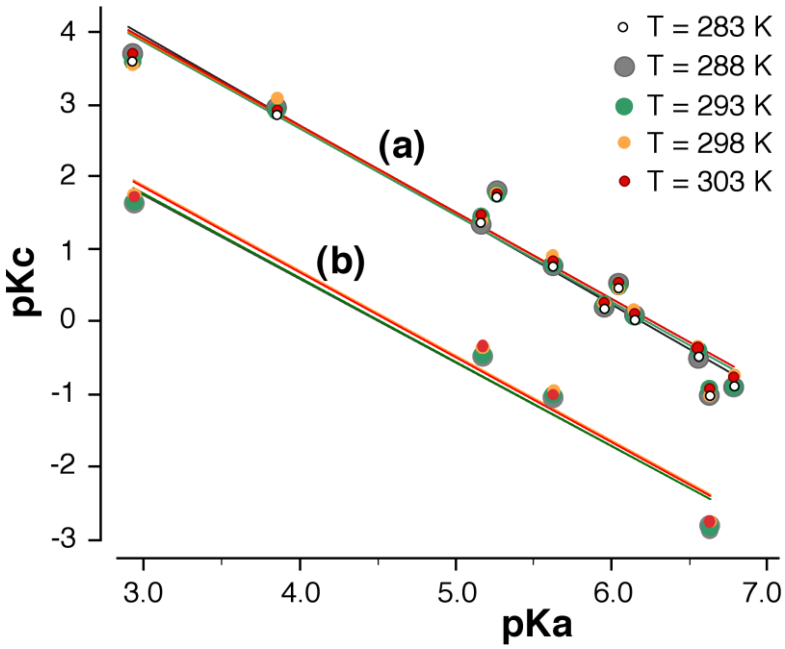

Fig. 10.5 - Plots of p*K*c vs. p*K*a for the pyridines in reactions (2′). The figure is the result of superimposing five R = ethyl (**a**) or four R = benzyl (**b**) different straight lines; each line in the groups (**a**, **b**) refers to a given temperature.

All the data for each single pyridine may be analyzed by means of the van't Hoff equation. According to this analysis, the contribution of $\Delta H°$ to the equilibrium constant for each pyridine is small or negligible; this could mean that the chlorohydrated pyridines have comparable enthalpy values with respect to the type **II** complexes. As a consequence, each p*K*c value for process (2′) depends largely on the entropy contribution. This also means that the value of the entropy contribution mainly depends on the basicity of the pyridine, in agreement with the trend of the straight lines in Figure 10.5.

In particular, the trends in Figure 10.5**a** and Figure 10.5**b**, that is, the grouped straight lines that show the dependence of the equilibrium constant for reactions (2′) at various temperatures, indicates that the sigma-donor power of a given R group (benzyl or ethyl), affects only the basicity of type **II** complexes; it means that a lower sigma-donor effect (smaller σ-taft value) produces less basic type **II** complexes and therefore a larger equilibrium constant.

It seems quite unusual that HCl interacts with about the same strength with both pyridine nitrogen and N···H⁻N moieties of type **III** species; nevertheless, this is proven by indisputable results. It is reasonable to think that the interaction between the species that appear in reaction (2′) and the solvent plays an essential role in determining the observed thermodynamic parameters.

Actually, the solvent interacts with type **II** and **III** ion pairs in which the coordinated dithiooxamide groups form δ / λ chelate rings. However, in solution, at room temperature, geminal protons of alkyl substituents in *S,S* Pt-chelated H_2R_2DTO groups do not perceive the asymmetry produced by the two tilted NCS frames and appear in the proton spectra as an A_2Xn spin system (n = 0, 2, 3);[16] this means that some fluxional motion in H_2R_2DTO groups coordinated to Pt(II) makes the Pt($S_2C_2N_2H_2Cl$ κ-*S,S* Pt) plane symmetrical.

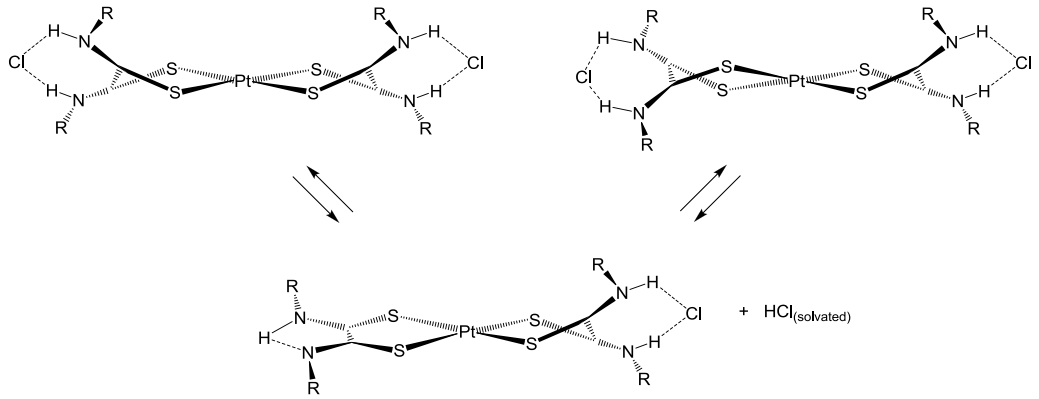

Scheme 10.4 - Proposed mechanism for the δ⇌λ conformational change of the PtSCCS plane. The same process rules δ⇌λ conformational change on the other DTO chelate ring.

Variable-temperature experiments[17,18] allowed to infer that fluxional motion happens according the mechanism represented in Scheme 10.4. In particular, in the monohydrohalogenated type **II** species the alkyl groups experience the same chemical environment, which indicates that HCl very rapidly moves from one to the other basic N⁻H···N sites of the molecule HCl cannot jump between two platinum-containing molecules, because of the distance between them; as a consequence, the transfer of hydrogen chloride between the basic sites of two Pt-containing molecules requires the mediation of a number of chloroform molecules. The fast and reversible formation of a tight ion pair, which is the essence of the δ⇌λ conformational change depicted in Scheme 10.4, could

also be represented by the following reaction, in which the role of the solvent is outlined in an explicit way:

$$[Pt(HR_2DTO)_2] + HCl(solvated) \rightleftharpoons [Pt(HR_2DTO)(H_2R_2DTO)][Cl] + solvent \quad (3)$$

I (δ,λ)**II**

Obviously, when **II** is subjected to reaction with a substituted pyridine, process (3') must also be taken into account. Reasonably, the observed entropy changes in process (2′) could depend on solvent released by a balance of processes (3) and (3'). Thus, a more basic pyridine, driving the balance of processes (3) and (3') towards a greater amount of solvent released, could produce a larger entropy content.

$$\text{substituted pyridine} + HCl\text{-(solvated)} \rightleftharpoons \text{substituted pyridine}\cdot HCl + solvent \quad (3')$$

The formation of a tight ion pair within a platinum complex is a reversible process, that is, a tight ion pair of the type **III** may be sequentially dehydrohalogenated to give complexes of the type **II** [reactions (1) and (2)]. In turn, type **I** complexes can sequentially assume HCl to restore ion pair **III** [reactions (4) and (5)]. (Scheme 10.5)

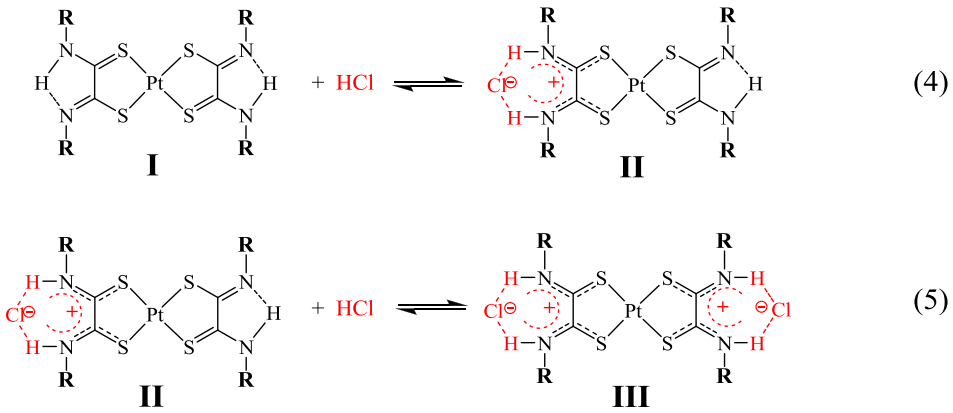

(4)

(5)

Scheme 10.5

The reaction (4) has not explored in detail, because this process is extensively shifted towards the products, to such an extent that the corresponding equilibrium constant values have very high experimental errors. On the contrary, the process (5) provided reliable values (Table 4)

Table 10.4 - Equilibrium constant values for reaction (5) determined at various temperatures and thermodynamic parameters.

	Kc						$\Delta H°$	$\Delta G°$	$\Delta S°$
	10°C	15°C	20°C	25°C	27°C	30°C	kJ/mol	kJ/mol	J/(K mol)
R = Ethyl;	1.47×10^{6}	6.40×10^{5}	2.80×10^{5}	5.82×10^{4}	2.88×10^{4}		-146.3±9.7	-28.1±1.0	-398±32
R = Benzyl		1.82×10^{4}	1.15×10^{4}	6.86×10^{3}		4.56×10^{3}	-67.7±2.0	-21.9±2.0	-154±7

Reaction (5) is an association process of the type A + B ⇌ A-B. The bonding in A-B may be viewed as a property of the interface between A and B, as this is a weak interaction. In similar cases it has been argued[21] that the overall loss of translational and rotational entropy that occurs when the association takes place is related to the exothermicity of the reaction. In some association processes,[23,24] enthalpy-entropy relations have been found that imply a motion restriction limit of $T\Delta S$ ≈50 to 60 kJ mol^{-1} for the immobilization of molecules up to 300 g mol^{-1}; this entropy loss has been generally found as a limiting value even when the interaction between the associating entities is weak.[19-22]

As for the results for process (5), it is puzzling that an enthalpy lowering of 146 kJ mol^{-1} (R = ethyl) and 67.7 kJ mol^{-1} (R = benzyl) may be related to a weak association between two neutral species; these values, in fact, are typical of a strong interaction. In the same processes, the entropy loss (398 J K^{-1} mol^{-1}, R = ethyl; 154 J K^{-1} mol^{-1}, R = benzyl) seems too large to be due to the restriction of motion upon association. However, it is known that, in association processes, the interactions of the reactants and products with the solvent can produce unexpected effects.[23]

Although processes (2′) and (5) occur in a noncoordinating, low-polarity solvent ($CHCl_3$), this solvent plays an essential role in such acid-base reactions. One wants to mean that HCl linked to [Pt(HR_2DTO)$_2$] is in a rapid exchange between chloroform and the N-H···N basic sites of dithiooxamide complexes (Scheme 10.4). The nature of the interaction between HCl and $CHCl_3$ may be represented as shown in Figure 10.6. HBD properties of CH groups of haloforms have been widely explored.[24]

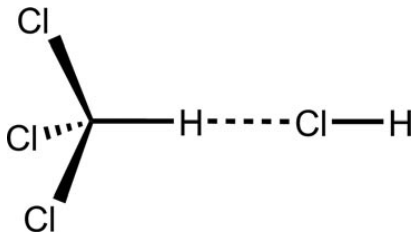

Fig. 10.6 - Suggested interaction between HCl and $CHCl_3$.

In other words, ion pairs **II** can lose HCl since the hydrogen atom is weakly bonded to the amidic nitrogen and strongly linked to the chloride ion; therefore, the frame NHCl should be represented with N···H as a weak bond, and with H-Cl as a strong bond, that is, N···H-Cl.[11] With this in view, the N···H bond energy should be less than 50 kJ mol^{-1},[25] which is in agreement with the present results once the effect of the solvent is taken into consideration (vide infra). Such a bond energy (50 kJ mol^{-1} or less) justifies the mobility of HCl, which, after leaving the N···H-N basic site, organizes the solvent as depicted in Figure 10.6. This justifies the unusual values of the thermodynamic parameters (Table 10.4) experimentally found for reaction (5).

A binding event, A + B $\rightleftharpoons$ A-B, can be represented schematically as a thermochemical cycle (Scheme 10.6). In the event of binding, a fraction of the solutes A (i.e., type **II** complexes), or B (i.e., HCl), or both (depending on the solvent used), does not interact with the solvent any more, so that the solvent released is returned to the bulk. The thermochemical cycle in Scheme 10.6 can be viewed as a useful guide for distinguishing the contribution of solute-solute interactions from solvation effects in binding phenomena.

A similar thermochemical cycle showing separation of the measured enthalpy of binding into an intrinsic (solute-solute) enthalpy and enthalpies of solution for the bound and unbound systems has already been proposed for protein-carbohydrate association in water.[26]

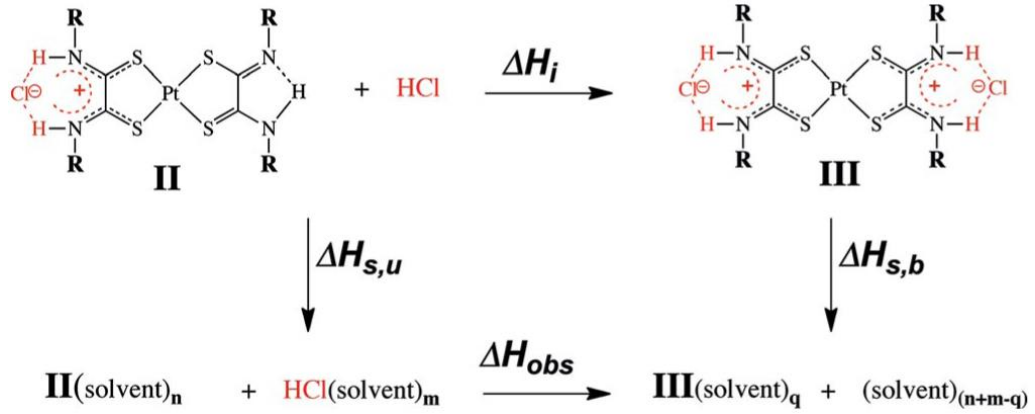

Scheme 10.6 - Thermochemical cycle showing separation of the measured enthalpy of binding (Δ*H*obs) into an intrinsic (solute–solute) enthalpy (Δ*Hi*) and enthalpies of solvation for the bound (Δ*H*s,b) and unbound (Δ*H*s,u) systems in the acid‑base reaction between complexes of type **II** and HCl.

According to Scheme 10.6, the enthalpy value of process (5) does not seem so unusual; in fact, the thermochemical cycle is supposed to reduce the intrinsic enthalpy of the association process to a minor portion (15‑30 %) of the observed value, once that the enthalpy of solvation is taken into account.[24] With this in view, the intrinsic enthalpy value for the association process (5) could range between more realistic values of 20‑42 kJ mol^{-1}.

One can argue that the measured enthalpy value for association reactions (5) seems adequate to justify the formation of type **II** ion pairs, because these species are very stable in chloroform solution. However, the stability of **II** and **III** would conflict with the intrinsic weakness of the N···H‑Cl interaction, which, in its turn, ensures the reversible formation of such species, as also demonstrated by the role of compounds **I**‑**III** as sensors and carriers.[18,27] The standard entropy change in reaction (5) also warrants a deeper discussion: in fact, according to the two terms of the free energy expression $\Delta G = \Delta H - T \Delta S$, in the case of an association process, as ΔH becomes more negative (stronger bonding), ΔS tends to decrease as a result of the tightening up of the system. As ΔH becomes less negative (weaker bonding), ΔS should increase as the system becomes more disordered. On the contrary, in reaction (5) the observed large lowering of enthalpy (Table 10.3) is matched by an exceedingly large lowering of the entropy term.

It has been already discussed that the rapid exchange of HCl between type **II** ion pairs and chloroform engages a significant quantity of solvent; consequently, an important decrease in the entropy of the system can occur in these kinds of processes. Thus, the entropy contribution of the solvent[28] needs to be taken into consideration in the enthalpy‑entropy balance in association process (5) in addition to the entropy lowering due to the tightening up of HCl and the type **II** species. It is noteworthy that the reported thermodynamic parameters give account of the capability of type II compounds to behave as efficient HCl transporters in chloroform solution.[18]

10.3. Pt(II)-dithiooxamide based anion receptors as self-indicating titrants: determination of amines

It has been observed that even a Broensted weak base, such as a solvent containing donor atoms (Me_2SO, ROH, acetonitrile and so on) is able to remove HCl from either II and IIa ion pairs; thus, in a low polar non coordinating solvent and in presence of a Broensted base :B, the acid-base equilibria show in the Scheme 10.7 take place.

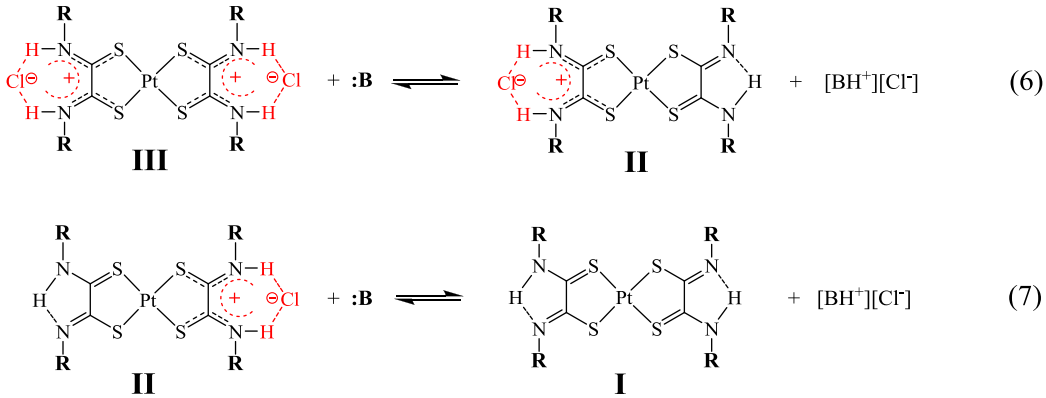

Scheme 10.7 - Equilibrium processes between $[Pt(H_2R_2DTO)_2]^{2+}[Cl^-]_2$ (**II**), $[(HR_2DTO)Pt(H_2R_2DTO)]^+[Cl^-]$ (**II**) and Broested bases (**:B**)

Equilibria 6 and 7 have been already studied, either changing the electron disposal on nitrogen chelating systems of **I**, **II** and **III**, or changing the base strength of :B (:B = pyridines ranging in a wide pKa range).

The Figure 10.7 shows the spectral changes referable to the process 7 when known amounts of amine are added to a known quantity of the complex $[(HR_2DTO)Pt(H_2R_2DTO)]^+[Cl^-]$; in the course of the titration the total concentration of Pt remains constant.

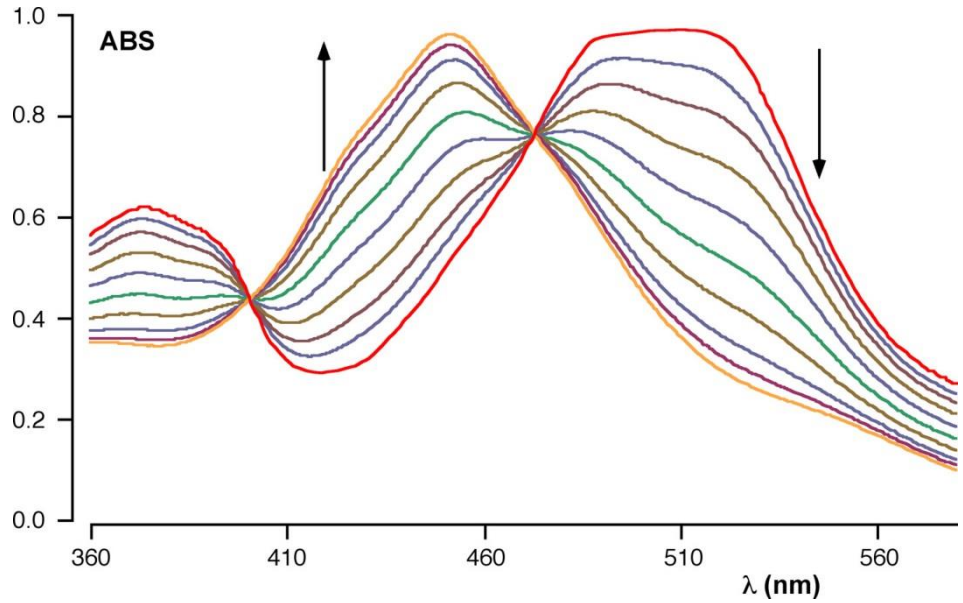

Fig. 10.7 - Spectral changes in the course of the process $[(HR_2DTO)Pt(H_2R_2DTO)]^+[Cl^-] + :B \rightleftharpoons [Pt(HR_2DTO)_2] + [BH^+][Cl^-]$ (R = Benzyl; :B = 1-hexylamine; solvent = chloroform); starting spectrum = $[(HR_2DTO)Pt(H_2R_2DTO)]^+[Cl^-]$ 1×10^{-4} mol dm^{-3}

By selecting the proper wavelength it is possible to obtain the equilibrium constant value for the process under examination

We found that the values of the equilibrium constant of processes (6) and (7) became greater i) when the basicity of B increases, ii) as well as when the acidity of ion pairs increases.

The analysis of the various equilibrium processes provides typical curves whose shape depends on the value of the relative equilibrium constant (Fig. 10.8).

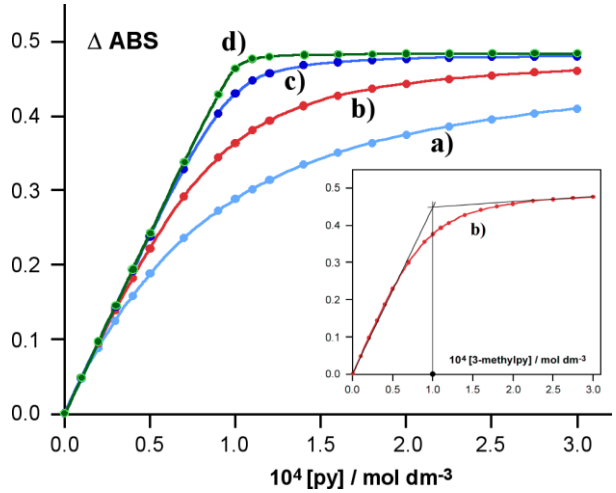

Fig. 10.8 - Variation of the absorbance during the process: $[(HR_2DTO)Pt(H_2R_2DTO)]^+[Cl^-]$ + :B $\rightleftharpoons$ $[Pt(HR_2DTO)_2]$ + $[BH^+][Cl^-]$ (R = Benzyl; solvent = chloroform; :B = (**a**) pyridine (Kc = 2.16); (**b**) 3-methylpyridine (Kc=9.18); (**c**) 3,6-ludidine (Kc = 63); (**d**) 1-hexylamine ($Kc>10^6$)).

In each titration curve absorbance values have been measured at 447 nm. In all cases the total concentration of Platinum was 1×10^{-4} mol dm^{-3}.

Looking at the figure 10.8 one can see that when the value of the equilibrium constant is big enough, it is quite easy to determine the equivalence points of the processes.

In other words, by using a complex $[(HR_2DTO)Pt(H_2R_2DTO)]^+[Cl^-]$ (R = Alkyl) it becomes possible determine the concentration of amines in chloroform. This can be done by adding to a solution of an amine of unknown concentration known volumes of the suitable $[(HR_2DTO)Pt(H_2R_2DTO)]^+[Cl^-]$. The spectral changes shown in figure 10.9 are obtained.

The first spectrum in the figure 10.9 is coincident with the baseline in that the amine solution is not light-absorbing in the explored spectral range.

As $[(HR_2DTO)Pt(H_2R_2DTO)]^+[Cl^-]$ (**II**) is added a spectrum appears which features almost all $[Pt(HR_2DTO)_2]$ (**III**). When **II** added is equivalent to the amine amount, the spectrum is mainly produced by **III**. Further addition of **II** produces spectra which mainly feature $[(HR_2DTO)Pt(H_2R_2DTO)]^+[Cl^-]$.

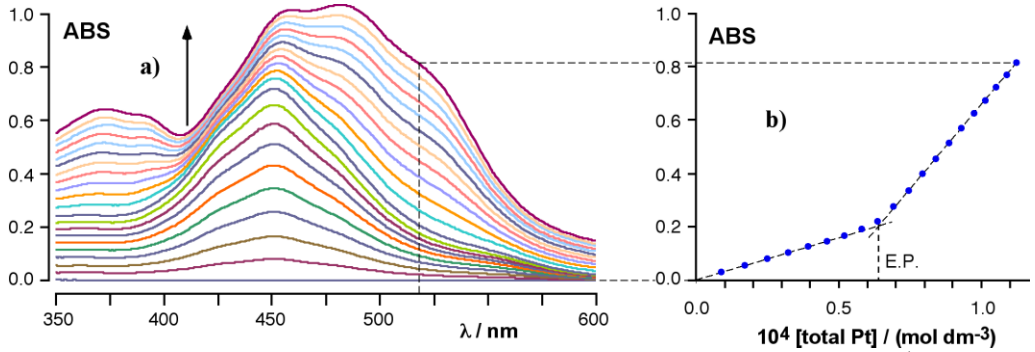

Fig. 10.9 - **a**) Spectral changes by addition of $[(HR_2DTO)Pt(H_2R_2DTO)]^+[Cl^-]$ (R = benzyl) to 1-hexylamine; **b**) detection of the equivalence point; absorbance values have been measured at 520 nm. The measured absorbance values lies very close to the straight lines of the graph **b** also in the proximity of the equivalence point.

By plotting the optical densities measured at a proper wavelength vs. concentration of total complex added, a plot as in Fig 10.9b is obtained so that the equivalence point is detectable without any ambiguity

When an amine whose pKa is greater than 7.5 is implied, the equivalent point of the relative acid-base process is detectable with confidence (Fig. 10.10). The titrations of amines whose pKa ranges between 5.0 and 7.5 require a greater care in handling data because the measured absorbance values in the proximity of the equivalence point deviates from the straight lines of the graph (Fig. 10.11).

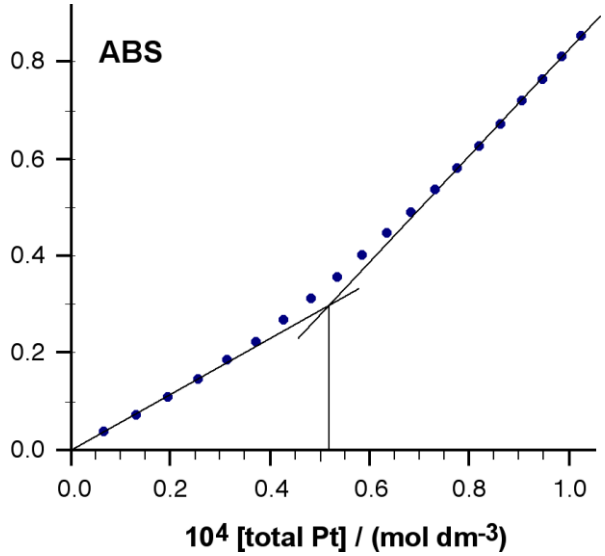

Fig. 10.11 – Titration curve obtained by addiction $[(HR_2DTO)Pt(H_2R_2DTO)]^+[Cl^-]$ (R = benzyl) to a pyridine (pKa = 5.17) solution. Absorbance values have been measured at 520 nm.

As a first approach it has been tested the reliability of the method proposed here for the spectrophotometric determination of the amine in chloroform by determining in the bulk the following fatty amines: 1-aminobutane, 1-aminohexane, 1-aminododecane, diethylamine, Triethylamine, ethylenediamine.

The above amines have been chosen because they vary in both the alkyl chain length and the substituents on the nitrogen. Finally, ethylenediamine was tested as a model of the bifunctionalised biogenic amines putrescine and cadaverine.

Starting from weighted amount of amines, stock of solutions 1×10^{-3} mol dm^{-3} in chloroform have been obtained. At least 100 μL of each of them were pipetted in a standard spectrophotometric cuvette (1 cm optical path) and then diluted to 2 mL. The complexes $[(HR_2DTO)Pt(H_2R_2DTO)]^+[Cl^-]$ (R = ethyl, **1**; R = benzyl, **2**), used as titrants, have been prepared according to ref. [16]. The mother solution of **1** and **2** have been prepared by using weighted amounts of complexes; titrant solutions have been prepared by proper dilution of mother solutions (the typical platinum concentration ranged from 4×10^{-4} to 8×10^{-4} mol dm^{-3}). In any case, the concentration of the titrant solutions was checked by their molar absorptivity at 513, which is 11500 mol $^{-1}$ dm^3 cm^{-1}.

Each amine underwent five independent determinations. The result are collected in table 10.5.

Table 10.5 - Results of amine determination

Amine	**Found (%)**
1-amino-butane	99.5±0.31
1-amino-hexane	100.1±0.2
1-amino-dodecane	98.8±0.4
diethylamine	100.3±0.1
Triethylamine	99.7±0.5
ethylenediamine	99.6±0.4

As one can see from date in Table 10.5 the recovery of the amines has been in all cases very good.

As already pointed out the method here proposed for the spectrophotometric determination of amine is not based on little procedural changes with respect to the official method: on the contrary it is basically different both in its theoretical bases and in experimental procedures. Nonetheless, the results provided by method here proposed are good, reproducible, easy to perform and finally of high sensitivity.

As a further step of this investigation, we tested the proposed spectrophotometric method in the determination of 1,4-benzodiazepines in tablets as a possible test of quality control for these drugs has been tested. Quality control is an essential operation of the pharmaceutical industry, which concerns also analyses of finished dosage forms to determine compliance with label claims for active ingredients.

Benzodiazepines are the type of psychotropic drug, in the sense that they concern the mind and can amend frame of mind.

The widespread use of this class of drugs has occasionally raised concern about recreational benzodiazepine abuse and has led to the erroneous impression that benzodiazepines have a relatively high abuse liability among recreational drug users. The abuse or misuse of benzodiazepines is internationally widespread which means that any forensic laboratory may encounter a range of these compounds. Therefore, development of rapid, easy to perform, sensitive and reproducible spectrophotometric methods for their preliminary screening may relieve the burden of criminology laboratories working with more sophisticated, but more expensive and laborious HPLC/MS instruments

In general, benzodiazepines encountered in the illicit market are diverted from legitimated sources. Benzodiazepine derivatives are prescribed in large quantities globally and are potentially new emerging environmental contaminants.

We have purchased from lo local market the dosage forms of the following benzodiazepines: diazepam,**1** (valium, Roche, 5 mg tablets), bromazepam, **2** (lexotan, Roche, 6 mg tablets), Triazolam, **3** (halcion, Pfizer, 0.25 mg tablets), flurazepam, **4** (flunox, 30 mg, Teofarma), chlordiazepoxide, **5** (Librium, 10 mg, MEDA) (Fig. 10.11).

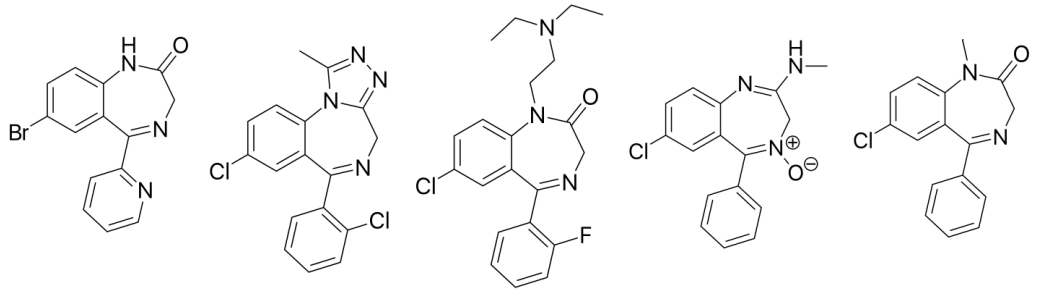

Fig. 10.11

We have chosen the above five benzodiazepine in the expectation that their structural differences could cause important changes in their basicity.

In particular, Diazepam and Bromazepam are characterized by a classical benzodiazepine structure; in addition to this, flurazepam is characterized by an alkylamine substituent on N1, Triazolam by 1,2,4 triazole group and chlordiazepoxide by amidine group.

As a preliminary experiment, samples of tablets of each investigated benzodiazepine have been finely powdered. A portion of each powdered sample has been suspended in one milliliter of $CDCl_3$ under magnetic stirring. Proton spectra of resulting solution showed that only pure benzodiazepines or bzd*HCl have been extracted. Only triazolam showed low quantity of other species whose signals were different from those attributable to the benzodiazepine molecule, in particular in the methylene region. This probably is due to some excipient contained in the tablets (Dihexyl sodium sulfosuccinate, food colorant E132 "indigo carmine"), which however contain groups not basic enough to interfere in the titration.

Looking at the structure formula of these compounds one can exclude that N1 in the diazepine ring can be significantly basic, either when is part of an amidic system (diazepam and bromazepam) or of a 1,2,4-triazolic ring. The lone pair of other nitrogen in the ring, N4, is responsible for the basicity of a classical benzodiazepine ring and then is scarcely available. Actually, the shape of the titration curve of **1**, **2** and **3** (Fig. 10.12) indicates that the basicity of these systems is lower than pyridine (pKa = 5.13).

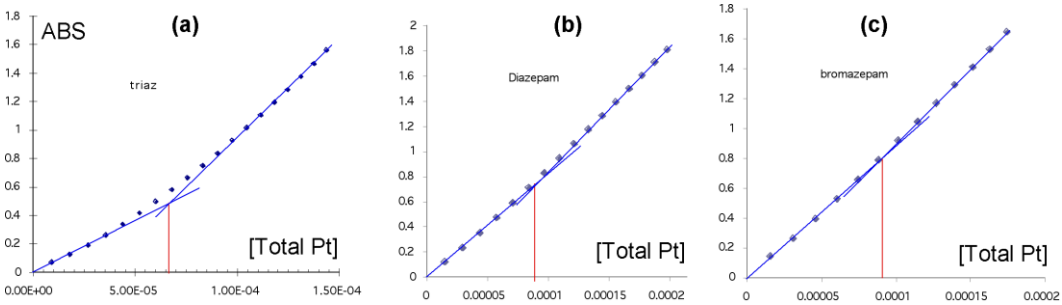

Fig. 10.12 - Titration plot for triazolam (**a**), diazepam (**b**) and bromazepam (**c**)

In an attempt to provide a reliable estimation of the above benzodiazepines pKa, we measured the equilibrium constants for the processes

bzd + $[(HR_2DTO)Pt(H_2R_2DTO)]^+[Cl^-]$ $\rightleftharpoons$ bzd*HCl + $[Pt(HR_2DTO)_2]$; (R = benzyl, bzd = Bromazepam, Diazepam)

The determined pKc are related to the pKa of the Benzodiazepines under examination according to a suitable free energy relationship described in a previous paper (rif [28]). The found pKc values support that Triazolam (pKc=0.04) Bromazepam (pKc=0.31) and Diazepam (pKc=0.98) are less basic than pyridine (pKc=-0.33) .

Flurazepam bears on N1 nitrogen a 2-(diethylamino)ethyl group as a substituent group which is basic like a generic tertiary alkylamine. Flurazepam is marketed as commercial tablets containing amine-hydrochloride. For this reason, after extraction from tablets, the benzodiadepine chloridrate need to be dehydroalogenated before titration. Then flurazepam as a free base has been determined with high accuracy and sensitivity (Fig. 10.13).

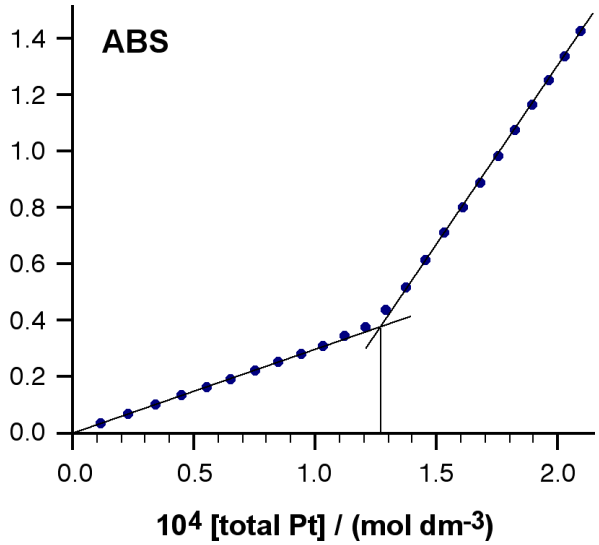

Fig. 10.13 - Titration plot for flurazepam.

Also Chlordiazepoxide has been purchased by us as a hydrochloride. However we have not been able to dehydrhoalogenate it. This means that Chlordiazepoxide is a very strong base. In fact 2-methylamino as substituent of C2 carbon of benzodiazepine ring makes with N1 atom a amidine group which is known to be a superbase for organic synthesis. (Superbases for Organic Synthesis: Guanidines, Amidines, Phosphazenes and Related Organocatalysts, pag. 20, TSUTOMU ISHIKAWA Ed. 2009 John Wiley & Sons)

A number of tablets of each pharmaceutical preparation, corresponding to an amount of active principle ranging from 5 to 30 mg was pulverized. Then each pulverized pharmaceutical preparation was extracted with four 5 mL portion of

chloroform which were transferred into a 25 mL volumetric flask using chloroform to adjust the final volume. Results are quite good: about the 95% of active principle is recovered by the analytical method here proposed. Anyway, for the heterocyclic bases the method here proposed require further refinement

Obviously, the spectrophotomeric methods for the determination of amines here proposed may be extended to the determination of biogenic amines in their natural matrices (blood, urine, tissues and so on); it is presumable that a more basic method of determination will allow many insights in the research fields in which biogenic amines are important matter of study.

10.4. Pt(II)-dithiooxamide based anion receptors as self-indicating titrants: determination acids in chloroform.

The equilibrium constants of the processes (4) and (5) in the Scheme 10.5 have been determined by exploiting chloroform solutions of HCl whose concentration has been obtained from a mother solution titrated according to standard methods.[28] That is chloroform solutions of hydrogen chloride were prepared by dripping HCl (38 %) in H_2SO_4 (98 %). The liberated HCl was then bubbled into sulfuric acid to remove any trace of water vapor, and then the dry gas was absorbed into anhydrous chloroform. The resulting hydrogen chloride solution (10 cm^3) was shaken vigorously with distilled water (10 cm^3) into a 50 cm^3 separating funnel. After separation of the layers, the aqueous phase was transferred into an Erlenmeyer flask, and the amount of HCl was determined by using sodium hydroxide solution (0.1 M). The hydrogen chloride solutions in chloroform were titrated before starting each set of experiments.

This procedure is time consuming, quite tedious and must be carefully performed; in particular a micro determination of HCl in chloroform is not reliable.

Actually, chloroform solutions of complex dehydrohalogenated type **I** prepared by weighting the dry complex even in small quantities (about three milligrams weighted with a standard analytical balance), behave as mother solution suitable to determinate low concentration of HCl in small volumes of chloroform solution.

Obviously, this is possible in that the equilibrium constants of process 6 and 7 in the Scheme 10.5 are very high.

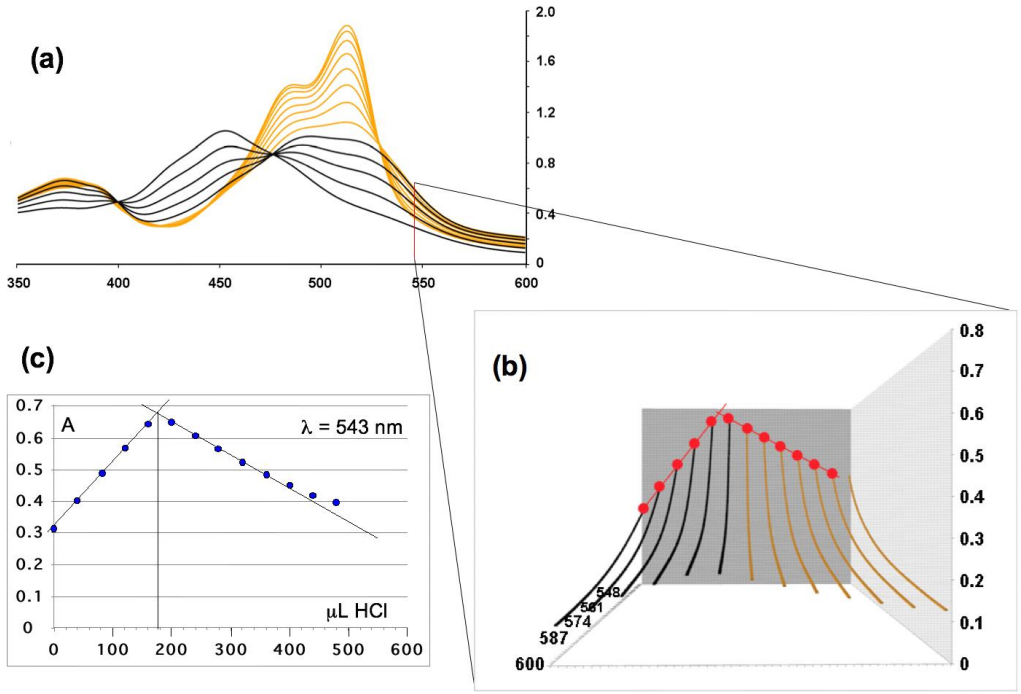

Fig. 10.14 - (**a**) Spectral changes of processes process 6 and 7 in the Scheme 10.5 in the interval 350-600 nm. (**b**) Sequence of the spectra in (a) taken in a narrower spectral range (543-600 nm). (**c**) Absorbance changes at 543 nm (the titration).

Figure 10.14 gives a synoptic view of the titration process and indicates the accuracy of the method, after having indicated the: i) the concentration of **I** (1×10^{-4} M); ii) the volume of solution titrated (2 mL); iii) the equivalent volume of the titrant. The concentration of the complex is kept constant during the course of the titration.

As for other acid dissolved in chloroform they could be titrated by compound type **I** if the equilibrium constant of their reaction with **I** e **II** were high enough to allow the detection of the equivalence point with precision.

Actually, the reaction with some acid of various strength with **I** species have been performed. The result are reported in the table 10.6

Table 10.6 - pKc of the reaction **I** + HA ⇌ **II** vs. pKa of HA

Acid	pKa	pKc
Picric acid	0.3	-4.49
Tricloroacetic acid	0.77	-4.26
Dichloroacetic acid	1.25	-2.60
2-nitrobenzoic acid	2.16	-1.45
2-chloropropionic acid	2.86	-0.78
Hydrochloric acid	negative	-6.40

The results indicate that only HCl is titratable with good accuracy. However also picric acid can be determinate with a good enough precision.

pKc values seems to be dependent on the pKa values of the corresponding acids. On plotting pKa vs. pKc of the whole series (Fig. 10.15) one can see that such dependence is linear.

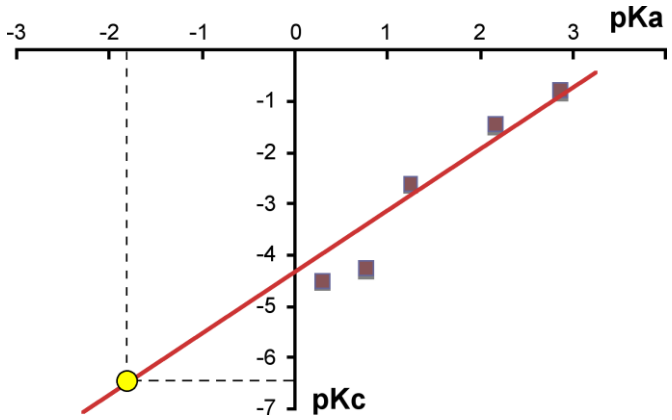

Fig 10.15 - Dependence of pKc of the reaction **I** + HA ⇌ **II** on pKa of the corresponding HA. pKa value of HCl is extrapolated from the corresponding pKc value.

According to such a linear relationship it would be possible, in principle , to extrapolate the pKa of HCl from the corresponding pKc value. The value found "-1.8" falls almost within the commonly accepted range (-7 ÷ -2) reported in the literature [29]. Indeed, a five order magnitude is a range too large even for a rough estimation. However, we reasonably believe that the extrapolation of the pKa (HCl) from the values of table 10.6 is quite realistic, assuming the

behavioral differences of acids in chloroform and water are not as dramatically different when HCl is compared to a series of relatively weak acids.

Conclusions.

This dissertation aims to show that the secondary dithiooxamides coordinated to a transition metal behave as an anion receptor, being able to achieve contact ion pairs with halides.

To better support these conclusions it was deemed useful to review the main classes of anion receptors, as well as the templating effect of metal ions which, through a preorganization of binding sites, lead to a more effective anion recognition. The metal-dithiooxamide-halide tight ion pairs, as well as their neutral counterpart $[Pt(HR_2DTO)_2]$ behave in chloroform solution as sensors, molecular carriers and finally as self-indicating titrants in acid-base processes in chloroform. Further investigations of these properties could produce noteworthy insight in the fields of phase transfer catalysis as well as in the selective transfer of anion between different aqueous phases.

Furthermore, the disposal of self indicating titrants could expand the current level of knowledge about acid base processes in chloroform.

References

[1] (a) Beer, P. D.; Gale, P. A. *Angew. Chem., Int. Ed*. **2001**, 40, 486. (b) Gale, P. A. *Coord. Chem. Rev*. **2003**, 240, 191. (c) Sessler, J. L.; Gale, P. A.; Cho, W.-S. *Anion Receptor Chemistry*; Royal Society of Chemistry: Cambridge, **2006**.

[2] (a) Manabe, K.; Okamura, K.; Date, T.; Koga, K. *J. Org. Chem*. **1993**, 58, 6692. (b) Motomura, T.; Aoyama, Y. *J. Org. Chem*. **1991**, 56, 7224. (c) Reetz, M. T.; Niemeyer, C. M.; Hermes, M.; Goddard, R. *Angew. Chem., Int. Ed*. **1992**, 31, 1017. (d) Dietrich, B.; Hosseini, M. W.; Lehn, J.-M.; Sessions, R. B. *J. Am. Chem. Soc*. **1981**, 103, 1282. (e) Dixon, R. P.; Geib, S. J.; Hamilton, A. D. *J. Am. Chem. Soc*. **1992**, 114, 365. (f) Ariga, K.; Anslyn, E. V. J. *Org. Chem*. **1992**, 57, 417. (g) Arduini, A.; Secchi, A.; Pochini, A. In Calyxarenes in the Nanoworld; Vicens, J., Harrowfield, J., Eds.; Springer: Berlin, **2007**; p 63, and refs. Therein

[3] Yoon, D.-W.; Gross, D. E.; Lynch, V. M.; Lee, C.-H.; Bennett, P. C.; Sessler, J. L. *Chem. Commun*. **2009**, 1109, and refs. therein.

[4] (a) Jeffrey, G. A.; Saenger, W. *Hydrogen Bonding in Biological Structures*; Springer-Verlag: Berlin, **1991**. (b) Hughes, M. P.; Smith, B. D. *J. Org. Chem*. **1997**, 62, 4492.

[5] Karaman, R.; Bruice, T. C. *Inorg. Chem*. **1992**, 31, 2455.

[6] (a) Sambrook, M. R.; Beer, P. D.; Wisner, J. A.; Paul, R. L; Cowley, A. R. *J. Am. Chem. Soc*. **2004**, 126, 15364. (b) Sambrook, M. R.; Beer, P. D.; Wisner, J. A.; Paul, R. L; Cowley,A. R.; Szemes, F.; Drew,M.G. B. *J. Am. Chem. Soc*. **2005**, 127, 2292.

[7] Rosace, G.; Bruno, G.; Monsù Scolaro, L.; Nicolò, F.; Sergi, S.; Lanza, S. *Inorg. Chim. Acta* **1993**, 208, 59

[8] Rosace, G.; Giuffrida, G.; Guglielmo, G.; Campagna, S.; Lanza, S. *Inorg. Chem*. **1996**, 35, 6816.

[9] See for example: Menger, F. M.; Singh, T. D.; Bayer, F. L. *J. Am. Chem. Soc*. **1976**, 98, 5011.

[10] (a) Taft, R. W. *J. Am. Chem. Soc*. **1953**, 75, 4231. (b) Hall, H. K., Jr. *J. Am. Chem. Soc*. **1957**, 79, 5441. (c) De Tar, D. F. *J. Am. Chem. Soc*. **1980**, 102, 7988.

[11] As Σσ* values, we used the values reported in ref 16b for the various amines. Note that we used the values for the amines employed to prepare the DTO ligands, and not the Σσ* of the DTO ligands, which should be used from a more rigorous point of view. However, this functional approximation should be acceptable, since the difference in the DTO properties are dictated by the R substituents on the nitrogens.

[12] (a) Robin, M. B.; Day, P. *Adv. Inorg. Radiochem*. **1967**, 10, 247. (b) Richardson, D. E.; Taube, H. *J. Am. Chem. Soc*. **1983**, 105, 40. (c) Creutz, C. *Prog. Inorg. Chem*. **1983**, 30, 1.

[13] Giuffrida, G.; Campagna, S. *Coord. Chem. Rev*. **1994**, 135-136, 517.

[14] The situation is even more general. This discussion applies indeed to any symmetric species with two identical redox-active sites, and has its explanation in the superexchange theory.[15] The dinuclear metal complexes oxidation splitting is taken as an example, and a simplified view is here used for immediate qualitative comparison with the present systems.

[15] (a) McConnell, H. H. *J. Chem. Phys*. **1961**, 35, 508. (b) Lambert, C.; No::ll, G. *J. Am. Chem. Soc*. **1999**, 121, 8434. (c) Demadis, K. D.; Hartshorn, C. M.; Meyer, T. *J. Chem. Rev* **2001**, 101, 2655. (d) Paddon-Row, M. N. *In Electron Transfer in Chemistry* (Ed.: Balzani, V.), Wiley-VCH, Weinheim, **2001**, Vol. 3, p. 179. (e) Brunschwig, B. S.; Creutz, C.; Sutin, *N. Chem. Soc. Rev*. **2002**, 31, 168.

[16] A. Giannetto, F. Puntoriero, A. Barattucci, S. Lanza, S. Campagna, *Inorg. Chem.* **2009**, *48*, 10397.

[17] S. Lanza, L. Monsu Scolaro, G. Rosace, *Inorg. Chim. Acta* **1994**, *227*, 63.

[18] A. Giannetto, S. Lanza, F. Puntoriero, M. Cordaro, S. Campagna, *Chem. Commun.* **2013**, *49*, 7611.

[19] D. H. Williams, M. S. Westwell, *Chem. Soc. Rev.* **1998**, *27*, 57.

[20] a) R. W. Taft, *J. Am. Chem. Soc.* **1953**, *75*, 4231; b) H. K. Hall, *J. Am. Chem. Soc.* **1957**, *79*, 5441; c) D. F. De Tar, *J. Am. Chem. Soc.* **1980**, *102*, 7988.

[21] a) M. S. Searle, M. S. Westwell, D. H. Williams, *J. Chem. Soc. Perkin Trans. 2* **1995**, *2*, 141; b) M. S. Westwell, J. Klein, D. H. Williams, *J. Phys. Chem.* **1996**, *100*, 16000; c) D. H. Williams, M. S. Westwell, *Chem. Soc. Rev.* **1998**, *27*, 57.

[22] R. M. Izatt, J. S. Bradshaw, K. Pawlak, R. L. Bruening, B. J. Tarbet, *Chem. Rev.* **1992**, *92*, 1261.

[23] a) P. L. Privalov, S. Gill, *J. Adv. Protein Chem.* **1988**, *39*, 191; b) W. P. Jencks, *Adv. Enzymol.* **1975**, *43*, 219; c) K. A. Dill, *Biochemistry* **1990**, *29*, 7133; d) A. R. Fersht, *Trends Biochem. Sci.* **1987**, *12*, 301; e) A. Ben-Naim, *J. Phys. Chem.* **1991**, *95*, 1437.

[24] a) P. R. Shirhatti, D. K. Maity, S. Wategaonkar, *J. Phys. Chem. A* **2013**, *117*, 2307; b) S. N. Delanoye, W. A. Herrebout, B. J. van der Veken, *J. Am. Chem. Soc.* **2002**, *124*, 7490.

[25] J. Emsley, *Chem. Soc. Rev*. **1980**, 9, 91.

[26] M. C. Chervenak, E. J. Toone, *J. Am. Chem. Soc.* 1994, *116*, 10533

[27] F. Nastasi, F. Puntoriero, N. Palmeri, S. Cavallaro, S. Campagna, S. Lanza, *Chem. Commun.* **2007**, 4740.

[28] I. Ielo, S. Lanza, S. Campagna and A. Giannetto, *Eur. J. Inorg. Chem.* **2016**, 281‑287

[29] (a) R. A. Robinson, R . Bates, *Analitical Chemistry*, Vol. 43, NO. 7, june **1971**; (b) B. R. Tagirov, A. W. Zotov and N. N. Akinfiev, *Geochimica et Cosmochimica* **Acta**, Vol. 61, No. 20, pp. 4267-4280, **1997**; (c) S. L. Clegg and P. Brimlecombe, *Atmospherik enviroment*, Vol. 20. No. 12. pp. 2403-245. **1996**; (d) A. R. W. Marsh and W. J. McElroy, *Atmospheric Environment* Vol. 19, No. 7, pp. 1075-1080, **1985**; (e) J. R. Ruaya and T. M. Seward, *Geochimica et Cosmochimica Acta* Vol. 51, pp. 121-130, **1987**

11. Experimental part

11.1. Preparation of Compounds

Secondary dithioxamides[1] and cis-Pt-$(Me_2SO)_2Cl_2$[2] were prepared according to the literature methods.

$\{[Pt(H_2R_2DTO)_2]^{++},2X^-\}$, (R = methyl, ethyl, n-propyl, n-butyl, benzyl, isopropyl, isoamyl; X = Cl, Br, I) compounds have been prepared according to reported general procedures.[3,4,5];
(1,4-Cyclooctadyene)Rh(μ-((S)-1-phenylEthyl)$_2$DTO κ-N,N Rh, κ-S,S Pt) Pt(H-(S)-1-phenylEthyl)$_2$DTO κ-S,S Pt) [6];

General procedure for the synthesis of [Pt(HR_2DTO κ-S,S Pt) (Me_2SO)Cl] (HR_2DTO- = N,N-Dialkyl-dithiooxamidate; R = methyl, ethyl, ^{n}propyl, ^{n}butyl, ^{n}decyl, isopropyl, {R}-(1-phenyl)ethyl; Me_2SO = S-bonded dimethyl sulphoxide.[7]

In 50 mL of chloroform containing cis-Pt$(Me_2SO)_2Cl_2$ (211 mg, 0.5mmol) and sodium bicarbonate (0.5 g) the equimolar quantity of H_2R_2DTO was added in small portions under magnetic stirring. The solution was turning orange while the suspension of the starting cis-Pt$(Me_2SO)_2CL_2$ slowly disappeared. Finally the orange solution was separated from sodium bicarbonate and chloroform was removed by vacuum evaporation till to the final volume of 25 ml. Then 50 mL of petroleum ether were added and [Pt(HR_2DTO κ-S,S Pt) (Me_2SO)Cl] complexes precipitated as yellow-orange powders.

Key to acronyms: *s*, singlet; *bs*, broad singlet; *d*, doublet; *t*, triplets; *q*, quartet; *sl*, seven lines; *m*, multiplets; Ph, phenyl groups; Cp, cyclopentadienyl groups; COD, 1,4-cyclooctadiene; PhPy, 2-phenylpyridine(both H and C of the phenyl group have been labelled with the symbol ').

[Pt(H-Me_2-DTO κ-S,S Pt)(Me_2SO)Cl]: Yield: 0.19 g (83.3%). ^{1}H NMR (300 MHz, $CDCl_3$): δ 3.48 (s, 6H, Pt-S(O)(CH_3)$_2$, $^3J_{Pt\text{-}H}$ = 18.5 Hz), 3.41 (*s*, 3H, N-CH_3), 3.38 (*s*, 3H, N-CH_3). ^{13}C NMR (75MHz, $CDCl_3$): δ 44.43 (Pt-S(O)(*C*H$_3$)$_2$, $^2J_{Pt\text{-}C}$ = 49.0 Hz), 35.65 (N-*C*H$_3$), 35.43 (N-*C*H$_3$). Anal. Calcd. for $C_6H_{13}N_2OS_3ClPt$: C, 15.81; H, 2.87; N, 6.14. Found: C, 15.88; H, 2.77; N, 6.01.

[Pt(H-Et_2-DTO κ-S,S Pt) (Me_2SO)Cl]: Yield, 0.205 g (84.7%). ^{1}H NMR (300 MHz, $CDCl_3$): δ 3.71 (*q*, 2H, N-CH_2-CH$_3$, $^3J_{H\text{-}H}$ = 7.4 Hz), 3.68 (*q*, 2H, N-CH_2-CH$_3$, $^3J_{H\text{-}H}$ = 7.4 Hz), 3.47 (*s*, 6H, Pt-S(O)(CH_3)$_2$, $^3J_{Pt\text{-}H}$ = 18.3 Hz), 1.38 (*t*, 3H, N-CH$_2$-CH_3, $^3J_{H\text{-}H}$ =

7.4 Hz), 3.38 (*s*, 3H, N- CH_2-C*H*$_3$, $^3J_{H-H}$ = 7.4 Hz). ^{13}C NMR (75MHz, $CDCl_3$): δ 44.46 (Pt-S(O)(*C*H_3)$_2$, $^2J_{Pt-C}$ = 46.5 Hz), 43.73, 43.57 (N-*C*H_2-CH_3), 13.91, 13.81 (N-CH_2-*C*H_3). Anal. Calcd. for $C_8H_{17}N_2OS_3ClPt$: C, 19.85; H, 3.54; N, 5.79. Found; C, 19.91; H, 3.77; N, 5.74.

[Pt(H-^{n}propyl$_2$-DTO κ-S,S Pt) (Me_2SO)Cl]: Yield, 0.200 g (78.1%). ^{1}H NMR (300 MHz, $CDCl_3$): δ 3.62 (*t*, 2H, N-C*H*$_2$-CH_2-CH_3, $^3J_{H-H}$ = 7.1 Hz), 3.59 (*t*, 2H, N-C*H*$_2$-CH_2-CH_3, $^3J_{H-H}$ = 7.1 Hz), 3.47 (*s*, 6H, Pt-S(O)(C*H*$_3$)$_2$, $^3J_{Pt-H}$ = 18.5 Hz), 1,794 (*six lines*, 2H, N-CH_2-C*H*$_2$-CH_3), 1,786 (*six lines*, 2H, N-CH_2-C*H*$_2$-CH_3), 1.11 (t, 6H, N-CH_2- CH_2-C*H*$_3$, $^3J_{H-H}$ = 7.1 Hz). ^{13}C NMR (75MHz, $CDCl_3$): δ 50.63, 50.38(N-*C*H_2-CH_2-CH_3), 41.90 (Pt-S(O)(*C*H_3)$_2$, $^2J_{Pt-C}$ = 48.2 Hz), 22.23, 22.13 (N-CH_2-*C*H_2-CH_3), 11.82 (N-CH_2-CH_2-*C*H_3). Anal. Calcd. for $C_{10}H_{21}N_2OS_3ClPt$: C, 23.46; H, 4.13; N, 6.92. Found; C, 23.23; H, 4.27; N, 6.84.

[Pt(H-^{n}decil$_2$-DTO κ-S,S Pt) (Me_2SO)Cl]: Yield, 0.282 g (79.1%). ^{1}H NMR (300 MHz, $CDCl_3$): δ 3.65 (*t*, 2H, N-C*H*$_2$-(C_8H_{16})-CH_3, $^3J_{H-H}$ = 7.1 Hz), 3.61 (*t*, 2H, N-C*H*$_2$-(C_8H_{16})-CH_3, $^3J_{H-H}$ = 7.10 Hz), 1.75 (*m*, 4H, N-CH_2-C*H*$_2$-(C_7H_{14})-CH_3, $^3J_{Pt-H}$ = 18.5 Hz), 1,44-1.22 (*m*, 28H, N-CH_2-CH_2-(C_7H_{14})-CH_3), 0.89 (*t*, 6H, N-CH_2-CH_2-(C_7H_{14})-C*H*$_3$), $^3J_{H-H}$ = 7.1 Hz). ^{13}C NMR (75MHz, $CDCl_3$): δ 49.06, 48.76 (N-*C*H_2-(C_8H_{16})-CH_3), 44.46 (Pt-S(O)(*C*H_3)$_2$, $^2J_{Pt-C}$ = 47.10 Hz), 31.90, 29.53, 29.31, 29.26, 28.85, 28.69, 27.30, 22.61, 14.64 (N-CH_2-C_9H_{19}). Anal. Calcd. for $C_{24}H_{49}N_2OS_3ClPt$: C, 40.69; H, 6.97; N, 3.95. Found: C, 40.93; H, 7.17; N, 4.06.

[Pt(H-isopropyl$_2$-DTO κ-S,S Pt)(Me_2SO)Cl]: Yield, 0.212 g (82.8%). ^{1}H NMR (300 MHz, $CDCl_3$): δ 4.320 (*seven lines*, 1H, N-C*H*-(CH_3)$_2$, $^3J_{H-H}$ = 6.6 Hz), 4.314 (*seven lines*,1H, N-C*H*-(CH_3)$_2$, $^3J_{H-H}$ = 6.6 Hz), 3.47 (*s*, 6H, Pt-S(O)(C*H*$_3$)$_2$, $^3J_{Pt-H}$ = 18.5 Hz), 1,30 (*d*, 6H, N-CH-(C*H*$_3$)$_2$, $^3J_{H-H}$ = 6.34 Hz 6.6 Hz). ^{13}C NMR (75MHz, $CDCl_3$): δ 50.10, 50.00 (N-*C*H_2-(CH_3)$_2$, 44.46 (Pt-S(O)(*C*H_3)$_2$, $^2J_{Pt-C}$ = 47.6 Hz), 21.73, 21.67 (N-CH-(*C*H_3)$_2$. Anal. Calcd. for $C_{10}H_{21}N_2OS_3ClPt$: C, 23.46; H, 4.13; N, 6.92. Found; C, 23.32; H, 4.07; N, 6.95.

[Pt(H-({R}-1-phenyl-ethyl)$_2$-DTO κ-S,S Pt)(Me_2SO)Cl]: Yield, 0.240 g (74.3%). ^{1}H NMR (300 MHz, $CDCl_3$): δ 7.44-7.31 (*m*, 10H, Ph), 5.338 (*q*, 1H, N-C*H*-(C_6H_5)-CH_3, $^3J_{H-H}$ = 6.6 Hz), 5.331 (*q*, 1H, N-C*H*-(C_6H_5)-CH_3, $^3J_{H-H}$ = 6.6 Hz), 3.47 (*s*, 6H, Pt-S(O)(C*H*$_3$)$_2$, $^3J_{Pt-H}$ = 18.5 Hz), 1,61 (*d*, 6H, N-CH-(C_6H_5)-C*H*$_3$, $^3J_{H-H}$ = 6.6 Hz). ^{13}C NMR (75MHz, $CDCl_3$): δ 128.9, 127.9, 126.6 (*multiplets*, Ph), 57.72, 57.66 (N-*C*H(C_6H_5)-(CH_3)$_2$, 44.46 (Pt-S(O)(*C*H_3)$_2$, $^2J_{Pt-C}$ = 49.2 Hz), 21.55, 21.50 (N-CH(C_6H_5)-(*C*H_3)$_2$. Anal. Calcd. for $C_{20}H_{25}N_2OS_3ClPt$: C, 37.76; H, 3.96; N, 5.57. Found; C, 37.95; H, 4.11; N, 6.05.

[Pt(H-({S}-2-hydroxy-propyl)$_2$-DTO κ-S,S Pt)(Me$_2$SO)Cl]: Yield, 0.219 g (80%).^{1}H NMR (300 MHz, $CDCl_3$): δ 4.15 (*m*, 2H, N-CH_2-C*H*(OH)-CH_3), 3.76 (1H, ABX spin pattern, part A, N-C*H*$_2$-CH(OH)-CH_3), 3.72 (1H, ABX spin pattern, part B, N-C*H*$_2$-CH(OH)-CH_3), 3.47 (*s*, SO(C*H*$_3$)2, superimposed the ABX spin pattern of the CH_2 fragment of the other N-C*H*$_2$-CH (OH)-CH_3 group, overall 8H), 1.32 (*d*, 3H, N-CH_2-CH(OH)-C*H*$_3$, $^3J_{H-H}$ = 6.3 Hz), 1.27 (d, 3H, N-CH_2-CH(OH)-C*H*$_3$, $^3J_{H-H}$ = 6.3 Hz). ^{13}C NMR (75MHz, $CDCl_3$): δ 65.91 (N-CH_2-*C*H(OH)-CH_3), 56.44 91 (N-*C*H_2-CH(OH)-CH_3), 45.11 (Pt-S(O)(*C*H_3)$_2$), 20,70 (N-CH_2-CH(OH)-*C*H_3), 21.10 (N-CH_2-CH(OH)-*C*H_3).

General procedure for the synthesis of complexes [Pt(HR$_2$DTO κ-S,S Pt)(dppf)]Cl (HR$_2$DTO$^-$ = N,N-Dialkyl-dithiooxamidate; R = methyl, ethyl, ^{n}propyl, ^{n}butyl, ^{n}decyl, isopropyl, {R}-(1-phenyl)ethyl; dppf 1,1'-bis-(diphenylphosphinoferrocene) P- Pt chelated).

0.5 mmol of the proper [Pt(HR$_2$DTO κ-S,S Pt)(Me$_2$SO)Cl] were dissolved in 25 mL of chloroform. To the resulting orange solution, the equimolar quantity of 1,1'-bis-(diphenylphosphinoferrocene) was added. The solution immediately turned yellow. Then 50 mL of petroleum ether were added and [Pt(HR$_2$DTO κ-S,S Pt)(dppf)]Cl precipitated as yellow powder in good yields.

[Pt(H-methyl$_2$-DTO κ-S,S Pt)(dppf)]Cl. Yield: 0.40 g (86%). ^{1}H NMR (300 MHz, $CDCl_3$): δ 7.92 ÷ 7.19 (*m*, 20H, Ph*)*, 4.39 *(bs*,4H, Cp*)* , 4.23 *(bs*, 4H, Cp*)*, 3.14 (*s*, 6H, N-C*H*$_3$). ^{13}C NMR (75MHz, $CDCl_3$): δ 164.6, 132.06, 128.47 (*m*, Ph); 76.17, 74.21 (*m*, Cp); 37.62 (N-*C*H_3). ^{31}P NMR (121.49 MHz, $CDCl_3$): δ 17.16 ($^1J_{Pt-P}$ 3127 Hz). Anal. Calcd. for $C_{38}H_{35}N_2P_2S_2ClFePt$: C, 48.96; H, 3.78; N, 3.01. Found; C, 48.88; H, 3.72; N, 3.11. Molar conductivity (MeOH): 102 ohm^{-1} cm^{-1} mol^{-1}.

[Pt(H-ethyl$_2$-DTO κ-S,S Pt)(dppf)]Cl. Yield: 0.42 g (88.6%). ^{1}H NMR (300 MHz, $CDCl_3$): δ 7.72 ÷ 7.41 (*m*, 20H, Ph*)*, 4.55*(bs*, 4H, Cp*)* , 4.273 *(bs*, 4H, Cp*)*, 3.56 (*q*, 4H, N-C*H*$_2$-CH_3, $^3J_{H-H}$ = 7.1 Hz), 1.19 (*t*, 6H, N-CH_2-C*H*$_3$, $^3J_{H-H}$ = 7.1 Hz). ^{13}C NMR (75MHz, $CDCl_3$): δ 134.60, 132.27, 128.47 (*multiplets*, Ph), 76.26, 74.50 (*multiplets*, Cp), 44.37 (N-*C*H_2-CH_3), 13.31 (N-CH_2-*C*H_3). ^{31}P NMR (121.49 MHz, $CDCl_3$): δ 16.62 ($^1J_{Pt-P}$ 3158 Hz). Anal: Calcd. for $C_{40}H_{39}N_2P_2S_2ClFePt$: C, 50.03; H, 4.09; N, 2.92. Found; C, 50.52; H, 4.01; N, 3.08. Molar conductivity (MeOH): 98 ohm^{-1} cm^{-1} mol^{-1}.

[Pt(H-^{n}propyl$_2$-DTO κ-S,S Pt)(dppf)]Cl. Yield: 0.44 g (89.0%). ^{1}H NMR (300MHz, $CDCl_3$): δ 7.80 ÷ 7.36 (*m*, 20H, Ph*)*, 4.42*(bs*, 4H, Cp*)* 4.24 *(bs*, 4H, Cp*)*, 3.30 (*t*, N-C*H*$_2$- CH_2-CH_3, $^3J_{H-H}$ =7.7 Hz), 1.63 (*six lines*, N-CH_2-C*H*$_2$-CH_3, , $^3J_{H-H}$ =7.7 Hz), 0.82 (*t*, N-CH_2- 7CH_2-C*H*$_3$, , $^3J_{H-H}$ = 7.7 Hz). ^{13}C NMR (75MHz, $CDCl_3$): δ 134.77, 131.40,

128.00 (*m*, Ph), 75.92, 73.48, (*m*, Cp), 54.91 (N-*C*H_2CH$_2$CH$_3$), 22.76 (N-CH$_2$*C*H$_2$CH$_3$), 12.23 (N-CH$_2$CH$_2$*C*H$_3$). ^{31}P NMR: δ 17.43 ppm (*s*, *P*-Pt ,$^{1}J_{(P\text{-}Pt)}$=3075Hz). Anal: Calcd. for $C_{42}H_{43}N_2P_2S_2ClFePt$: C, 52.00; H, 4.61; N, 2.76. Found; C, 52.20; H, 4.61; N, 2.79. Molar conductivity (MeOH): 102 ohm^{-1} cm^{-1} mol^{-1}.

[Pt(H-^{n}decyl$_2$-DTO κ-S,S Pt)(dppf)]Cl. Yield: 0.50 g (85%).^{1}H NMR (300MHz, $CDCl_3$): δ 7.80 ÷ 7.26 (*m*, 20H, Ph*)*, 4.38*(bs*, 4H, Cp*)* 4.22 *(bs*, 4H, Cp*)*, 3.32 (m, 4H, n-C*H*$_2$-(C$_8$H$_{16}$)-CH$_3$), 1.64, 1.29, 1.24, 1.20 (*m* , 32H, n-CH$_2$-(C$_8$*H*$_{16}$)-CH$_3$), 0.89 (*t*, 6H, $^{3}J_{H\text{-}H}$ = 6.6 Hz). ^{13}C NMR (75MHz, $CDCl_3$): δ 134.92, 131.20, 127.89 (*m*, Ph), 75.86, 73.29, (*m*, Cp), 53.9 (N-*C*H$_2$-(C$_9$H$_{19}$)), 41.00, 31.94. 29.72, 29.66, 29.58, 29.50, 29.38, 22.70, 14.16 (N-CH$_2$-(*C*$_9$H$_{19}$). ^{31}P NMR: δ 18.81 ppm (*s*, *P*-Pt ,$^{1}J_{(P\text{-}Pt)}$=3079Hz). Anal. Calcd. for $C_{56}H_{71}N_2P_2S_2ClFePt$: C, 56.78; H, 6.04; N, 2.36. Found; C, 56.60; H, 5.81; N, 2.30. Molar conductivity (MeOH): 95 ohm^{-1} cm^{-1} mol^{-1}.

[Pt(H-isopropyl$_2$-DTO κ-S,S Pt)(dppf)]Cl. Yield: 0.415 g (84%). ^{1}H NMR (300MHz, $CDCl_3$): δ 7.71 ÷ 7.40 (*m*, 20H, Ph*)*, 4.58 (*bs*, 4H, Cp) , 4.28 (*bs*, 4H, Cp), 3.80 (*sl*, 2H, N-C*H*(CH$_3$)$_2$, $^{3}J_{H\text{-}H}$ = 6.4 Hz), 1.28 (*d*, 12H, N-CH(C*H*$_3$)$_2$, $^{3}J_{H\text{-}H}$ = 6.4 Hz).). ^{13}C NMR (75MHz, $CDCl_3$): δ 134.40, 132.40, 128.70 (*m*, Ph), 76.34, 74.75, (*m*, Cp), 50,69 (N-*C*H(CH$_3$)$_2$), 21.34 (N-CH(*C*H$_3$)$_2$). ^{31}P NMR: δ 16.75 ppm (*s*, *P*-Pt ,$^{1}J_{(P\text{-}Pt)}$=3160Hz). Anal. Calcd. for $C_{42}H_{43}N_2P_2S_2ClFePt$: C, 52.00; H, 4.61; N, 2.76. Found; C, 52.35; H, 4.59; N, 2.81. Molar conductivity (MeOH): 92 ohm^{-1} cm^{-1} mol^{-1}.

[Pt(H-({R}-1-phenyl-ethyl)$_2$-DTO κ-S,S Pt)(dppf)]Cl. Yield: 0.50 g (81%). ^{1}H NMR (300MHz, $CDCl_3$): δ 7.71 ÷ 7.10 ppm (*m*, 30H, Ph*)*, 4.77 (*q*, 2H, N-C*H*(CH$_3$)C$_6$H$_5$, $^{3}J_{H\text{-}H}$ = 6.6 Hz), ^{1}H NMR (300MHz, $CDCl_3$): δ 7.80 ÷ 7.26 ppm (*m*, 20H, Ph*)*, 4.47*(bs*, 4H, Cp*)*, 4.23*(bs*, 4H, Cp*)*, 1.44 (*d*, 6H, N-CH(C*H*$_3$)C$_6$H$_5$, $^{3}J_{H\text{-}H}$ = 6.6 Hz). ^{13}C NMR (75MHz, $CDCl_3$): δ 134.50, 131.80, 128.30, 127.28, 126.97 (*m*, Ph), 76.11, 74.04, (*m*, Cp), 59.91 (N-*C*H(CH$_3$)C$_6$H$_5$), 22.5 (N-CH(*C*H$_3$)C$_6$H$_5$). ^{31}P NMR: δ 17.68 ppm (*s*, *P*-Pt ,$^{1}J_{(P\text{-}Pt)}$=3115 Hz). Anal: Calcd. for $C_{52}H_{47}N_2P_2S_2ClFePt$: C, 56.15; H, 4.26; N, 2.52. Found; C, 56.01; H, 4.16; N, 2.49. Molar conductivity (MeOH): 108 ohm^{-1} cm^{-1} mol^{-1}.

[Pt(H-({S}-2-hydroxy-propyl)$_2$-DTO κ-S,S Pt) (dppf)] Cl. Yield: 0.420 g (85.3 %). ^{1}H NMR (300MHz, $CDCl_3$): δ 7.80 ÷ 7.30 ppm (*m*, 20H, Ph), 4.42 *(bs*, 4H, Cp*)*, 4.23*(bs*, 4H, Cp*)*, 4.02 (*m*, 2H, N-C*H*-CH$_2$(OH)-CH$_3$), 3.31 (ABX spin pattern, part A, 2H , N-CH-C*H*$_2$(OH)-CH$_3$), 3.11 (ABX spin pattern, part B, 2H , N-CH-C*H*$_2$(OH)-CH$_3$), 1.11 (*d*, 6H, N-CH-CH$_2$(OH)-C*H*$_3$). ^{13}C NMR (75MHz, $CDCl_3$): δ 134.70, 131.53, 128.16, (*m*, Ph), 75.93, 73.60, (*m*, Cp), 66.90 (N-*C*H-CH$_2$(OH)-CH$_3$), 60.58 (N-CH-*C*H$_2$(OH)-CH$_3$), 20.40 (N-CH-CH$_2$(OH)-*C*H$_3$). ^{31}P NMR: δ 18.24 ppm (*s*, *P*-Pt ,$^{1}J_{(P\text{-}Pt)}$=3084 Hz).

General procedure for the synthesis of compounds [Pt(HR_2DTO κ-S,S Pt)(dppf)]$_6$$Cl_6$ (HR_2DTO^- = N,N-Dialkyl-dithiooxamidate; R = methyl, ethyl, ^{n}propyl, ^{n}butyl, ^{n}decyl; dppf 1,1'-bis-(diphenylphosphinoferrocene) PPt-P′Pt′ bridged).

0.25 mmol of the proper [Pt(HR_2DTO κ-S,S Pt)(dppf)]Cl precursor, dissolved in 25 mL of methanol, was allowed to stand for two days at room temperature. From the resulting solution, which after this time has became deep blue, solvent has been removed. The resulting blue powder has been dissolved in the minimum volume of chloroform and then has been put at the head of an alumina column equilibrated with petroleum ether. Elution with chloroform/MeOH mixture 97/3 v/v removed all the impurities while the blue compound stayed over the head of the column. Finally, when all the impurities were removed, the blue compound was eluted with a chloroform/MeOH mixture 88/12 v/v. Then, the blue eluate was concentrated to a small volume (10 mL) to which petroleum ether was added (50 mL). [Pt(HR_2DTO κ-S,S Pt) (dppf)]$_6$ Cl_6 species precipitated as blue powder.

[Pt(H-methyl$_2$-DTO κ-S,S Pt) (dppf)]$_6$ Cl_6. Yield: 0.140 g (60%). Ph ^{1}H NMR (300MHz, $CDCl_3$): *δ* 7.71÷7.37 (*m*, 20 H, Ph*)*, 4.50 *(bs*, 4 H, Cp), 4.25 (*bs*, *4H*, Cp*)*, 2.44 *(s*, 6 H, N-C*H*$_3$). ^{13}C NMR (75MHz, $CDCl_3$): *δ* 134.61, 132.07, 128.44 (*m*, Ph), 76.18, 74.28 (*m*, Cp), 40.63 (N-*C*H_3). ^{31}*P* NMR: *δ* 16.73, (*s*, *P*-Pt $^1J_{(P\text{-}Pt)}$=3067Hz). Anal. Calcd. for $C_{38}H_{35}N_2P_2S_2ClFePt$: C, 48.96; H, 3.78; N, 3.01. Found; C, 49.12; H, 3.75; N, 3.14.

[Pt(H-ethyl$_2$-DTO κ-S,S Pt) (dppf)]$_6$ Cl_6. Yield: 0.155 g (64.6%). ^{1}H NMR (300MHz, $CDCl_3$): *δ* 7.73÷7.35 (*m*, 20 H, Ph), 4.50 *(bs*, 4 H, Cp), 4.24 (*bs*, 4H, Cp*)*, *3.40 (m*, ABX_3 spin pattern, N-C*H*$_2$-CH_3 part A, 2H), 2.46 (*m*, ABX_3 spin pattern, N-C*H*$_2$-CH_3 part *B*, 2H), 0.62 (*t*, N-CH_2-C*H*$_3$, $^3J_{H\text{-}H}$=7.2Hz). ^{13}C NMR (75MHz, $CDCl_3$): *δ* 134.60, 131.92, 126.28 (*m*, Ph), 76.09, 74.14 (*m*, Cp), 50.13 (N-*C*H_2-), 11.84 (N-CH_2-*C*H_3*)*. ^{31}*P* NMR: *δ* 17.25 ppm (*s*, $^2J_{(P\text{-}Pt)}$=3090 Hz). Anal: Calcd. for $C_{240}H_{396}N_{12}P_{12}S_{12}Cl_6Fe_6Pt_6$: C, 50.03; H, 4.09; N, 2.92. Found; C, 49.82; H, 4.19; N, 3.10.

[Pt(H-^{n}propyl$_2$-DTO κ-S,S Pt) (dppf)]$_6$ Cl_6. Yield: 0.130 g (52.5%). ^{1}H NMR (300MHz, $CDCl_3$): δ 7.71÷7.34 (*mm*, 20 H, Ph), 4.52 (bs, 4 H, Cp), 4.26 (d, 4 H, $^3J_{H\text{-}H}$ =10.7 Hz), 3.19 (*m*, ABX_2 spin pattern, part A, 2 H, N-C*H*$_2$-CH_2-CH_3), 2.24 (*m*, ABX_2 spin pattern, part B, 2 H, N-C*H*$_2$-CH_2-CH_3), 1.22 (*m*, 4H, N-CH_2-C*H*$_2$-CH_3), 0.56 (*t*, 6H, $^3J_{H\text{-}H}$ =6.6 Hz). ^{13}C NMR (75MHz, $CDCl_3$): δ 134.63, 131.95, 128.28 ppm (*m*, Ph), 76.17, 74.23 (*m*, Cp), 57.73 (N-*C*H_2-CH_2-CH_3*)*, 20.16 (N-CH_2-*C*H_2-*C*H_3*)*, 12.31 (N-CH_2-CH_2-*C*H_3). ^{31}*P* NMR: δ 17.42 (s, *P*-Pt, $^2J_{(P\text{-}Pt)}$=3101 Hz). Anal: Calcd. for

$C_{252}H_{258}N_{12}P_{12}S_{12}Cl_6Fe_6Pt_6$: C, 52.00; H, 4.61; N, 2.76. Found; C, 52.20; H, 4.61; N, 2.79.

[Pt(H-^{n}decyl$_2$-DTO κ-S,S Pt) (dppf)]$_6$ Cl$_6$. Yield: 0.140 g (45.4%). ^{1}H NMR (300MHz, $CDCl_3$): δ 7.71÷7.34 (*m*, 20 H, Ph), 4.52 (*bs*, 4H), 4.22 (*d*, 4H, Cp, $^3J_{H-H}$=6.0Hz), 3.25 (ABX_2 spin pattern, 2H, N-CH_2-(C_9H_{19}), part A), 2.22 (ABX_2 spin pattern, 2H, N-CH_2-(C_9H_{19}), part B), 1.76, 1.26, 1.21 (*m*, 32 H, , N-CH_2-(C_8H_{16})CH_3, 0.91 (t, 6H, N-CH_2-(C_8H_{16})CH_3, $^3J_{H-H}$=6.8Hz). ^{13}C NMR (75MHz, $CDCl_3$): δ 134.60, 131.92, 128.28 (*m*, Ph), 76.15, 74.17 (*m*, Cp), 57.17, 32.04, 29.87, 29.52, 29.43, 27.90, 26.69, 22.75, 22.65, 14.20 (N-$C_{10}H_{21}$). *P* NMR: δ 17.70 ppm (*s*, $^2J_{(P-Pt)}$=3096 Hz). Anal: Calcd. for $C_{336}H_{426}N_{12}P_{12}S_{12}Cl_6Fe_6Pt_6$: C, 56.78; H, 6.04; N, 2.36. Found; C, 56.15; H, 5.90; N, 2.28.

General procedure for the synthesis of [(dppf)Pt(HMe$_2$DTO κ-S,S Pt κ-N,N M)MLn)]Cl (HMe$_2$DTO$^-$ = N,N-Dimethyl-dithiooxamidate; dppf = 1,1'-bis-(diphenylphosphinoferrocene) P-Pt chelated); MLn$^+$ = Pd(η^3-allyl)$^+$; Rh(COD)$^+$; Ru(η^6-p-cymene)Cl$^+$; Ir(2-phenylpyridine κ-N,C Ir)$_2^+$; Rh(2-phenylpyridine κ-N,C Rh)$_2^+$.

0.5 mmol of the [Pt(HMe$_2$DTO κ-S,S Pt)(dppf)]Cl species were dissolved in 100 mL of $CHCl_3$/MeOH mixture 97/3 v/v. To the resulting solution the half molar quantity of the proper $[MLnCl]_2$ chloro-bridged dimer was added. The resulting mixture was kept under reflux at 60 °C for two hours. After this time solvent was removed by rotary evaporation. The residuum, dissolved in the minimum quantity of chloroform, was put at the head of an alumina column equilibrated with petroleum ether. The compound was eluted with chloroform/MeOH by varying MeOH content from 1 to 5%. The pure [(dppf)Pt(HMe$_2$DTO κ-S,S Pt κ-N,N M)MLn)]Cl species were collected as yellow fraction and concentrated to a small volume (10 ml). Then petroleum ether (50 mL) was added and the pure trimetallic species precipitated as yellow powder.

[(dppf)Pt(H-methyl$_2$-DTO κ-S,S Pt κ-N,N Pd)Pd(η^3-allyl)Cl]. Yield: 0.35 g (65%). ^{1}H NMR (300MHz, $CDCl_3$): δ 7.7 ÷ 7.36 (*m*, 20H,CH), 5.58 (*m*, 1H, allyl CH_2CHCH_2), 4.52(*bs*, 4H, Cp),4.23(*bs*,4H,Cp), 3.67 (*d*, 2H, allyl $CHH_{syn}CHCHH_{syn}$, J_{syn}=6.8 Hz), 3.04 (*d*, 2H, allyl $CHH_{anti}CHCHH_{anti}$, J_{anti}= 12.5 Hz), 3.19 (*s*, 6H, NCH_3). ^{13}C NMR (75MHz, $CDCl_3$): δ 134.40, 132.10, 128.50 (*m*, Ph), 117.7 (allyl CH_2CHCH_2), 76.18, 74.5 (*m*,Cp), 60.0 (allyl CH_2CHCH_2), 46.4 (N-CH_3). ^{31}*P*NMR: δ 17.35 (s, *P*Pt,$^1J_{P-Pt}$: 3121Hz). Anal: Calcd. for $C_{41}H_{39}N_2P_2S_2ClFePdPt$: C, 45.65; H, 3.64; N, 2.60. Found: C, 45.18; H, 3.35; N, 2.73. Molar conductivity (MeOH): 91 ohm^{-1} cm^{-1} mol^{-1}.

[(dppf)Pt(H-methyl$_2$-DTO κ-S,S Pt κ-N,N Rh)Rh(COD)]Cl. Yield: 0.385 g (67,5%). ^{1}H NMR (300MHz, $CDCl_3$): δ 7.7 ÷ 7.37 (*m*, 20H, Ph), 4.55 (*bs* ,4H, Cp), 4.25 (*bs*, 4H,

Cp), 4.00 (m, 4H, COD C*H*), 2.51 (s, 6H, N-CH_3), 2.42 (m,4H, COD CH_2), 1.91(m ,4H, COD CH_2). ^{13}C NMR (75MHz, $CDCl_3$): δ 134.50, 132.30,128.60 (*m*, ,Ph), 84.20 (d ,COD *C*H,$^1J_{Rh-C}$ = 12.6Hz), 76.18, 74.57 (*m*,Cp), 38.98 (N-*CH$_3$)*, 30.58(COD *C*H$_2$). ^{31}PNMR: δ 17.25 (s, *P*Pt,$^1J_{P-Pt}$=3127Hz*)*. Anal: Calcd. for $C_{46}H_{46}$ N_2P_2 $S_2ClFeRhPt$: C, 48.37; H, 4.06; N, 2.45. Found: C, 48.60; H, 4.15; N, 2.53. Molar conductivity (MeOH): 89 ohm^{-1} cm^{-1} mol^{-1}.

[(dppf)Pt(H-methyl$_2$-DTO κ-S,S Pt κ-N,N Ru)Ru(p-cymene)Cl]Cl. Yield: 0.427 g (71,0%).^{1}H NMR (300MHz, $CDCl_3$): δ 7.70 ÷ 7.36 (*m*, phenyl C*H*), 5.66 (AA' X X' spin system, 4*H*, H^{2,3,5,6} cymene), 4.48 (*bs*, 4H, Cp), 4.26 (*bs*, 2H,Cp), *4.20* (bs, *2H*, Cp C*H*), 3.63*(s*, 6H, N-C*H$_3$)*, 2.79 (*sl*,1H,C*H*(CH$_3$)$_2$,$^3J_{H-H}$=6.6Hz), 2.22 (*s*,3H, cymene C*H$_3$*), 1.21 (*d*, CH*(CH$_3$)$_2$*,$^3J_{H-H}$ = 6.6 Hz). ^{13}C NMR (75MHz, $CDCl_3$): δ 134.53, 132.13 ,128.52 (*m*, Ph), 104.94, 100.08 (cymene *C*^{1,4}), 85.33, 84.84 (cymene *C*^{2,3,5,6}), 76.22 , 74.17 (*m*, Cp), 49.02 (N-*C*H$_3$), 31.36 (cymene *C*H(CH$_3$)$_2$), 22.33 (cymene CH-(*C*H$_3$)$_2$), 19.10*(*cymene *C*H$_3$). ^{31}*P*NMR: *δ* 16.85 (s,$^1J_{Pt-P}$=3113Hz). Anal: Calcd. for $C_{48}H_{48}$ N_2P_2 $S_2Cl_2FeRuPt$: C, 47.97; H, 4.03; N, 2.45. Found: C, 48.16; H, 4.12; N, 2.53. Molar conductivity (MeOH): 84 ohm^{-1} cm^{-1} mol^{-1}.

[(dppf)Pt(H-methyl$_2$-DTO κ-S,S Pt κ-N,N Ru)Ir(2-phenylpyridine)Cl]Cl. Yield: 0.450 g (63,0%). ^{1}H NMR (300MHz, $CDCl_3$): *δ* 7.87 (m, 4H, *PhPy H*^{4}, *H*^{6}), 7.76 - 7.35 (*m*, 26H, PhPy *H*$^{3'}$, *H*^{5},*H*^{3}, Ph), 6.85 (*t*, 2H, PhPy *H*$^{4'}$,$^3J_{H-H}$ = 7.4 Hz), 6.72 (*t*, 2H, PhPy *H*$^{5'}$,$^3J_{H-H}$ = 7.4 Hz), 6.03 (*d*, 2H, PhPy *H*$^{6'}$, $^3J_{H-H}$7.4 Hz), 4.52 (*bs*, 4H, Cp), 4.27 (*bs*, 4H, Cp), 2.77 (*s*, 6H, N-C*H$_3$*). ^{13}C NMR (75MHz, $CDCl_3$): δ 168.13 (PhPy *C*$^{1'}$), 155.19 (PhPy *C*^{2}), 150.00 (PhPy *C*^{6}), 134.54, 132.11 , 128.52 (*m*, Ph), 131.06 (PhPy *C*$^{6'}$), 130.19 (PhPy *C*$^{5'}$), 124.2 (PhPy *C*$^{3'}$), 123.4 (PhPy *C*^{5}), 121.7 (PhPy *C*$^{4'}$), 119.04 (PhPy *C*^{3}), ^{31}*P*NMR: δ 17.56 (*s*, $^1J_{Pt-P}$ =3096 Hz). Anal: Calcd. for $C_{60}H_{50}$ N_4P_2 $S_2ClFeIrPt$: C, 50.33; H, 3.52; N, 3.91. Found: C, 50.63; H, 3.48; N, 3.86. Molar conductivity (MeOH): 82 ohm^{-1} cm^{-1} mol^{-1}.

[(dppf)Pt(H-methyl$_2$-DTO κ-S,S Pt κ-N,N Ru)Rh(2-phenylpyridine)Cl]Cl. Yield: 0.438 g (65,3%). ^{1}H NMR (300MHz, $CDCl_3$): *δ* 7.89 (m, 4H, PhPy *H*^{4}, *H*^{6}), 7.77- 7.33 (*m*, 26H, PhPy *H*$^{3'}$, *H*^{5}, *H*,^{3} Ph), 6.92 (*t*, 1H, PhPy *H*$^{4'}$, $^3J_{H-H}$ = 7.4 Hz), 6.79 (*t*, 1H, PhPy *H*$^{5'}$,$^3J_{H-H}$ = 7.4 Hz), 6.05 (*d*,1H, PhPy PhPy *H*$^{6'}$, $^3J_{H-H}$7.4 Hz), 4.55 (*bs*, 4H, Cp), 4.28 (*bs*, 4H, Cp), 2.70 (*s*, 6H, N-C*H$_3$*). ^{13}C NMR (75MHz, $CDCl_3$): δ 169.5 (*d*, PhPy *C*$^{1'}$, $^1J_{Rh-C}$ = 31.5Hz), 163.0 (*d*, PhPy *C*$^{2'}$, $^1J_{Rh-C}$ = 1.7 Hz), 149.6 (PhPy *C*^{6}), 143.0 (PhPy *C*$^{2'}$), 137.9 (PhPy *C*^{4}), 134.00, 132.00 and 128.46 (*m*, PhPy *C*^{2}), 129.0 (PhPy *C*$^{5'}$), 123.8 (PhPy *C*$^{3'}$), 123.4 (PhPy *C*^{5}), 122.60 (PhPy *C*$^{4'}$), 123.40 (PhPy *C*^{5}), 119.2 (PhPy *C*^{3}) 76.2 (*m*, Cp), 74.3 (*m*, Cp), 40.7 (N-*CH$_3$*). ^{31}*P*NMR: δ 17.28 (*s*, $^1J_{Pt-P}$ =3088 Hz). Anal: Calcd. for $C_{60}H_{50}$ N_4P_2 $S_2ClFeIrPt$: C, 53.68; H, 3.75; N, 4.17. Found: C, 53.50; H, 3.68; N, 4.02. Molar conductivity (MeOH): 87 ohm^{-1} cm^{-1} mol^{-1}.

[(dppe)Pt(H-isopropyl$_2$-DTO □-S,S Pt)]Cl. This compound as been prepared following the same procedure of type II compounds. Obviously, in this case 1,2-diphenylphophine ethane (dppe) has been used instead of 1,1'-diphenylphosphinoferrocene. Yield: 85%. ^{1}H NMR (300MHz, $CDCl_3$): δ 7.64÷7.42 (*m*, 20H, Ph), 4.15 (*sl*, 2H, N-C*H* $(CH_3)_2$, 2.72 (*m*, 4H, P-CH_2-CH_2-P), 1.26 (*d*, 12H, N-CH(CH_3)$_2$). ^{13}C NMR (75MHz, $CDCl_3$): δ 133.3, 132.2, 129.2 (*m*, Ph), 52.48, (N-*C*H$(CH_3)_2$, 28.66 (m, P-*C*H_2-*C*H_2-P), 22.03, (N-CH(*C*H_3)$_2$). ^{1}*P*NMR: δ 16,10 (s, $^1J_{Pt-P}$ = 2910 Hz). Anal: Calcd for $C_{34}H_{41}N_2P_2S_2ClPt$: C, 48.95; H, 4.95; N, 3.36. Found: C, 49.12; H, 5.05; N, 3.28. Molar conductivity (MeOH): 98 ohm^{-1} cm^{-1} mol^{-1}.

[{(dppf)Pt(H-methyl$_2$-DTO κ-S,S Pt)$^+$,Cl$^-$}]Cl. 0.67 mL of a chloroform solution containing 53,6 mM of hydrogen chloride were added to 50 mg (8.92 mmol) of **[Pt(H-methyl$_2$-DTO κ-S,S Pt) (dppf)]$_6$Cl$_6$,** dissolved in 20 mL of chloroform. The deep blue solution slowly turned to brown yellow in about 1.5 hours. After this time, the volume of the solution was reduced about to the half and petroleum ether (50 mL) was added. A brown yellow precipitate was immediately formed. Upon rimotion of the solvent, 39 mg of brown yellow powder were collected. Elemental analysis and NMR spectrometry allowed to formulate the powder as the hydroalogenated form of the IIa species. In particular, the split of the N-CH3 singlet strongly supports the formation of a tight contact ion pair through the hosting of hydrogen chloride in the N-H…N frame of **[Pt(H-methyl$_2$-DTO κ-S,S Pt)(dppf)]Cl**. Yield: 75%. ^{1}H NMR (300MHz, $CDCl_3$): δ 7.91÷7.41 (*m*, 20H, Ph), 4.39 (*bs*, 4H, Cp), 4.21 (*bs*, 4H, Cp), 3.31 (*d*, 6H, N-CH_3, $^3J_{H-H}$ = 5.5Hz). ^{13}C NMR (75MHz, $CDCl_3$): δ 135.12, 131.28, 127.72 (*m*, Ph), 76.11, 73.20 (*m*, Cp), 33.9 (N-*C*H_3). ^{1}*P*NMR: δ 13,19 (s, $^1J_{Pt-P}$ = 3760 Hz). Anal: Calcd for $C_{38}H_{38}FeN_2P_2S_2Cl_2Pt$: C, 47.02; H, 3.95; N, 2.89. Molar conductivity (MeOH): 105 ohm^{-1} cm^{-1} mol^{-1}.

11.2. Equilibrium Constant and Curve fitting

For reactions of the following type:

	M-HCl	+	py	⇌	**M**	+	pyHCl
initial	C_0		L_0		-		-
equil.	C_0 - x		L_0 - x		x		x

$$Kc = \frac{[M]\,[pyHCl]}{[M\text{-}HCl]\,[py]} = \frac{x \cdot x}{(C_0 - x)\,(L_0 - x)} = \frac{x^2}{C_0 \cdot L_0 - C_0 \cdot x - L_0 \cdot x + x^2};$$

$$(Kc-1) \cdot x^2 - (Kc \cdot C_0 + Kc \cdot L_0) \cdot x + Kc \cdot C_0 \cdot L_0 = 0; \qquad (1)$$

The absorbance depends on x:

$$A = A_0 + \frac{A_{lim} - A_0}{C_0} x \qquad (2)$$

A was the recorded absorbance intensity, A_0 was the start value without the addition of pyridine, A_{lim} was the limiting value (left as a floating parameter), C_0 was the complex ion-pair concentration (mol dm^{-3}), L_0 was the added pyridine concentration. You can solve the implicit equation (1) and insert the result into the equation (2) and use it for the non linear least squares analysis to determine the Kc. We used the program "**MicroMath Scientist**" to fit the equation (2) and the equation (1) was used as an implicit equation.

MicroMath SCIENTIST model file used

```
// Equilibrium type:  M-HCl + B  =  M + BHCl   (absorbing species M-HCl and M)
// Absorbing species M-HCl and M (Mtot = constant)
// Independent and dependent variables definition
IndVars: L0
DepVars: A
// parameters definition. A0 e C0 must be fixex (costant)
Params: Kc, Alim, A0, C0
// implicit equation
(Kc-1)*x*x-(Kc*C0+Kc*L0)*x+Kc*C0*L0=0
// Constraints implicit solution
0<x<C0
// Global equation A=f(x)
A=A0+(Alim-A0)*x/C0
```

For reactions of the following type:

	M	+	L	⇌	**ML**
initial	C_0		L_0		-
equil.	$C_0 - x$		$L_0 - x$		x

$$Kc = \frac{[ML]}{[M]\,[L]} = \frac{x}{(C_0 - x)\,(L_0 - x)} = \frac{x}{C_0 \cdot L_0 - C_0 \cdot x - L_0 \cdot x + x^2};$$

$$Kc \cdot x^2 - (Kc \cdot C_0 + Kc \cdot L_0 + 1) \cdot x + Kc \cdot C_0 \cdot L_0 = 0; \qquad (3)$$

The absorbance depends on x:

$$A = A_0 + \frac{A_{lim} - A_0}{C_0} x \qquad (4)$$

We used the program "**MicroMath Scientist**" to fit the equation (3) and the equation (4) was used as an implicit equation.

MicroMath SCIENTIST model file used:

```
// Equilibrium type:  M + L  =  ML
// Absorbing species M and ML (Mtot = constant)
// Independent and dependent variables definition
IndVars: L0
DepVars: A
// parameters definition. A0 e C0 must be fixex (costant)
Params: Kc, Alim, A0, C0
// implicit equation
Kc*x*x-(Kc*C0+Kc*L0+1)*x+Kc*C0*L0=0
// Constraints implicit solution
0<x<C0
// Global equation A=f(x)
A=A0+(Alim-A0)*x/C0
```

11.3. Instruments

Electronic spectra were recorded with a PE Lambda35 UV VIS spectrometer. ^{1}H NMR and ^{13}C-{^{1}H}NMR spectra were recorded at 298 K on a Bruker ARX-300, equipped with a broadband probe operating at 300.13 and 75.56MHz, respectively. Chemical shifts (δ, ppm) were referred to $SiMe_4$.

Conductivity measurements were carried out with a Radiometer CDM3 conductivity bridge at 25°C. Electrochemical measurements were carried out in argon purged 1,2-dichloroethane at room temperature with an Autolab multipurpose equipment interfaced to a PC. The working electrode was a glassy carbon (8 mm^2, Amel) electrode. The counter electrode was a Pt wire, and the reference electrode was an SCE separated with a fine glass frit. The concentration of the complexes was about 5×10^{-4} M. Tetrabutylammonium hexafluorophosphate was used as a supporting electrolyte and its concentration was 0.05 M. Differential pulse voltammetry (DPV) was obtained at scan rates of 4, 10, 20 mV s^{-1}. Redox potentials were corrected by the internal reference ferrocene.

Diffusion Ordered NMR Spectroscopy (DOSY) studies were performed on a Varian 500 MHz spectrometer equipped with a pulse-field gradient probe. Spectra were recorded at 25 °C using a gradient stimulated echo with spin-lock and a convection compensation pulse sequence (DgcsteSL_cc).[8] Experimental parameters were optimized according to the sample under investigation. Diffusion gradients were incremented in 30 steps with gradient pulse amplitudes varying from 2.4 to 59.7 gauss/cm, 32 number of transients were acquired for each increment, with a diffusion gradient length of 2 ms and diffusion delays in 50–60 ms range. All measurements were performed in triplicate and the reported values are the mean±standard deviation of the mean. The hydrodynamic radii (R_h) were obtained using the Stokes-Einstein equation: $D_{obs} = k_B T/6\pi\eta R_h$, where k_B is the Boltzmann constant, T is the temperature and η is the viscosity of the solvent.

X-ray Crystal Structure Determination Data were collected at room temperature with a Bruker APEX II CCD area-detector diffractometer using Mo Kα radiation (λ = 0.71073 Å). Data collection, cell refinement, data reduction and absorption correction were performed by multiscan methods by means of the Bruker software.[9] The structures were solved by direct methods using SIR2004.[10] The nonhydrogen atoms were refined anisotropically by the full-matrix least-squares method on F^2 using SHELXL.[11] All the hydrogen (H) atoms were introduced in calculated positions and constrained to ride on their parent atoms

References

[1] Hurd, R. N.; De La Mater, G.; McElheny, C. G.; Turner, R. J.; Vallingford, V. H. *J. Org. Chem*. **1961**, 26, 3980.

[2] Kukushkin, Y. N.; Viaz'menskii, Y. E.; Zorina, L. I.; Pazhukina, Y. L. *Russ. J. Inorg. Chem*. **1968**, 13.

[3] Rosace, G.; Bruno, G.; Mons_u Scolaro, L.; Nicol_o, F.; Sergi, S.; Lanza, S. *Inorg. Chim. Acta* **1993**, 208, 59.

[4] Rosace, G.; Giuffrida, G.; Guglielmo, G.; Campagna, S.; Lanza, S. *Inorg. Chem.* **1996**, 35, 6816.

[5] Rosace, G.; Giuffrida, G.; Saitta, M.; Guglielmo, G.; Campagna, S., Lanza, S. *Inorg. Chem*. (**1996**) 35 6816

[6] Lanza, S.; Bruno, G.; Nicolò, F.; Callipari, G.; Tresoldi G. *Inorg. Chem*. (**2003**) 42 4545

[7] Giannetto, A.; Puntoriero, F.; Notti, A.; Parisi, MF; Ielo, I.; Nastasi, F. Bruno, G.; Campagna, S.; Lanza, S. *Eur. J. Inorg. Chem.* **2015**, 5730–5742

[8] Jerchow, A.; Müller, N. *J. Magn. Reson.* **1997**, 125, 372.

[9] (a) COSMO, version 1.60; Bruker AXS Inc.: Madison,Wisconsin, 2005. (b) SAINT, version 7.06A; Bruker AXS Inc.: Madison, Wisconsin, 2005. (c) SADABS, version 2.10; Bruker AXS Inc.: Madison, Wisconsin, 2005.

[10] Burla, M. C.; Caliandro, R.; Camalli, M.; Carrozzini, B.; Cascarano, G. L.; De Caro, L.; Giacovazzo, C.; Polidori, G.; Spagna, R. SIR2004, J. Appl. Crystallogr. 2005, 38, 381.

[11] Sheldrick, G. M. SHELXL97, University of Göttingen, Göttingen, Germany, 1997**.**